

https://dspace.org/

Bord stability evaluation and support design at Thorncliffe Chrome Mine in the Bushveld Complex: a case study

Khoza, Akani Trust

2025-08

University of the Witwatersrand, Johannesburg

https://hdl.handle.net/10539/49734

Khoza, Akani Trust. (2025). Bord stability evaluation and support design at Thorncliffe Chrome Mine in the Bushveld Complex: a case study. [Master's dissertation, University of the Witwatersrand, Johannesburg]. WIReDSpace. https://hdl.handle.net/10539/49734

Downloaded from a DSpace repository. https://dspace.org/

[

School of Mining Engineering



UNIVERSITY OF THE
WITWATERSRAND,
JOHANNESBURG

BORD STABILITY EVALUATION AND SUPPORT DESIGN AT THORNCLIFFE CHROME MINE IN THE BUSHVELD COMPLEX: A CASE STUDY

Akani Trust Khoza

I declare that this research report is my own unaided work. It is being submitted for the degree of Master of Science at the University of the Witwatersrand, Johannesburg. It has not been submitted before for any degree or examination to any other university.

Johannesburg, 2025

DECLARATION

I have familiarised myself with the University of the Witwatersrand Student Academic Misconduct Policy (SAMP). I hereby declare that the work I am submitting for assessment is my original work. I affirm that I have not plagiarised, misrepresented, or colluded with any other person or source. I have properly acknowledged, cited, and referenced all the sources that I have used in my work. I also declare that where I have used artificial intelligence (AI) tools it has only been as a means of guidance. The ideas and arguments presented in my work are my original thoughts and interpretations. I acknowledge that any academic misconduct, such as plagiarism or collusion will result in serious consequences. According to the SAMP, these consequences may include a reduced grade, a fail mark, or disciplinary action. The Faculty of Engineering and the University of the Witwatersrand have my consent to investigate any potential academic misconduct in my work. This investigation may include the use of similarity and AI detection software to check the originality of my work. I undertake to abide by the decision of any such investigation.

A.T Khoza

Signature of Candidate

25/08/2025

Date

“Excellence is never an accident. It is always the result of high intention, sincere effort, and intelligent execution; it represents the wise choice of many alternatives – choice, not chance, determines your destiny”

- Aristotle

ABSTRACT

Thorncliffe Chrome Mine is one of Glencore's Eastern Chrome Mines (ECM) bord and pillar mining operations. It is in the process of revising its mine design criteria with a focus on the stability of mining spans between pillars. The process includes the development of appropriate standard support requirements. A methodology developed by the Mine Health and Safety Council (MHSC) for designing stable bord spans in shallow Bushveld Complex operations was applied in the case study. Important factors considered included the rock mass quality, degree of safety required in different production drives, engineering requirements, local rock engineering environment, and various rock mass failure mechanisms. The rock mass classification analysis found that the ground conditions ranged from very poor to very good. Empirical design results indicated that maximum unsupported spans for short-term production drives varied between 3 m to 15 m. Due to higher safety requirements, maximum unsupported spans in medium-term production drives varied between 2 m to 8 m. However, engineering requirements dictated the mine maintains a minimum of 6 m in all the production drives, travelling roadways, and strike conveyor belt drives, to accommodate the manoeuvrability of the Trackless Mobile Machinery (TMM) used in production and belt conveyor equipment. Sufficient space is also required for workers to travel to workplaces. As an additional safety factor in the design of bord spans, the largest (diagonal) spans across intersections were used to design maximum stable bord widths. Poor ground conditions and spans larger than 17 m (formed by 12 m spans of orthogonal bords) showed costly standard support requirements. An optimised tendon support design was proposed. An opportunity to reduce the current tendon length from 1.5 m to 1.2 m was identified. The newly proposed primary tendon support system will achieve the desired stable conditions whilst reducing support costs for the mine.

ACKNOWLEDGMENTS

I would like to express my sincere gratitude to the following people who supported me throughout my master's journey:

My loving parents for their unwavering faith in me, encouragement, and sacrifices you made to ensure I complete my master's studies.

Thank you to my supervisor, Professor Bryan Watson, for his consistent guidance and patience throughout the completion of this project report. Your knowledge of the subject matter and feedback steered me through the research.

Lebogang Baloyi, you always availed yourself to assist with brainstorming and having meaningful geotechnical discussions. We improved each other as young professionals, thank you.

Thank you to the Glencore Eastern Chrome Mines team for the great effort we expended in collecting underground geotechnical data, which was used in this project.

TABLE OF CONTENTS

DECLARATION i

ABSTRACT iii

ACKNOWLEDGMENTS iv

LIST OF FIGURES viii

LIST OF TABLES xvi

1 INTRODUCTION 1

1.1 Research Context 1

1.2 Research Background 2

1.3 Problem Statement 19

1.4 Justification for Research 20

1.5 Research Objectives 20

1.6 Research Methods 21

1.7 Research Validation 22

1.8 Structure of the Research Report 22

2 LITERATURE REVIEW 24

2.1 Review of Rock Engineering Design Methods 24

2.2 Methodology for Designing Stable Bord Spans 25

2.3 Rock Mass Characterization 27

2.4 Geotechnical Data Collection Methods 43

2.5 Evaluation of Boundary Conditions 49

2.6 Evaluation of Rock Mass Quality 54

2.7 Estimation of In Situ Rock Mass Properties 55

2.8 Stability Evaluation Methods (Stability Analyses) 70

2.9 Evaluation of Support Requirements for Shallow Bord and Pillar Mines 81
2.10 Monitoring of Underground Excavations 91
2.11 Summary of Chapter 92
3 GEOTECHNICAL INVESTIGATION 93
3.1 Scanline Mapping of Hangingwall and Sidewall 93
3.2 Laboratory Testing of Rock Material 97
3.3 Summary of Chapter 97
4 ROCK MASS CHARACTERIZATION 98
4.1 Orientation of Discontinuities 98
4.2 Discontinuity Properties 101
4.3 Rock Mass Classification Results 110
4.4 Rock Test Results and Rock Mass Properties 118
4.5 Summary of Chapter 123
5 DESIGN OF STABLE BORD SPANS 124
5.1 Maximum Unsupported Bord Spans 124
5.2 Stability Evaluation of Bord Spans 131
5.3 Chapter Summary 179
6 DETERMINATION OF IN-STOPE SUPPORT REQUIREMENTS 181
6.1 Support Requirements using Rock Mass Classification Systems 183
6.2 Case Study Support Requirements 201
6.3 Support for Identified Keyblocks and Wedges 204
6.4 Support from Stress Analysis 213
6.5 Support for a Stratified Rock Mass 214
6.6 JBlock Probabilistic Stability Analysis 214
6.7 Support Cost Saving Analysis 224

6.8 Chapter Summary 226

7 PROJECT FINDINGS 228

7.1 Rock Mass Failure Analysis 228

7.2 Hangingwall Beam Failure Analysis 230

7.3 Structural Failure Analysis 231

7.4 Intact Rock Failure Analysis 232

7.5 Support Requirements 233

7.6 Chapter Summary 234

8 CONCLUSIONS AND RECOMMENDATIONS 235

8.1 Summary of Chapters 235

8.2 Research Key Findings and Observations 237

8.3 Research Contributions 240

8.4 Research Limitations 241

8.5 Recommendations to Thorncliffe Mine 242

9 REFERENCE LIST 245

LIST OF FIGURES

Figure 1-1: Setting of the Thorncliffe mine in the eastern limb of the BC 3

Figure 1-2: Schematic stratigraphic column of the Rustenburg Layered Suite of the Bushveld Complex 4

Figure 1-3: A surface outcrop of the interlayer between Chromitite and Anorthosite layers (Upper Critical Zone) at the Dwarsrivier National Monument 5

Figure 1-4: Geological map of the Eastern Limb showing outcrop of layers of the Rustenburg Layered Suite 6

Figure 1-5: General stratigraphic column of the Chromitite Layers at Thorncliffe Mine 7

Figure 1-6: Detailed MG1 Chromitite Package with hangingwall and footwall layers 8

Figure 1-7: ECM major geological structures 10

Figure 1-8: Typical production section layout used at Thorncliffe Mine 12

Figure 1-9: Enlarged typical bord and pillar layout used at Thorncliffe Mine 13

Figure 1-10: Cumulative frequency of the FOG thickness at Thorncliffe Mine 15

Figure 1-11: Cumulative frequency of the FOG areal extent at Thorncliffe Mine 16

Figure 1-12: Number of FOGs occurring at different types of excavations at the mine 17

Figure 1-13: FOG average distance from face for different excavation types 17

Figure 1-14: Location of recorded FOGs at Thorncliffe Mine..... 18

Figure 1-15: Geological structures contributing to FOGs at Thorncliffe Mine..... 18

Figure 1-16: Number of FOGs per activity..... 19

Figure 2-1: Flowchart for the design of stable bord spans..... 26

Figure 2-2: Geometrical terms describing discontinuity orientation 31

Figure 2-3: Illustrating measurement of true spacing and apparent spacing for a single discontinuity set..... 32

Figure 2-4: ISRM Roughness profiles and suggested nomenclature..... 33

Figure 2-5: Suggested definitions of aperture of open discontinuities and width of filled discontinuities..... 36

Figure 2-6: Effect of increasing discontinuity sets on the rock mass..... 41

Figure 2-7: Schematic illustration of a scanline survey..... 45

Figure 2-8: Orientation of horizontal principal stresses 51

Figure 2-9: Variation of major horizontal principal stress with depth..... 52

Figure 2-10: Variation of minor horizontal principal stress with depth..... 53

Figure 2-11: Variation of the ratio of major horizontal principal stress to vertical stress (K_1) with depth..... 53

Figure 2-12: Variation of the ratio of minor horizontal principal stress to vertical stress (K_3) with depth..... 54

Figure 2-13: Stress-strain curve showing the progressive deformation of a specimen in uniaxial compression 56

Figure 2-14: Mohr-Coulomb strength envelopes in terms of a) normal vs shear stress and b) principal stresses 61

Figure 2-15: Rock beam failure in stratified rock masses 72

Figure 2-16: (a) Jointed rock beams; (b) Voussoir beam with compressive arch, and (c) Voussoir model showing the trajectory of the compressive forces 73

Figure 2-17: Failure modes of the voussoir beam 74

Figure 2-18: Maximum height of bed separation due to hangingwall tensile zone 78

Figure 2-19: Example of a tunnel layout in a high horizontal stress environment 80

Figure 2-20: Estimation of the tributary area requirements 86

Figure 2-21: Determination of support influence 87

Figure 3-1: Thorncliffe Mining Sections (not to scale) 94

Figure 4-1: Example contour plot showing major discontinuity sets 99

Figure 4-2: Thorncliffe Mining sections with a compass showing all discontinuity directions (not to scale) 101

Figure 4-3: Frequency distribution of RMR_{89} values for all production sections 111

Figure 4-4: Frequency distribution of GSI values for all production sections 113

Figure 4-5: Frequency distribution of Q-Index values for all production sections 115

Figure 4-6: Frequency distribution of MRMR values for all production sections 117

Figure 4-7: Frequency distribution of Pyroxenite UCS values 119

Figure 4-8: Frequency distribution of Chromitite UCS values 119

Figure 4-9: Output from RocLab for Pyroxenite rock 120

Figure 4-10: Output from RocLab for MG1 Chromitite rock 121

Figure 5-1: Thorncliffe Life of Mine (LOM) Footprint (not to scale) 125

Figure 5-2: Enlarged typical bord and pillar layout showing the working area and back area 127

Figure 5-3: Bord spans are designed to accommodate the critical diagonal span across intersections 132

Figure 5-4: Stability number versus hydraulic radius for Rig 47 mining section 137

Figure 5-5: Stability number versus hydraulic radius for Rig 50 mining section 138

Figure 5-6: Stability number versus hydraulic radius for TC1 mining section 139

Figure 5-7: Stability number versus hydraulic radius for RIG 2 mining section 140

Figure 5-8: Stability number versus hydraulic radius for RIG 14 mining section 141

Figure 5-9: Adjusted MRMR versus hydraulic radius for RIG 47 mining section 143

Figure 5-10: Adjusted MRMR versus hydraulic radius for RIG 50 mining section 144

Figure 5-11: Adjusted MRMR versus hydraulic radius for TC1 mining section 145

Figure 5-12: Adjusted MRMR versus hydraulic radius for Rig 2 mining section 146

Figure 5-13: Adjusted MRMR versus hydraulic radius for Rig 14 mining section 147

Figure 5-14: Interaction of a Rig 47 strike bords with the identified discontinuity sets 160

Figure 5-15: Wedges formed in the hangingwall, footwall, and sidewall of RIG 47 strike bords 160

Figure 5-16: Interaction of a Rig 47 ventilation holings with the identified discontinuity sets 161

Figure 5-17: Wedges formed in the hangingwall, footwall, and sidewall of RIG 47 ventilation holings 162

Figure 5-18: Interaction of Rig 50 strike bords with the identified discontinuity sets 163

Figure 5-19: Wedges formed in the hangingwall, footwall, and sidewall of RIG 50 strike bords 164

Figure 5-20: Interaction of Rig 50 ventilation holings with the identified discontinuity sets 167

Figure 5-21: Wedges formed in the hangingwall, footwall, and sidewall of RIG 50 ventilation holings 167

Figure 5-22: Interaction of TC1 strike bords with the identified discontinuity sets 170

Figure 5-23: Wedges formed in the hangingwall, footwall, and sidewall of TC1 strike bords 170

Figure 5-24: Interaction of TC1 ventilation holings with the identified discontinuity sets 171

Figure 5-25: Wedges formed in the hangingwall, footwall, and sidewall of TC1 ventilation holings 171

Figure 5-26: Constructed RS2 model with MG1L1 Chrome stringer 175

Figure 5-27: Enlarged section of the RS2 model showing the position and thickness of the MG1L1 stringer 175

Figure 5-28: RS2 results showing measurements of the vertical tensile zone 176

Figure 6-1: Q-support design chart for an 8.0 m medium-term span in RIG 47 185

Figure 6-2: 1.5 m long resin grouted bolts installed on a 1.5 m by 1.5 m grid spacing in RIG 47 206

Figure 6-3: 1.5 m long resin grouted bolts installed on a 1.0 m by 1.0 m grid spacing in RIG 47 206

Figure 6-4: 1.2 m long resin grouted bolts installed on a 1.5 m by 1.5 m grid spacing in RIG 47 207

Figure 6-5: 30 mm Shotcrete and 1.5m long resin grouted bolts installed on a 1.5 m by 1.5 m grid spacing in RIG 47 207

Figure 6-6: 1.5 m long resin grouted bolts installed on a 1.5 m by 1.5 m grid spacing in RIG 50 208

Figure 6-7: 1.2 m long resin grouted bolts installed on a 1.0 m by 1.0 m grid spacing in RIG 50 208

Figure 6-8: 30 mm Shotcrete and 1.5m long resin grouted bolts installed on a 1.5 m by 1.5 m grid spacing in RIG 50 209

Figure 6-9: 1.5 m long resin grouted bolts installed on a 1.5 m by 1.5 m grid spacing in TC1 209

Figure 6-10: 1.5 m long resin grouted bolts installed on a 1.0 m by 1.0 m grid spacing in TC1 210

Figure 6-11: 1.2 m long resin grouted bolts installed on a 1.5 m by 1.5 m grid spacing in TC1 210

Figure 6-12: 30 mm Shotcrete and 1.5m long resin grouted bolts installed on a 1.5 m by 1.5 m grid spacing in TC1 211

Figure 6-13: JBlock Model of a 10 m Span with no support in Rig 47 217

Figure 6-14: JBlock Model of a 10 m Span with support installed at 1.5 m by 1.5 m in Rig 47 218

Figure 6-15: Distribution of rockfalls in the face area of a 10 m bord span with no support in Rig 47 219

Figure 6-16: Key block stability frequency distribution chart for a 10 m bord span with no support in Rig 47 220

Figure 6-17: Hazard and risk results for a 10 m bord span with no support in Rig 47 220

Figure 6-18: Distribution of rockfalls in the face area of a 10 m bord span with support in Rig 47 221

Figure 6-19: Keyblock stability frequency distribution chart for a 10 m bord span with support in Rig 47 221

Figure 6-20: Hazard and risk results for a 10 m bord span with support in Rig 47 222

LIST OF TABLES

Table 1-1: Thorncliffe Mine pillar dimensions and FOS with depth below surface 14

Table 1-2: FOG 95th Percentile variables for Thorncliffe Mine 16

Table 2-1: Description of discontinuity spacing 32

Table 2-2: Suggested classification and description of discontinuity roughness 33

Table 2-3: Description and classification of discontinuity persistence 34

Table 2-4: Weathering classification of rocks 35

Table 2-5: Field classification of discontinuity wall strength 36

Table 2-6: Classification of discontinuity aperture 37

Table 2-7: The modified Wentworth scale for grain size classification 38

Table 2-8: Weathering types for filled discontinuities 39

Table 2-9: Field classification of filling material strength 39

Table 2-10: Water seepage classification of filled discontinuities 40

Table 2-11: Water seepage classification of unfilled discontinuities 40

Table 2-12: Field description of discontinuity sets 41

Table 2-13: Block size classification according to the volumetric joint count 42

Table 2-14: Description of the Blockiness of the rock mass 43

Table 2-15: Values of the Hoek-Brown constant m_i for intact rock 63

Table 2-16: Guidelines for estimating the disturbance factor D 65

Table 2-17: Estimation of the peak friction angle from joint roughness number and joint alteration number 68

Table 2-18: Shear strength of filled discontinuities 69

Table 2-19: Rock engineering parameters associated with different mining depths 82

Table 3-1: Orientation of bords (strike direction) and splits (dip direction) in the five production sections 93

Table 3-2: Meters mapped per mining section 95

Table 3-3: Example of a scanline mapping sheet used in collecting geotechnical data 96

Table 3-4: Summary of laboratory tests conducted 97

Table 4-1: Major discontinuity sets identified in each mining section 100

Table 4-2: Summary of Rig 47 hangingwall discontinuity sets 102

Table 4-3: Properties of Rig 47 hangingwall discontinuity sets 103

Table 4-4: Summary of Rig 50 hangingwall discontinuity sets 104

Table 4-5: Properties of Rig 50 hangingwall discontinuity sets 105

Table 4-6: Summary of TC1 hangingwall discontinuity sets 106

Table 4-7: Properties of TC1 hangingwall discontinuity sets 107

Table 4-8: Summary of Rig 2 hangingwall discontinuity sets..... 108

Table 4-9: Properties of Rig 2 hangingwall discontinuity sets..... 108

Table 4-10: Summary of Rig 14 hangingwall discontinuity sets..... 109

Table 4-11: Properties of Rig 14 hangingwall discontinuity sets..... 109

Table 4-12: Statistical analysis of the hanging wall RMR_{89} results 112

Table 4-13: Statistical analysis of the hanging wall GSI results..... 113

Table 4-14: Statistical analysis of the hanging wall Q-Rating results..... 116

Table 4-15: Summary of $MRMR_{2000}$ Adjustment Factors 117

Table 4-16: Statistical Analysis of the $MRMR_{2000}$ Results..... 118

Table 4-17: Statistical analysis of UCM results for Pyroxenite and Chromitite rock 120

Table 4-18: Rock mass properties for the hangingwall and the mineralised zone..... 122

Table 4-19: Frictional properties of discontinuities with serpentine infill material..... 122

Table 5-1: ESR values assigned to different production drives in a bord and pillar section..... 128

Table 5-2: Maximum unsupported spans for short-term panels in the five production sections..... 129

Table 5-3: Maximum unsupported spans for medium-term panels in the five production sections..... 130

Table 5-4: Diagonal spans across intersections of various orthogonal bords ... 133

Table 5-5: Results of the Modified Rock Quality Index (Q') per mining section ... 134

Table 5-6: Modified Stability Number Multiplying factors (A, B, and C) per production section ... 134

Table 5-7: Calculated Modified Stability Number (N') in each section for different rock qualities ... 135

Table 5-8: Bord spans, hydraulic radii, and stability number for the Rig 47 section ... 136

Table 5-9: Bord spans, hydraulic radii, and stability number for Rig 50 mining section ... 137

Table 5-10: Bord spans, hydraulic radii, and stability number for TC1 mining section ... 139

Table 5-11: Bord spans, hydraulic radii, and stability number for Rig 2 mining section ... 140

Table 5-12: Bord spans, hydraulic radii, and stability number for Rig 14 mining section ... 141

Table 5-13: Bord spans, hydraulic radii, and MRMRs for Rig 47 mining section ... 143

Table 5-14: Bord spans, hydraulic radii, and MRMRs for Rig 50 mining section ... 144

Table 5-15: Bord spans, hydraulic radii, and MRMRs for TC1 mining section ... 145

Table 5-16: Bord spans, hydraulic radii, and MRMRs for Rig 2 mining section 146

Table 5-17: Bord spans, hydraulic radii, and MRMRs for Rig 14 mining section 147

Table 5-18: Input parameters for Voussoir beam stability analysis 149

Table 5-19: Voussoir buckling or snap-through failure analysis at Thorncliffe Mine 151

Table 5-20: Voussoir beam shear failure analysis at 200 mbs at Thorncliffe Mine 152

Table 5-21: Voussoir beam shear failure analysis at 400 mbs at Thorncliffe Mine 153

Table 5-22: Voussoir beam shear failure analysis at 600 mbs at Thorncliffe Mine 154

Table 5-23: Voussoir beam shear failure analysis at 800 mbs at Thorncliffe Mine 155

Table 5-24: Voussoir beam shear failure analysis at 1000 mbs at Thorncliffe Mine 156

Table 5-25: Results of the maximum wedges formed in RIG 47 strike bord 161

Table 5-26: Results of the maximum wedges formed in RIG 47 ventilation holings 162

Table 5-27: Results of the maximum wedges formed in the hangingwall of RIG 50 strike bords 164

Table 5-28: Results of the maximum wedges formed in the upper right side of RIG 50 strike bords 165

Table 5-29: Results of the maximum wedges formed in the upper left side of RIG 50 strike bords 165

Table 5-30: Results of the maximum wedges formed in the lower left side of RIG 50 strike bords 165

Table 5-31: Results of the maximum wedges formed in the lower right side of RIG 50 strike bords 166

Table 5-32: Results of the maximum wedges formed in the floor of RIG 50 strike bords 166

Table 5-33: Results of the maximum wedges formed in the roof of RIG 50 ventilation holings 168

Table 5-34: Results of the maximum wedges formed in the upper right side of RIG 50 ventilation holings 168

Table 5-35: Results of the maximum wedges formed in the upper left side of RIG 50 ventilation holings 168

Table 5-36: Results of the maximum wedges formed in the lower left side of RIG 50 ventilation holings 169

Table 5-37: Results of the maximum wedges formed in the floor of RIG 50 ventilation holings 169

Table 5-38: Results of the maximum wedges formed in TC1 strike bords 172

Table 5-39: Results of the maximum wedges formed in TC1 ventilation holings 172

Table 5-40: In-situ field stress parameters 174

Table 5-41: Summary of material properties used in the RS2 model 174

Table 5-42: Empirical and modelled tensile zone height results at 200 mbs..... 177

Table 5-43: Empirical and modelled tensile zone height results at 400 mbs..... 177

Table 5-44: Empirical and modelled tensile zone height results at 600 mbs..... 178

Table 5-45: Empirical and modelled tensile zone height results at 800 mbs..... 178

Table 5-46: Empirical and modelled tensile zone height results at 1000 mbs... 178

Table 6-1: Current in-stope tendon support used at Thorncliffe mine..... 181

Table 6-2: Specifications of the shotcrete support used at Thorncliffe Mine..... 182

Table 6-3: Equivalent dimension (De) for medium-term production drives 184

Table 6-4: Equivalent dimension (De) for short-term production drives..... 184

Table 6-5: Support requirements for an 8.0 m medium-term span in different ground conditions..... 186

Table 6-6: Support requirements for an 11.0 m medium-term span in different ground conditions..... 187

Table 6-7: Support requirements for a 14.0 m medium-term span in different ground conditions..... 188

Table 6-8: Support requirements for a 17.0 m medium-term span in different ground conditions..... 189

Table 6-9: Support requirements for a 20.0 m medium-term span in different ground conditions..... 190

Table 6-10: Support requirements for a 21.0 m medium-term span in different ground conditions..... 191

Table 6-11: Support requirements for an 8.0 m short-term span in different ground conditions 192

Table 6-12: Support requirements for a 11.0 m short-term span in different ground conditions 193

Table 6-13: Support requirements for a 14.0 m short-term span in different ground conditions 194

Table 6-14: Support requirements for a 17.0 m short-term span in different ground conditions 195

Table 6-15: Support requirements for a 20.0 m short-term span in different ground conditions 196

Table 6-16: Support requirements for a 21.0 m short-term span in different ground conditions 197

Table 6-17: Parameters used for primary support design of short-term panels 199

Table 6-18: Parameters used for primary support design of medium-term panels 200

Table 6-19: Design of primary support systems for short-term production drives 200

Table 6-20: Design of primary support systems for medium-term production drives 200

Table 6-21: Support demand at Thorncliffe based on 100% fallout height 202

Table 6-22: Determination of standard bolt minimum length 203

Table 6-23: Comparison of ECM and Case Study primary support FOS 204

Table 6-24: Support scenarios evaluated in Unwedge 205

Table 6-25: Bolt properties specified in Unwedge 205

Table 6-26: Shotcrete support specified in Unwedge 205

Table 6-27: FOS results of generated wedges after applying various support systems..... 211

Table 6-28: Results of the FOS of the roof wedge in RIG 50 after applying different support..... 212

Table 6-29: Results of the FOS of the lower left wedge in RIG 50 after applying different support..... 212

Table 6-30: Results of the FOS of the upper left wedge in RIG 50 after applying different support..... 212

Table 6-31: Results of the FOS of the lower right wedge in RIG 50 after applying different support..... 213

Table 6-32: Results of the FOS of different wedges in TC1 after applying different support..... 213

Table 6-33: Support scenarios to assess the effect of support spacing, bolt length, and shotcrete 215

Table 6-34: Summary of discontinuity characteristics in each mining section... 216

Table 6-35: Results of statistical keyblock analysis, Rig 47 10 m span 223

Table 6-36: Results of statistical keyblock analysis, Rig 50 10 m span 223

Table 6-37: Results of statistical key block analysis, TC1 10 m span..... 223

Table 6-38: Effect of increasing supported bord spans on rockfall risk..... 224

Table 6-39: Roof bolts and resin capsules pricing 224

Table 6-40: Support cost saved annually 226

LIST OF ABBREVIATIONS AND SYMBOLS

Abbreviation	Description
2D	Two Dimensional
3D	Three Dimensional
AMS	Airborne Magnetic Surveys
BC	Bushveld Complex
BIC	Bushveld Igneous Complex
BTS	Brazilian Tensile Strength Test
COP	Code of Practice
DBS	Depth Below Surface
DEM	Discrete Element Method
ECM	Eastern Chrome Mines
ERR	Energy Release Rate
ESR	Excavation Support Ratio
FDM	Finite Difference Method
FEA	Finite Element Analysis
FLAC	Fast Lagrangian Analysis of Continua
FOG	Fall of ground
FOS	Factor of Safety
FW	Footwall
GCMP	Ground Control Management Plan
GSI	Geological Strength Index
HW	Hangingwall
ISRM	International Society for Rock Mechanics
LHD	Load Haul and Dump Truck
LOM	Life of Mine
Mbs	Metres below Surface
M-C	Mohr-Coulomb Failure Criterion
MDC	Mine Design Criteria
MG1	Middle Chromitite Group 1 Reef
MG1L1	MG1 leader 1 Chromitite stringer
MHSC	Mine Health and Safety Council
MRMR	Mining Rock Mass Rating
RMR	Rock Mass Rating
RS2	Rock and Soil 2-dimensional analysis program
RS3	Rock and Soil 3-dimensional analysis program
SAMRASS	South African Mines Reportable Accidents Statistics System
SEPT	Short Encapsulations Pull Out Test
TARP	Trigger Action Response Plan
TCS	Triaxial Compressive Strength
TMM	Trackless Mobile Machinery
UCS	Uniaxial Compressive Strength
UDEC	Universal Distinct Element Code
VTZ	Vertical Tensile Zone

Symbol	Description	Units
ϕ_b	Basic friction angle of rock	°
ϕ_i	Internal angle of friction	°
τ	Shear Strength of rock	MPa
σ_{cm}	Uniaxial Compressive Strength of rock mass	MPa
σ_{ci}	Uniaxial Compressive Strength of intact rock	MPa
σ_3	Minor Principal Stress	MPa
σ_2	Intermediate Principal Stress	MPa
σ_1	Major Principal Stress	MPa
p	Rock density	kg/m^3
γ	Unit Weight	N/m^3
g	Gravitational acceleration	m/s^2
E	Young's Modulus	MPa
c	Cohesion of intact rock	MPa

1 INTRODUCTION

Falls of ground (FOGs) are the main cause of injuries and fatalities in shallow mining operations (Murphy, et al., 2016). A proper process of rock mass stability evaluation is vital to ensure the maximum extraction of ore under safe working conditions. The process must include an evaluation of excavation stability and determine optimum support requirements (Stacey, 2001). Stacey (2001) stated that the "stability of the excavation must be evaluated to the quality of the rock mass in which it is located". This means that the design of stable mining excavations requires an in-depth knowledge of:

- the rock mass characteristics,
- understanding of the geotechnical aspects surrounding the orebody, and
- the mechanisms controlling stability.

Thorncliffe Chrome Mine is one of Glencore's Eastern Chrome Mines (ECM). It is a hard rock bord and pillar mining operation situated within the Eastern Limb of the Bushveld Complex (BC). The mine is in the process of reviewing and revising the mine design criteria with a focus on the stability of mining spans between pillars. This process entails bord span analysis and the review of current support practices. This investigation aims to apply an improved method of determining maximum stable bord spans in conjunction with optimum support systems. This research work will form an essential part of the Ground Control Management Plan (GCMP) of the mine. It will assist in improving the mine's mandatory Code Of Practice (COP) to combat rock falls.

1.1 Research Context

Bord and pillar mining involves leaving unmined blocks or sections of the orebody known as *'Pillars'*. These pillars perform the role of maintaining the stability of the openings and supporting the overburden. Methods for designing stable hard-rock pillars have been based on empirical studies (Esterhuizen, 2007). There are no universally adopted methodologies for the design and evaluation of maximum stable spans between pillars (Murphy, et al., 2016). Swart & Handley (2005) also affirmed that only a few mining operations are designing bord spans based on adequate knowledge of the existing local factors governing instability. Instead, the

design of bord spans is often largely predetermined, being informed by the size of equipment used or dictated by previous experience, that is, benchmarking against mines operating under similar conditions. Such design methods can lead to unexpected FOGs. There is variability in parameters controlling rock behaviour from one mine to another, or even from one area of a mine to another. The parameters include geological structures, rock strength, in-situ stress, rock durability, and other rock characteristics. This variability in ground conditions must be considered in the design of mining excavations (Stacey, 2021).

The MHSC commissioned research for developing a reliable engineering methodology for designing stable bord spans in shallow mining operations (Murphy, et al., 2016). The proposed methodology was applied in this study.

1.2 Research Background

1.2.1 Locality

Thorncliffe Mine is geologically situated along the southern part of the Eastern Limb of the Bushveld Complex (Figure 1-1). Geographically, the mine is located approximately 30 km south of the Steelpoort Fault and 50 km south-west of Burgersfort Town. The regional setting of the project area is depicted with a red star in Figure 1-1. The mine exploits a Chromite ore-bearing orebody found within the Critical Zone of the Rustenburg Layered Suite of the BC (Glencore ECM, 2021). The characteristics of the orebody will be discussed in greater detail in Sections 1.2.2 and 1.2.3.

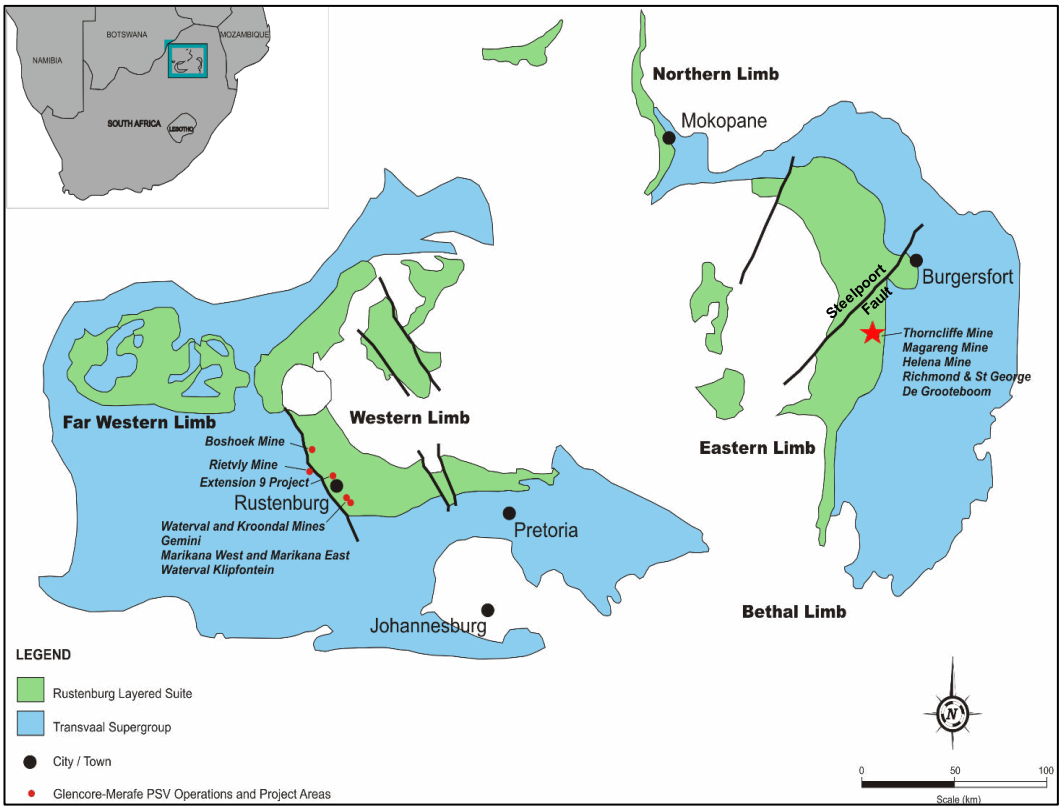


Figure 1-1: Setting of the Thorncliffe mine in the eastern limb of the BC (adapted from Merafe Resources (2021))

1.2.2 Regional Geology

The project area falls within the mafic Rustenburg Layered Suite in the Eastern Limb of the BC. The Rustenburg Layered Suite is subdivided into five zones, namely the Marginal Zone, which occurs at the base, and overlain by the Lower Zone, Critical Zone, Main Zone, and Upper Zone. Figure 1-2 provides a stratigraphic column of the Rustenburg Layered Suite. The Critical Zone of the Rustenburg Layered Suite contains many of the valuable mineralized layers. The Critical Zone, which is up to 1500 m thick and characterized by great layering, contains Chromium and Platinum-rich deposits (Deseta, 2020). The highly continuous and world-class Chromitite layers in the Critical Zone carry significant amounts of PGMs, but the Chromite mineral is dominant. The Chromitite seams in the Critical Zone host the largest Chromitite resources on earth (Scoon & Viljoen, 2016).

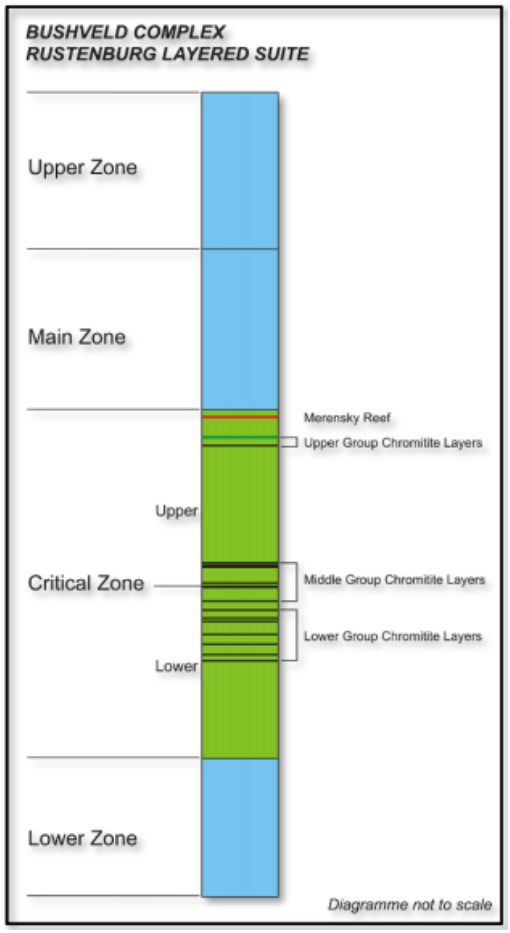


Figure 1-2: Schematic stratigraphic column of the Rustenburg Layered Suite of the Bushveld Complex (Merafe Resources, 2021)

The Critical Zone is divided into the Lower Critical Zone, which is characterized by small-scale Harzburgites and dominated by thick successions/layering of feldspathic orthopyroxenes and the Upper Critical Zone, which consists of packages of Anorthosites, Norites, Chromitite, Harzburgite, and Pyroxenite rocks in the footwall and hangingwall (Deseta, 2020). The Critical Zone hosts a total of 15 main Chromitite layers with varying grades and thicknesses ranging from 25 mm to over 2 m. These Chromitite layers are classified into three groups (as shown in Figure 1-2): the ultramafic Lower Group, which comprises seven Chromitite seams (LG1-7), the Middle Group containing four Chromitite seams (MG1-4), and the Upper Group (UG1-3) comprising three Chromitite seams (Hasch & Latypov, 2021).

The Lower Group Chromitite layers are hosted within the Lower Critical Zone, and the Upper Critical Zone contains the Middle Group Chromitite layer, the Upper Group Chromitite Layer, and the famous Merensky Reef at the top of the Critical Zone. Figure 1-3 shows a surface outcrop of the Upper Critical Zone found at Dwarsrivier National Monument, near Steelpoort, Limpopo Province.



Figure 1-3: A surface outcrop of the interlayer between Chromitite and Anorthosite layers (Upper Critical Zone) at the Dwarsrivier National Monument

In Figure 1-3 the Upper Group 1 (UG1) Chromitite layer is underlain by an interlayer between Anorthosite (light-brown rock) and thin Chromitite (black-colour) layers. Figure 1-4 shows the outcrop of the various mineralized layers/areas of the Rustenburg Layered Suite in the Eastern limb of the Bushveld Complex. The project area is located where there is a highly continuous MG1 Chromitite layer outcrop. Section 1.2.3 discusses the local geology in the project area.

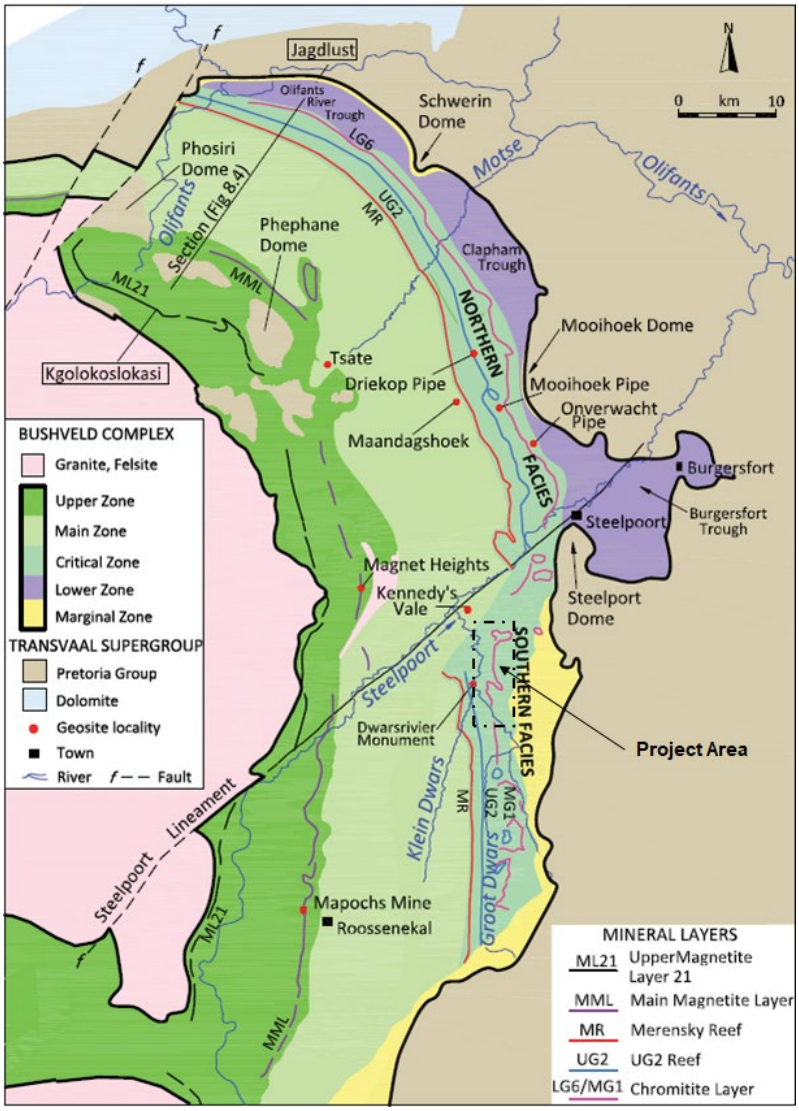


Figure 1-4: Geological map of the Eastern Limb showing outcrop of layers of the Rustenburg Layered Suite (adapted from Scoon & Viljoen (2016)*)*

1.2.3 Local Geology

The stratigraphic column in Figure 1-5 shows the positions of various Chromitite layers relative to the MG1 Chromitite layer in the critical zone. The Middle Group Chromitite package is comprised of four Chromitite layers (MG1 – MG4) where the MG1 and MG2 reefs are embedded/hosted in Pyroxenite layers, while the MG3 and MG4 seams are between Norites and Anorthosites of the Upper Critical Zone (Glencore ECM, 2021).

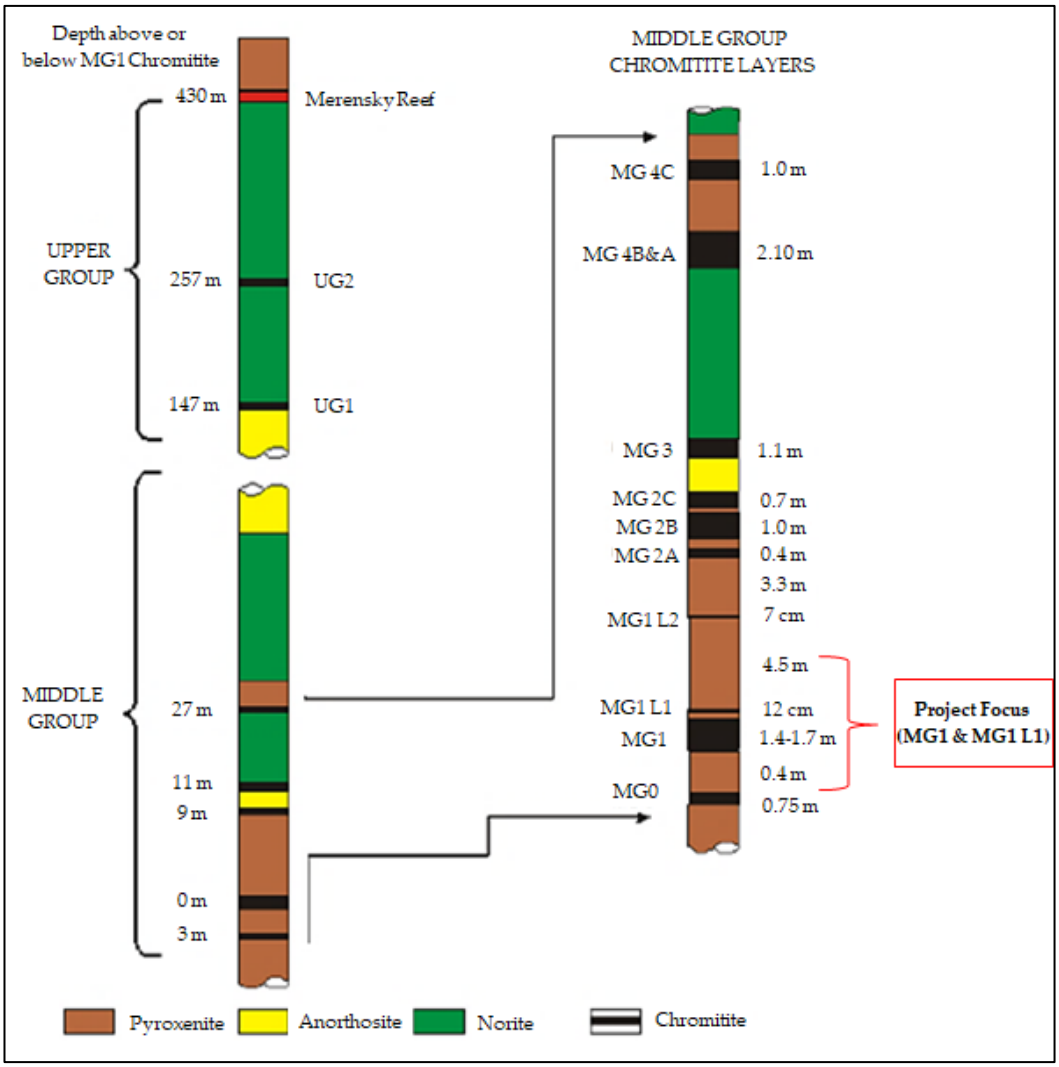


Figure 1-5: General stratigraphic column of the Chromitite Layers at Thorncliffe Mine (Glencore ECM, 2021)

After the MG1 Chromitite package is extracted, a pyroxenite hangingwall with an average thickness of 4.5 m is exposed and supported primarily by tendon units. The rocks of the MG1 layer are striking close to the North-South direction and dipping at shallow angles of between 10° – 12° to the west (Xtrata Alloys, 2005).

The average thickness of the MG1 Chrome package at Thorncliffe Mine is 1.8 m. The hangingwall layering and a disseminated MG1 leader 1 (MG1L1) Chromitite stringer in the hangingwall result in average stoping heights of up to 2.2 m at Thorncliffe Mine. However, there are underground working areas where the mining cut does not include the disseminated chromite leaders (Xtrata Alloys, 2005). A

detailed description of the MG1 Chromitite reef package with footwall and hangingwall layers is presented in Figure 1-6.

Thickness	STRAT	LITHOLOGY	UNIT	PACKAGE	REMARKS
11cm		MG1L2	MG1L2	MG1HW	Disseminated Leader occur in PX
8.9m		PX	MG1HW2		Pyroxenite
17cm		CHRDISS	MG1L1	MG1	Disseminated chromitite Leader band
45cm		PX	MG1HW1		
1.3 - 1.7m (1.98m)		CHR	MG1		MG1 package with disseminated MG1 Leader band included
		PX			
		CHR			
5cm		PX	MGFW1	MG1FW	MG1 footwall with Chromitite footwall marker bands
8cm		PXCHRDISS			
1.80m		PX			
57cm		CHR	MG1FM2		
		PX			
		CHR			
75cm		PX	MG1FW2		
64cm		CHR	MG0		
		PX			
		CHR			
		PX	MG1FW3		

Figure 1-6: Detailed MG1 Chromitite Package with hangingwall and footwall layers (adapted from Xtrata Alloys (2005))

Figure 1-6 shows the layered hangingwall of the MG1 Chrome reef. It is made up of the disseminated MG1L1 and a pyroxenite hangingwall layer (MG1HW1) immediately above the MG1 seam. The Pyroxenite MG1HW1 has a variable thickness of 250 mm to 450 mm across the study area, while the MG1L1 thickness ranges between 20 mm to 200 mm. The footwall of the MG1 reef (MG1FW1) consists of pyroxenite immediately below the MG1, which is often included in the mining cut as an overbreak (Xtrata Alloys, 2005).

1.2.4 Regional and Local Structural Geology

The BC contains many geological features that pose a threat to the safe and productive extraction of orebodies. Geological structures in mining environments often result in geological losses, modification of mining layouts, and require additional support systems (Leach, et al., 2002). In a structural geology investigation conducted at Glencore ECM, lineaments derived from aerial surveys were identified as fault zones (Xtrata Alloys, 2005). High-resolution Airborne Magnetic Surveys (AMS) indicated the occurrence of dolerite dyke swarms with variable orientations (Xtrata Alloys, 2005). The orientation of major faults and dykes is illustrated in red and green lines, respectively, in Figure 1-7.

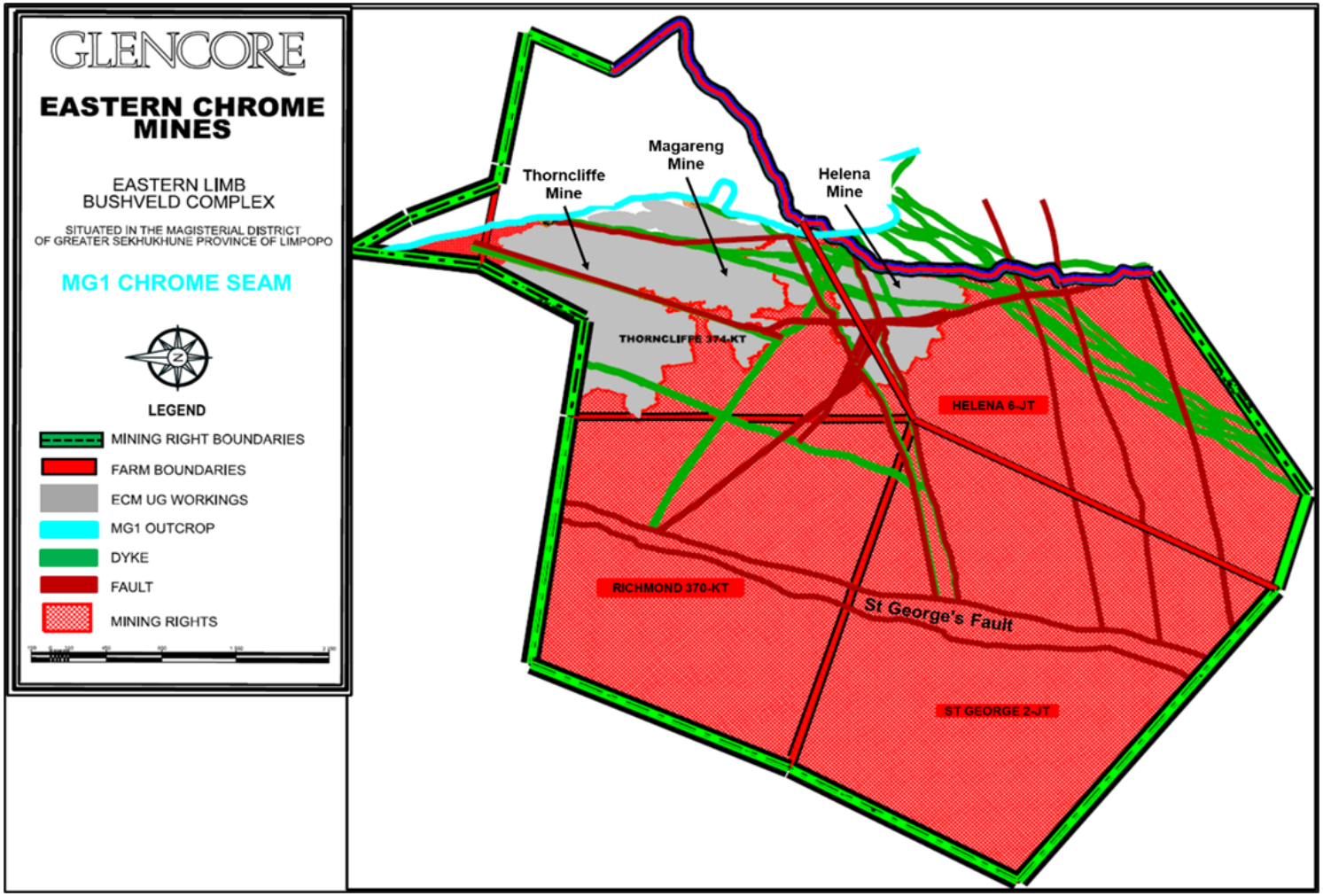


Figure 1-7: ECM major geological structures (Glencore ECM, 2021)

The identified major faults are near vertical/steeply dipping and are characterised as combinations of thrust-faulting, normal, and reverse faulting. The vertical displacements vary between 2 m and 15 m. The St. George's fault (Figure 1-7) displaces the reef package considerably more, with an up-throw of approximately 40 m and a total damage zone width that varies between 180 m–200 m to the west (Glencore ECM, 2021). The major dolerite dykes illustrated in Figure 1-7 vary in thickness from several metres to more than 50 m and are associated with blocky/friable ground conditions and water ingress. Geological losses are estimated to be in the order of 11% due to the occurrence of dykes, faults, shear zones, and potholes (Lousteau, 2014). Production rates in the vicinity of these major geological structures are often reduced as additional support is required for safe production (Xtrata Alloys, 2005).

Jointing, minor faulting, small-scale brittle shear zones, small dykes (<5 m thick), disseminated vein structures, localised domes, and potholes are confirmed across the mine property by boreholes. It is important to correctly identify, support and negotiate these geological features (du Preez, 2018). The most common local structural features occurring in the underground workings include the following (Glencore ECM, 2021):

- joints;
- shear zones;
- vein structures;
- domes (thrust faults);
- potholes;
- faults; and
- dykes.

1.2.5 Mine Design Criteria: Mining layout

Thorncliffe Mine functions at depths varying between 30 m and 590 m below the surface. The mine utilizes a trackless mechanised bord and pillar layout for the extraction of the MG1 Chromitite reef. Currently, the bord spans in a normal 2.2 m high stope spans are designed to be in a range of 6 m to 8 m. Where stoping heights are less than 1.5 m, spans range between 10 m and 13 m (Glencore ECM,

2021). A plan view of a typical bord and pillar layout used at Thorncliffe Mine is shown in Figure 1-8.

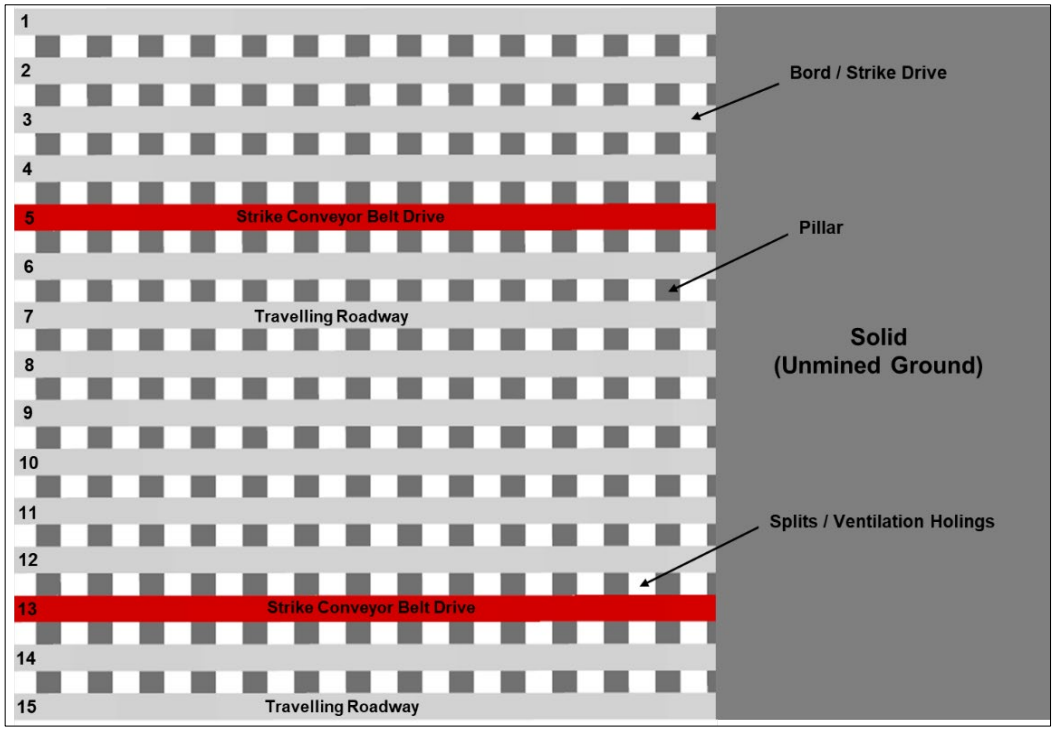


Figure 1-8: Typical production section layout used at Thorncliffe Mine

Each production section typically consists of 15 bords and is equipped with two strike conveyor belt drives for transporting broken ore to the main conveyor. A production section usually has two travelling roadways for access of the TMMs and workforce to the stopes. The strike conveyor belt drives (highlighted in red in Figure 1-8) are ideally positioned on the fifth (5^{th}) and 13^{th} strike drives, whilst the travelling roadways are placed below the belt drives (Glencore ECM, 2021). The splits/ventilation holings or dip roadways are typically holed up-dip. Figure 1-9 shows an enlarged illustration of Figure 1-8. Pillar sizes in each production section are a function of the depth below the surface and are designed at a minimum Factor of Safety (FOS) of 1.5. Table 1-1 summarises the change in pillar dimensions and FOS with increasing depth below surface at Thorncliffe Mine

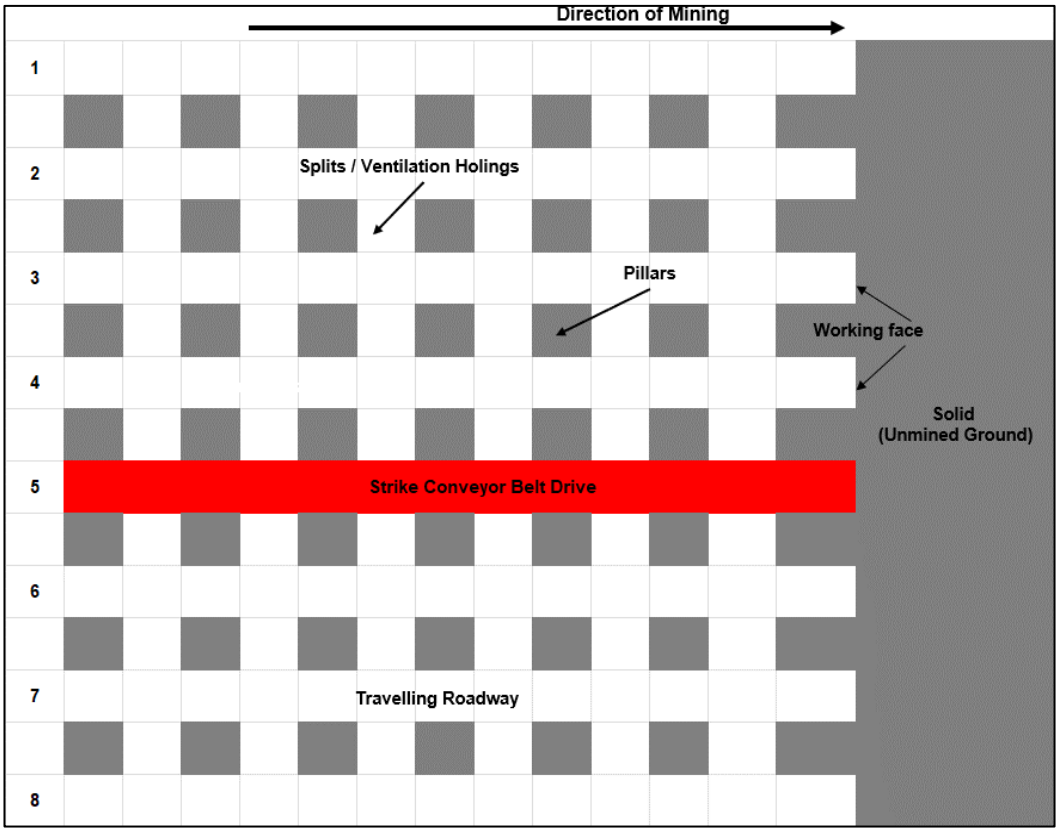


*Figure 1-9: Enlarged typical bord and pillar layout used at Thorncliffe Mine (*adapted from Egerton (2004))

Table 1-1: Thorncliffe Mine pillar dimensions and FOS with depth below surface (Glencore ECM, 2021)

Depth Below Surface (m)	Pillar Dimensions (m)		Factor of Safety (FOS)
	Along Strike (m)	Along Dip (m)	
30	6.0	6.0	8.6
80	6.0	6.0	4.3
120	6.0	6.0	2.9
160	6.0	6.0	2.2
200	6.0	6.0	1.7
240	7.0	7.0	1.8
280	8.0	7.0	1.8
300	8.0	8.0	1.8
320	8.0	8.0	1.7
340	9.0	8.0	1.7
360	10.0	8.0	1.8
380	10.0	8.0	1.7
400	10.0	9.0	1.7
420	11.0	9.0	1.8
440	11.0	9.0	1.7
460	11.0	10.0	1.7
480	11.0	10.0	1.7
500	11.0	11.0	1.7
520	12.0	11.0	1.7
540	12.0	11.0	1.7
560	13.0	11.0	1.7
580	13.0	12.0	1.7
600	13.0	12.0	1.7
620	13.0	12.0	1.6
640	14.0	12.0	1.6
660	14.0	12.0	1.6
680	14.0	13.0	1.6
700	14.0	13.0	1.6
720	14.0	14.0	1.6
740	14.0	14.0	1.6
760	15.0	14.0	1.6
780	15.0	14.0	1.6
800	15.0	15.0	1.6

1.2.6 Thorncliffe Mine FOG Incident Analysis

The database consisted of all FOG instabilities between 2006 and 2022. All the FOG incidents were reported following the South African Mines Reportable

Accidents Statistics System (SAMRASS) and are included in the analysis. The mine's FOG database is summarised in Appendix A.

Various FOG dimension variables were analysed. Figure 1-10 and Figure 1-11 present the cumulative frequency plots of the fallout height and FOGs areal extent, respectively. Figure 1-10 shows that the 95% fallout thickness of all FOG occurrences from the mine is 0.5 m, and the largest height of instability recorded is 0.8 m. The 95th cumulative fallout area value of 1.2 m^2 in Figure 1-11 together with the 95% fallout thickness, were used in the determination of other important FOG dimension variables, as summarised in Table 1-2 (Glencore ECM, 2021).

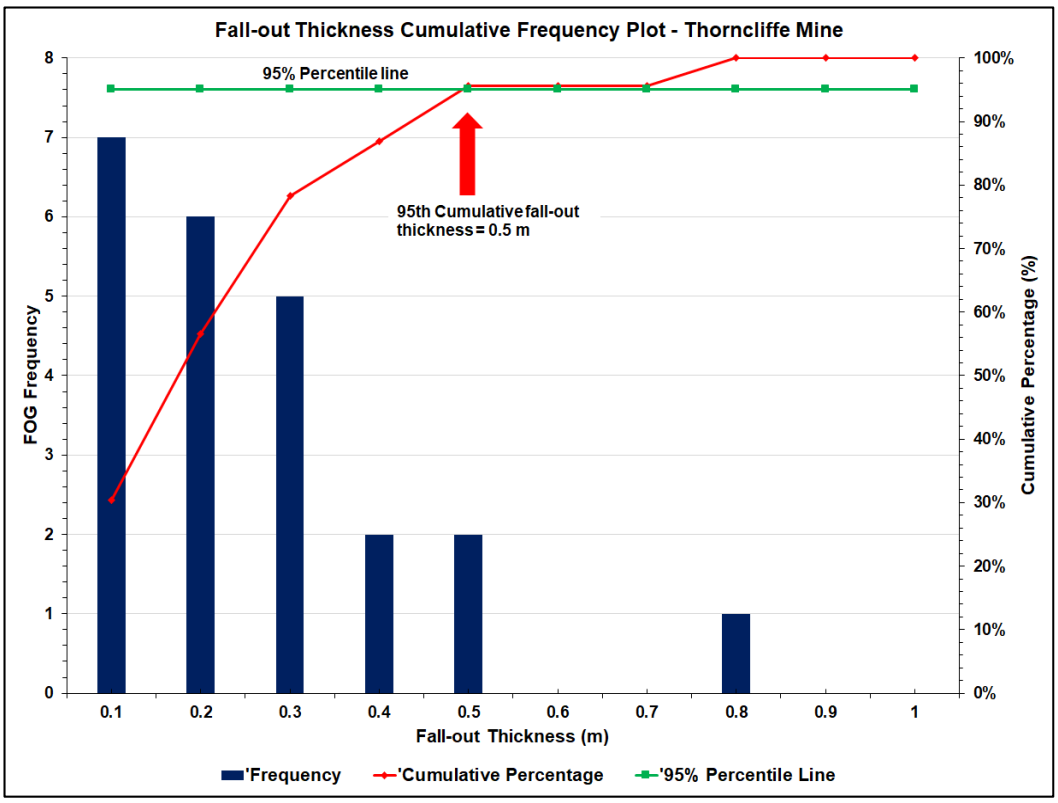


Figure 1-10: Cumulative frequency of the FOG thickness at Thorncliffe Mine

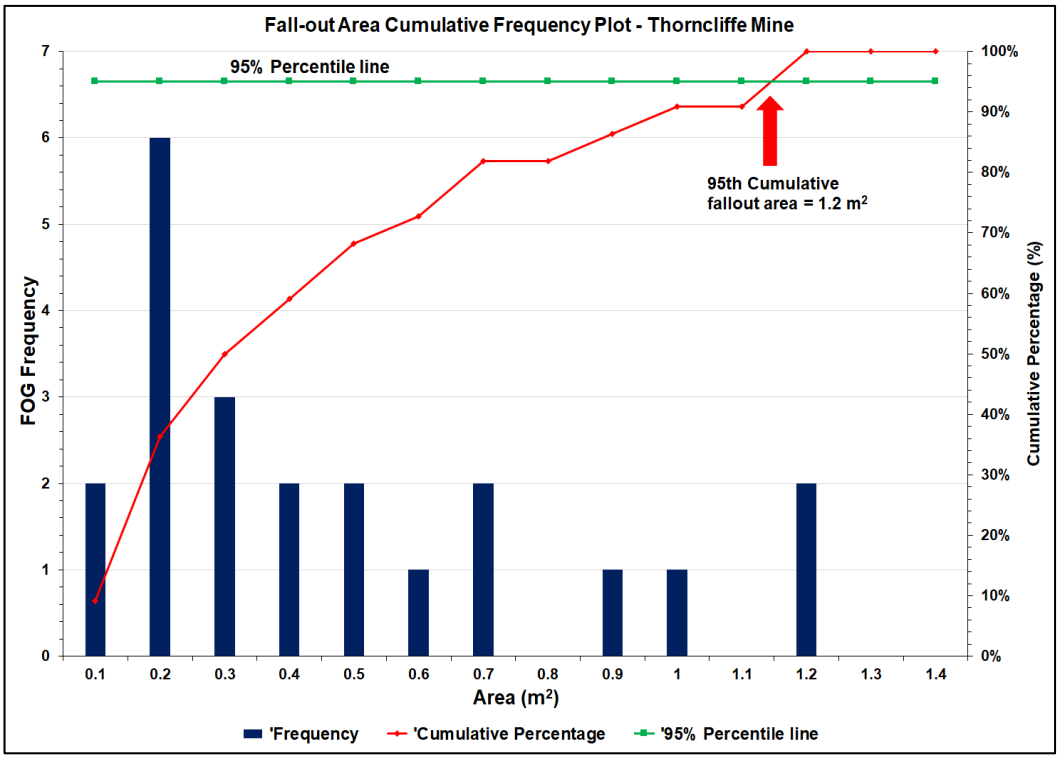


Figure 1-11: Cumulative frequency of the FOG areal extent at Thorncliffe Mine

Table 1-2: FOG 95th Percentile variables for Thorncliffe Mine

95th Percentile variable	Value
Fall-out height (m)	0.5
Area (m^2)	1.2
Volume (m^3) (calculated from the above Area & Fall-out thickness)	0.6
Mass (tonnes) (using density of 3.2t/m^3)	1.92

Figure 1-12 to Figure 1-16 presents an overview of analyses performed on the database. Figure 1-12 showed that 60% of the recorded FOG incidents occurred in the strike panels at an average distance of 3.1 m from the advancing face (Figure 1-13). This region is called the face area and is located between the last line of permanent support and the face. Therefore, most of the recorded FOGs occurred in an unsupported area. A few FOGs were recorded at varying average distances when breaking away for ventilation holings (from the up-dip and down-dip faces). Figure 1-14 shows that 90% of the recorded incidents occurred in the hangingwall whilst only 10% of FOGs emanated from the ore zone (sidewall). Figure 1-15 illustrates that all recorded hangingwall fallouts occurred due to the existence of structural features where both partings in the hangingwall and wedge or brow features contributed almost equally to the fallouts. So far, only a few roof fallouts

have been caused by faults or dyke features in the mine. Figure 1-16 shows that most FOGs occurred during production activities such as drilling of blast holes, installation of support, and barring of loose rocks in the face area.

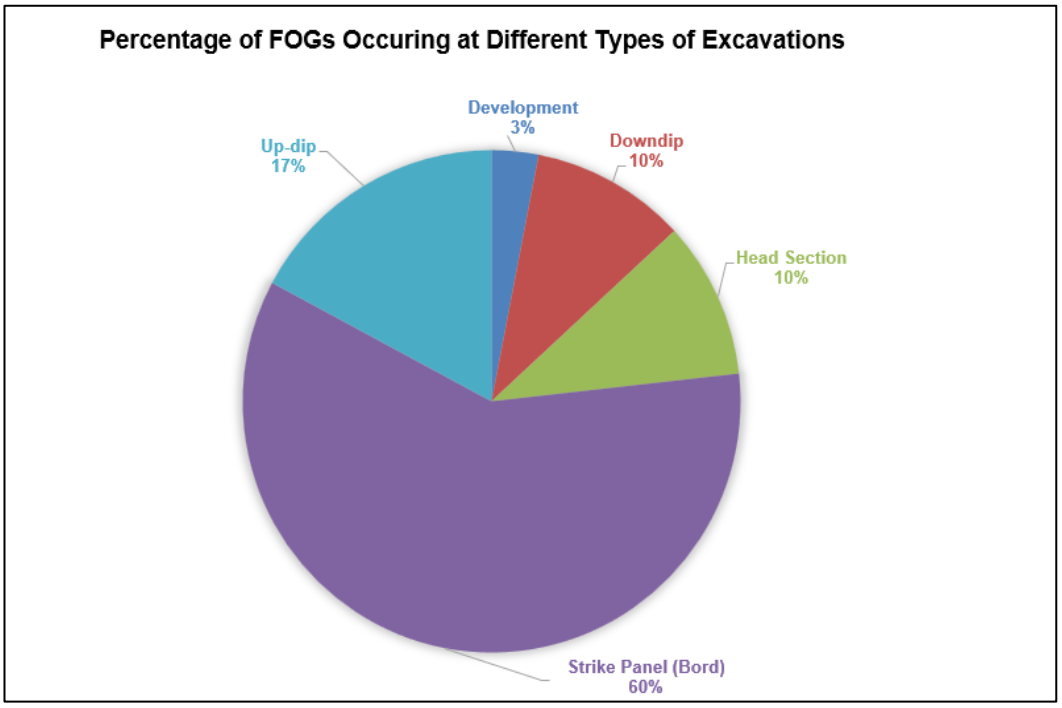


Figure 1-12: Number of FOGs occurring at different types of excavations at the mine

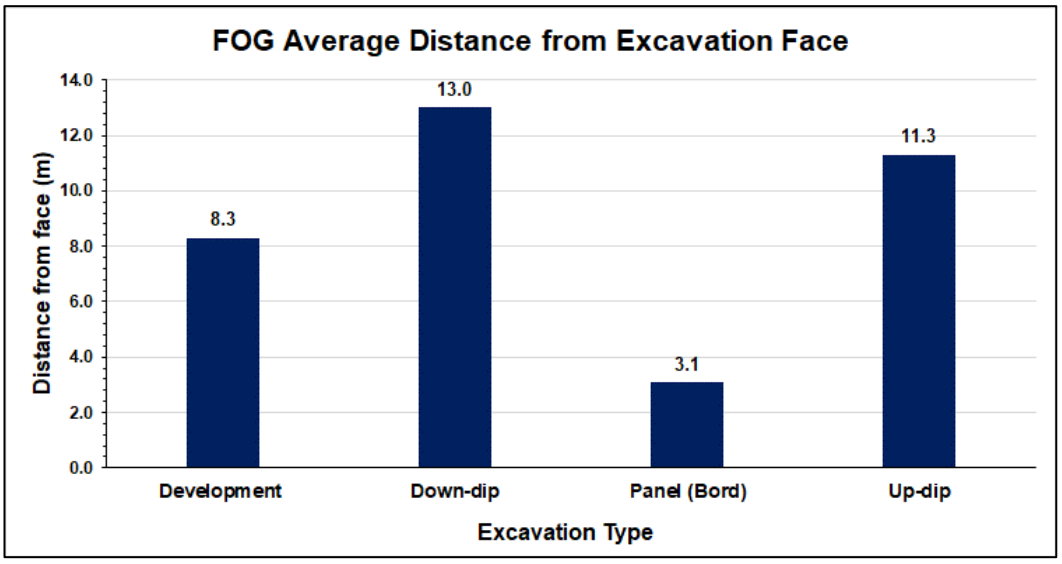


Figure 1-13: FOG average distance from face for different excavation types

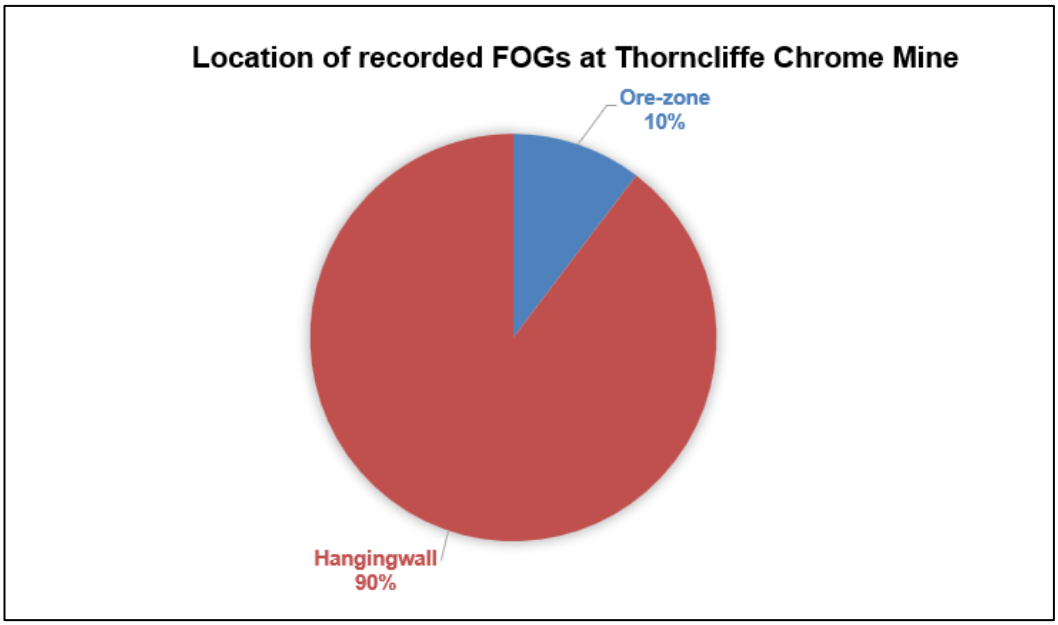


Figure 1-14: Location of recorded FOGs at Thorncliffe Mine

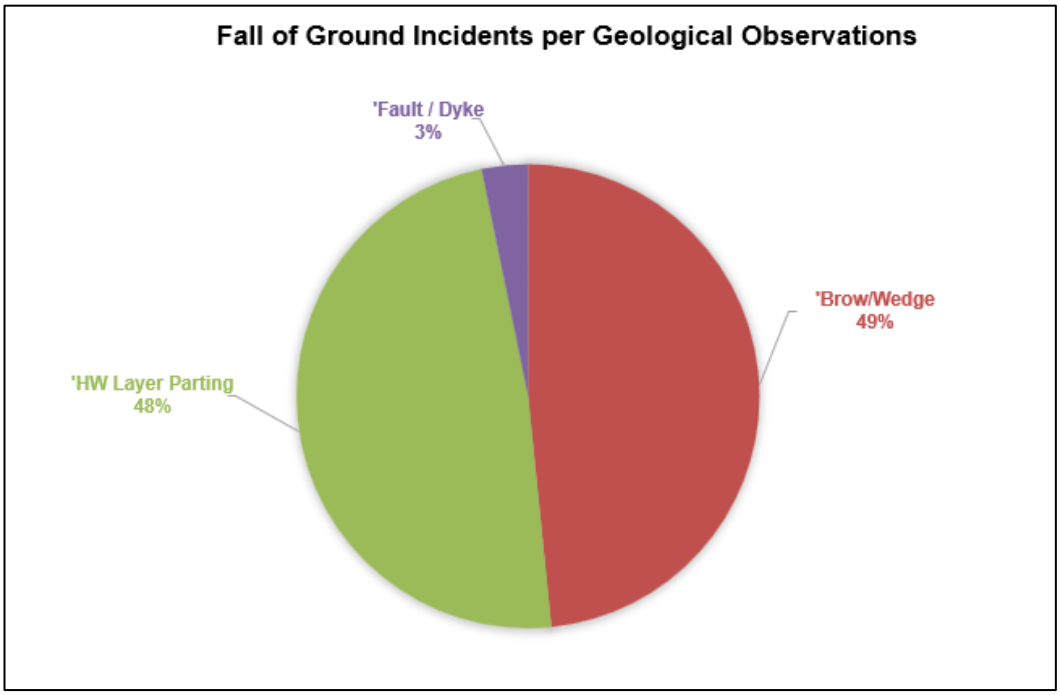


Figure 1-15: Geological structures contributing to FOGs at Thorncliffe Mine

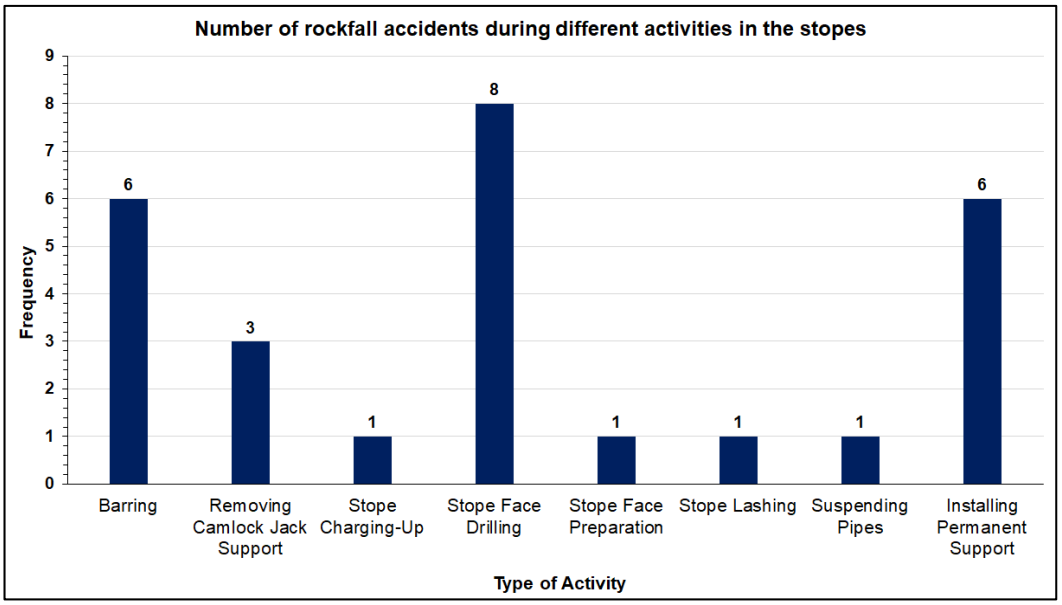


Figure 1-16: Number of FOGs per activity

1.3 Problem Statement

Since Thorncliffe Chrome Mine went into production in 2006, unplanned, uncontrolled FOG incidents have occurred in the stopes each year. Historically, the design of bord spans at Thorncliffe mine has been dictated by the equipment in use and benchmarking against other bord and pillar mines operating under similar conditions. This has contributed to the unplanned panel collapses, which are a threat to the safe and economic extraction of the orebody. The mine needs to follow a holistic and systematic engineering approach which takes critical factors into account for the stability of bords (Swart & Handley, 2005).

Support capacity requirements are solely based on previous experience, the 'tributary area' concept, and the '95% fallout criterion' (fall-out height). In this concept, a given weight of rock that is determined by a potentially unstable area in the plane of rock and the height of possible fall is supported by a fixed number of support elements (Jager & Ryder, 2002). The height of potential fall is determined statistically/empirically, in which historical fallout heights/thicknesses where falls of ground had occurred are analysed (Murphy, et al., 2016). While this engineering approach mostly informs the determination of support requirements at the mine, it does not adequately address the fact that there are discontinuities between the

support units, which can cause instabilities and fallouts (Jager & Ryder, 2002). Murphy et al. (2016) added that the 95% fallout criterion can be misused and misinterpreted as it 'does not cater for the largest rockfalls'.

Since various rock mass failure mechanisms control the occurrence of the FOGs between the pillars at the mine, the support design should be informed by results from assessing all potential instability modes. By considering critical parameters that adequately quantify and describe the rock mass structure, the mine will ensure the maximum extraction of ore under safe working conditions.

1.4 Justification for Research

Unplanned FOGs and panel collapses occur each year at Thorncliffe Mine. Historically, the mine has not considered critical geotechnical factors controlling stability in the design of mining spans between pillars. Therefore, research needed to be done for the following reasons:

- Establish an understanding of the relationship between the stability of bord spans and existing geotechnical conditions (factors controlling stability/instability at the mine),
- Follow a holistic engineering approach in determining stable bord spans that can be safely mined and optimized ground support systems to ensure safe and productive mine production, and
- Improve the mine's mandatory code of practice to combat rockfalls and rock burst accidents.

1.5 Research Objectives

The objective of this research is to provide Thorncliffe Mine with bord design guidelines, derived from a holistic and systematic engineering methodology, to determine (Murphy, et al., 2016):

- maximum stable bord spans that can be safely mined;
- a standard support system that is adequate for most of the expected ground conditions within the mine;

- reduce FOGs; and
- save costs by using fit-for-purpose support.

1.6 Research Methods

The systematic engineering methodology developed by the MHSC for designing stope excavations in shallow mining operations guided the design of stable bord spans at Thorncliffe Mine. The methodology is based on adequate knowledge of all critical factors controlling rock mass instability. These parameters were used for the quantitative description of the mine's rock mass structure to enable the design of maximum safe bord widths. To achieve the objectives of this research study, the quantitative research approach outlined below was followed:

- Conducted a geotechnical investigation in the mine's underground workings using various geotechnical data acquisition techniques. The acquired data included scanlines from mapping of underground exposed hangingwall and pillar rock surfaces, laboratory testing of rock material, and the mine's FOG database since commencement of production to date (2006 – 2022).
- The acquired geotechnical data were used to quantitatively describe the geotechnical character and properties of discontinuities, rocks and the rock mass at Thorncliffe Mine. Analysis of the mine's historic FOG database enabled the establishment of FOG occurrence trends, which informed the mine's current and future support system design requirements.
- The characterisation results were used in the identification of potential hangingwall failure modes such as intact rock mass failure, structural failure, beam failure and rock mass failure. Evaluation of the various failure modes was carried out using numerical analysis, statistical analysis, voussoir beam analysis, and rock mass classification methods, respectively.
- Used a combination of recommended methods to determine the requirements of optimal support systems to maintain stability for the expected ground conditions at the mine.

1.7 Research Validation

The proposed system for designing stable bord spans considers the critical factors which influence and control hangingwall instability. The research study was verified by determining if the newly developed ground support systems provided the desired support to achieve stable conditions in areas where FOGs had previously occurred. The improved support system was shown to reduce costs.

1.8 Structure of the Research Report

The research report chapter outline is as follows:

- Chapter 1 introduces the research report. The introduction chapter includes the purpose of the study, research background, research motivation, and the problem statement.
- Chapter 2 will comprise the literature review of different rock engineering design methods used for the design and stability evaluation of underground excavations. The MHSC methodology for the design of maximum stable bord widths will be discussed in detail in this chapter.
- Chapter 3 will present the geotechnical investigation which was undertaken at the mine. The chapter will cover the geotechnical data acquired from the underground workings, as well as laboratory rock tests conducted.
- Chapter 4 will discuss the characterisation of the discontinuous rock mass at the mine. This chapter will present the quantitative geotechnical description of intact rock blocks and the condition of discontinuities, which both make up the structure of the jointed rock mass at the mine.
- Chapter 5 will first present the determination of maximum stable or safety spans with no support. This is followed by a stability evaluation exercise, which involves the assessment of different failure mechanisms in the stope excavations.
- Chapter 6 will present the application of various methods to determine standard support strategies required to maintain stability at Thorncliffe Mine.
- Chapter 7 will be used to analyse and discuss the findings from the research study.

- Chapter 8 will provide conclusions to the research report by concisely presenting the research key findings and observations, contributions and limitations, and will provide some recommendations.

2 LITERATURE REVIEW

Chapter 1 outlined the research background and main objective of this study. This chapter presents a review of existing rock engineering methods for evaluating stability and determining support requirements. This is followed by presenting and discussing in detail the MHSC systematic methodology for evaluating stability and determining maximum stable bord spans. Determinations of in-stope standard support requirements are presented later in the chapter. A summary of the findings is presented at the end of the chapter.

2.1 Review of Rock Engineering Design Methods

In rock engineering, the methods available for the design of stope excavations are broadly classified into three (3) categories. These categories are Empirical, Analytical, and Observational (Bieniawski, 1984). The design methods are discussed in greater detail below.

2.1.1 Empirical design methods

Empirical methods are solely based on experience gained from previous projects or the results of experiments. The empirical design approach is often used to relate the practical experience gained from previous projects to the conditions anticipated or encountered at a proposed site (Rehman, et al., 2021).

Due to their success in the design of mine structures, empirical design methods are the most widely used design techniques in the mining industry. Rock mass classification systems are the most widely used empirical design methods.

2.1.2 Analytical or Closed-Form Solutions

Analytical design methods use advanced techniques such as closed-form mathematical solutions and numerical modelling techniques, including probabilistic and deterministic assessments for the evaluation of stability. These design methods are useful for assessing the influence of varying input parameters on the stability of stope panels and for comparing alternative designs.

In the stability assessment of stope panels, analytical methods are commonly used together with appropriate failure criteria to model failure modes or anticipated

failure mechanisms (Rehman, et al., 2021). It is recommended that more than one analytical design approach be used to predict failure and its extent.

2.1.3 Observational Design Methods

Observational methods entail the monitoring and collection of ground movement and stope instability data during mining to verify that design performance is acceptable. The observational method enables the determination and confirmation of the rock mass behaviour around an excavation over an extended period (Swart, 2005). These methods also enable the verification of the appropriateness and performance of the input parameters and assumptions established in the design stage of underground excavations. The collected data is continually used to further revise and refine the initial designs.

2.1.4 General Comments

When undertaking bord and pillar design problems, the design techniques described above are combined to obtain the best possible design. It is recommended that none of these techniques should be used solely or separately (Malan & Napier, 2011).

2.2 Methodology for Designing Stable Bord Spans

The design of stable stope spans aims at enabling optimum orebody extraction while maintaining safe working conditions for the duration of the mining period. Stacey & Swart (2001) stated that a sound rock engineering approach to underground excavation design and stability evaluation first considers the purpose of the excavation, which determines its geometry and size. Secondly, the process of designing practical and stable excavations is guided by answering the following questions:

- Will the planned excavation be stable?
- What is the existing mode of rock mass instability, if any?
- Can excavation stability be improved by modifying or optimising its geometry? and
- What support is required to ensure the excavation is sufficiently stable?

The methodology proposed by the MHSC for designing maximum stable bord spans is presented in Figure 2-1. The methodology was developed to be used during all stages of mining, from the pre-feasibility stage through to implementation, and when compiling mandatory codes of practice to combat rockfalls (Swart, 2005). The systematic methodology outlines the analysis to be carried out and will be applied as a guide in this study. The components of the design methodology are discussed in the following sections.

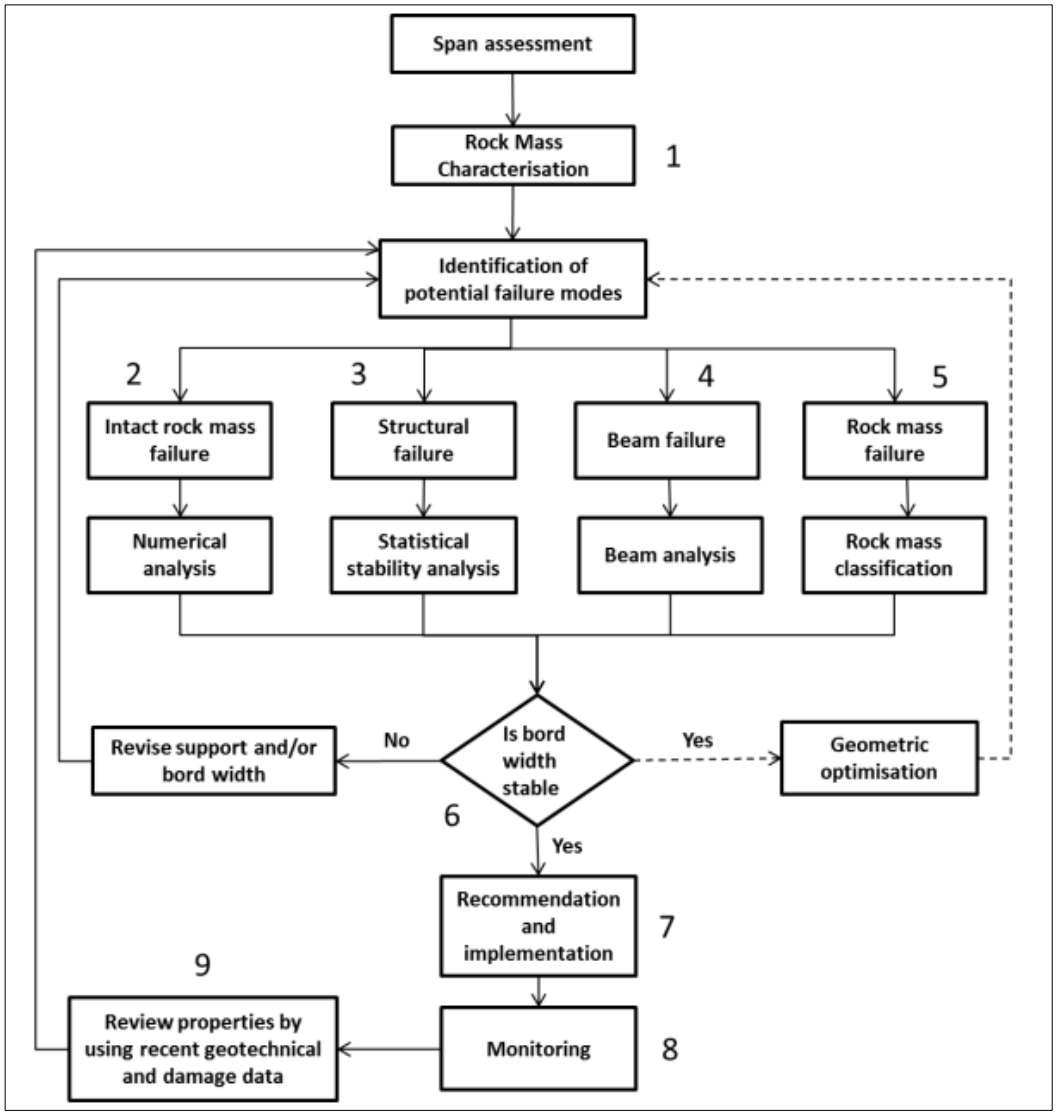


Figure 2-1: Flowchart for the design of stable bord spans (Murphy, et al., 2016)

2.3 Rock Mass Characterization

Thorncliffe Mine operates at depths ranging between 30 m and 590 m below the surface, which are considered shallow mining depths (Jager & Ryder, 1999). Rock masses in these shallow mining conditions behave as a discontinuum, as hangingwall instability is controlled by the presence and properties of naturally occurring geological structures (Jager & Ryder, 1999). The geological structures present at Thorncliffe Mine, which include joints, shear zones, vein structures, domes (thrust faults), potholes, faults, and dykes can be described as follows:

2.3.1 Joints

Fractures or breaks in the rock mass along which no shear displacement has occurred (du Preez, 2018). Joints create planes of weakness, which commonly contain infill material. Generally, the fill material in pyroxenite joints is serpentinite, which further reduces the shear strength of rock masses. The intersection of two or more joints (or with other structures) often causes wedge-shaped roof rock fallouts. Thorncliffe mine classifies joints according to their orientation, length and frequency of occurrence (du Preez, 2018). Examples are:

- Prominent joints – when the strike length of the joint feature exceeds 10 m.
- Low-angle or flat-dipping joints – joints dipping less than 60° from the hangingwall plane. When these are prominent, a large area of weakness can be exposed, which can cause large collapses if not adequately supported.
- Steep dipping joints – joints dipping more than 60° from the hangingwall plane. These can be continuous or discontinuous.
- Joint zones – Multiple closely spaced joints. The joints within a joint zone may have a different trend and dip. Joint zones significantly decrease the competency of the intersected rock mass and often cause roof fallouts.

2.3.2 Shear zones

Shear zones are characterised by multiple faulting with little noticeable movement and multiple closely spaced joints with the same dip and strike. Shear zones often cause the unravelling of the hangingwall and creation of brows when intersected by other geological features (du Preez, 2018). Thorncliffe consists of both minor and major shear zones with varying thicknesses between 100 mm to greater than 5 m (Glencore ECM, 2021).

2.3.3 Vein structures

These structures represent planes of weakness in the rock mass. Veins are disseminated dilated fractures filled with mineral deposits. These are formed when mineral constituents carried by water are deposited in fissures through precipitation. The project area consists of calcite and pegmatite veins with thicknesses varying between 100 mm–250 mm (Glencore ECM, 2021).

2.3.4 Domes (thrust faults)

Commonly referred to as ‘curved joints’ or ‘low-angle faults’. Domes or thrust faults are formed by upwarping of the rock strata, causing older strata from the bottom to meet younger strata on top when displacement along fault features occurs. These deformations result in large loose blocks/wedges in the roof. Domes often occur in sets commonly called ‘piggy-back doming’ where multiple ramp-flat geometries are formed (du Preez, 2018).

2.3.5 Potholes

Where the reef package and surrounding stratigraphy have slumped or transgressed into the footwall with a change in dip and strike and usually disappear altogether. Slumping of the reef results in off-reef mining and fracturing of the surrounding ground, which causes instabilities (du Preez, 2018).

2.3.6 Faults

Breaks in the strata along which displacement or movement has occurred. Localised near-vertical normal and reverse minor faults are common at the mine (du Preez, 2018).

2.3.7 Dykes

Near-vertical dolerite intrusions that cut across the strata form when molten magma fills pre-existing planes of weakness in older rocks. The dykes in the project area vary in thickness from a few centimetres to tens of meters. Dykes are associated with blocky/friable ground conditions and sympathetic jointing and/or faulting running sub-parallel to them (Xtrata Alloys, 2005).

2.3.8 Influence of structures on stability

Brady & Brown (2004) describe how that structurally influenced failures are of prime concern at shallow depths of mining. Jointed rock masses have the following properties (Amadei, 2019):

- Reduced shear strength along discontinuity planes;
- the discontinuities separate the hangingwall rock into varied sizes of blocks; which become unstable and fall if not adequately supported;
- exhibits anisotropy during loading and unloading due to the existence of different discontinuity sets; and
- often heterogeneous and have higher permeability.

The nature and distribution of discontinuities have a weakening effect on the rock mass behaviour. It is therefore vital to initially provide a quantitative description of the nature of discontinuities to obtain a better understanding of the rock mass structure. The rock mass structure will influence the following (Brady & Brown, 2004):

- response of the rock mass to the creation of excavations;
- selection of Mining method;
- design of mining layouts;
- stability of excavation spans;
- support requirements/strategies; and
- rock mass cavability.

The successful application of the design methodology for evaluating the stability and support requirements of the rock mass is reliant on a proper rock mass characterization exercise (Stacey, 2001). Rock mass characterization entails the collection of field parameters that adequately describe and quantify the

geotechnical character of the rock mass. The acquired geotechnical data are then used to quantify and describe the mechanical behaviour (deformability) of the rock mass, evaluate rock mass strength, identify potential failure mechanisms, and delineate geotechnical areas in a mining environment (Stacey, 2001). According to the International Society for Rock Mechanics (ISRM, 1978c), the ten important parameters selected to adequately describe the geometrical and mechanical properties of discontinuities and rock masses include the following:

- Orientation;
- Spacing;
- Roughness;
- Persistence;
- Wall strength;
- Aperture;
- Filling;
- Water Seepage;
- Number of discontinuity Sets; and
- Block Size.

2.3.9 Discontinuity orientation

Discontinuity orientation describes the attitude of discontinuities in space measured relative to each other and to underground excavations. Field orientation data are often measured by equipment such as a clinometer and a geological compass. The parameters describing discontinuity orientation are listed below and illustrated in Figure 2-2 (ISRM, 1978c):

(i) Dip angle – also called the true dip angle, this is the steepest angle measured between a horizontal plane and the plane of the discontinuity. The dip angle varies between 0 and 90°. When the discontinuity dip angle is measured in any direction other than the true dip direction, it is called an apparent dip.

(ii) Dip direction (azimuth) – the angle measured clockwise between the North direction and the true dip (the direction that water runs down on a plane of a geological feature). The azimuth describes the trend of a feature on the surface of the Earth and varies between 0 and 360°.

(iii) Strike – the strike of a discontinuity refers to the direction of the line (measured clockwise from the North) formed by the intersection of the discontinuity plane with the horizontal plane. The strike line is always perpendicular to the true dip angle.

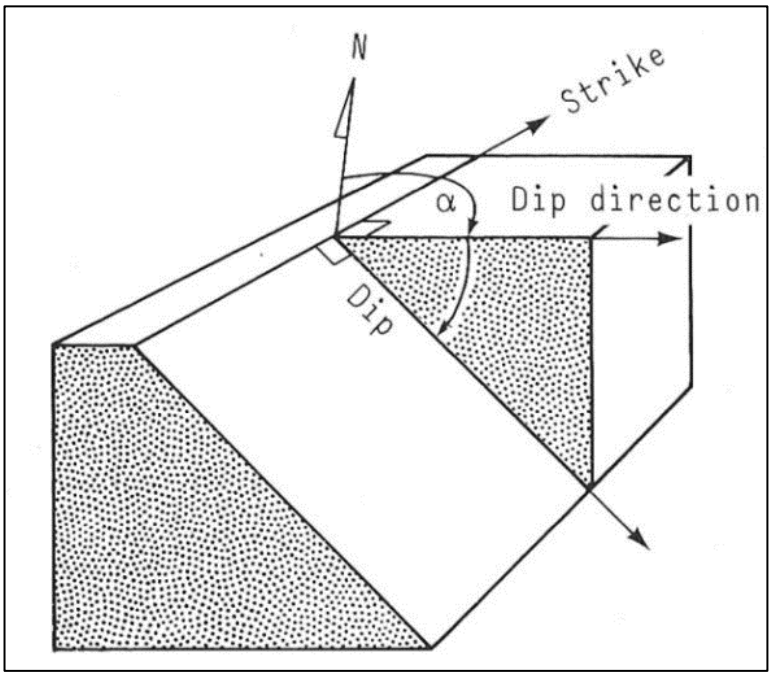


Figure 2-2: Geometrical terms describing discontinuity orientation (Hyldahl, 2018)

2.3.10 Discontinuity spacing

Spacing describes the measurement of the shortest/perpendicular distance between two adjacent discontinuities. The spacing between discontinuities determines the size of rock blocks/intact rock pieces in the rock mass. A measuring tape of at least 3 m in length and a clinometer are often used to measure the spacing between discontinuities. The true spacing between consecutive discontinuities, instead of the apparent spacing, is used in the quantitative description of discontinuities (ISRM, 1978c). The difference is illustrated in Figure 2-3.

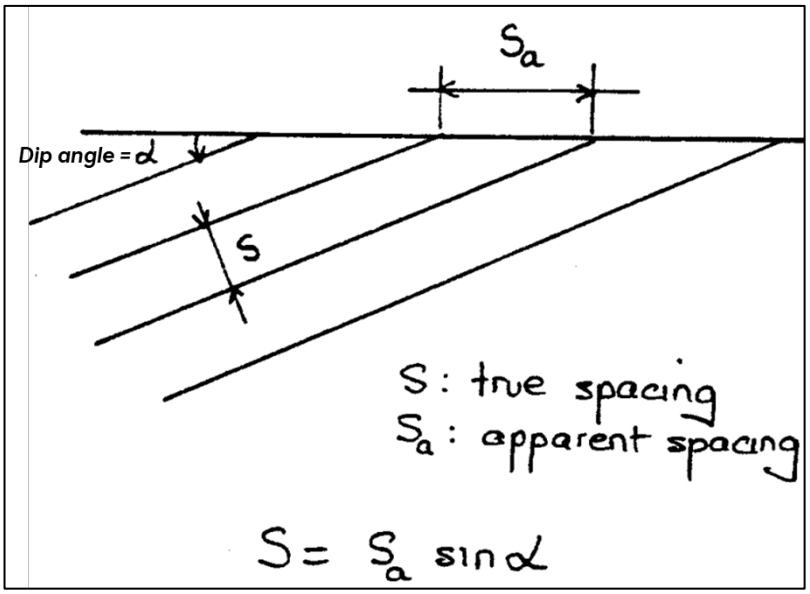


Figure 2-3: Illustrating measurement of true spacing and apparent spacing for a single discontinuity set (adapted from Amadei (2019))

The minimum, maximum, and modal spacing are recorded and used to describe the spacing of each discontinuity set. The following discontinuity spacing descriptions are used (ISRM, 1978c):

Table 2-1: Description of discontinuity spacing (ISRM, 1978c)

Descrption	Spacing (mm)
Extremely close spacing	<20
Very close spacing	20-60
Close spacing	60-200
Moderate spacing	200-600
Wide spacing	600-2000
Very wide spacing	2000-6000
Extremely wide spacing	>6000

2.3.11 Discontinuity roughness

Roughness refers to the inherent discontinuity surface roughness and waviness relative to the mean plane of a discontinuity. Roughness and waviness influence the overall shear strength of discontinuities. Discontinuities with rough surfaces tend to have higher shear strengths than smooth surface discontinuities (ISRM, 1978c). Table 2-2 presents the ISRM-suggested classification and descriptive terms to describe discontinuity roughness during field mapping. The illustration of

the typical discontinuity roughness profiles to match the nomenclature in Table 2-2 is presented in Figure 2-4.

Table 2-2: Suggested classification and description of discontinuity roughness (ISRM, 1978c)

Class	Description
I	Rough (or irregular), stepped
II	Smooth, stepped
III	Slickensided, stepped
IV	Rough (or irregular), undulating
V	Smooth, undulating
VI	Slickensided, undulating
VII	Rough (or irregular), planar
VIII	Smooth, planar
IX	Slickensided, planar

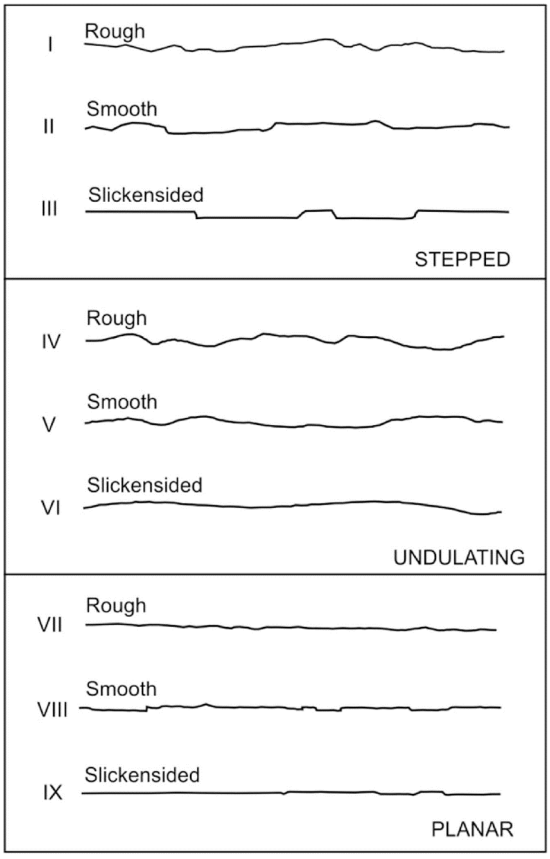


Figure 2-4: ISRM Roughness profiles and suggested nomenclature (Korkanç & Savran, 2017)

2.3.12 Discontinuity persistence

Persistence describes the crude measure of the continuity or trace lengths of discontinuities as observed in the field. In jointed rock masses, discontinuities often terminate at the intersection of other discontinuities, resulting in the formation of rock blocks/intact rocks in the rock mass. The ISRM (1978c) suggests the use of the modal trace length to describe or classify the persistence of a discontinuity set. Table 2-3 presents the classification of discontinuity persistence from collected field data.

Table 2-3: Description and classification of discontinuity persistence (ISRM, 1978c)

Description	Persistence or length (m)
Very low persistence	<1
Low persistence	1-3
Medium persistence	3-10
High persistence	10-20
Very high persistence	>20

2.3.13 Discontinuity wall strength

Discontinuity wall strength is sometimes called joint surface hardness and refers to the compression strength of a discontinuity surface/wall. Discontinuity wall strength may sometimes be lower than the strength of rock blocks due to weathering or alteration of the discontinuity walls. In underground metalliferous mines, experience has shown that the field strength classification of rocks can be determined by the following test procedures (ISRM, 1978c; Miller, et al., 1986).

(i) The number of geological hammer blows required to break a drill core specimen,
(ii) Effect of fracturing a core sample with the sharp end of a geological pick, and
(iii) Effect of scraping a core specimen with a fingernail and a pocketknife.

The discontinuity wall strength is usually some fraction of the strength of fresh rock since the alteration/weathering caused by hydrothermal processes mostly affects discontinuity walls and not the interior of a rock mass (ISRM, 1978c). A description of a discontinuity wall strength must therefore include the description and grading

of weathering/alteration states of intact rocks and the rock masses (ISRM, 1978c). The Schmidt hammer test is commonly used to obtain estimates of the hardness and strength of discontinuity walls. Table 2-4 presents the suggested weathering classification and grading of rock material and rock masses. Table 2-5 summarises the suggested field strength classification of rock and discontinuity wall strength.

Table 2-4: Weathering classification of rocks (ISRM, 1978c)

Classification	Description	Grade
Fresh/Unweathered	No visible signs of rock material weathering; perhaps slight discolouration on major discontinuity surfaces.	I
Slightly Weathered	Discoloration indicates weathering of rock material and discontinuity surfaces. All the rock material may be somewhat weaker externally than in its fresh condition.	II
Moderately Weathered	Less than half of the rock material is decomposed and/or disintegrated to soil. Fresh or discolored rock is present in either continuous framework or as core stones.	III
Highly Weathered	More than half of the rock material is decomposed and/or disintegrated to soil. Fresh or discoloured rock is present either as a discontinuous framework or as corestones.	IV
Completely Weathered	All rock material is decomposed and/or disintegrated to soil. The original mass structure is still largely intact.	V
Residual Soil	All rock material is converted to soil. The mass structure and material fabric are destroyed. There is a large change in volume, but the soil has not been significantly transported.	VI

Table 2-5: Field classification of discontinuity wall strength (ISRM, 1978c)

Grade	Description	Field identification	Approx. range of uniaxial compressive strength (MPa)
R0	Extremely weak rock	Can be indented by thumbnail	0.25-1.0
R1	Very weak	Material crumbles under firm blows of geological hammer, can be peeled by a pocket knife	1.0-5.0
R2	Weak rock	Can be peeled by a pocket knife with difficulty, shallow indentations made by firm blow with point of geological hammer	5.0-25
R3	Medium strong rock	Cannot be scraped or peeled with pocket knife, specimen can be fractured with single firm blow of geological hammer	25-50
R4	Strong rock	Specimen requires more than one blow of geological hammer to fracture it	50-100
R5	Very strong rock	Specimen requires many blows of a geological hammer to fracture it	100-250
R6	Extremely strong rock	Specimen can only be chipped with geological hammer	>250

2.3.14 Discontinuity aperture

Aperture measures the separation or openness between two discontinuity walls, in which the space between the discontinuity walls is air or water filled. It is obtained by measuring the perpendicular distance separating adjacent rock walls of an open discontinuity. The aperture is therefore different from the width of a fracture with mineral filling (ISRM, 1978c). The difference is illustrated in Figure 2-5.

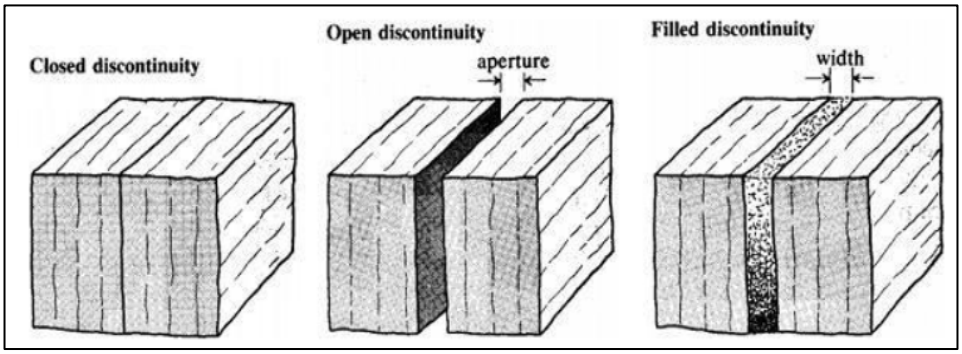


Figure 2-5: Suggested definitions of aperture of open discontinuities and width of filled discontinuities (Brady & Brown, 2004)

The modal aperture is usually used in the description of a discontinuity set. The field description and classification of discontinuity aperture is presented in Table 2-6.

Table 2-6: Classification of discontinuity aperture (ISRM, 1978c)

Aperture	Description	
<0.1mm	Very tight	"Closed" features
0.1-0.25mm	Tight	
0.25-0.5mm	Partly open	
0.5-2.5mm	Open	"Gapped" features
2.5-10mm	Moderately wide	
>10mm	Wide	
1-10cm	Very wide	"Open" features
10-100cm	Extremely wide	
>1m	Cavernous	

2.3.15 Discontinuity filling

Discontinuity filling refers to the presence of infill material/minerals between adjacent discontinuity walls. The width of discontinuities refers to the perpendicular distance containing infill materials between adjacent discontinuity walls. Filling materials are usually weaker than the host rock and influence the shear strength properties of discontinuities (ISRM, 1978c). Examples include Calcite, Clay, Chlorite, and Serpentinite. Filled discontinuities display a wide range of physical behaviour due to several geo-mechanical factors, which will be discussed below. It is therefore suggested that the description of discontinuity infill materials in a project should include the following (ISRM, 1978c):

a) Geometry of filling material

In the field, filling geometry is described by the discontinuity width. This entails recording the minimum, maximum, and finally estimating the modal widths of filled discontinuities. Secondly, taking measurements of the amplitude of discontinuity wall roughness helps determine detailed shear characteristics of discontinuities. Thirdly, it is recommended to provide a field sketch of the discontinuity walls to illustrate the degree of any fracturing or alteration (ISRM, 1978c).

b) Infill type

The filling type is described firstly by the mineralogy of the infill material. Finer filling material controls the long-term shear deformation of discontinuities. Therefore, this involves describing the mineralogical composition and characteristics of the finest filling material for the filled discontinuities (ISRM, 1978c).

Secondly, particle size or grading is used to describe the infill type between discontinuities. To identify and classify particle size, the use of the modified Wentworth scale for classifying and describing coarse sediments in Table 2-7 is suggested.

Table 2-7: The modified Wentworth scale for grain size classification (ISRM, 1978c)

The Wentworth Scale		
Category	**Type**	**Particle Size/Diamater (mm)**
Boulder	Boulders	200 - 600
Gravel	Cobbles	60 -200
	Course Gravel	20 - 60
	Medium Gravel	6 - 20
	Fine Gravel	2 - 6
Sand	Course Sand	0.6 - 2
	Medium Sand	0.2 - 0.6
	Fine Sand	0.06 - 0.2
Mud	Silt, Clay	<0.06

Lastly, sometimes filled discontinuities are a result of some preferential weathering along discontinuities. Therefore, the filling may be composed of either decomposed rock or disintegrated rock. It is suggested that the weathering types should be recorded (ISRM, 1978c). Table 2-8 presents the weathering types for filled discontinuities.

Table 2-8: Weathering types for filled discontinuities (ISRM, 1978c)

Weathering Classification	Description
Decomposed	The rock is weathered to the condition of a soil in which the original material fabric is still intact, but some or all of the mineral grains are not decomposed.
Disintegrated	The rock is weathered to the condition of a soil, in which the original material fabric is still intact. The rock is friable, but the mineral grains are not decomposed.

c) Filling material strength

The strength of the filling material can be assessed using Table 2-9, recommended under Wall Strength. These are also applicable for cohesive soils such as clays, silty clays, and combinations of silty clays with sand (ISRM, 1978c).

Table 2-9: Field classification of filling material strength (ISRM, 1978c)

Grade	Description	Field identification	Approx. range of uniaxial compressive strength (MPa)
S1	Very soft clay	Easily penetrated several inches by fist	<0.025
S2	Soft clay	Easily penetrated several inches by thumb	0.025 - 0.05
S3	Firm clay	Can be penetrated several inches by thumb with moderate effort	0.05 - 0.10
S4	Stiff clay	Readily indented by thumb but penetrated only with great effort	0.1 - 0.25
S5	Very stiff clay	Readily indented by thumbnail	0.25 - 0.50
S6	Hard clay	Indented with difficulty by thumbnail	>0.50

d) Seepage of filled discontinuities

Seepage of filled discontinuities is described by water content and permeability. The suggested field identification and classification of the seepage of filled discontinuities is presented in Table 2-10.

Table 2-10: Water seepage classification of filled discontinuities (ISRM, 1978c)

Seepage Classification/Rating	Field Identification
W1	The filling materials are heavily consolidated and dry, significant flow appears unlikely due to very low permeability.
W2	The filling materials are damp, but no free water is present.
W3	The filling materials are wet, occasiional drops of water
W4	The filling materials show signs of outwash, continuous flow of water (estimate litres/minute)
W5	The filling materials are washed out locally, considerable water flow along out-wash channels (estimate litres/minute and describe pressure i.e. low, medium, high).

2.3.16 Discontinuity water seepage

Water seepage refers to the amount of water flowing along discontinuities in a rock mass. Water seepage in rock masses is influenced by the permeability of the rock material making up the rock mass. Discontinuity moisture conditions vary from dry to continuous flow. Groundwater influences discontinuity shear strength. Slip-type failures along dry discontinuities tend to be minimal. On the other hand, the shear strength of wet discontinuities is reduced by water pressure, resulting in slip failure along such discontinuities (ISRM, 1978c). The water seepage of filled and unfilled discontinuities can be assessed according to the suggested descriptive tables in Table 2-10 and Table 2-11, respectively.

Table 2-11: Water seepage classification of unfilled discontinuities (ISRM, 1978c)

Water Seepage Rating	Description
I	The discontinuity is very tight and dry, water flow along it does not appear possible.
II	The discontinuity is dry with no evidence of water flow.
III	The discontinuity is dry but shows evidence of water flow, i.e rust staining, etc.
IV	The discontinuity is damp but no free water is present.
V	The discontinuity shows seepage, occassional drops of water, but no continuous flow.
VI	The discontinuity shows a continuous flow of water. (Estimate 1/min and describe pressure i.e low, medium, high).

2.3.17 Number of Discontinuity Sets

Discontinuities usually occur in sets in jointed rock masses. Each discontinuity set consists of discontinuities which have similar orientation data (azimuth and dip angle) and usually display similar mechanical properties too. The number of intersecting discontinuity sets influences the appearance and overall mechanical or stability behaviour of a rock mass. Rock masses with many intersecting discontinuity sets have a blocky appearance than ones with few discontinuity sets (ISRM, 1978c). This contrast is illustrated in Figure 2-6.

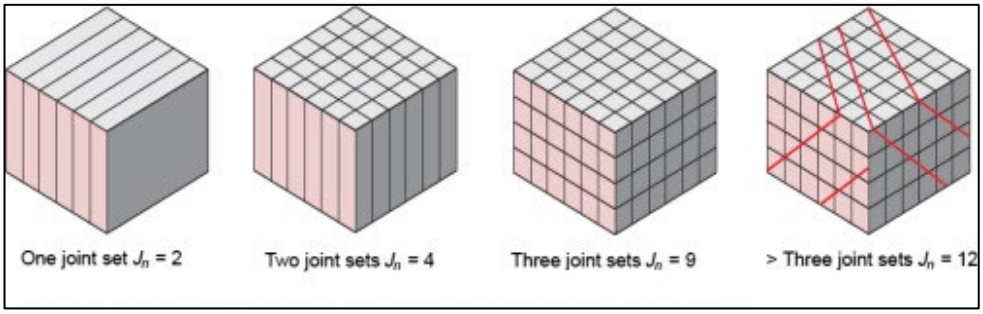


Figure 2-6: Effect of increasing discontinuity sets on the rock mass (Yun, 2018)

In terms of stability, rock blocks formed by three or more discontinuity sets in a rock mass have a higher degree of freedom of deformation than in a rock mass with fewer discontinuity sets (ISRM, 1978c). Table 2-12 presents the suggested scheme that can be used to describe discontinuity sets in the field.

Table 2-12: Field description of discontinuity sets (ISRM, 1978c)

Discontinuity Set Description	
I	Massive, occassional random joints
II	One joint set
III	One joint set plus random
IV	Two joint sets
V	Two joint sets plus random
VI	Three joint sets
VII	Three joint sets plus random
VIII	Four or more joint sets
IX	Crushed rock, earth-like

2.3.18 Block Size

Blocks refer to individual rock blocks formed/bounded by intersecting discontinuities and discontinuity sets in jointed rock masses. The shape and size of the rock blocks influence the overall response and behaviour of the rock mass. The dimension and shape of the blocks in the rock mass are determined by the spacing between discontinuities, the number of discontinuity sets, and the persistence of the discontinuities delineating the blocks (ISRM, 1978c). To describe the block size of a geotechnical domain of interest, it is suggested to first record the block size index (I_b), which represents the average dimension of typical rock blocks. I_b is estimated by visually selecting and measuring dimensions of typical block sizes and taking their mode. Each geotechnical domain is therefore characterised by stating the smallest, largest, and modal I_b. The volumetric joint count (J_v) is also used to indicate the block size of jointed rock masses. J_v is determined by summing the number of joints per meter for each discontinuity set in the rock mass. The mean true spacing, instead of the modal spacing, is used in the determination of J_v (ISRM, 1978c). Table 2-13 presents the classification of block size according to the volumetric joint count.

Table 2-13: Block size classification according to the volumetric joint count (ISRM, 1978c)

Description	J_v (joints/m^3)
Very large blocks	<1.0
Large blocks	1-3
Medium-sized blocks	3-10
Small blocks	10-30
Very small blocks	>30
Note: Values of J_v > 60 would represent crushed rock, typical of clay-free crushed zone.	

When defining block size in a rock mass, it is suggested to describe the blockiness of the rock mass as tabulated in Table 2 14. If it aids in the better communication of the block size and shape, photographs and field sketches of exposures are recommended (ISRM, 1978c).

Table 2-14: Description of the Blockiness of the rock mass (ISRM, 1978c)

Classification	Description
Massive	Few joints or very wide spacing
Blocky	Approximately equidimensional
Tabular	One dimension considerably smaller than the other two
Columnar	One dimension considerably larger than the other two
Irregular	Wide variations of block size and shape
Crushed	Heavily jointed to "sugar cube"

2.4 Geotechnical Data Collection Methods

As noted in Section 2.2, the planning and design of a shallow mining operation requires an in-depth understanding of the mine's overall rock mass structure and geological setting. Hoek (2007) stated that *"The cornerstone of any practical rock mechanics analysis is the geological model and the geological database upon which the definition of rock types, structural discontinuities and material properties is based."* The geotechnical data which describes the rock mass structure comprises the types, and important engineering properties of structural features found within a jointed rock mass (Brady & Brown, 2004).

The local geology in a mining operation, is often obtained through geological exploration programs that only outline the general lithologies and major structural data. While this data is essential, it does not adequately or entirely serve the purpose of informing the engineering understanding of a mine's rock mass structure or establishing of a complete structural and geological model for mine-design. Therefore, two (2) mainstream structural data acquisition techniques are commonly used to collect the data required to sufficiently quantify the geotechnical characteristics of structural features in the rock mass. The two (2) structural data acquisition methods have not changed a great deal in many years and there is still no acceptable substitute for them (Hoek, 2007). The methods are:

(i) Mapping of underground exposures; and
(ii) Geotechnical Core Logging

2.4.1 Mapping of Underground Exposures

Mapping of underground exposures for acquiring structural data is usually concentrated on areas adjacent to the orebody from which the design of stopes can be based. There are three (3) types of approaches used for mapping of underground exposures, which are:

1. Scanline mapping;
2. Window Mapping; and
3. Digital Mapping

Scanline Mapping - involves extending a measuring tape (the sampling line) across an exposed rock surface, and all the discontinuities intersecting the scanline along its length are mapped. In the scanline survey, geotechnical attributes of all the discontinuities intersecting the sampling line are recorded. The minimum number of scanline measurements required to define a discontinuity set usually differs from site to site (Read & Stacey, 2008). The structural data collected through a scanline survey enables the application of rock mass classification systems and further characterisation of the rock mass. *Figure 2-7* shows a schematic illustration of a scanline mapping survey on an exposed rock surface. The following discontinuity features are recorded for the quantitative description of the rock mass:

- distance at which discontinuities intersect the scanline;
- type of discontinuity intersected along the scanline;
- discontinuity orientation (dip angle and dip direction), which is measured using a geological compass;
- persistence (continuity or trace length);
- weathering condition of discontinuities;
- roughness (joint inherent surface roughness and waviness);
- discontinuity wall strength;
- aperture (discontinuity wall separation);
- water condition (signs of water seepage);
- infill material type and thickness; and
- number of discontinuity sets.

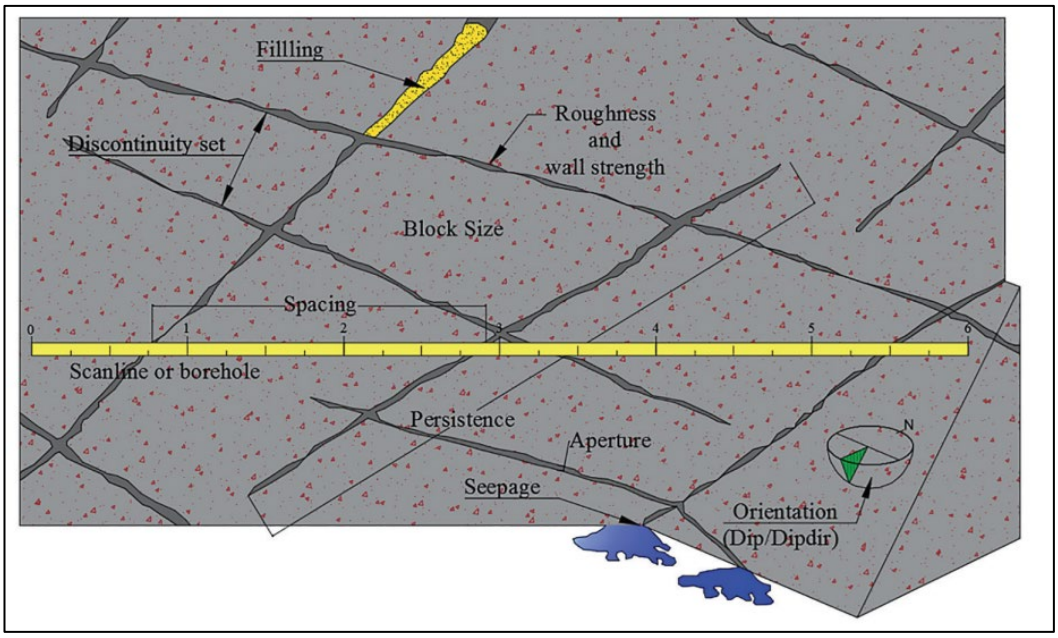


Figure 2-7: Schematic illustration of a scanline survey (Monsalve, et al., 2018)

Additional valuable information recorded in a scanline survey includes photos of the scanline location (if possible), scanline grid coordinates, host rock type, scanline orientation, and face orientation. Scanlines are used for the collection of structural data on all three components of the orebody, namely the immediate hangingwall, footwall, and the mineralised zone.

Window Mapping - Sometimes referred to as 'areal mapping', this approach involves the collection of all structural data within a specified or selected area (the window) of an underground/surface rock exposure. This type of specific mapping is conducted when the orientation and other characteristics of structural features or discontinuity sets are judged to influence the stability behaviour of excavations (Stacey, 2001). The variability of the following parameters in each discontinuity set is usually established (Stacey, 2001):

- discontinuity orientation;
- discontinuity spacing; and
- discontinuity trace lengths.

Typical statistical analyses and distributions for the above-listed parameters are produced to serve as inputs in stability assessment studies. Caution is required

when using this approach as it may introduce bias into the data (Stacey, 2001). The bias introduced during mapping will be discussed in detail below.

Digital Mapping - The scanline and window mapping described above are traditional/conventional methods which require manual effort for the collection of structural data. This may mean exposure to dangerous/unsafe working areas while mapping, taking longer mapping times, and recording a small sample size (Monsalve, et al., 2018). Over the years, there have been advances in the equipment and technology used for geotechnical data collection. Development of digital mapping techniques such as Terrestrial Laser Scanning (TLS) (laser imaging) and three-dimensional (3D) Photogrammetry has enabled optimal characterisation and design of underground or surface structures (Monsalve, et al., 2018). This technology offers a more effective process of collecting structural data, is faster, cheaper, and provides better characterisation results (representation of the rock mass structure) than traditional techniques.

Digital photogrammetry uses two-dimensional (2D) images from high-resolution cameras and photogrammetry software to generate detailed and spatially accurate 3D digital terrain models (Torkan, et al., 2022). The 3D models enable the accurate determination of the mechanical properties of geological structures over longer distances, remotely. The photogrammetric data can be integrated into mine planning software and used as real-time data for mine design and planning (Read & Stacey, 2008). In an underground setting, photogrammetry may require illumination to obtain high-resolution and better images.

Laser imaging (laser scanning) entails using a laser scanner to send out laser pulses to scan the position of an exposed rock surface and produce a massive point cloud of the scanned area, with millimetre precision (Monsalve, et al., 2018). The laser scans produce a detailed 3D image of the rock mass from which attributes of discontinuities composing the rock mass can be statistically analysed for further characterization. Laser imaging enables mapping with more precision and less bias, and collects copious quantities of data in a short time (Monsalve, et al., 2018).

2.4.2 Challenges Associated with Exposure Mapping

Sampling bias is the main issue introduced by several factors in exposure mapping results. Four (4) types of sampling bias are known to be associated with traditional scanline and window mapping, these are (Brady & Brown, 2004; Read & Stacey, 2008):

- orientation bias;
- size bias;
- truncation or size cut-off bias; and
- censoring bias.

Orientation bias – the frequency of discontinuities intersected and recorded in a particular scanline/window depends on the orientation of the sampling line relative to the orientation of discontinuity sets in the rock mass. When a discontinuity set is parallel to the sampling scanline/window, a few structural features of that set will be recorded (Brady & Brown (2004) and Read & Stacey (2008)).

Size bias – larger and prominent structural features in the rock mass are more likely to be sampled by a scanline or window than smaller structures (Brady & Brown (2004) and Read & Stacey (2008)).

Truncation or size cut-off bias – sampling size cut-off is often applied in exposure mapping. This, for example, entails choosing to ignore discontinuities of a certain length during mapping. If a smaller size cut-off is used in a scanline survey, this affects overall discontinuity statistically and the size distribution of all the structural features may not be properly accounted for (Brady & Brown (2004) and Read & Stacey (2008)).

Censoring bias – this type of bias is introduced when 'artificial' boundaries exist when carrying out scanline surveys. A 'censor window' is an artificial boundary or area in which discontinuity trace lengths can be accurately measured or estimated. Discontinuities with trace lengths extending outside the artificial boundary are called 'censored'. Uncensored discontinuities have trace lengths that terminate within the censor window. In underground mines, the height of excavations is often one of the main limiting boundaries (Brady & Brown (2004) and Read & Stacey (2008)).

2.4.3 Geotechnical logging of diamond-drilled core

Core drilling is a reliable method of investigating the structure and geo-mechanical properties of the interior of a rock mass. The structural logging of the core provides valuable geotechnical parameters for characterising the rock mass and conducting stability assessments. Geotechnical core data management requires taking colour photographs of the undisturbed drilled core before logging commences. The process of geotechnical core logging involves dividing the core into geotechnical domains/zones (intervals of similar geotechnical characteristics), then assigning geotechnical attributes to each domain (Stacey, 2001). To eliminate logging errors, naturally open discontinuities are often distinguished from artificial fractures/defects introduced by core drilling and the handling of core (Read & Stacey, 2008). Artificial defects are marked and excluded from the collection of structural data. The geotechnical logging of the core involves the collection of the following information (Stacey, 2001):

- orientation of core;
- borehole position (coordinates);
- drill run (From, To);
- rock type (Major and minor Lithology);
- core recovery (Total and solid core recovery);
- depth at which discontinuities are intersected;
- type of discontinuity intersected;
- orientation of discontinuities;
- strength index (hardness of rock);
- roughness and waviness of discontinuities;
- infilling materials (type and thickness of infill);
- open/closed discontinuities;
- weathering;
- alteration of discontinuities; and
- water conditions.

The acquired geotechnical data are used for providing a quantitative description of the rock mass quality using rock mass classification systems and conducting strength assessments. The geotechnical logging of the core can be supplemented by advanced technology, such as digital logging techniques for the determination

of attributes of discontinuities that intersect a drilled core. These include the use of downhole logging equipment and geophysical logging systems (Stacey, 2001).

Downhole scanners include borehole cameras used for logging borehole walls. These digital photographic systems are enhanced with digital imaging software to provide high-resolution core images from which logging is conducted (Hoek, 2007). Downhole imaging technology also includes borehole-acoustic (ATV) and optical (OTV) televiewers, which provide continuous high-resolution images of the borehole wall. The magnetically oriented colour images are then used for mapping the mechanical properties of planar structural features intersecting the borehole. Geophysical logging systems usually consist of a downhole geophysical probe, which is lowered down a borehole. The probe collects mechanical properties and attributes of the rock mass and discontinuities intersecting the borehole.

2.4.4 Challenges associated with geotechnical core logging

Like the mapping of rock exposures, sampling issues are introduced to geotechnical core logging results by several factors. These sampling issues also apply to digital logging methods. The major challenges in geotechnical core logging are as follows (Jakubec & Laubscher, 2000; Brady & Brown, 2004; Jakubec, 2013):

- The rock mass cannot be seen or studied on a 3D large scale. Therefore, the continuity (persistence or trace lengths) of structural features, orientation, and their large-scale expression/geometry are impossible to correctly establish with confidence.
- Drill hole (sampling) orientation bias – the frequency and attributes of structural features parallel to the core axis cannot be determined unless the core drilling is oriented in several directions.
- Difficult to distinguish between artificial (drill-or-handling induced) defects and natural open fractures, especially in laminated/bedded rock masses.

2.5 Evaluation of Boundary Conditions

The determination of in situ rock mass properties in the roof of stope panels includes the estimation of in situ stress conditions, which informs excavation boundary conditions (Stacey, 2001). In mining environments, *in situ* field stresses

determine the confinement imposed on the rock mass surrounding stope openings. In-situ stresses are therefore an essential boundary condition and input parameter in the numerical stability analyses and design of safe mining excavations (Swart & Handley, 2005). Depending on their magnitude, in situ stresses can have the following impact on rock mass stability (Stacey & Wesseloo, 1998):

- If in-situ stresses are of sufficient magnitude, the rock mass will be well confined and thus have a beneficial effect of promoting stability.
- If in-situ stress magnitudes are low, instability may result since confinement is reduced and rock blocks in the rock mass have the freedom to fall out.
- Finally, if the stresses are sufficiently high, fracture and failure of the rock mass may be induced, resulting in instability.

Several methods are used in the field to estimate the complete in-situ state of stress in the rock mass for design purposes. These include an overcoring method when underground access is available, in-situ stress tests based on small flat jacks, and/or hydrofracturing. However, these methods are usually expensive and time-consuming. Swart & Handley (2005) suggested that the estimation of the in-situ stress field can be based on the work by Stacey & Wesseloo (1998).

Stacey & Wesseloo (1998) collated and evaluated a database of in situ stress measurements carried out in different mining and civil projects in Southern Africa over the past 30 to 40 years. The database consists of in situ stress measurement data from the Carletonville-Klerksdorp-Free State area and the Bushveld Complex (Rustenburg Platinum Mine, Impala Platinum Mine, and Northam Mine). The database was used to determine the magnitude and orientation (trend) of principal horizontal and vertical stresses. If no site-specific in situ stress measurements are carried out for a specific project, extrapolation of in situ/virgin stress conditions can be achieved from the existing database.

The virgin vertical stress, which is directly proportional to rock density, is commonly used to express the in-situ stress state. The magnitude of the vertical component of the virgin stress is given by Equation 2-1. The horizontal virgin stress is a fraction of the virgin vertical stress. Dividing the virgin horizontal stress by the vertical stress gives the ‘virgin stress ratio’ or simply the ‘k-ratio’, which varies with direction. Sellers, et al. (2002) added that in South Africa, the major principal stress is usually

not vertical, indicating that the in-situ stress state has been altered by tectonic movements/action.

$$\sigma_{virgin} = p\ g\ H$$ ***Equation 2-1***

Where: p is the rock density (kg/m^3); g is the gravitation acceleration (kg/m^2); and H is the depth below the surface (m).

Figure 2-8 shows the variation in the orientation of horizontal principal stresses measured at various locations in Southern and Central Africa. As shown in Figure 2-8, horizontal major principal stresses commonly trend in the northwest-southeast (NW–SE) and northeast-southwest (NE-SW) directions in South Africa. Secondly, the collated in situ stress field database indicated that the magnitude of horizontal principal stresses is often equal to or greater than the magnitude of vertical stresses at shallow depth (Stacey & Wesseloo, 1998).

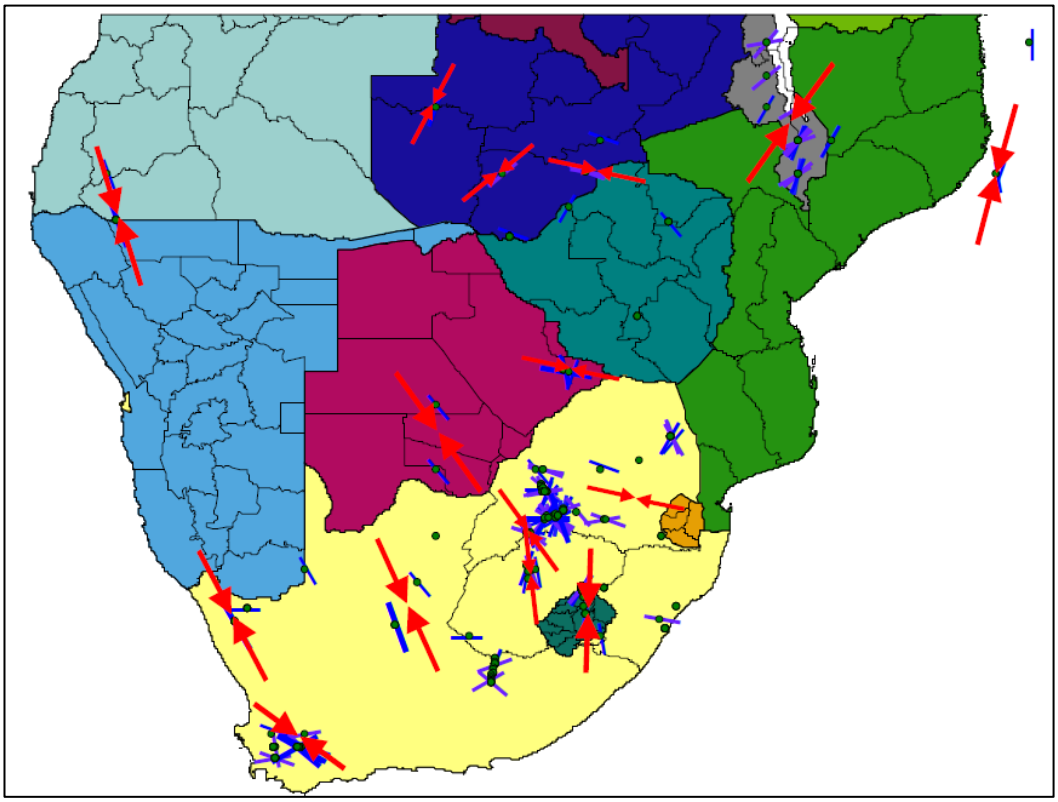


Figure 2-8: Orientation of horizontal principal stresses (Stacey & Wesseloo, 1998)

Figure 2-9 and Figure 2-10 indicate the variation of minor and major horizontal principal stress with increasing depth, respectively. Figure 2-11 and Figure 2-12 show the ratio of major (K_1) and minor (K_3) horizontal in situ stress to vertical stress, respectively. The k-ratio decreases with depth, with high values (>1) in shallow mining conditions to low values (<0.5) in deeper mines.

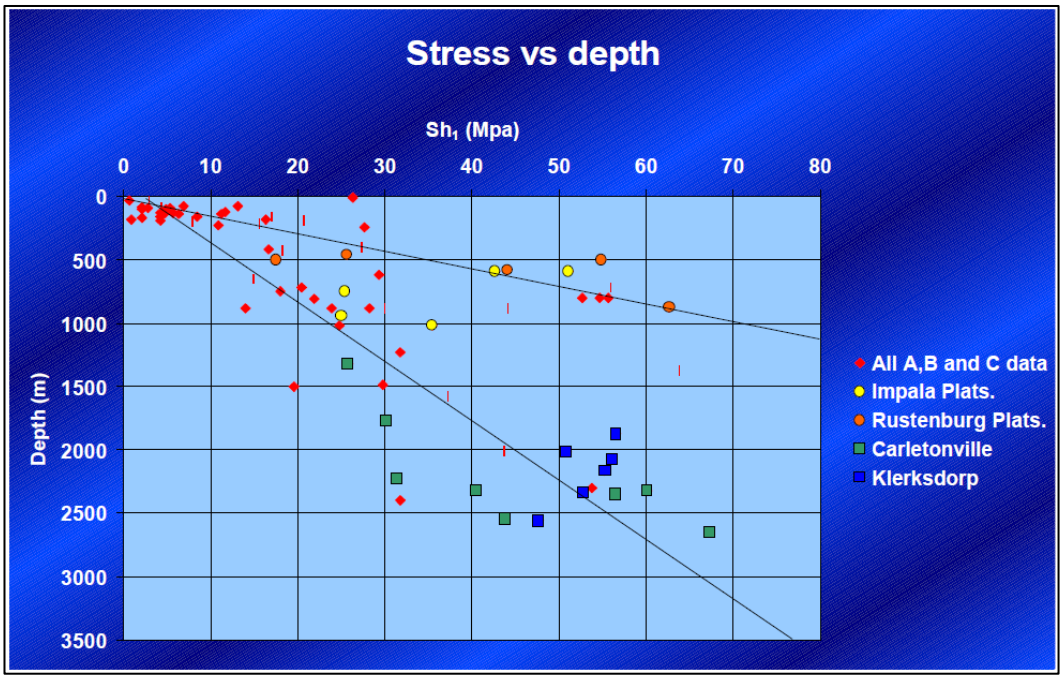


Figure 2-9: Variation of major horizontal principal stress with depth (Stacey & Wesseloo, 1998)

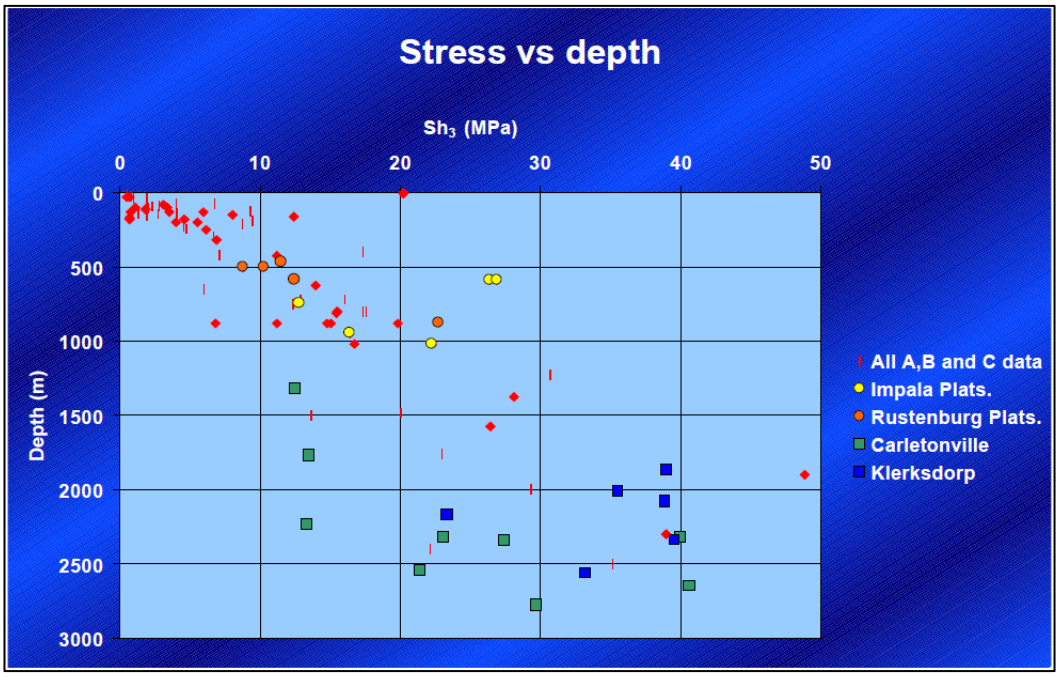


Figure 2-10: Variation of minor horizontal principal stress with depth (Stacey & Wesseloo, 1998)

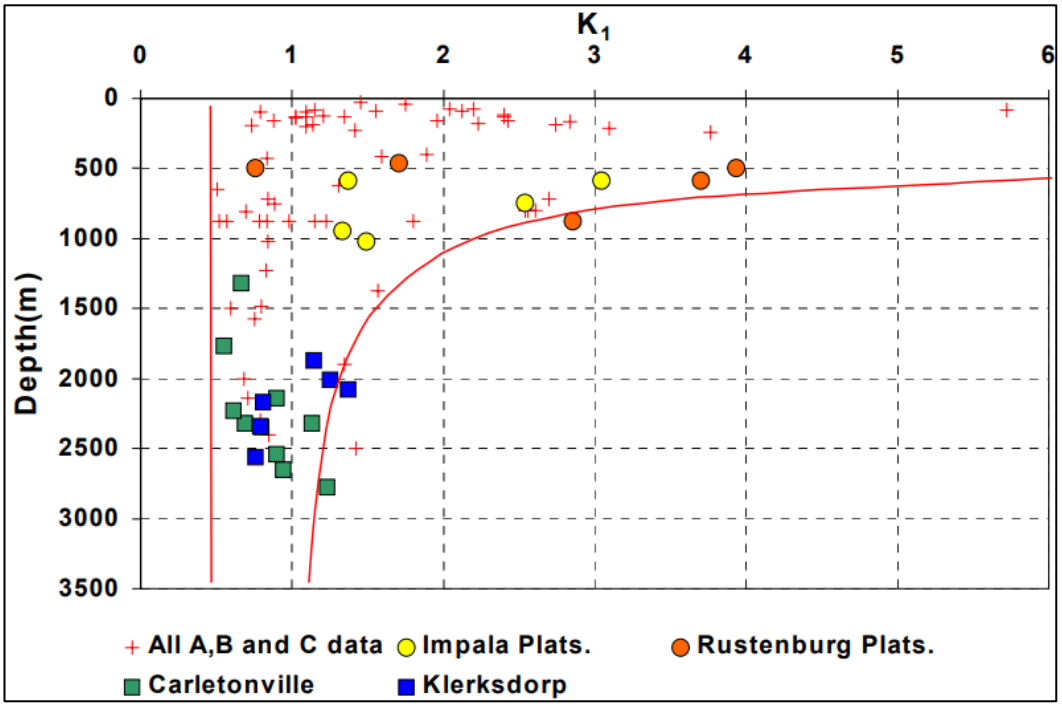


Figure 2-11: Variation of the ratio of major horizontal principal stress to vertical stress (K_1) with depth (Stacey, 2001)

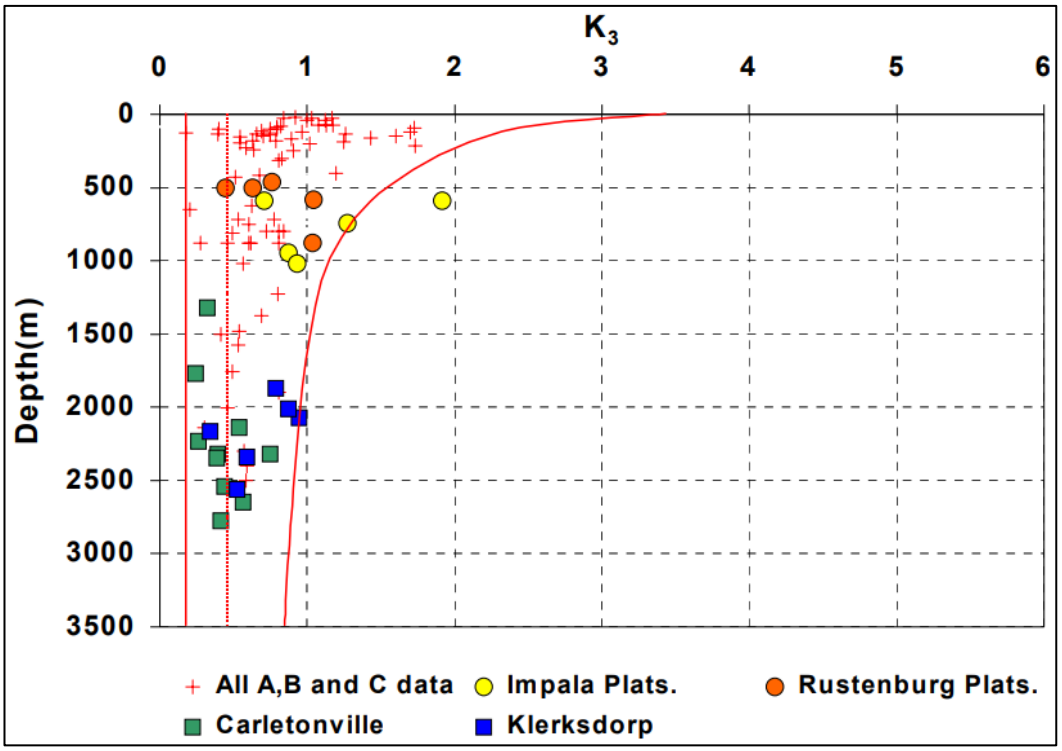


Figure 2-12: Variation of the ratio of minor horizontal principal stress to vertical stress (K_3) with depth (Stacey, 2001)

2.6 Evaluation of Rock Mass Quality

Rock mass classification systems are used as a means of quantifying the rock mass quality (Stacey, 2001). The geotechnical data collected from geotechnical core logging or mapping and laboratory rock tests are used as input data in the rock mass classification systems. The resulting numerical value, which quantitatively describes the quality of the rock mass, is correlated with many rock mass properties. This value is used in evaluating excavation stability and determining support requirements.

In this project report, a review of 12 rock mass classification methods for characterisation of the rock mass is provided in Appendix B. It is recommended to use at least two rock mass classification systems to gain greater confidence in the results. The RMR_{89}, Q-Index, and MRMR systems are recommended (Stacey, 2001).

2.7 Estimation of In Situ Rock Mass Properties

The strength of jointed rock masses is controlled by the deformation properties of intact rock material and the frictional properties of existing discontinuities (Brady & Brown, 2004). Rock mass classification systems and results from intact rock tests are usually combined to provide estimates of the strength and stiffness properties of the rock mass (Swart & Handley, 2005).

The estimated rock mass properties are used in different rock engineering design methods (analytical & empirical models) for evaluating the stability of jointed rock masses and determination of support requirements. The rock mass geotechnical parameters include stiffness, strength, and frictional properties such as:

- Intact rock elastic (Young's) modulus (*E*), Poisson's ratio (*v*), uniaxial compressive strength (intact rock σ_{ci}, and rock mass σ_{cm}), and the tensile strength of rock,
- Rock mass modulus of deformation (E_M),
- Rock strength criteria input parameters, such as Hoek-Brown criterion for jointed rock masses parameters (mb, s, m_r and s_r), and
- Mohr-Coulomb failure criterion frictional parameters (cohesion (C) and the friction angle (ϕ)).

2.7.1 Rock Testing

Small-scale laboratory rock material tests under different loading conditions are usually performed to establish important mechanical properties of intact rocks and rock masses. Rock material tests are carried out according to methods standardized by the International Society for Rock Mechanics (ISRM). The strength and rigidity of rock masses are expected to be lower than that of intact rocks, as full-scale rock masses contain discontinuities. To sufficiently "tie down" the rock mass characterization exercise, the following laboratory test procedures are recommended and are discussed below (Stacey, 2001):

- Uniaxial Compressive Strength (UCS) test;
- Triaxial Compressive Strength (TCS) tests,
- indirect Uniaxial Tensile Brazilian (UTB) Strength test, and
- shear strength tests (Direct Shear).

Uniaxial Compression Strength Test with Elastic Properties - Uniaxial Compressive tests with Modulus and deformation measurements (UCM) are conducted for the strength classification and characterisation of the rock material in a mining environment. It is the most widely used strength test. The test determines the deformability and strength of the rock materials in uniaxial compression (Bieniawski, et al., 1979). The test involves uniaxially loading a rock specimen of cross-sectional area 'A' with a uniaxial force 'F' until it fails. The resulting stress-strain curves in this test describe the progressive brittle fracture process of intact rock material (Abioye, 2019). Figure 2-13 shows the progressive deformation process of intact rock in uniaxial compression.

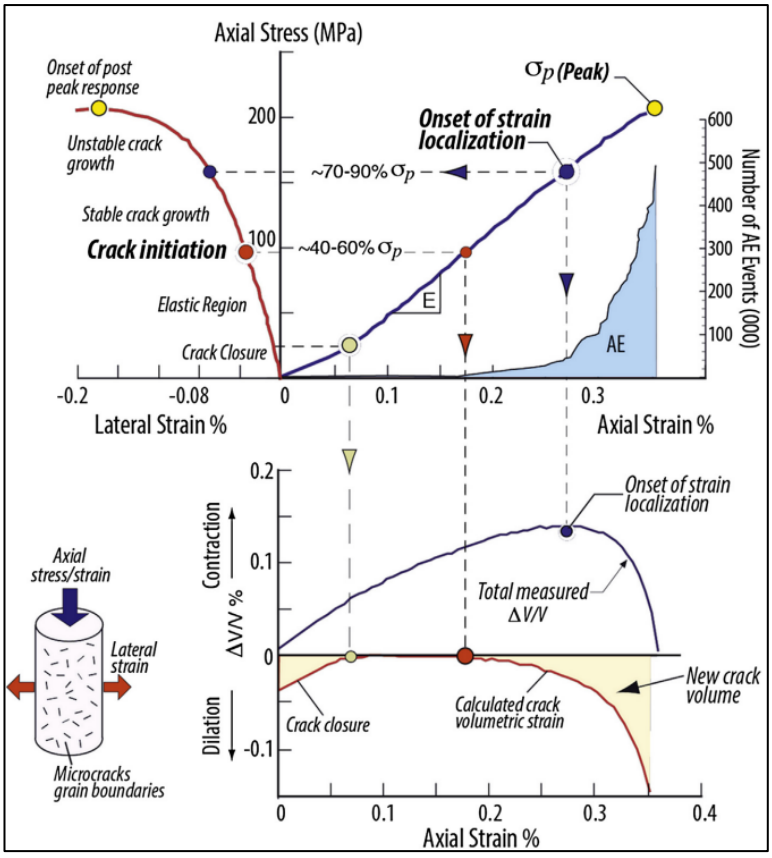


Figure 2-13: Stress-strain curve showing the progressive deformation of a specimen in uniaxial compression (Hoek & Martin, 2014)

At peak stress and specimen failure, the UCS of the rock material is calculated from Equation 2-2. In this test, important elastic properties of rock materials, such

as Young's modulus (*E)*, and Poisson's ratio (*v*) are determined (Bieniawski, et al., 1979).

$$\sigma_c = \frac{F}{A} \qquad \textit{Equation 2-2}$$

Where: F is the recorded force when the specimen fails (N) and A is the cross-sectional area of the specimen (m^2).

The elastic modulus of rock is determined by Equation 2-3. Equation 2-4 is used to determine Poisson's ratio (Bieniawski, et al., 1979).

$$E = \frac{\sigma}{\varepsilon} \qquad \textit{Equation 2-3}$$

Where: E is the elastic modulus or Young's modulus (MPa); σ is the stress (MPa); and ε is the strain.

$$v = |\frac{\varepsilon_2}{\varepsilon_1}| \qquad \textit{Equation 2-4}$$

Where: v is the Poisson's ratio; ε_2 is the radial or lateral strain, and ε_1 is the axial strain.

Triaxial Compressive Strength Test - TCS tests are conducted to determine the behaviour of rock material when compressed in three directions (triaxial) (σ_1, σ_2, and σ_3) (ISRM, 1978a). The test enables the evaluation of the strengthening effect of confining stresses on the rock. Triaxial tests have indicated that the strength of rock increases with increasing confining stress. The procedure for the determination of the triaxial compressive strength of rock is described by the ISRM (1978). The principal stress state is obtained and described at the point of rock failure, providing Major Principal Stress vs Minor Principal Stress plots. Shear Stress vs Normal Stress plots and Mohr's envelopes can be determined from this information. In addition, rock strength parameters such as input for Hoek-Brown (mi, mb, s and a) and Mohr-Coulomb (cohesion (c) and friction angle (ϕ)) failure) Criteria can be determined from the test results. These parameters are necessary

inputs for evaluating the stability behaviour of jointed rock masses (Hoek & Brown, 1977).

Brazilian Indirect Tensile Strength Test - Shallow bord and pillar mines within the BC experience vertical tensile stresses in the stope hangingwall, which cause instabilities by promoting the opening of discontinuities and bed separation in the hangingwall (MHSC, 2016). The resistance of rock to fracturing under the influence of tensile stresses determines the tensile strength of the rock (Perras & Diederichs, 2014). Laboratory Brazilian tensile strength tests are performed according to procedures described by the ISRM (1978) to indirectly determine the tensile strength property of rock material. In this test, a short rock cylinder (thin disc with a thickness-to-diameter ratio (*t*/*D*) of 0.5) is compressed diametrically until failure (ISRM, 1978b). The compression applied across the diameter induces a tensile stress normal to the loading lines and causes a tensile fracture (Li & Wong, 2012). The indirect tensile strength σ_t (MPa) of a rock specimen is a function of the load at failure P (N), the diameter of the test specimen D (mm), and the thickness t (mm) and is calculated by using **Equation 2-5** (ISRM, 1978b).

$$\sigma_t = -\frac{2P}{\pi D t} \quad \text{(MPa)} \qquad \textit{Equation 2-5}$$

Direct Shear Testing of Rock Discontinuities - The shear strength of rock discontinuities influences the stability of jointed rock masses. Consequently, the shearing loads on discontinuities must be considered during the design of underground excavations. Shear failure along discontinuities is common in underground structures; thus the determination of the peak shear strength of rock discontinuities is important (Larsson, 2021). Laboratory direct shear testing of rock material containing discontinuities is conducted to determine the shear strength properties of the discontinuities. The methods for conducting laboratory direct shear tests are provided by the ISRM (Muralha, et al., 2013). Plotting the shear strength versus normal stress graphs enables the calculation of the basic friction angle (BFA), cohesion (C), and angle of friction of rock (ϕ); which are geotechnical parameters used to provide estimates of the shear strength of rock discontinuities (Zhang, et al., 2019).

2.7.2 Estimation of Elastic Properties from Rock Mass Classification Systems

While intact rock elastic properties such as Young's modulus and Poisson's ratio can be determined from laboratory tests, some important in situ rock mass strength and deformation properties are usually estimated by incorporating results from rock mass ratings (Hoek & Diederichs, 2006). This includes the deformation modulus of a rock mass, which is an important input parameter in numerical modelling programs for the analysis of the deformation behaviour of rock masses (Cai, et al., 2004). Due to the high costs and difficulties associated with conducting in situ measurements of rock mass modulus of deformation values, Equation 2-6 and Equation 2-7 are empirical equations proposed to provide estimates of the deformation modulus (Swart, 2005). In these equations, the deformation modulus is related to the Geological Strength Index (GSI) classification system. If the uniaxial compressive strength (σ_{ci}) of intact rock is greater than 100 MPa, Equation 2-6 is used. If the σ_{ci} is less than 100 MPa, Equation 2-7 is used.

$$E_m = \sqrt{\frac{\sigma_{ci}}{100}} \text{x } 10^{(\frac{GSI-10}{40})} \qquad \textit{Equation 2-6}$$

$$E_m = 10^{(\frac{GSI-10}{40})} \qquad \textit{Equation 2-7}$$

Where: E_m is the Modulus of deformation of rock masses (in GPa); GSI is the Geological Strength Index; σ_{ci} is the intact rock uniaxial compressive strength (in MPa)

The GSI rock mass classification technique is primarily used in the characterization of jointed rock masses and is detailed in Appendix B. Rock test results and the GSI are incorporated in the derivation of empirical formulas for the calculation of the following rock mass parameters (Hoek & Brown, 2019):

- Constants in the Hoek-Brown failure criterion (mb, s, and a),
- UCS of the rock mass, and
- the tensile strength of the rock mass.

The combination of both intact rock results and rock mass ratings in deriving the above-listed parameters is presented in Section 2.7.3.

2.7.3 Rock Mass Failure Criteria

The stability behaviour of jointed rock masses is complex, as deformations and failures occur along discontinuities and in the intact rock blocks of the rock mass. Knowledge and understanding of the rock failure process and prediction of the rock mass strength improve the design of underground excavations and support systems (Edelbro, 2004). Rock mass failure criteria are used to reliably predict the load-bearing capacity of rock masses. This section presents only the most well-known and suggested empirical rock mass failure criteria for reliably predicting and describing the strength of jointed rock masses in the BC. These are (Edelbro, 2004; MHSC, 2016):

- Mohr-Coulomb Criterion,
- Generalised Hoek-Brown Criterion for jointed rock masses, and
- Extension-Strain Criterion.

Mohr-Coulomb Failure Criterion - The Mohr-Coulomb theory states that the shear failure of rock is caused by a critical combination of normal and shear stresses and not solely from either the maximum normal or shear stress (Giwangkara, et al., 2020). The shear strength of rock is characterized and described by two distinct shear properties, namely the internal friction angle (ϕ_i) and cohesion value (c). The cohesion parameter is used to identify the bond strength between internal rock particles (inherent strength), whilst the internal friction angle represents the internal friction between the rock particles (Giwangkara, et al., 2020). **Equation 2-8** represents the Mohr-Coulomb failure criterion, which relates the normal and shear stresses across a shear plane. The graphical representation of the criterion, where shear stresses are plotted against normal stresses from direct shear tests, or triaxial shear test results, enables the estimation of the internal angle of friction and cohesion of rock (Giwangkara, et al., 2020). Figure 2-14 shows the Mohr-Coulomb failure envelopes, which are determined by drawing a tangential line to the Mohr circles (Figure 2-14).

$$\tau_{max} = c + \sigma_n \tan\phi$$ **Equation 2-8**

Where:

- τ_{max} is the shear strength along a shear plane obtained at failure (MPa),
- σ_n is the normal stress acting on the shear plane (MPa),
- c refers to the cohesion of a shear plane (kPa), and
- ϕ is the internal friction angle of the shear plane (°).

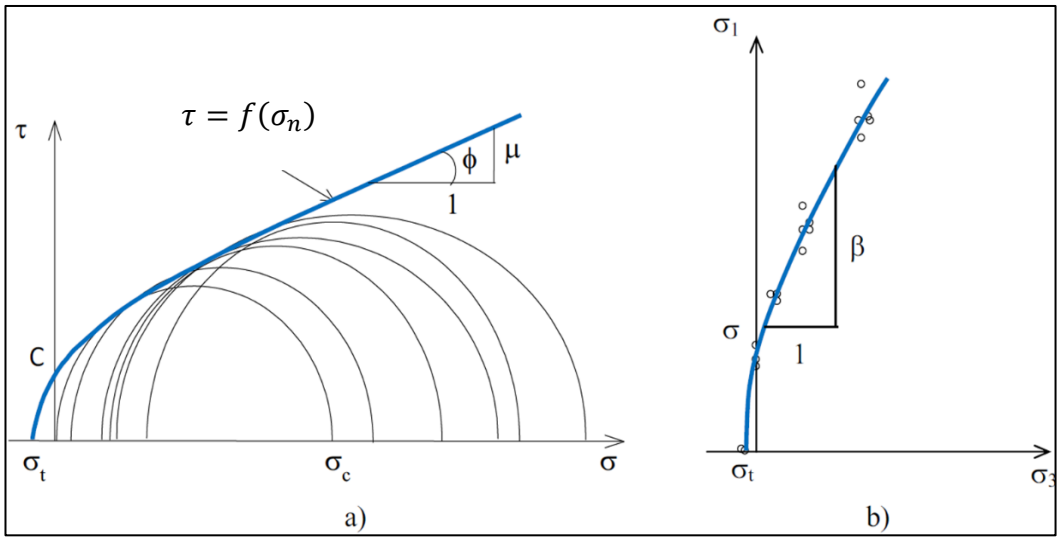


Figure 2-14: Mohr-Coulomb strength envelopes in terms of a) normal vs shear stress and b) principal stresses (Yilmaz, 2010)

Generalised Hoek-Brown Criterion - Hoek & Brown (1980) proposed a method for estimating the triaxial strength of jointed rock masses, based on the assessment of the interlocking (intact) rock blocks and the condition of discontinuities. Over the years, the original rock mass failure criterion was modified to suit different engineering applications; with a major revision being made in 2002 to ensure the criterion can be applied in numerical models and update the methods for estimating Mohr-Coulomb parameters (Hoek, et al., 2002). Equation 2-9 presents the generalised Hoek-Brown criterion for jointed rock masses.

$$\sigma_1 = \sigma_3 + \sigma_{ci}(m_b \frac{\sigma_3}{\sigma_{ci}} + s)^a$$ ***Equation 2-9***

Where: σ_1 and σ_3 are the maximum and minimum effective principal stresses at failure, respectively (MPa); σ_{ci} is the UCS of intact rock blocks making up the rock mass (MPa); m_b is the Hoek-Brown constant for the rock mass; and a and s are Hoek-Browm empirical constants which vary for distinct types of rocks (Hoek & Brown, 1980).

The estimation of the strength and deformability of jointed rock masses using the Hoek-Brown criterion involves the determination of three rock mass properties. These are:

- UCS of intact rock pieces making up the rock mass,
- the Hoek-Brown constant m_i of the intact rock pieces, and
- the value of the GSI for the rock mass.

For intact rock material "s" is equated to one and m becomes m_i. Therefore, Equation 2-9 simplifies to Equation 2-10 (Hoek & Brown, 1980):

$$\sigma_1 = \sigma_3 + \sigma_{ci}(m_i \frac{\sigma_3}{\sigma_{ci}} + 1)^{0.5}$$ ***Equation 2-10***

Values for m_i and σ_{ci} can be determined from the results of laboratory triaxial testing of core specimens. When laboratory triaxial testing is not possible, Table 2-5 in Section 2.3 and Table 2-15 are used to obtain estimates of σ_{ci} and m_i, respectively (Hoek, et al., 2002).

Table 2-15: Values of the Hoek-Brown constant m_i for intact rock *(Hoek, et al., 2002)*

Rock type	Class	Group	Texture			
			Coarse	Medium	Fine	Very fine
SEDIMENTARY	Clastic		Conglomerates (21±3) Breccias (19±5)	Sandstones 17±4	Siltstones 7±2 Greywackes (18±3)	Claystones 4±2 Shales (6±2) Marls (7±2)
	Non-Clastic	Carbonates	Crystalline Limestone (12±3)	Sparitic Limestones (10±2)	Micritic Limestones (9±2)	Dolomites (9±3)
		Evaporites		Gypsum 8±2	Anhydrite 12±2	
		Organic				Chalk 7±2
METAMORPHIC	Non foliated		Marble 9±3	Hornfels (19±4) Metasandstone (19±3)	Quartzites 20±3	
	Slightly foliated		Migmatite (29±3)	Amphibolites 26±6	Gneiss 28±5	
	Foliated*			Schists 12±3	Phyllites (7±3)	Slates 7±4
IGNEOUS	Plutonic	Light	Granite 32±3 Granodiorite (29±3)	Diorite 25±5		
		Dark	Gabbro 27±3 Norite 20±5	Dolerite (16±5)		
	Hypabyssal		Porphyries (20±5)		Diabase (15±5)	Peridotite (25±5)
	Volcanic	Lava		Rhyolite (25±5) Andesite 25±5	Dacite (25±3) Basalt (25±5)	Obsidian (19±3)
		Pyroclastic	Agglomerate (19±3)	Breccia (19±5)	Tuff (13±5)	

In jointed rock masses, when the size of the underground excavation is large and the rock blocks (defined by discontinuity spacing) in comparison are smaller, the GSI and Hoek-Brown criterion are combined to evaluate the strength of the rock mass (Hoek, et al., 2002). The m_b, s, and Hoek-Brown parameters in ***Equation 2-9*** for jointed rock masses are computed using ***Equation 2-11*** to ***Equation 2-13***. In

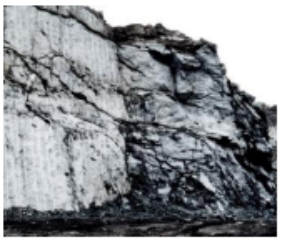
the 2002 edition of the Hoek-Brown rock mass failure criterion, the influence of blast damage is considered. In Equation 2-10 to Equation 2-11, “D” depends on the degree of disturbance of the rock mass due to blast damage and varies between 0 for undisturbed in situ rock masses to 1 for very disturbed rock masses. Hoek, et al., (2002) suggested guidelines for estimating the disturbance factor D in Table 2-16.

$$m_b = m_i \exp\left(\frac{GSI - 100}{28 - 14D}\right)$$ ***Equation 2-11***

$$s = \exp\left(\frac{GSI - 100}{9 - 3D}\right)$$ ***Equation 2-12***

$$a = \frac{1}{2} + \frac{1}{6}\left(e^{-\frac{GSI}{15}} - e^{-\frac{20}{3}}\right)$$ ***Equation 2-13***

Table 2-16: Guidelines for estimating the disturbance factor D (Hoek, et al., 2002)

Appearance of rock mass	Description of rock mass	Suggested value of D
	Excellent quality controlled blasting or excavation by Tunnel Boring Machine results in minimal disturbance to the confined rock mass surrounding a tunnel.	D = 0
	Mechanical or hand excavation in poor quality rock masses (no blasting) results in minimal disturbance to the surrounding rock mass. Where squeezing problems result in significant floor heave, disturbance can be severe unless a temporary invert, as shown in the photograph, is placed.	D = 0 D = 0.5 No invert
	Very poor quality blasting in a hard rock tunnel results in severe local damage, extending 2 or 3 m, in the surrounding rock mass.	D = 0.8
	Small scale blasting in civil engineering slopes results in modest rock mass damage, particularly if controlled blasting is used as shown on the left hand side of the photograph. However, stress relief results in some disturbance.	D = 0.7 Good blasting D = 1.0 Poor blasting
	Very large open pit mine slopes suffer significant disturbance due to heavy production blasting and also due to stress relief from overburden removal. In some softer rocks excavation can be carried out by ripping and dozing and the degree of damage to the slopes is less.	D = 1.0 Production blasting D = 0.7 Mechanical excavation

The UCS of the rock mass can be obtained by setting $\sigma_3 = 0$ in the original version of the Hoek-Brown criterion (Equation 2-9), giving Equation 2-14. Again, by setting $\sigma_1 = \sigma_3 = \sigma_t$ in Equation 2-9 to represent a condition of biaxial tension, the uniaxial tensile strength of the rock mass is calculated by Equation 2-14:

$$\sigma_{cm} = \sigma_{ci}.s^{a}$$ ***Equation 2-14***

Where σ_{cm} is the UCS of the rock mass (MPa)

$$\sigma_t = -\frac{s\sigma_{ci}}{m_b}$$ ***Equation 2-15***

Where: σ_t is the tensile strength of the rock mass (MPa).

In the design of underground mining excavations, Table 2-15 and Table 2-16 are used as built-in charts in the Rocscience program 'RocLab' to estimate the mi and D inputs for various rock types. The 'RocLab' program enables users to obtain reliable estimates of rock mass strength parameters (Roscscience, 2007). The program often involves importing the triaxial laboratory test data and specification of the following Hoek-Brown parameters as input:

- Intact rock UCS,
- GSI,
- Intact rock parameter mi, and the
- Disturbance factor due to blasting (D).

The Hoek-Brown failure envelope parameters mb, s, and a and equivalent Mohr-Coulomb parameters (cohesion and friction angle) are then calculated by the program. The RocLab program also calculated important rock mass strength parameters such as the tensile strength, UCS of the rock mass, deformation modulus and global rock mass strength (Roscscience, 2007).

Extension-Strain Criterion - Murphy et al. (2016) recommended the use of the critical extension strain criterion to assess the extension fracturing of the brittle rock in underground excavations. Stacey (1981) proposed the criterion, and it states that ''a fracture of brittle rock will initiate when the total extension strain (ε) in the rock exceeds a critical value which is characteristic of that rock type''. According to this criterion, the fracturing of brittle rock initiates when the following is satisfied (Stacey, 1981):

$$\varepsilon_3 \geq \varepsilon_{cr}$$ ***Equation 2-16***

Where ε_{cr} is the critical extension strain and ε_3 is the minimum extension strain. For material that shows ideal linear deformation behaviour, the strain in this direction is related to the three principal stresses (σ_1, σ_2, σ_3) using Equation 2-17.

$$\varepsilon_3 = \frac{1}{E}\left[\sigma_3 - v\left(\sigma_1 + \sigma_2\right)\right.$$ ***Equation 2-17***

Where:

- E is the Young's Modulus (MPa)
- v is the Poisson's ratio

2.7.4 Influence of Discontinuity Infill Material and Surface Roughness on Shear Strength

The stability of jointed rock masses is governed by the shear strength of rock discontinuities and their mechanical properties. As discussed in Section 2.3, the presence of infill material has a significant impact on the shear strength of discontinuities since they are weaker than the host rock. It is therefore vital to assign appropriate discontinuity shear strength parameters taking cognisance of the effect of infillings when designing underground excavations.

According to Read & Stacey (2008), infillings are broadly classified into two groups, namely, clays and crushed infill materials found in faults and sheared zones. Clays include montmorillonite and bentonitic clays, which typically have a cohesion ranging from 0 kPa to about 200 kPa. The friction angle of the clays ranges from about 8° to 20°. The infill material formed in faults and shear zones has a friction angle of between 25° to 45°, whilst the cohesion values range between 0 kPa to 100 kPa. Equation 2-18 presents the estimation of the peak friction angle by considering discontinuity roughness and wall rock strength (Read & Stacey, 2008). Table 2-17 presents various peak friction angle values determined from this equation. Table 2-18 presents Barton's (1974) estimation of shear strength parameters for filled discontinuities.

$$\phi_j \approx tan^{-1}(\frac{J_r}{Ja})$$ ***Equation 2-18***

Where: Jr is the joint roughness; Ja is the joint alteration number.

Table 2-17: Estimation of the peak friction angle from joint roughness number and joint alteration number (Read & Stacey, 2008)

			Joint alteration number, J_a				
			Tightly healed, hard, non-softening, impermeable filling, i.e. quartz or epidote	Unaltered joint walls, surface staining only	Slightly altered joint walls, non-softening mineral coatings, sandy particles, clay-free disintegrated rock etc.	Silty- or sandy-clay coatings, small clay fraction (non-softening)	Softening or low-friction clay mineral coatings, i.e. kaolinite or mica. Also chlorite, talc, gypsum, graphite etc. and small quantities of swelling clays
			A	B	C	D	E
Joint roughness number, J_r					J_a		
Description		J_r	0.75	1	2	3	4
A	Discontinuous joints	4	70°		60°	55°	45°
B	Rough, undulating joints	3	70°		55°	45°	35°
C	Smooth, undulating joints	2	65°	60°	45°	35°	25°
D	Slickensided, undulating joints	1.5	60°	55°	35°	25°	20°
E	Rough or irregular, planar joints	1.5	60°	55°	35°	25°	20°
F	Smooth, planar joints	1.0	50°	45°	25°	18°	15°
G	Slickensided, planar joints	0.5	35°	25°	15°	<10°	

Notes
The joint roughness number assumes rock wall contact or rock wall contact before 10 cm of shear displacement.
The descriptions of different cases for J_r refer to small-scale features and intermediate-scale features, in that order.
The joint alteration number assumes rock wall contact.
These are first estimates of peak friction angle and may not be appropriate for site-specific design purposes.

Table 2-18: Shear strength of filled discontinuities (Barton, et al., 1974)

Rock	Description	Peak c' (MPa)	Peak $\phi°$	Residual c' (MPa)	Residual $\phi°$
Basalt	Clayey basaltic breccia, wide variation from clay to basalt content	0.24	42		
Bentonite	Bentonite seam in chalk	0.015	7.5		
	Thin layers	0.09-0.12	12-17		
	Triaxial tests	0.06-0.1	9-13		
Bentonitic shale	Triaxial tests	0-0.27	8.5-29		
	Direct shear tests			0.03	8.5
Clays	Over-consolidated, slips, joints and minor shears	0-0.18	12-18.5	0-0.003	10.5-16
Clay shale	Triaxial tests	0.06	32		
	Stratification surfaces			0	19-25
Coal measure rocks	Clay mylonite seams, 10 to 25 mm	0.012	16	0	11-11.5
Dolomite	Altered shale bed, ± 150 mm thick	0.04	1(5)	0.02	17
Diorite, granodiorite and porphyry	Clay gouge (2% clay, PI = 17%)	0	26.5		
Granite	Clay filled faults	0-0.1	24-45		
	Sandy loam fault filling	0.05	40		
	Tectonic shear zone, schistose and broken granites, disintegrated rock and gouge	0.24	42		
Greywacke	1-2 mm clay in bedding planes			0	21
Limestone	6 mm clay layer			0	13
	10-20 mm clay fillings	0.1	13-14		
	<1 mm clay filling	0.05-0.2	17-21		
Limestone, marl and lignites	Interbedded lignite layers	0.08	38		
	Lignite/marl contact	0.1	10		
Limestone	Marlaceous joints, 20 mm thick	0	25	0	15-24
Lignite	Layer between lignite and clay	0.014-.03	15-17.5		
Montmorillonite Bentonite clay	80 mm seams of bentonite (mont-morillonite) clay in chalk	0.36 0.016-.02	14 7.5-11.5	0.08	11
Schists, quartzites and siliceous schists	100-15- mm thick clay filling	0.03-0.08	32		
	Stratification with thin clay	0.61-0.74	41		
	Stratification with thick clay	0.38	31		
Slates	Finely laminated and altered	0.05	33		
Quartz / kaolin / pyrolusite	Remoulded triaxial tests	0.042-.09	36-38		

2.8 Stability Evaluation Methods (Stability Analyses)

The design of effective mine support strategies for underground excavations requires the evaluation of the inherent or natural stability of the rock mass. This means excavation support design must be informed by a thorough assessment of all rock mass failure mechanisms in the mine. There are different stability evaluation approaches for specific classes of excavations with unique purposes. For example, instability may be necessary for mining by caving methods, temporary mine openings require short-term stability, and important permanent mining excavations require maintaining long-term stability. Swart (2005) stated that the proposed systematic engineering methodology for the design of maximum stable bord widths considers all potential failure/instability modes that may occur between pillars. As shown in the methodology presented in Figure 2-1, instabilities between pillars were identified and categorised into four types, which are (Murphy, et al., 2016):

- rock mass failure;
- beam failure;
- structural Failure; and
- intact Rock Mass Failure.

There are well-defined rock engineering models and procedures recommended for carrying out stability evaluations for each of these failure mechanisms between pillars. This section discusses the methods for identifying each failure mode and the techniques for conducting stability evaluation.

2.8.1 Rock Mass Stability Evaluation using Rock Mass Classification Systems

Rock mass classification systems form the primary empirical approach for the evaluation of jointed rock mass stability and the design of stope panels (Stacey, 2001). In the stability evaluation of stope panels, rock mass classification methods are used for (Stacey, 2001) (Murphy, et al., 2016):

- prediction of the potential of rock mass failure (unravelling). Unravelling failure is usually expected to take place in poor rock quality;

- provide indications of unsupported stable span dimensions and the ability of a rock mass to remain stable for a specific time until supported; and
- providing preliminary indications of excavation support requirements.

The degree of stability required in stope excavations is informed by the exposure of the workforce in the stopes. If more personnel work in the stopes, then a conservative approach is taken. If few to no people will work in the stope, a more "marginal stability condition" is often tolerated (Stacey, 2001). To assess rock mass failure in production-oriented excavations such as the shallow stopes in the Bushveld Complex, Swart et al (2000) suggested the following four rock mass classification systems:

- the Geomechanics Classification or Rock Mass Rating (RMR) system developed by Bieniawski (1989);
- the Norwegian Geotechnical Institute (NGI), rock quality index or Q-system developed by Barton et al (1974);
- the Modified Rock Mass Rating or Mining Rock Mass Rating (MRMR) system (Laubscher, 1990); and
- the Modified Stability Graph Method using the Modified Stability Number, *N'*, originally developed by Mathews et al (1981) and later modified by Potvin (1988) and others.

The above-listed rock classification methods for evaluating the stability of pillar-supported shallow stopes are discussed in Appendix B. In the stability evaluation of excavations, it is also recommended to use at least two rock mass classification systems to gain greater confidence in the results (Murphy, et al., 2016).

2.8.2 Stability Evaluation of Stratified Rock (Rock Beams)

Stratified rock masses in the Bushveld Complex are a result of excavation-parallel fracturing of massive rock or stratification created during the igneous and metamorphic formation of the rock mass (Swart & Handley, 2005). In such a structure of the rock mass, parting planes between rock beams occur and can fail if not properly supported. The possible excavation failure modes, which are bed separation and interbed slip in laminated rock masses, are shown in Table 2-9. The discussion of Thorncliffe Mine's local geology setting in Section 1.2.3 showed that there is interlayering of disseminated Chromitite layers and the pyroxenite host

rock, which form rock beams and parting planes in the hangingwall. Therefore, it is vital to test for the stability of rock beams to ensure the roofs between bords are stable. Two crucial factors influence the stability behaviour of a stratified hangingwall (Swart & Handley, 2005):

- the tensile strength perpendicular to the stratification is very low or zero, and;
- the shear strength on the laminations is very low compared to the shear strength of the intact rock.

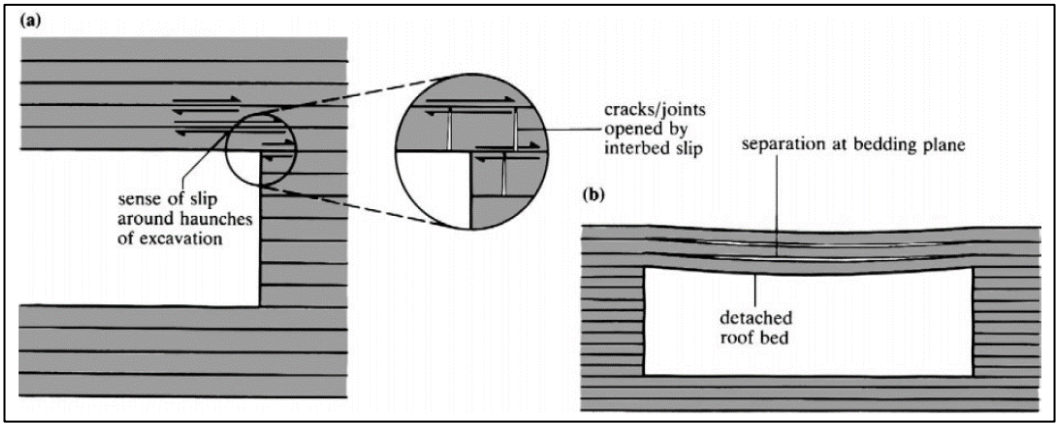


Figure 2-15: Rock beam failure in stratified rock masses (Brady & Brown, 2004)

In the evaluation of the stability of rock beams in stratified rock masses, the '*Elastic beam theory*' is used to explain the deformation and failure of hangingwall beams, which are intact and contain no joints or cracks. When the roof between pillars contains sub-vertical jointing (which is common in the Bushveld Complex), the design of the roof between pillars in stratified rock is carried out using the *'Voussoir beam theory'* (Swart & Handley, 2005). The near-vertical jointing in a Voussoir beam material results in zero tensile strength in the horizontal direction.

In rock engineering, the Voussoir arch concept illustrated in Figure 2-16 is used to describe the deformation and stability behaviour of jointed rock beams. As illustrated in Figure 2-16 (a), When a jointed beam deflects, the central part of the beam will deflect downwards under its weight, which causes its lower central part to be in tension and likely to form a tensile crack (Figure 2-16b). The upper central part together with the lower parts at each end of the beam will be in compression

(Figure 2-16c). The trajectory of these compressive thrust forces from the lower parts at each end of the beam towards the upper central zone is effectively the *'Voussoir beam'*. This arching effectively promotes compressive zones in the existing sub-vertical joints and subsequently, a stable roof beam in a bord will form if this compressive arch (Voussoir arch) can develop (Garg, 2018).

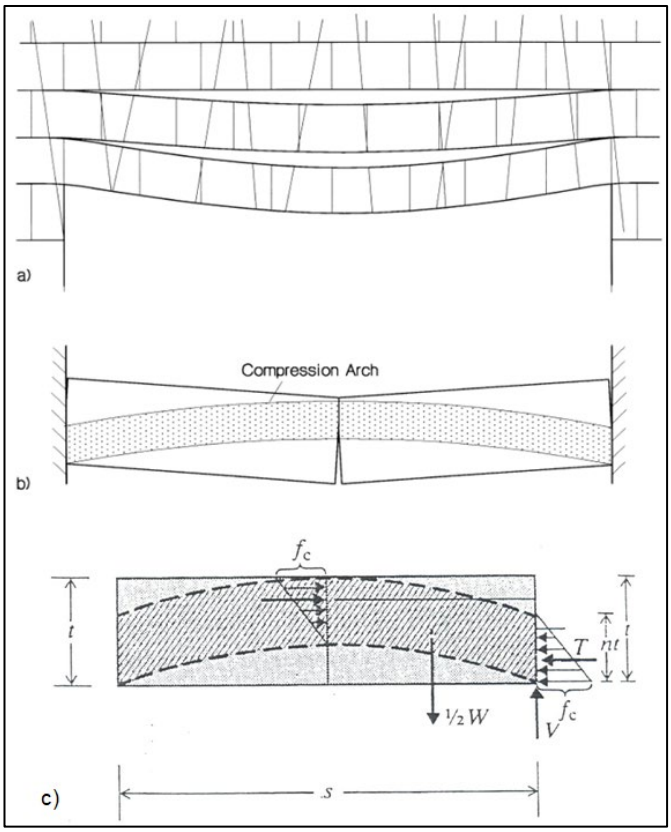


Figure 2-16: (a) Jointed rock beams; (b) Voussoir beam with compressive arch, and (c) Voussoir model showing the trajectory of the compressive forces (adapted from Garg (2018))

There are three failure mechanisms associated with the Voussoir beam, which are Buckling or snap-through failure, Crush failure, and Shear (Sliding) failure (Oliveira & Pells, 2014). According to the study conducted by the MHSC (2016), when applying the Voussoir arch in the pillar-supported mines situated in the Bushveld Complex, only two of the three failure modes are common and evaluated. The failure modes of the Voussoir beam are illustrated in Figure 2-17. The two failure modes are:

- buckling or snap-through Failure (Figure 2-17a); and
- shear or sliding Failure (Figure 2-17c).

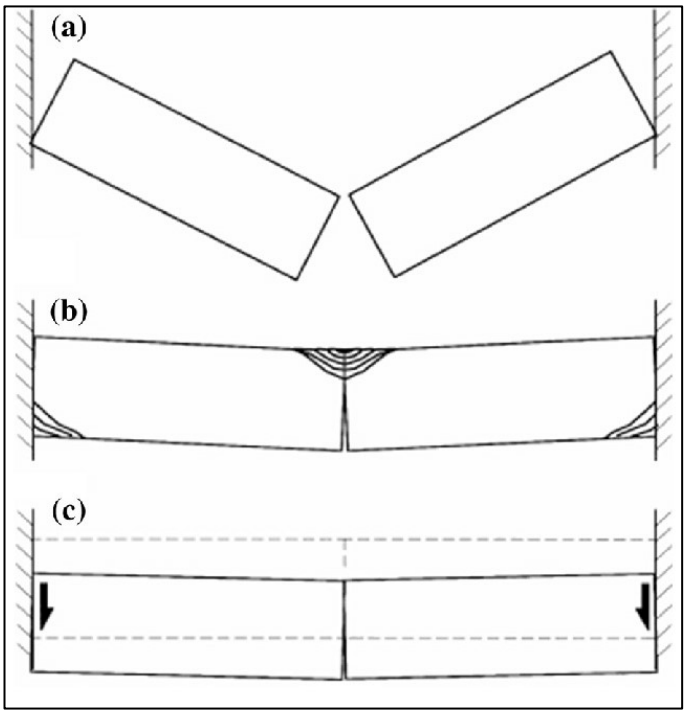


Figure 2-17: Failure modes of the voussoir beam (Shabanimaschool, et al., 2014)

The analytical solution to these failure modes is based on an iterative solution system which determines the deflection and stability of the Voussoir beam. The models used for evaluating buckling and shear failure of the Voussoir beam are discussed below.

Evaluation of Buckling failure - Buckling or snap-through beam failure occurs when the lateral loads cause beam deflection to exceed the beam material's yield strength. This causes the beam to fracture or crack. When gradual deflection of the beam occurs, the beam bends from straight to curved under a compressive load due to increasing horizontal or lateral thrust. The Buckling Limit (BL) Index, which is an engineering estimate for the yield threshold of the buckling limit, was established. The BL was established by relating the midspan deflection (δ) and the beam thickness (t). According to Brady & Brown (2004), in roof design, the

allowable yield threshold of the buckling limit is when deflection is equivalent to about 10% of the beam thickness.

$$\text{Buckling Limit Index} = 0.1\text{t} \qquad \textbf{Equation 2-19}$$

where 't' is the beam thickness measured (in metres).

Beam shear failure - Beam shear failure occurs at the abutments when the abutment shear force (*V*) exceeds the beam material's shear resistance/capacity. Slip is usually initiated along the sub-vertical joint planes. The calculated shear beam forces are used to assess the possibility of shear failure of the hangingwall beam at the abutments *(*Shabanimaschool, et al., 2014*)*. The maximum frictional resistance (*F*) that can be mobilised is calculated from:

$$F = T \tan \varphi = \frac{1}{2} f_c \tan \varphi \qquad \textbf{\textit{Equation 2-20}}$$

Where: T is the lateral thrust force measured in N; φ is the friction angle of the sub-vertical planes of weakness in degrees; f_c is the calculated maximum compressive stress in the beam in Pascals.

The shear force acting at the abutment:

$$V = \frac{1}{2} \gamma \, st \qquad \textbf{Equation 2-21}$$

Where: γ is the specific weight of the beam in kN/m^3; *s* is the bord span in m; and *t* is the thickness of the beam in metres. The factor of safety against sliding of shear failure at the abutments is therefore defined by:

$$FOS_{slip} = \frac{f_c n}{\gamma s} \tan \varphi \qquad \textbf{\textit{Equation 2-22}}$$

where *n* is the thickness coefficient; *n* is typically taken as 0.75.

2.8.3 Evaluation of Structurally Controlled Instability

As described in Section 2.2, hangingwall instabilities in the shallow bord and pillar mines in the Bushveld Complex are largely controlled by the presence of discontinuities (Swart, 2005). According to Murphy et al. (2016), the three common hangingwall structural failure mechanisms in the pillar-supported mines within the Bushveld Complex that can be evaluated statistically are:

- keyblock failure – Discontinuities occur in sets that trend in different directions and the intersection of at least three of these discontinuities separates the rock mass into discrete but interlocked unstable keyblocks (Murphy, et al., 2016);
- wedge failure – Wedge structures occur where low-angled joints in the stope hangingwall intersect other major planes of weakness and cause a wedge-shaped fallout. Wedge failures usually cover a larger areal extent than keyblocks (Murphy, et al., 2016); and
- dome/ramp fault failure – A dome is where low-angled discontinuities dip away from each other at angles between 15° to 45°. One of these discontinuities is usually part of a thrust structure, which forms an upward-curving block of rock (Murphy, et al., 2016).

A free face created by introducing an excavation removes the constraint from the keyblocks and allows failure (Keykha, et al., 2011). The keyblocks can fall (topple) or slide from an excavation surface if their weight exceeds the support capacity in place or if they occur between support units (Esterhuizen & Streuders, 1998). The geometry and possibility of the keyblocks failing by either falling or sliding depends on (Zerradi, et al., 2020):

- the orientation and geotechnical characteristics of significant discontinuity sets;
- excavation or tunnel orientation; and
- rock material properties and shear strength properties of discontinuities.

In rock engineering, the block theory proposed by Goodman & Shi (1985) forms the foundation for keyblock stability evaluations. The block theory evaluates potential keyblock failure and determines whether selected support systems will ensure stability. The suggested general steps taken to address hangingwall

structural instabilities and achieve acceptable levels of stability can be summarized as follows (Swart, 2005):

- interpret the structural geology to determine the average (true) dip and dip direction of major discontinuity sets;
- identify potential keyblocks which can slide or fall;
- assess stability by determination of keyblock factors of safety; and
- determination of a support system required to achieve stability of the keyblocks.

Esterhuizen & Streuders (1998) and Swart (2005) concluded that the stability of keyblocks in jointed rock masses is best evaluated using a probabilistic design approach. Probabilistic keyblock evaluations are conducted using a computer program called '*Jblock'*, which evaluates the potential for gravity-driven FOGs. The Jblock program uses properties of discontinuities as input data and follows a probabilistic approach to determine the types, sizes, and frequency of keyblocks that can occur in underground excavations. Jblock is also used to optimize support strategies by evaluating the effectiveness of support systems in preventing falls of ground of a particular size (Swart, 2005).

Deterministic methods are also used to assess the stability of wedge failures around excavations. This involves the use of Rocscience's programme '*UNWEDGE*', which also uses the block theory proposed by Goodman & Shi (1985) to evaluate the stability of multi-sided wedges. The programme determines the size and safety factors of the largest unstable wedges that can be formed around an excavation, and the support system required to achieve stability (Zerradi, et al., 2020). The UNWEDGE software integrates well with a popular software capable of kinematic and jointing analysis called 'Dips'. Dips is a stereographic projection software designed for the interactive modelling and statistical analysis of geological orientation data (Rocscience, 2023). Dips enable users to analyse and visualise structural data and determine joint sets following the same method used in manual stereonets. Additionally, the Dips programme enables the analysis of various failure modes, including planar and wedge sliding, direct and flexural toppling failure of rock. The integration of the two software enables the importation of orientation data from Dips for deterministic and probabilistic evaluation of rock failure in UNWEDGE (Rocscience, 2023).

2.8.4 Evaluation of Intact Rock Failure

Intact rock failure in shallow BC bord and pillar mines is associated with the presence of a relatively large vertical tensile zone (VTZ) in the hangingwall and stress failures due to relatively high virgin horizontal stresses (Murphy, et al., 2016). Intact rock failures are therefore defined by the widely spaced tensile fractures (opened-up bedding planes and joints) and extension stress failures in the hangingwall (Jager & Ryder, 1999). Watson, et al. (2021) noted that the vertical tensile zone extends high into the hangingwall of stope excavations in the depth range from the surface to about 1 400 m below the surface. The vertical tensile zone defines the maximum height of bed separation between pillars (Figure 2-18), which can cause beam failure or keyblock fallouts, followed by major stope collapses. In-stope pillars are used to control the tensile zone on a regional scale to prevent large collapses (Jager & Ryder, 2002). To stabilise the immediate stope hangingwall and prevent local FOGs between pillars, it is essential to keep the immediate 'roof-softening zone' stable by installing a high resistance support system consisting of support units of adequate lengths (Canbulat, et al. (2006) and Watson, et al. (2021)).

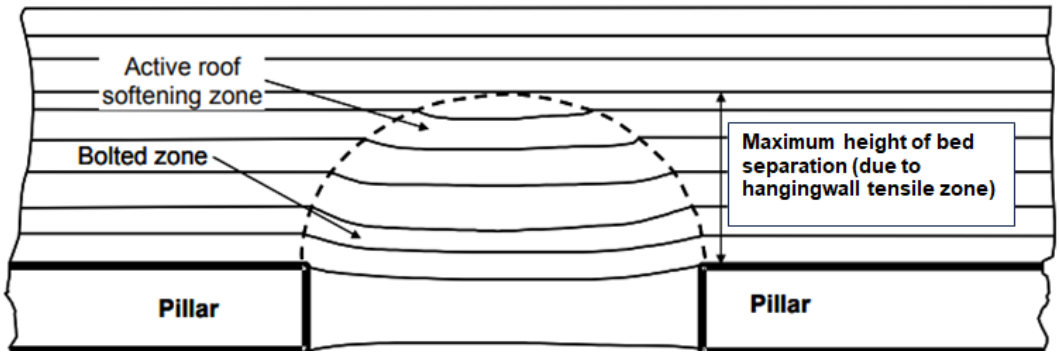


Figure 2-18: Maximum height of bed separation due to hangingwall tensile zone (adapted from Canbulat, et al. (2006))

Analytical solutions are used to estimate the maximum height of the VTZ in the stope hangingwall. The crude approximation estimates the height of the VTZ above the centre of a circular excavation and relates the VTZ to the stope span and its depth below the surface. For a circular stope and a 2D stope of equal half span, the following equation is proposed (O'Ferrall & Malan, 2012):

$$\frac{Z_o(circular\ stope)}{Z_o(2D\ panel)} = \frac{1}{\sqrt{\frac{16}{3\pi}}} \approx 0.77$$ ***Equation 2-23***

Where Z_0 is the height of the VTZ at the centre of the excavations

For an isolated 2D bord, the following equation can be used to estimate the height of VTZ (O'Ferrall & Malan, 2012):

$$\frac{Z_o(2D\ panel)}{l} \approx \frac{1}{\sqrt{\frac{H}{l}-\frac{3}{2}}}$$ ***Equation 2-24***

Where: Z_o = The height of the tensile zone at the centre of the excavations; H = Excavation depth below the surface; and *l* = Half span of the stope

If Equation 2-24 is inserted in Equation 2-23, it gives:

$$Z_o(circular\ stope) = \frac{0.77l}{\sqrt{\frac{H}{l}-\frac{3}{2}}}$$ ***Equation 2-25***

Where *l* is the radius of the circular stope

Jager & Ryder (1999) noted that the high horizontal stress observed in the Bushveld Complex led to breakouts/poor conditions in the hangingwall of stope excavations and caused 'Gothic-arch' shaped tunnels in some of the platinum mines. Practical methods implemented to prevent roof stress fracturing and arching include the creation of Gothic-arch-shaped tunnels to expose a small area of the tunnel to major horizontal stresses and advance the tunnels in the direction of the high stresses (Jager & Ryder, 1999). Figure 2-19 shows an example of a tunnel layout consisting of crosscuts from the shaft infrastructure to the footwall haulages (showing a gothic-arch fracturing profile) in a high horizontal stress environment.

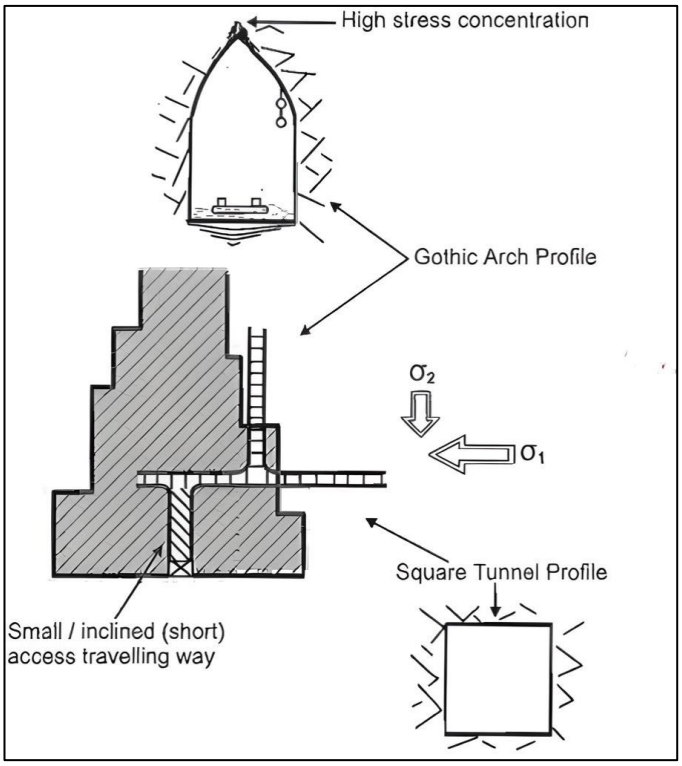


Figure 2-19: Example of a tunnel layout in a high horizontal stress environment (Jager & Ryder, 1999)

Stress-induced failure is predicted by evaluating the in-situ stress field in the rock surrounding the excavations to determine overstressed zones around stope panels (Swart, 2005). The MHSC suggests the use of numerical modelling techniques such as finite element codes to determine the extent of fracturing around excavations. These numerical modelling codes can also be used to estimate tensile zone heights for proposed stope layouts, since they can analyse tensile failure (Murphy, et al., 2016).

2.8.5 Stope Geometrical Optimisation to Improve Stability

If the stability assessment procedures indicate that stability cannot be improved by installing roof support, then stope geometrical changes must be considered (Stacey & Swart, 2001). Stoping layouts are optimised by altering the location, orientation, shape, and size of stope panels. The orientation of stope panels can be altered such that (Swart, 2005):

- the geometric instability and the number of keyblocks are minimised;

- stope panels are not advancing parallel to the direction of major discontinuities; and
- Under low-stress conditions, mining in the direction of minor principal stresses (σ_3) is achieved.

Stacey & Swart (2001) added that larger stope spans tend to be less stable than smaller spans. This is because reducing stope spans reduces the number of discontinuities exposed in the hangingwall and limits the development of uncontrolled stress-induced instabilities. Therefore, only the minimum appropriate panel span should be created if stability is a problem. If stress-induced rock failures are possible, stability can be improved by optimising stress distribution around stope excavations. In strong rock, elliptical-shaped excavations with their long cross-sectional axis oriented in the direction of the major principal stress (σ_1) are designed. If high field stresses exist and stress-induced failures are impossible to contain, the long axis of the elliptical-shaped stope excavations is oriented parallel to the minor principal stress direction.

2.9 Evaluation of Support Requirements for Shallow Bord and Pillar Mines

Section 2.8 discussed the rock engineering procedures for 'testing' and predicting different failure mechanisms between pillars. If instability is detected in the stopes, some means of local ground support or reinforcement is required to maintain stability. Stacey (2001) stated, *"It is almost certain that, even in good quality rock masses, rock support will be required. It is most important that the stability of the excavation and the corresponding support requirements are determined for the worst conditions to be encountered over the life of the excavation. The aim must be to install support that will ensure stability for the full life of the excavation, not only during development."* Support units of appropriate length and strength are installed at optimum spacing and orientation between pillars to achieve the following:

- to ensure the safety of the working places;
- to prevent the occurrence of FOGs by preventing keyblock failure; and

- control the movement of unstable rock blocks in the periphery of the excavations.

Optimal stope support systems are recognised as the ultimate strategy to combat rockfalls between pillars. An optimised engineering approach for designing support systems in a mine considers the following critical rock mass and support parameters (Jager & Ryder, 2002):

- height of potential rockfall;
- quasi-static stope closure rates;
- dynamic closure rates;
- compressive hangingwall stresses and strength; and
- discontinuity spacing, orientation, and interface properties.

The critical support parameters are:

- effect of support length on stability;
- effect of compression rate on support;
- support performance consistency; and
- areal coverage of support systems.

The depths at which mining activities take place are also a dominant factor influencing the characteristics of both mining strategies and support systems employed (Jager & Ryder, 1999). Table 2-19 summarises the typical quantities of some of the critical rock engineering parameters at different mining environments (mining depths).

Table 2-19: Rock engineering parameters associated with different mining depths (Jager & Ryder, 1999)

Parameter	Shallow	Intermediate	Deep	Ultra-deep
Typical Depth (m)	< 1000	1000 - 2250	2250 - 3500	>3500
Typical Energy Release Rate, ERR (MJ/m^2)	<8	8 - 40	40 - 80	>80*
Vertical virgin stress (MPa)	<25	25 - 60	60 - 95	>95
Stress fracturing	Little/None	Moderate	Deep	Very Deep
Stope Closure rate (mm/m face advance)	Low (<10)	Moderate (10 - 30)	High (30 - 60)	Very High (>60)*
Influence of geology on HW stability	Strong	Moderate	Moderate	Moderate
Possible extent of falls of ground	Can be large	Often small	Usually small	Small
Rockburst hazard	Minimal	Moderate to Severe	Severe	Very Severe*
Notes:	* If regional support were not used			

Table 2-19 shows that shallow mining environments are characterised by low stress (no stress-fracturing), low ERR, low compressive (clamping) stresses, little to no stope closure, and competent hangingwalls. The principal source of FOGs in shallow bord and pillar operations is the formation of unstable keyblocks due to the interaction of geological discontinuities and reduced rockmass confinement due to low in-situ stress magnitudes (Stacey, 2001). In shallow bord and pillar mines, the most important rock mass parameters influencing the design of support systems are therefore:

- the height of potential rock mass instability; and
- discontinuity orientation, spacing, and interface (frictional) properties.

The height of the potential rockfall informs the length of selected support units and the demand that a support system is required to meet. Support resistance will be discussed further below. Discontinuity orientation determines the size and shape of instabilities forming in the hangingwall. A hangingwall consisting of closely spaced discontinuities is densely fractured and therefore likely to unravel. The frictional characteristics (such as effective friction angles and cohesion) of discontinuities in the rock mass affect the zone of influence of a support system (Jager & Ryder, 2002).

According to Murphy et al (2016), common support elements used to provide primary reinforcement of the immediate hangingwall between pillars consist of tendons such as fully grouted (resin or cement) rockbolts and tensioned cable anchors. This type of support is stiff; therefore, rock displacement is minimised. Tendons provide a supporting mechanism of ‘suspending’ unstable keyblocks to the competent rock/self-supporting layer overlying the keyblocks. Shallow mining environments experience instabilities of bed/layer separation and large collapses due to an extended tensile zone in the hangingwall. A ‘beam-building’ support mechanism is therefore also applicable where roof rockbolts/cable anchors can be used to combine individual beams to form a self-supporting composite beam (Canbulat, et al., 2006).

O'Ferrall & Malan (2012) stated that while spot bolting can successfully support keyblocks, a systematic support layout is often used to minimise unexpected rock fallouts due to failure to identify individual keyblocks. Jager & Ryder (2002) added

that a highly discontinuous hangingwall requires areal coverage such as mesh, nets and super-skin/spray-on membranes such as shotcrete or Thin-Skin Liners (TSL)) to maintain its integrity. Areal coverage is effective in preventing FOGs that occur between support units.

2.9.1 Types of Support Elements

Before presenting specific support elements, it is vital to distinguish between the following support types:

- permanent support and temporary support;
- primary support and secondary support; and
- active and passive support.

Permanent support refers to support that is installed without the intention of removing it later. Temporary support, usually installed close to the face area, is any support that is installed for a limited time (Stacey, 2001). Primary support refers to the initial permanent support installed that is expected to maintain adequate support. The additional support installed after the primary support to achieve long-term stability is called secondary support (Stacey, 2001). Active support (which requires pre-tensioning) refers to support that exerts a supporting force immediately after installation, while passive support starts exerting a supporting force as a response to some rock deformation (Stacey, 2001). The selection of appropriate support is associated with the loading conditions in a rock mass. Typical support elements commonly used in the mining industry include the following (Stacey, 2001 and Harshil, et al., 2018):

- mechanical anchored bolts;
- grout (resin or cement) end-anchored rockbolts;
- full-column grouted rockbolts;
- friction bolts;
- cable anchors;
- mesh (welded or wire); and
- shotcrete and TSL.

2.9.2 Evaluation of in-stope support requirements

The support design of shallow underground excavations is based on two aspects, namely demand and capacity, which are both measured in kN/m^2 (Stacey, 2001). As mentioned above, demand refers to the load from the hangingwall imposed on the support system and the maximum resistance each support unit is required to meet. Equation 2-26 is used to calculate the demand for a support system. Capacity is the maximum load that can be carried by each support unit. Equation 2-27 presents the calculation of the support resistance generated by a support unit (Stacey, 2001).

$$Demand = p\ g\ t \quad (\text{kN/m}^2) \qquad \textbf{\textit{Equation 2-26}}$$

Where: *p* is the rock density (kg/m^3); *t* is the height of potential rock fall (in metres), and *g* is the gravitational acceleration (in m/s^2).

$$Support\ Resistance = \frac{F}{A} \quad (\text{kN/m}^2) \qquad \textbf{\textit{Equation 2-27}}$$

Where: *F* is the force generated by the support unit (N); and *A* is the Tributary area of the hangingwall to be supported by a support unit.

The FOS of a support system is obtained by dividing the support capacity by the demand imposed by the deadweight of a potential rockfall. It is recommended that the support system capacity should be at least 1.5 times the demand (Stacey, 2001). Harshil, et al (2018) added that in rock bolting design, the FOS ranges between 1.5 to 3.

The height of potential rockfall 't' in Equation 2-26 is often determined by back analysis of a mine's historical fall of ground data. Stacey (2001) added that '*t*' is usually taken as equal or greater than 95% of the fallout thickness of all FOG occurrences. The Guidelines for the Prevention of Rockfall and Rockburst Accidents issued by the Department of Mineral Resources require the same analysis (O'Ferrall & Malan, 2012).

2.9.3 Tributary Area and Zone of Support Influence

The tributary area theory forms the basis of tendon support design, irrespective of the zone of influence of support units or stable ground between support units (Daehnke, et al., 2001). The tributary area that can be supported by a support unit for rockfall conditions is given by Equation 2-28. The demand for support is shown as a function of the height of instability in *Figure 2-20* for various tributary areas.

$$A_T = \frac{F}{p\,g\,t} \text{ (m}^2\text{)} \qquad \textit{Equation 2-28}$$

Where: A_T is the maximum supported tributary area (m^2); F is the support unit capacity (kN); p is the rock density (kg/m^3); g is the gravitational acceleration (m/s^2); and t is the fallout thickness (m).

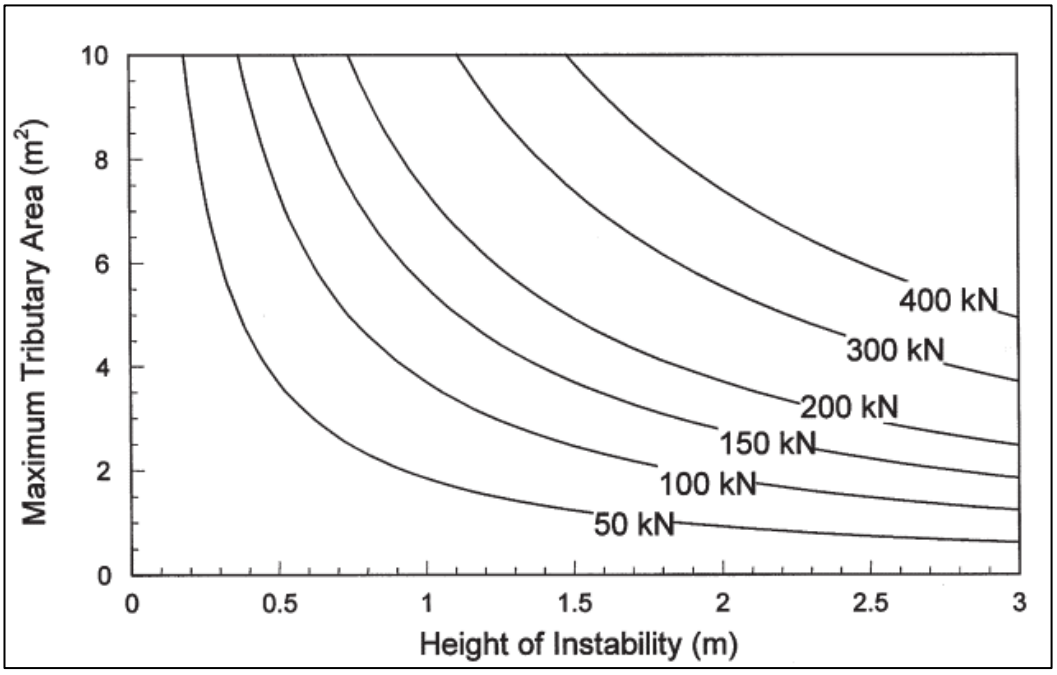


Figure 2-20: Estimation of the tributary area requirements (Daehnke, et al., 2001)

The area supported by individual tendon support units in a support system is known to interact if the units are closely spaced. Tendon support units, therefore, have a zone of influence, which can assist in determining correct and optimum spacing

between units. According to Roberts (1999), the extent of the zone of influence from the side of the support unit typically ranges between 1.0 m to 1.5 m. Daehnke, et al. (2001) proposed Equation 2-29 to determine the extent of the zone of support influence in a homogenous hangingwall beam. Equation 2-29 was derived from Figure 2-21.

$$z = b \tan \varphi \qquad \textit{Equation 2-29}$$

Where: *z* is the lateral extent of the zone of influence measured from the edge of the support unit (m); *b* is the height of the first parting plane in the hangingwall; and ϕ is the friction angle at the parting plane.

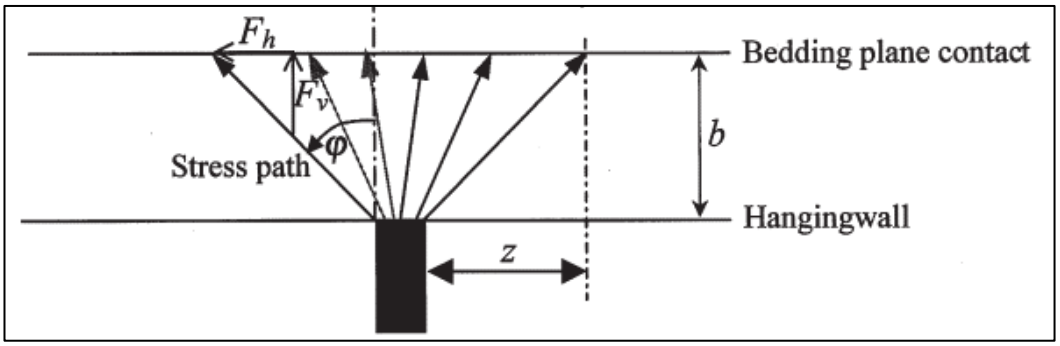


Figure 2-21: Determination of support influence (Daehnke, et al., 2001)

2.9.4 Tendon support length design

Stacey (2001) stated that rockbolts must be at least 0.2 m (critical bond length) longer than the selected fallout thickness to anchor the unstable zone with the competent rock in the hangingwall. Barton and Grimstad (1993) also proposed empirical equations for estimating rockbolt length and support pressure required to maintain stability. The use of empirical equations in tendon support design is suggested before mining commences. Once operations commence, historical FOG data and the height of the vertical tensile stress zone above stope excavations will inform tendon support length design in shallow stopes (O'Ferrall & Malan, 2012).

2.9.5 Different Approaches for Estimation of Support Requirements

The assessment and understanding of different failure modes between pillars eventually inform the determination of the appropriate support systems required to achieve desired stable conditions. Stacey (2001) stated that there are five approaches to the determination of support requirements. These are:

- precedent practice;
- Rock Mass Classification Systems;
- kinematic analysis of keyblocks and wedges,
- support based on stress analysis, and
- support of stratified rock masses.

Precedent Practice - This is a pragmatic approach where support requirements are based on experience or what has worked well in the past. The Trigger Action Response Plan (TARP) system is an example of this approach. The TARP system is a daily risk assessment tool devised to dictate a level of response to adverse geological structures and ground conditions that are commonly encountered in underground workings (Glencore ECM, 2021). It is recommended to always verify if the recommended support capacity is sufficient or if the rock is not overly supported.

Support requirements from Rock Mass Classification - Rock mass classification methods originated in 1879 when Ritter (1879) proposed a formal empirical approach to tunnel design for determining support requirements. Since then, all rock mass classification systems have the capability of providing indications of support requirements. Estimation of support requirements using rock mass classification systems is often conservative since they originated from civil engineering, and they do not consider any mechanism of rock instability (Stacey, 2001). The Q-System by Barton et al. (1974) (provided in Appendix B) is popular for including a tunnel support design chart that provides initial indications of rockbolt specifications (length and spacing). The Barton and Grimstad (1993) tunnel support design chart also provides indications of shotcrete requirements.

Kinematic analysis of Keyblocks and Wedges - Structural stability analyses involve the kinematic evaluation of formed keyblocks and wedges. Computer programs such as Rocscience's UNWEDGE and Jblock are often used to assess

the stability of keyblocks and therefore provide support pressure requirements to ensure stability. Support requirements are therefore informed by the dimensions of the largest identified blocks or wedges (Stacey, 2001). The capabilities of the Jblock software and UNWEDGE programme were discussed in detail in Section 2.8.3. The following factors must be considered in the kinematic analysis:

- geometry of block/wedge;
- size (mass, volume) of the block/wedge;
- factor of safety of keyblocks/wedges;
- capacity of rockbolts or shotcrete;
- support bond length and strength; and
- effect of block rotation.

Support Requirements from Stress Analysis - Stress analysis methods are often employed in conditions which require more specific support design calculations, such as poor ground conditions or larger bord spans (Stacey, 2001). Different commercially available numerical modelling computer programs, such as the Fast Lagrangian Analysis of Continua (FLAC), Rock and Soil 2-dimensional analysis program (RS2), and the Universal Distinct Element Code (UDEC), are often used for conducting stress analysis. Stacey (2001) suggests an in-depth understanding of the limitations and requirements of each numerical program before stability evaluations are conducted. The selection of applicable rock failure criteria is also important in simulating correct stress conditions and carrying out stability evaluations.

FLAC - FLAC is a finite difference method (FDM)-based program developed by ITASCA Software (Hoek, 2007). In rock engineering, FLAC enables users to create detailed models for studying the behaviour of rock and soil under varying loading conditions. FLAC provides the benefit of studying the behaviour of jointed rock masses, simulation and analysis of rock mass response to tunnelling and installation of support in underground excavations (ITASCA Software, 2025). Additionally, the FLAC software enables the modelling of complex rock mass behaviour involving tunnel-rock interaction scenarios consisting of huge geometries and large-strain failure of rock (Chiwaye, 2010).

Limitations of the FLAC program include slower running times for linear (simple) simulations compared to equivalent finite element method software. This is because FLAC is most effective when solving non-linear or large-strain failure of rock problems and scenarios in which the physical instability of rock may occur (Roberts, 2020). Lastly, the FLAC programme may experience efficiency issues when modelling problems involving rock beams modelled as solids rather than structural elements, or problems involving major differences in material properties or element sizes (Roberts, 2020).

RS2 – RS2, formerly called RS^2 or $Phase^2$, is a 2D elasto-plastic finite element analysis (FEA) software for analysing the stability of rock and soil structures (Ayamamani, 2014). RS2 provides capabilities to model and analyse stress distributions and ground deformations around mining excavations for project planning and risk mitigation. RS2 has found application in a wide range of rock engineering projects, including underground excavation design in jointed rock masses, optimisation of rock support systems, groundwater seepage analysis, and probabilistic and dynamic analysis (Rocscience Inc, 2022).

The RS2 program can easily create and analyse multi-stage models or scenarios with complex geometries, boundary or loading conditions, and differences in material properties. RS2 integrates well with the Rock and Soil 3-dimensional analysis program (RS3) for verifying and increasing confidence in results (Rocscience Inc, 2022). RS3 is used for performing 3D stress evaluations of both underground and surface excavations. It is a tradition for geotechnical engineers to analyse problems using the RS2 program to obtain starting insights into a problem and transition to complex 3D analysis (Hammah, 2025). Since real-world rock engineering problems exist in 3D space, Hammah (2025) suggests a change in the traditional workflow paradigm. This is because 2D models often simplify geometric nuances that a 3D analysis can compute easily. RS3 can represent complex rock anisotropic behaviour better than RS2. Lastly, starting with 2D programs such as RS2 can also overestimate or underestimate excavation stability and reinforcement (support) requirements (Hammah, 2025).

UDEC – UDEC is a 2D distinct element method (DEA)-based program developed by ITASCA Software for simulating the behaviour of discontinuous media (such as

jointed rock masses) under quasi-static and dynamic loading (ITASCA Software, 2025). In rock engineering, UDEC is used to analyse and predict the behaviour of rock masses under different loading conditions. Additionally, the program is used for evaluating underground excavation stability, rockfall analysis, and stope stability analysis (ITASCA Software, 2025). The UDEC program provides the benefits of simulating complex rock engineering problems involving large displacements and rotations, modelling problems with multiple discontinuities in the rock mass, and the flexibility of modelling the behaviour of different rock types (Lee, 2025). Limitations of the UDEC program include high computational costs associated with running large-scale models (Lee, 2025). The program also requires high-quality input data, including properties and characteristics of joints for creating reliable models and has limited ability in the simulation of certain types of rock behaviour, such as time-dependent behaviour (Lee, 2025).

Support of stratified rock masses - In Section 2.8.2, the behaviour of stratified rock masses in excavations was described. The stability of stratified rock masses depends on the stability of the hangingwall rock. The rockbolt support employed must therefore be of sufficient length and capacity to achieve the following (Stacey, 2001):

- to suspend unstable to a higher level above the unstable strata; and
- to clamp unstable strata together (using pre-stressed tendons) to form a composite voussoir beam.

2.10 Monitoring of Underground Excavations

Monitoring is an important observational design method implemented to give early warning of unexpected or excessive rock mass deformations. It is used to verify the validity of assumptions used in initial designs and monitor support performance (Jager & Ryder, 1999). The initial design is then progressively modified towards an optimal solution that suits the actual observed conditions (Spross, 2016). Monitoring, therefore, ensures the construction of sustainable underground structures in rock (Spross, 2016).

The closure of stope excavations is monitored using closure-ride stations and closure meters (Malan, et al., 2007). Extensometers are used to measure the opening of rock mass discontinuities, which indicate signs of deformation or displacement occurring in the hangingwall strata (Shacker, 2019). The extent of fracturing and position of weak planes in the rock mass is monitored with instruments such as borehole cameras, Ground Penetrating Radar (GPR), and borehole petroscopes (Jager & Ryder, 2002). The load in tendon support units is measured using Tendon load cells (Jager & Ryder, 2002).

2.11 Summary of Chapter

The review of the literature indicated that the safe creation of underground structures should be informed by an in-depth understanding of the rock mass structure in a mining environment. Therefore, acquiring reliable geotechnical data which characterize the jointed rock mass is an important stage in the design process. The methodology proposed by the MHSC utilizes a combination of different rock engineering design methods, such as empirical, analytical, and observational methods, to obtain the best possible design (Murphy, et al., 2016). It is vital to evaluate all failure modes in the design of underground excavations. This will inform the determination of optimum support systems required to achieve stability. Chapter 3 describes the geotechnical investigation performed at Thorncliffe Mine. It includes scanline mapping and geo-mechanical laboratory testing.

3 GEOTECHNICAL INVESTIGATION

Chapter 2 reviewed different rock engineering methods for evaluating the stability of underground excavations in shallow mining conditions. The MHSC holistic methodology for the design of stable bord spans and determination of support requirements was also discussed in detail. A major highlight was that the rock mass structure controls the stability or instability around underground excavations at the depth of Thorncliffe Mine. Additionally, the literature study outlined that a proper quantitative description of the rock mass structure depends on a thorough geotechnical investigation. This chapter presents the geotechnical investigation undertaken at Thorncliffe Mine. Critical parameters that adequately describe and quantify the geotechnical character of the rock mass were collected.

3.1 Scanline Mapping of Hangingwall and Sidewall

Thorncliffe mine is currently mining five 'ore blocks' or 'rig sections' for the extraction of the MG1 Chromitite orebody. A mechanised bord and pillar mining method is being used. Figure 3-1 shows the current five ore mining blocks. Three production sections, RIG 47, RIG 50, and TC1, are mining towards the South-strike direction. The declines (development in TC1) are advancing downdip to the west of the orebody, whilst the remaining two sections, RIG 2 and RIG 14, are both mining towards the North strike direction. The orientation of production panels in each mining section is summarised in Table 3-1.

Table 3-1: Orientation of bords (strike direction) and splits (dip direction) in the five production sections

Mining Section	Strike Direction (°) (North-South)	Dip Direction (°) (East-West)	Average Dip HW (°)
RIG 47	167	271	9
RIG 50	170	274	9
TC1	306	269	7
RIG 2	309	267	8
RIG 14	329	274	7

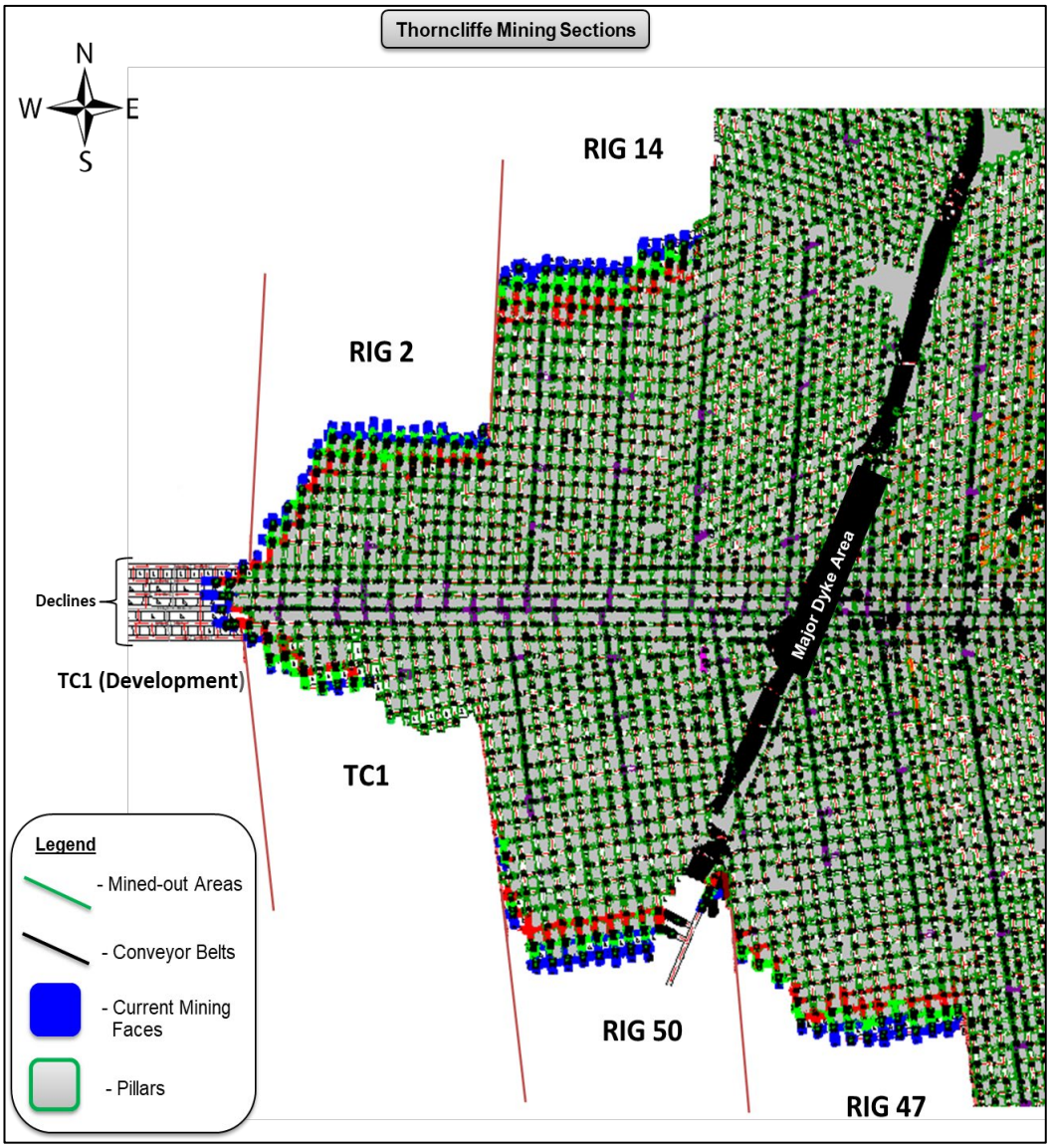


Figure 3-1: Thorncliffe Mining Sections (not to scale)

To cover all ground conditions likely to be encountered at the mine, geotechnical data gathering was conducted in all the current production sections. Since exposed hangingwall and pillar rock surfaces were available in the stopes, the 'Scanline Mapping' technique described in Section 2.4.1 was used for the collection of geotechnical data. It was necessary to geotechnically map both the hangingwall (Pyroxenite rock) and pillars (MG1 Chromitite layer) since there are disseminated Chromitite seams in the hangingwall. The properties of both geotechnical domains informed the design of safe stope excavations and the determination of support

requirements. Geotechnical mapping of underground workings was performed between February and April 2022.

Scanline surveys involved extending a 20 m long measuring tape (the scanline) across exposed hangingwall and sidewall rock surfaces. All the geological structures that intersected the scanline along its length were mapped. The ten properties (described in Section 2.3) of all natural discontinuities were recorded. This enabled the quantitative description of the rock mass structure in the mine, which will be discussed in Chapter 4. Approximately 1500 m of combined scanline mapping data was collected from the underground mining sections. *Table 3-2* presents the total metres mapped in the hangingwall and sidewall of each mining section.

Table 3-2: Meters mapped per mining section

Mining Section	Metres mapped per section (m)	
	Hangingwall (Pyroxenite rock)	Sidewall (MG1 Chromitite Layer)
1. RIG 47	162	186
2. RIG 50	173	115
3. TC1 (Including Declines)	145	122
4. RIG 2	166	164
5. RIG 14	120	120
Total metres mapped	**766**	**707**

In the mining sections shown in Figure 3-1, hangingwall and sidewall scanline mapping was conducted in two directions, along strike (North-South direction), and along dip (East-West direction). The mapping was conducted close to the advancing faces as the back areas were supported and sprayed with 50 mm-thick shotcrete. Accurate discontinuity orientation data (dip and dip direction) for each scanline were acquired using the GeoID tool. GeoID is an advanced professional tool with a built-in geological compass and a clinometer for accurately measuring and analysing geological structures. Efforts were made to take pictures of the scanline mapping set-up underground, but due to poor visibility in the underground workings, the pictures are of poor quality and cannot be included in this report. An example of the scanline mapping sheet used is provided in *Table 3-3*. All the scanline mapping data sheets for each production section are attached in Appendix C.

Table 3-3: Example of a scanline mapping sheet used in collecting geotechnical data



ROCK MASS SCANLINE MAPPING SHEET

ProJointect name:	Scanline Mapping	Shaft:	THORNCLIFFE MINE
Mapping area:	RIG2 Str13 HW on Dip	Mapped	A.Khoza & R.Mashige
Scanline orientation :	07/265	Date:	17/03/2022

Excavation width (m)	Excavation Height (m)	Rock type	Structures intersected along scanline	Structure intersected at (m)	Dip (°)	Dip direction (°)	Persistence (length) (m)	Hardness	Roughness	Infilling type	Infilling thickness	F (Joint Infill)	Weathering	Water Condition	End	Comment
7.3	2.4	Pyroxenite	Joint	0.22	88	218	4	4	3	-	-	-	1	W1	E2	Location: G8618 - 10m (Going Updip)
		Pyroxenite	Joint	1.00	76	233	4	4	3	-	-	-	1	W1	E2	
		Pyroxenite	Joint	1.00	75	250	4	4	3	-	-	-	1	W1	E2	
		Pyroxenite	Joint	1.42	81	248	4	4	3	-	-	-	1	W1	E2	
		Pyroxenite	Joint	2.00	78	232	4	4	3	-	-	-	1	W1	E2	
		Pyroxenite	Pegmatite Vein	2.25	83	114	3	4	2	Serp,Cal,Mica	3	6	1	W1	E0	
		Pyroxenite	Joint	2.25	81	136	4	4	2	Serp	1	7	1	W1	E2	
		Pyroxenite	Joint	3.12	74	126	3	4	2	Serp	2	7	1	W1	E2	
		Pyroxenite	Pegmatite Vein	3.56	88	143	4	4	2	Serp,Cal,Mica	2	6	1	W1	E2	
		Pyroxenite	Joint	4.26	78	145	3	4	3	-	-	-	1	W1	E0	
		Pyroxenite	Joint	4.64	88	120	3	4	3	-	-	-	1	W1	E0	
		Pyroxenite	Joint	5.00	86	139	3	4	3	-	-	-	1	W1	E0	
		Pyroxenite	Joint	5.61	88	318	3	4	2	-	-	-	1	W1	E2	
		Pyroxenite	Joint	6.39	84	138	3	4	2	Serp	1	7	1	W1	E2	
		Pyroxenite	Joint	7.00	87	037	3	4	2	Serp	1		1	W1	E0	
		Pyroxenite	Joint	7.59	81	226	4	4	2	Serp	1	7	1	W1	E2	
		Pyroxenite	Joint	7.59	89	122	3	4	2	Serp	1	7	1	W1	E2	
		Pyroxenite	Pegmatite Vein	8.15	87	116	3	4	2	Serp,Cal,Mica	3	6	1	W1	E2	
		Pyroxenite	Joint	8.82	87	312	3	4	2	Serp	1	7	1	W1	E0	
		Pyroxenite	Joint	9.00	75	211	3	4	2	Serp	1	7	1	W1	E2	
		Pyroxenite	Pegmatite Vein	10.69	85	300	3	4	2	Serp,Cal,Mica	3	6	1	W1	E2	
		Pyroxenite	Joint	10.69	85	227	3	4	2	Serp	2	7	1	W1	E0	

Joint Roughness (R)	
1	Planar Slickensided
2	Planar Smooth
3	Planar Rough
4	Undulating Slickensided
5	Undulating Smooth
6	Undulating Rough
7	Stepped Slickensided
8	Stepped Smooth
9	Stepped Rough

Joint Infill (F)	
1	No Infill
2	Non-softening coarse
3	Non-softening medium
4	Non-softening fine
5	Soft sheared coarse
6	Soft sheared medium
7	Soft sheared fine
8	Gouge thickness < irregularities
9	Gouge thickness > irregularities

Weathering	
1	Unweathered
2	Slightly weathered
3	Moderately weathered
4	Highly weathered
5	Decomposed

Hardness (Strength)	
M	Extremely weak
R0	Very weak
R1	Weak
R2	Medium Strong
R3	Strong
R4	Very Strong
R5	Extremely Strong

Water Condition	
W1	Completely Dry
W2	Damp
W3	Wet
W4	Dripping
W5	Flowing

Infill Thickness (mm)	
0	Tight
1	< 1mm
2	1 - 3 mm
3	3 mm - 10 mm
4	10 - 30 mm
5	> 30 mm

End	
E0	One end visible
E1	Both ends visible
E2	Both ends not visible

Discontinuity Length (m)	
1	<1 m
2	1 - 3 m
3	3 - 10 m
4	10 - 30 m
5	>30 m

The scanline mapping sheet in Table 3-3 comprises the critical parameters selected by the ISRM (1978c) to adequately characterise the discontinuous rock mass at Thorncliffe Mine. These parameters were described in Section 2.3.

3.2 Laboratory Testing of Rock Material

The geotechnical investigation undertaken in 2022 for this research included the laboratory compressive testing of rock samples. The results of these geo-mechanical tests were added to an existing database on the mine. The final database consisted of Pyroxenite and Chromitite rock materials tested as follows:

- UCS test with Elastic Modulus and Poisson's Ratio (UCM); and
- TCS tests.

Tensile tests are important to tie down the characterisation study; however, tensile tests were not done due to budget constraints at the mine. Table 3-4 summarises the number of laboratory tests conducted. The derivation of important rock strength parameters for design purposes from the rock test results is discussed in Chapter 4. All rock test results are attached in Appendix C.

Table 3-4: Summary of laboratory tests conducted

Test	Pyroxenite	Chromitite
UCM	20	13
TCS	6 (1 Set)	-

3.3 Summary of Chapter

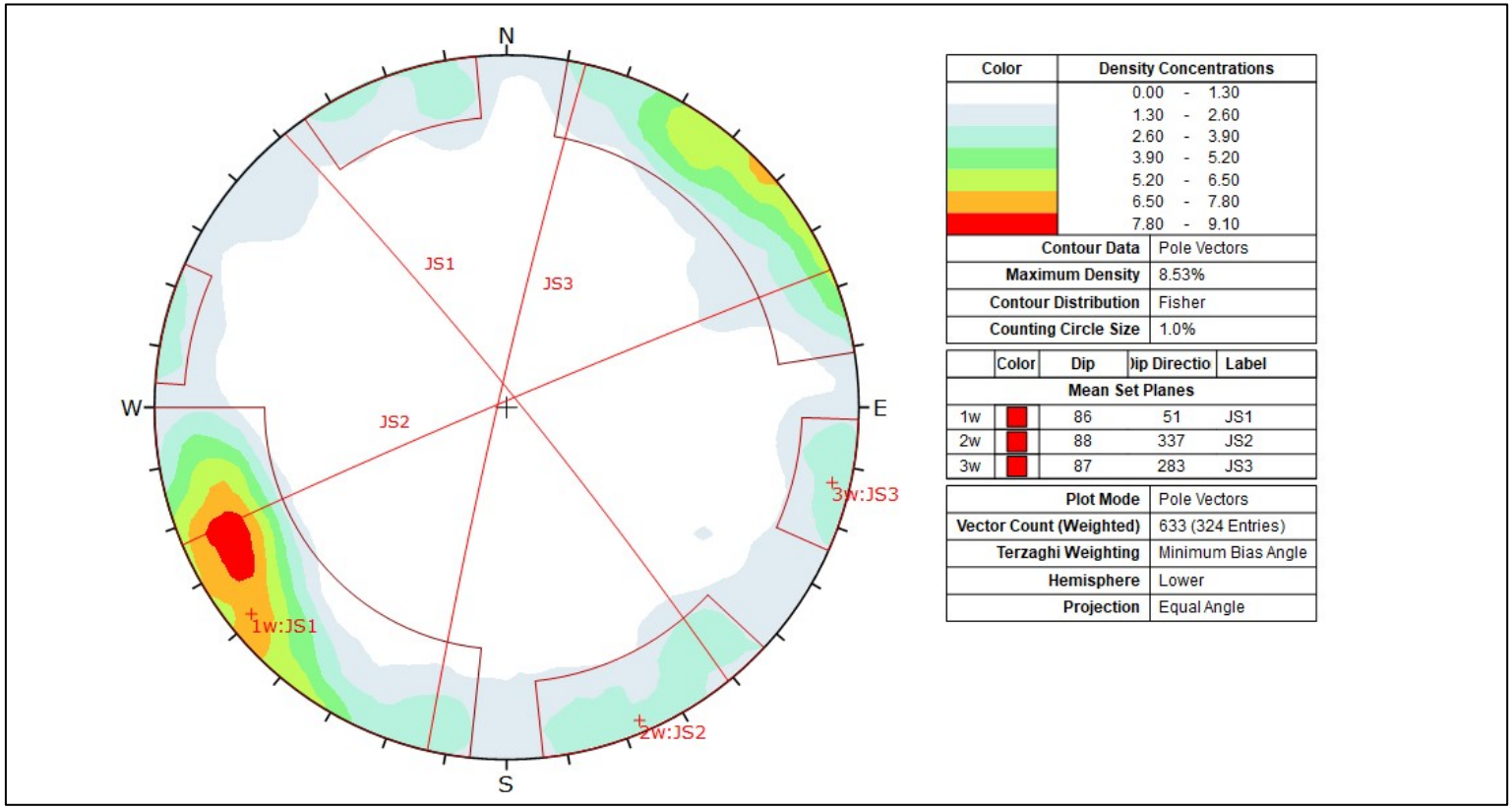
The geotechnical investigation undertaken at Thorncliffe Mine consisted of scanline mapping and laboratory rock tests which captured parameters that adequately describe the variability of the local discontinuous rock mass. The geotechnical data will be used to quantitatively describe characteristics of the rock mass and inform the design of maximum stable bord spans and support requirements. The next chapter focuses on presenting characterization results of the underground workings.

4 ROCK MASS CHARACTERIZATION

Chapter 3 outlined the geotechnical investigation undertaken at the mine. This Chapter presents the rock mass characterisation results, which involved using the acquired geotechnical data to characterise the jointed underground rock mass at Thorncliffe Mine. Discontinuity types, orientation, spacing and interface properties have a direct influence on the stability of the rock mass surrounding stope excavations, and the properties of support selected to maintain stability. The characterisation exercise focused on the MG1 immediate hangingwall rock mass (Pyroxenite rock). The only Chromitite layer characterisation results included were those used for comparison and/or deemed necessary to serve as input parameters in the numerical stability analyses of stope excavations.

4.1 Orientation of Discontinuities

All recorded hangingwall discontinuities were analysed using the Rocscience software 'Dips' to produce stereonet contour plots for identifying major discontinuity sets in each of the five (5) mining sections. The modelling in Dips enabled the identification of major discontinuity sets by using orientation data (both dip directions and dip angles) of the discontinuities to plot great circles of planes of weakness. Figure 4-1 shows an example of the results of contour plots in Dips with the identified major discontinuity planes in the hangingwall of the Rig 47 production section. The contour plots showing individual discontinuity sets in all the mining sections are provided in Appendix D.



Color	Density Concentrations
	0.00 - 1.30
	1.30 - 2.60
	2.60 - 3.90
	3.90 - 5.20
	5.20 - 6.50
	6.50 - 7.80
	7.80 - 9.10
Contour Data	Pole Vectors
Maximum Density	8.53%
Contour Distribution	Fisher
Counting Circle Size	1.0%

	Color	Dip	Dip Directio	Label
Mean Set Planes				
1w		86	51	JS1
2w		88	337	JS2
3w		87	283	JS3

Plot Mode	Pole Vectors
Vector Count (Weighted)	633 (324 Entries)
Terzaghi Weighting	Minimum Bias Angle
Hemisphere	Lower
Projection	Equal Angle

Figure 4-1: Example contour plot showing major discontinuity sets

Table 4-1 summarises the major discontinuity sets identified in each mining section. Colour coding was used to indicate the strike direction of the discontinuity sets. Discontinuity sets trending in a similar direction in the different production sections have the same colour code in the 'Strike Direction' column.

Table 4-1: Major discontinuity sets identified in each mining section

Notes	Ore production block	Discontinuity Set (JS)	Average Dip (°)	Average Dip Direction (°)	Strike Direction	Possibility of unstable wedge (s) forming
Production sections mining towards the South direction	RIG 47	JS1	86	051	NE - SW	Yes
		JS2	88	337	SSE - NNW	
		JS3	87	283	ESE - WNW	
	RIG 50	JS1	87	258	ENE - WSW	Yes
		JS2	85	030	NNE - SSW	
		JS3	87	351	SSE - NNW	
		JS4	88	124	SE - NW	
		JS5	62	215	NE - SW	
	TC1	JS1	87	299	ESE - WNW	Yes
		JS2	85	219	NE - SW	
		JS3	90	342	SSE - NNW	
Production sections mining towards the North direction	RIG 2	JS1	89	226	NE - SW	No
		JS2	87	124	SE - NW	
	RIG 14	JS1	89	054	NE - SW	No
		JS2	89	160	SSE - NNW	

As summarised in Table 4 1, the stereonet plots (provided in Appendix D) enabled a preliminary assessment of stability in each mining block. It was observed that the three sections mining towards the South direction (RIG 47, RIG 50, and TC1) consisted of the intersection of three or more major discontinuity sets, which was an indication that there are potentially unstable blocks (keyblocks), according to the block theory by Goodman & Shi (1985). The two sections mining towards the North direction both indicated an intersection of less than three major discontinuity sets, which indicated the probability of fewer instabilities occurring.

Additionally, the geometry of the potentially unstable wedges was analysed. The area defined by the great circles of intersecting major planes in each mining section is small (Appendix D). This was an early indication that the size of the keyblocks forming from the spatial distribution and interaction of discontinuities in the mining sections is small. It was only in the Rig 50 mining block, which is comprised of more discontinuity sets than any other mining section, where a larger intersection area was defined, which indicated the existence of larger keyblocks. In Figure 4-2, a compass rose (showing both cardinal and intercardinal directions) was included to enable the tracing of the trend or strike directions of the major discontinuity sets in each mining section.

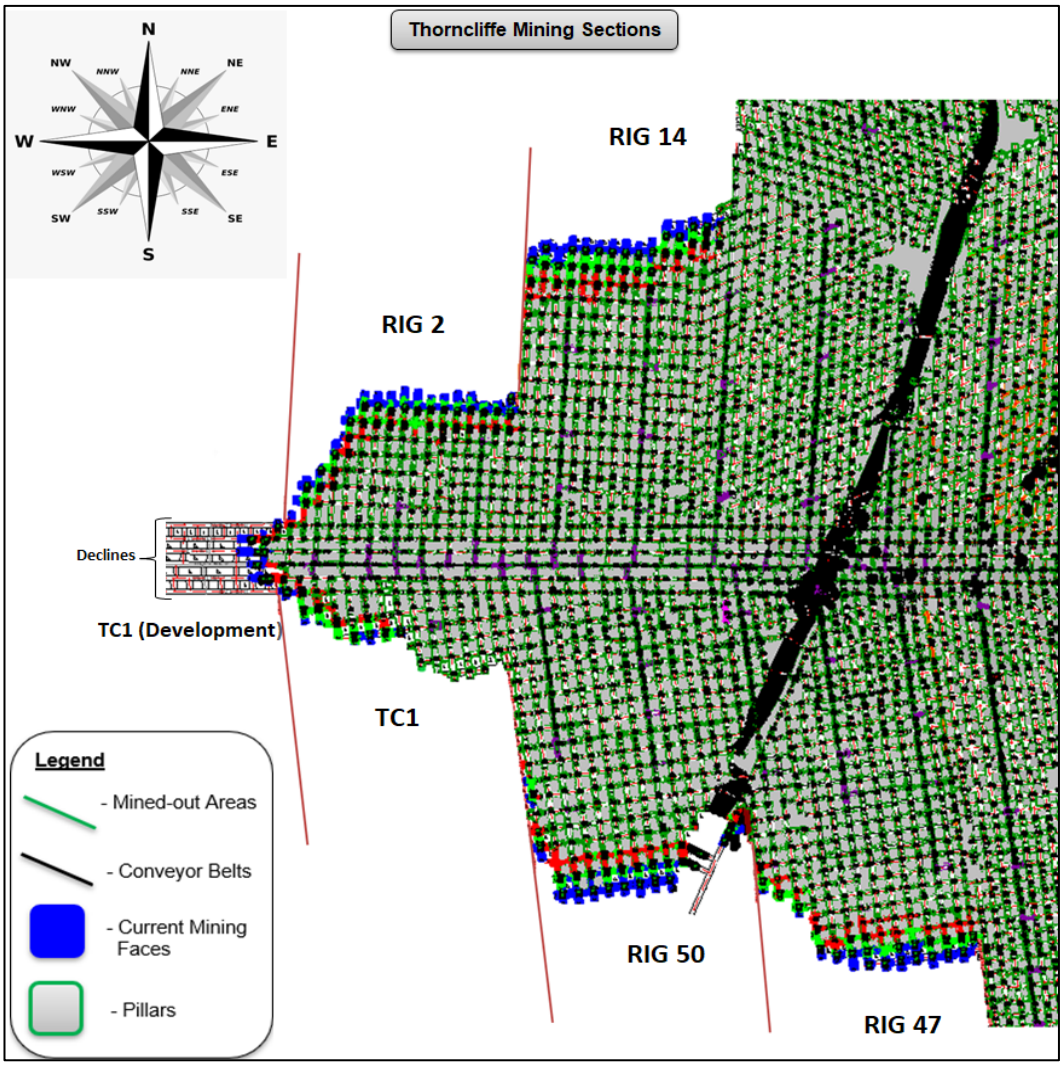


Figure 4-2: Thorncliffe Mining sections with a compass showing all discontinuity directions (not to scale)

In-depth structural stability analyses, which consider the frictional characteristics of the discontinuities in each section, will be discussed in detail in Chapter 5. The actual size (face area, mass, and volume) of the hangingwall wedges, maximum possible wedge dimensions, and the potential wedge failure modes (sliding failure or gravity falls) will be discussed in Chapter 5.

4.2 Discontinuity Properties

In-depth characterisation was conducted from the acquired geotechnical mapping data to quantify and describe the properties of major discontinuity sets in each

mining section. In addition to the identified major discontinuity sets, each production section consisted of 'random' discontinuities, which are discontinuities that are 'scattered' throughout the mine and do not form part of any discontinuity set. The intersection of major discontinuity sets and random discontinuities can also result in instabilities in the mine.

The frequency of jointing in the rock mass influences tunnel stability. The spacing of the hangingwall discontinuities in each discontinuity set was therefore quantified in the different production sections. The statistical analysis of the true (or actual) discontinuity spacing in each discontinuity set in each section was also computed in the Dips Software. The charts which provide the statistical analysis of the true spacing of discontinuities in each discontinuity set are provided in Appendix D.

Descriptions of the geotechnical properties of the major discontinuity sets are provided for all the various mining sections in *Table 4-2* to Table *4-11*. Bar graphs and tables, which quantify and contrast the properties of discontinuity sets and the random discontinuities in each mining section, are attached in Appendix D.

RIG 47 Discontinuity Properties

Table 4-2: Summary of Rig 47 hangingwall discontinuity sets

RIG 47 HW Discontinuity Sets				
Discontinuity Set	JS1	JS2	JS3	Random Discontinuities
Discontinuity Count	145	48	20	111
Total Recorded Discontinuities	324	324	324	324
Percentage (%)	45%	15%	6%	34%

Table 4-3: Properties of Rig 47 hangingwall discontinuity sets

Rig 47 Discontinuity Properties			
Joint Set (JS)	**Average Dip (°)**	**Average Dip Direction (°)**	**Description of Discontinuity Properties**
JS1	86	051	JS1 discontinuities are steeply dipping (near-vertical) and trending in a similar NE-SW direction as JS5 discontinuities in Rig 47, JS2 in TC1, and JS1 in both Rig 2 and Rig 14. Majority of these discontinuities have planar rough surfaces with few discontinuities having planar smooth surfaces. All recorded discontinuties have no rust staining along joint walls and have natural dry surfaces. The discontinuities have an average true spacing of 0.45 m. Serpentine infill materiall was recorded in most of the discontinuities while others had no infill material. An equal number of discontinuties having <1 mm and 3 - 10 mm infill thicknesses were recorded. Majority of JS1 discontinuities are prominent joints with one end visible to both ends not visible and have trace lenghs of approximately 3 - 10 m. There is only few discontinuities with both ends visible (1 - 3 m trace lengths). Lastly, JS1 discontiniuties consist mainly of joints, shear zones, joint zones, and few pegmatite veins).
JS2	88	337	The steeply dipping JS2 discontinuties are trending in the SSE-NNW direction, and have an average true spacing of 1.5 m. The discontinuities are trending in a similar direction as JS3 discontinuities in both Rig 50 and TC1, and JS2 in Rig 14. These discontinuities consist of a majority of planar rough surfaces, with few undulating rough and planar smooth surfaces recorded. No surface weathering and groundwater was recorded for JS2 discontinuities. Most of the recorded discontinuities have serpentine infill material and only a few have no infill material. Similarly to JS1, an equal number of JS2 discontinuties having <1 mm and 3 - 10 mm infill thicknesses were recorded. Majority of JS2 discontinuities have trace lenghs of approximately 3 - 10 m (with both ends not visible) and only few joints having one end or both ends visible (1 - 3 m trace lengths). JS2 discontiniuties also consist mainly of prominent joints, few shear zones and pegmatite veins).
JS3	87	283	JS3 discontinuities are steeply dipping and trending in the ESE-WNW direction, which is a similar trend direction as JS1 discontinuities in TC1. JS3 discontinuties have a wider average true spacing of 2.2 m. These discontinuities consist mainly of planar rough surfaces, with a few planar smooth surfaces; and have dry unweathered walls/surfaces. An equal number of discontinuties consisting of <1 mm and 3 - 10 mm serpentine infill material were recorded while few discontinuities are tight with no infill material. Generally, JS3 discontinuities have tracelengths of approximately 3 - 10 m (ends not visible) with few joints having 1 - 3 m tracelenghs (one or both ends visible). This set consists mainly of joints, Shear Zones, and few pegmatite veins containing serpentine, calcite and mica infill material at the same time.
Random discontinuities	Rig 47 hanging wall has random discontinuities with different orientations which consist mainly of low angle joints, prominent joints, and few pegmatite veins. Generally, these random discontinuities consist of both planar rough and planar smooth surfaces, and have unweathered dry walls. Majority of these discontinuities have 3 - 10 mm serpentine infill material, with few discontinuities containing no infill material. These random discontinuities have varying trace lengths of between <1 m to >30 m.		

RIG 50 Discontinuity Properties

Table 4-4: Summary of Rig 50 hangingwall discontinuity sets

RIG 50 HW						
Discontinuity Set	JS1	JS2	JS3	JS4	JS5	Random Discontinuities
Discontinuity Count	107	65	48	42	12	77
Total Recorded Discontinuities	351	351	351	351	351	351
Percentage (%)	30%	19%	14%	12%	3%	22%

Table 4-5: Properties of Rig 50 hangingwall discontinuity sets

Rig 50 Discontinuity Properties			
Joint Set (JS)	**Average Dip (°)**	**Average Dip Direction (°)**	**Description of Discontinuity Properties**
JS1	87	258	In Rig 50, the steeply dipping JS1 discontinuities are trending in the ENE-WSW direction and have an average true spacing of 0.71 m. Majority of these discontinuities have planar smooth surfaces with few discontinuities having planar and undulating rough surfaces. No rust staining along joint walls and no wet surfaces were recorded. Most JS1 discontinuities have serpentine infill materiall while few discontinuities have no infill material. All pegmatite veins recorded are comprised of a combination of serpentine, calcite, and mica infill materials. Almost an equal number of JS1 discontinuties with infill thickness of <1 mm and 1 - 3 mm infill thickness were recorded. The recorded Pegmatite veins generally have a 3 - 10 mm to 10 - 30 mm infill thickness. Majority of JS1 discontinuities were prominent joints and have trace lengths of approximately 3 - 10 m (both ends not visible) with few joints having one end or both ends visible (1 - 3m trace lengths). The pegmatite veins are quite prominent with trace lengths of approximately 10 - 30 m. JS1 discontiniuties consist mainly of joints, low angle joints, pegmatite veins, and the only set comprised of shear zones in Rig 50.
JS2	85	030	JS2 discontinuties are steeply dipping and trending in the NNE-SSW direction. These discontinuities have an average true spacing of 0.93 m. JS2 discontinuities consist of mainly planar smooth surfaces, with few planar to undulating rough discontinuities. The discontinuity walls show no evidence of weathering and no groundwater was recorded for JS2 discontinuities. Majority of the discontinuities have serpentine infill material with thicknesses of <1 mm to 1 - 3 mm, while the pegmatite veins consist of serpentine, calcite and mica infill material with thicknesses of 3 - 10 mm. Majority of JS2 discontinuities have trace lenghs of approximately 3 - 10 m (with both ends not visible) and only few joints having one end or both ends visible (1 - 3 m trace lengths). JS2 discontiniuties consist mainly of prominent joints, and prominent pegmatite veins (10 - 30 m trace length).
JS3	87	351	JS3 discontinuities in Rig 50 are steeply dipping and trending in the SSE-NNW direction, a similar trend direction as Rig 47 JS2 discontinuities, JS3 discontinuities in TC1, and JS2 discontinuities in Rig14. JS3 discontinuities have an average true spacing of 0.92 m. These discontinuities consist mainly of smooth (planar and undulating) discontinuities and few planar rough surfaces. These discontinuities have dry unweathered walls/surfaces. JS3 discontinuities consist of mainly <1 mm serpentine infill material, with only a few discontinuities having serpentine infill material of 1 - 3 mm in thickness. The pegmatite veins contain 3 - 10 mm to 10 - 30 mm infill material (serpentine, calcite, and mica), while few discontinuities are tight with no infill material. JS3 discontinuities have tracelengths of approximately 3 - 10 m (ends not visible) with few joints having 1 - 3 m tracelenghs (one or both ends visible). The pegmatite veins are prominent with trace lengths of approximately 10 -30 m. This set consists mainly of joints and few pegmatite veins.
JS4	88	124	JS4 discontinuities are steeply dipping and trending in the SE-NW direction, a similar trend direction as JS2 discontinuities in Rig2. These discontinuities have an average true spacing of 1.4 m. JS4 discontinuities consist mainly of planar smooth discontinuities and few planar/undulating rough surfaces. The discontinuities have unweathered surfaces and have no groundwater. The prominent joints in JS4 consists of <1 mm and 1 - 3 mm serpentine infill material. The pegmatite veins contain 10 - 30 mm and 3 - 10 mm infill material (serpentine, calcite, and mica), while few discontinuities are tight with no infill material. JS4 discontinuities have tracelengths of approximately 3 - 10 m (ends not visible) with joints having 1 - 3 m tracelenghs (one or both ends visible). The pegmatite veins are prominent with trace lengths of approximately 10 - 30 m. This set also consists mainly of joints and pegmatite veins.

Table 4-5: Properties of Rig 50 hangingwall discontinuity sets continued

Rig 50 Discontinuity Properties			
Joint Set (JS)	**Average Dip (°)**	**Average Dip Direction (°)**	**Description of Discontinuity Properties**
JS5	62	215	In Rig 50, a fifth discontinuity set (JS5) consiting of low angle (dip) discontinuities trending in the NE-SW direction was identified. This set of discontinuitites is trending in the same direction as JS1 in Rig 47, JS2 in TC1, JS1 in Rig 2, and JS1 in Rig 14. JS5 discontinuities measured an average true spacing of 0.68 m. This set of discontinuities also consists mainly of planar smooth discontinuities and a few planar rough surfaces. The discontinuities have unweathered surfaces and have no groundwater. These prominent joints in JS5 consists of mainly 1 - 3 mm and <1 mm thick serpentine infill material. No pegmatiite veins were identified in this set. JS5 discontinuities have tracelengths of approximately 3 - 10 m with both ends not visible, and a few joints having 1 - 3 m tracelengths (one or both ends visible). This set consists mainly of joints.
Random discontinuities	Rig 50 hanging wall also consist of random discontinuities with different orientations which consist mainly of prominent joints, few low angle joints, and pegmatite veins. These random discontinuities consist of both planar smooth and planar srough surfaces, and have unweathered dry walls. The prominent joints have 1- 3 mm and 3 - 10 mm thick serpentine infill material, while the pegmatite veins have at-most 10 - 30 mm thick infill material (serpentine, mica and calcite), with few discontinuities containing no infill material. Rig 50 random discontinuities have varying trace lengths from 1 - 3 m to >30 m.		

TC1 Discontinuity Properties

Table 4-6: Summary of TC1 hangingwall discontinuity sets

TC1 HW Discontinuity Sets				
Discontinuity Set	JS1	JS2	JS3	Random Discontinuities
Discontinuity Count	69	89	28	75
Total Recorded Discontinuities	261	261	261	261
Percentage (%)	26%	34%	11%	29%

Table 4-7: Properties of TC1 hangingwall discontinuity sets

TC1 Discontinuity Properties			
Joint Set (JS)	**Average Dip (°)**	**Average Dip Direction (°)**	**Description of Discontinuity Properties**
JS1	88	299	In TC1 mining section, JS1 discontinuities are trending in a similar ESE-WNW direction as JS3 discontinuities in Rig 47 and are steeply dipping. These discontinuities have an average true spacing of 1.3 m. Almost an equal number of JS1 discontinuities with planar smooth and planar rough surfaces were recorded. These discontinuities have fresh joint walls (unweathered) and dry surfaces. JS1 discontinuities consist mainly of serpentine infill materiall with few discontinuities containing no infill material was. Only the pegmatite veins consist of a combination of serpentine, calcite, and mica infill materials. Majority of JS1 discontinuties are joints with an infill thickness of <1 mm, followed by discontinuties with a 1 - 3 mm infill thickness. JS1 pegmatite veins generally have an infill thickness ranging from 3 - 10 mm to 10 - 30 mm or >30 mm. The prominent joints have trace lenghs of approximately 3 - 10 m (both ends not visible) with few joints having one end or both ends visible (1 - 3 m trace lengths). The pegmatite veins are quite prominent with trace lengths of approximately 10 - 30 m or >30 m. JS1 discontiniuties consist mainly of prominent joints and pegmatite veins.
JS2	85	219	TC1 JS2 discontinuties are trending in a similar NE-SW direction as JS1 discontinuities in Rig 47, Rig 2, and Rig 14; and JS5 in Rig 50. These discontinuities are steeply dipping and have an average true spacing of 0.46 m. JS2 discontinuities consist of mostly planar smooth and a few planar rough surfaces. The discontinuities have unweathered walls and no groundwater along the surfaces was recorded. JS1 discontinuities consist of serpentine infill materiall while almost an equal number of discontinuities with no infill material was recorded in this section. The pegmatite veins recorded have serpentine, calcite, and mica infill materials with thicknesses of 3 - 10 mm. Majority of JS2 discontinuities have trace lenghs of approximately 3 - 10 m (with both ends not visible) and only few joints having one end or both ends visible (1 - 3 m trace lengths). JS2 discontiniuties consist mainly of prominent joints, and a few prominent pegmatite veins (10 - 30 m trace length).
JS3	90	342	JS3 discontinuities in TC1 are steeply dipping and trending in a similar SSE-NNW direction as JS2 discontinuities in both Rig 47 and Rig 14; and JS3 in Rig 50. These discontinuities have an average true spacing of 1.1 m. JS3 discontinuities consist of mostly planar smooth surfaces and a few planar rough surfaces. These discontinuities have dry unweathered walls/surfaces. More JS3 discontinuities with no serpentine infill materiall were recorded than discontinuities with serpentine infill material. The infill thickness of the prominent joints with serpentine material is <1 mm. The pegmatite veins contain 3 - 10 mm thick infill material (serpentine, calcite, and mica). JS3 discontinuities have tracelengths of approximately 3 - 10 m (ends not visible) with joints having 1 - 3 m tracelenghs (one or both ends visible). The pegmatite veins are prominent with trace lengths of approximately 10 - 30 m. This set consists mainly of joints and few pegmatite veins.
Random discontinuities	The random discontinuities in TC1 hangingwall consist of prominent joints, low angle joints, and pegmatite veins. These random discontinuities are mainly planar smooth have few planar rough surfaces. These discontinuities have unweathered dry walls. The prominent joints have <1 mm, 1 - 3 mm, and 3 - 10 mm thick serpentine infill material, while the pegmatite veins have at-most 10 - 30 mm thick infill material (serpentine, mica and calcite), with few discontinuities containing no infill material. Most TC1 random discontinuities have trace lengths of 3 - 10 m, while the pegmatite veins have trace lengths of 10 - 30 m.		

RIG 2 Discontinuity Properties

Table 4-8: Summary of Rig 2 hangingwall discontinuity sets

RIG 2 HW Discontinuity Sets			
Discontinuity Set	JS1	JS2	Random Discontinuities
Discontinuity Count	241	79	139
Total Recorded Discontinuities	459	459	459
Percentage (%)	53%	17%	30%

Table 4-9: Properties of Rig 2 hangingwall discontinuity sets

RIG 2 Discontinuity Properties			
Joint Set (JS)	**Average Dip (°)**	**Average Dip Direction (°)**	**Description of Discontinuity Properties**
JS1	89	226	While most of the adverse geological features were recorded in Rig 2, only two discontinuity sets were determined. Rig 2 JS1 discontinuities consist mainly of prominent joints, joint zones, pegmatite veins and shear zones. These discontinuities are trending in a similar NE-SW direction as JS1 discontinuities in both Rig 47 and Rig 14; and JS2 in TC1. These discontinuities are steeply dipping and have an average true spacing of 0.31 m. JS1 discontinuities consist of mainly planar smooth surfaces with few planar rough surfaces. These discontinuities have fresh joint walls (unweathered) and dry surfaces. Majority of JS1 discontinuities are joints with an infill thickness of <1 mm, and also have few discontinuties with a 1 - 3 mm infill thickness. JS1 pegmatite veins generally have an infill thickness of 10 - 30 mm. Prominent discontinuities in this set have trace lengths of approximately 3 - 10 m (both ends not visible) with few joints having one end or both ends visible (1 - 3 m trace lengths). The pegmatite veins are prominent with trace lengths of approximately 10 - 30 m.
JS2	87	124	Rig 2 JS2 discontinuties are trending in a similar SE-NW direction as JS4 discontinuities in Rig 50, and are steeply dipping. These discontinuities also consist of prominent joints, joint zones, pegmatite veins and shear zones. This discontinuity set has an average true spacing of 0.88 m. JS2 discontinuities consist mainly of planar smooth surfaces with a few planar rough surfaces. The discontinuity set surfaces are unweathered and no groundwater along the surfaces was recorded. Majority of JS2 discontinuities consist of <1 mm to 1 - 3 mm serpentine infill materiall while only a few discontinuities have no infill material. The pegmatite veins recorded have serpentine, calcite, and mica infill materials with thicknesses of 3 - 10 mm and 10 - 30 mm. Majority of JS2 discontinuities have trace lengths of approximately 3 - 10 m (with both ends not visible) and only few joints having one end or both ends visible (1 - 3 m trace lengths). JS2 discontiniuties prominent pegmatite veins have trace lengths of approximately 10 - 30 m with both ends not visible.
Random discontinuities	Rig 2 hangingwall random discontinuities consist of prominent joints, low angle joints, joint zones, and pegmatite veins. These random discontinuities have planar smooth surfaces and a few planar rough surfaces. The random discontinuities have unweathered dry walls. Most of these discontinuities have <1 mm thick serpentine infill material, while the pegmatite veins have at-most 1 - 3 mm thick infill material (serpentine, mica and calcite), with few discontinuities containing no infill material. Rig 2 random discontinuities have trace lengths of 3 - 10 m, while trace lengths of 10 - 30 m were recorded on the pegmatite veins.		

RIG 14 Discontinuity Properties

Table 4-10: Summary of Rig 14 hangingwall discontinuity sets

RIG 14 HW Discontinuity Sets			
Discontinuity Set	JS1	JS2	Random Discontinuities
Discontinuity Count	83	50	73
Total Recorded Discontinuities	206	206	206
Percentage (%)	40%	24%	35%

Table 4-11: Properties of Rig 14 hangingwall discontinuity sets

RIG 14 Discontinuity Properties			
Joint Set (JS)	**Average Dip (°)**	**Average Dip Direction (°)**	**Description of Discontinuity Properties**
JS1	89	054	Rig 14 JS1 discontinuities consist mainly of prominent joints and shear zones. These steeply dipping discontinuities are trending in a similar direction as JS1 discontinuities in both Rig 47 and Rig 2, JS5 in Rig 50, and JS2 in TC1. JS1 discontinuities measured an average true spacing of 0.52 m. JS1 discontinuities mainly consist of planar smooth surfaces with few planar rough surfaces. These discontinuities have fresh joint walls (unweathered) and dry surfaces. All recorded dicontinuities contain serpentine infill material. Almost an equal number of JS1 discontinuties containing an infill thickness of <1 mm and 1 - 3 mm were recorded. The prominent discontinuities in this set have trace lenghs of approximately 3 - 10 m to 10 - 30 m (both ends not visible), with few joints having one end or both ends visible (1 - 3 m trace lengths).
JS2	89	160	Rig 2 JS2 discontinuties are steeply dipping and trending in a similar SSE-NNW direction as JS2 discontinuities in Rig 47, and JS3 discontinuities in both Rig 50 and TC1. These discontinuities consist of prominent joints, shear zones and pegmatite veins. The true spacing between JS2 discontonuities averaged 0.82 m. JS2 discontinuities consist of an equal number of planar smooth and planar rough surfaces. The discontinuity set surfaces are unweathered and no groundwater along the surfaces was recorded. Majority of JS2 prominent joints consist of <1 mm to 3 - 10 mm serpentine infill materiall while few discontinuities have no infill material. The pegmatite veins recorded have combined serpentine, calcite, and mica infill materials with thicknesses of 10 - 30 mm and 3 - 10 mm. Majority of JS2 discontinuities have trace lenghs of approximately 3 - 10 m (with both ends not visible) and only few joints having one end or both ends visible (1 - 3 m trace lengths). JS2 pegmatite veins are prominent, having 10 - 30 m to >30 m trace lengths.
Random discontinuities	Rig 2 hangingwall random discontinuities consist of Domes, prominent joints, shear zones, low angle joints, and pegmatite veins. These random discontinuities consist nainly of planar smooth surfaces and a large number of planar rough surfaces. The random discontinuities have unweathered dry walls. Most of these discontinuities have <1 mm to 1 - 3 mm thick serpentine infill material, while the pegmatite veins have 3 - 10 mm to 10 - 30 mm thick infill material (serpentine, mica and calcite), with few discontinuities containing no infill material. Rig 2 random discontinuities have trace lengths of 3 - 10 m, while trace lengths of atmost 10 - 30 m were recorded on the pegmatite veins.		

4.3 Rock Mass Classification Results

In this study, geotechnical mapping data were collected at distances varying between 5 m to 20 m behind the advancing production faces. Since these areas were not covered with shotcrete yet, the identification of different ground quality classes in each production section was achieved. The in-depth characterization results described in Section 4.2 were used as input in rock mass classification systems to derive hangingwall and ore zone rock mass quality indicators. The parameters which feed into the final rating results in each rock mass classification system were derived from raw scanline mapping data.

To obtain reliable rock mass quality indicator results, rock mass ratings were derived for 3 m runs of raw scanline mapping data. To obtain rock mass quality indicator values that are conservative, rock mass ratings of input parameters that are least favourable for stability were chosen in each rock mass classification system. The RMR_{89}, Q-system, and $MRMR_{2000}$ evaluation systems, which are comprehensively discussed in Appendix B, were selected for quantifying the underground rock mass quality. Additionally, the GSI system results were included as it was outlined in Section 2.7.2 that it is an important empirical characterization tool for the estimation of geo-mechanical properties. These geo-mechanical properties subsequently feed into the stability evaluation of underground engineering structures using numerical analysis or closed-form solutions.

The results from the rock mass classification exercise indicated that the hangingwall rock mass in each production section consists of different zones of rock mass quality. These zones range from very poor quality to very good ground conditions, which correlated well with the underground observations made during the data collection stage of this project. The rock mass characterization and classification exercise indicated that zones of very poor and poor ground quality were caused by the existence of adverse geological discontinuities. These discontinuities are pegmatite veins, shear zones, joint zones, fracturing associated with dykes, minor faults, and domes. Additionally, these areas consist of many intersecting discontinuities that are closely spaced, where most individual discontinuities have planar, slickenside or smooth surfaces with thick infill material of low strength, such as serpentine infill. The results from each rock mass classification method are presented in Sections 4.3.1 to 4.3.4. The results feature

frequency measurements of the occurrence of different rock qualities associated with the ground conditions in each production section. The analysis also included the statistical analysis of each ground quality class. Lastly, the statistical analysis for all scanline mapping data points combined is included in Appendix D.

4.3.1 Rock Mass Rating (RMR_{89}) Results

The RMR_{89} results, which include the ratings assigned to each RMR_{89} parameter determined for 3 m runs in all the production sections, are provided in Appendix D. Figure 4-3 presents the frequency distribution of RMR_{89} values for all identified rock quality classes per 3 m in each production section. Figure 4-3 shows that the ground conditions in each ore production section generally range between fair to good according to the RMR_{89}. Additionally, the existence of very good ground conditions was identified in one ore production block, namely RIG 47.

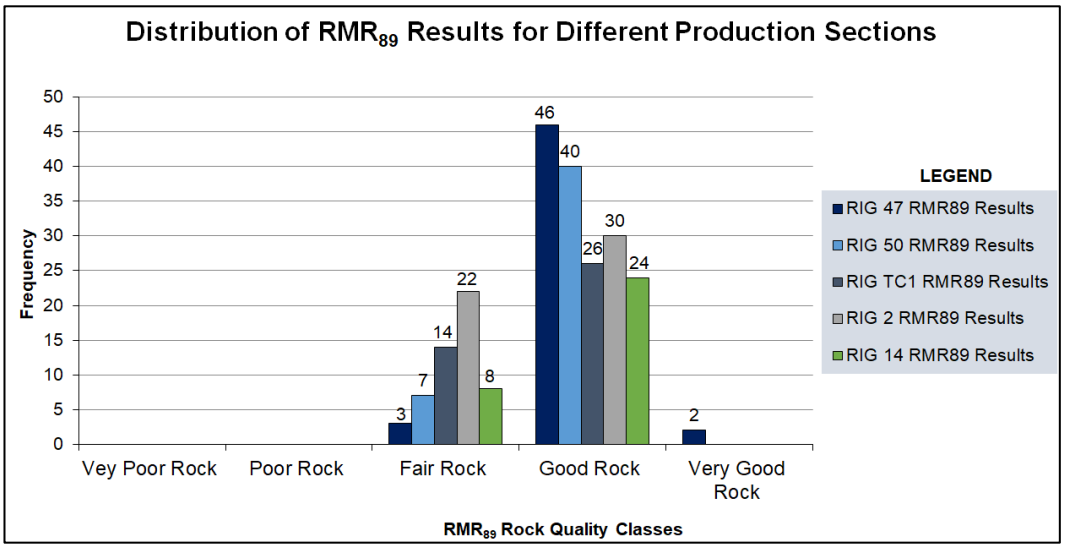


Figure 4-3: Frequency distribution of RMR_{89} values for all production sections

Table 4-12 provides the statistical analysis of the values in each identified rock mass quality class according to the RMR_{89} in each ore production section. According to the statistical analysis of RMR_{89}, the variability in the rock mass quality in each production section can be considered medium to high, indicating an irregular rock mass which requires careful mine and support design.

Table 4-12: Statistical analysis of the hanging wall RMR_{89} results

(RMR_{89}) Rock Mass Quality	Statistical Parameters	RIG 47	RIG 50	TC1	RIG 2	RIG 14
Vey Poor Rock (<20)	Minimum	0	0	0	0	0
	Maximum	0	0	0	0	0
	Mean	0	0	0	0	0
Poor Rock (21-40)	Minimum	0	0	0	0	0
	Maximum	0	0	0	0	0
	Mean	0	0	0	0	0
Fair Rock (41-60)	Minimum	51.00	59.00	59.00	53.00	51.00
	Maximum	60.00	59.00	60.00	60.00	59.00
	Mean	56.67	59.00	59.36	58.55	57.63
Good Rock (61-80)	Minimum	61.00	61.00	61.00	61.00	61.00
	Maximum	76.00	73.00	78.00	78.00	79.00
	Mean	68.04	65.98	68.38	67.90	69.04
Very Good Rock (81-100)	Minimum	82.00	0	0	0	0
	Maximum	86.00	0	0	0	0
	Mean	84.00	0	0	0	0

4.3.2 Geological Strength Index (GSI) Results

In the RMR_{89} results presented above, no poor rock mass quality was identified. Therefore, Equation B-13 (in Appendix B), which correlates the GSI system to Bieniawski's RMR_{89} was used to quantify the GSI in all the production sections. The GSI also ranges from 0 to 100, which is consistent with the RMR_{89} scale (Marinos, et al., 2005). The frequency distribution of GSI values for all identified rock quality classes in each production section is presented in Figure 4-4. Figure 4-4 confirmed that the ground conditions in each mining section generally ranged between fair to good according to the GSI. GSI results also indicated that very good ground conditions existed in one ore production block, which is RIG 47.

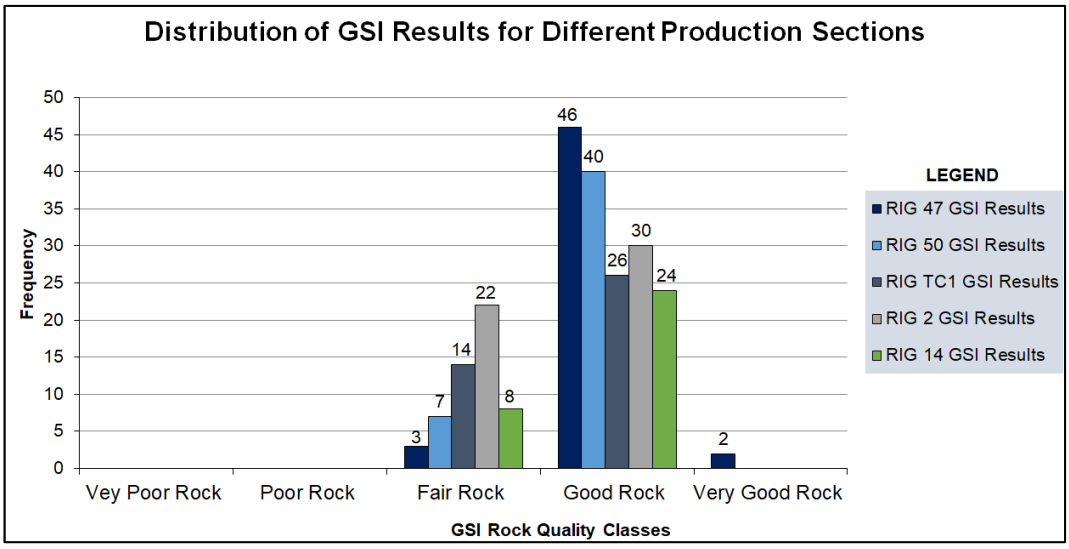


Figure 4-4: Frequency distribution of GSI values for all production sections

Table 4-13 presents the statistical analysis of the values in each identified rock mass quality class according to the GSI. The GSI system results determined for 3 m runs in all the production sections are also provided in Appendix D. Similar to the RMR_{89} results, the statistical analysis of the GSI values indicated medium to high variability in the rock mass quality in each production section.

Table 4-13: Statistical analysis of the hanging wall GSI results

GSI (Rock Mass Quality)	Statistical Parameters	RIG 47	RIG 50	TC1	RIG 2	RIG 14
Vey Poor Rock (<20)	Minimum	0	0	0	0	0
	Maximum	0	0	0	0	0
	Mean	0	0	0	0	0
Poor Rock (21-40)	Minimum	0	0	0	0	0
	Maximum	0	0	0	0	0
	Mean	0	0	0	0	0
Fair Rock (41-60)	Minimum	51.00	59.00	59.00	53.00	51.00
	Maximum	60.00	59.00	60.00	60.00	59.00
	Mean	56.67	59.00	59.36	58.55	57.63
Good Rock (61-80)	Minimum	61.00	61.00	61.00	61.00	61.00
	Maximum	76.00	73.00	78.00	78.00	79.00
	Mean	68.04	65.98	68.38	67.90	69.04
Very Good Rock (81-100)	Minimum	82.00	0	0	0	0
	Maximum	86.00	0	0	0	0
	Mean	84.00	0	0	0	0

4.3.3 Q - System Results

Q-ratings were determined for 3 m runs of raw hangingwall scanline mapping data in all the production sections. The Q-system results, which include the ratings assigned to each Q-system parameter per 3 m zone in all the production sections, are provided in Appendix D. *Figure 4-5* presents the frequency distribution of Q-Index values in each production section. The range of Q-values for the pyroxenite material, as shown in *Figure 4-5* indicated that the rock quality ranges from very poor to fair rock in each ore production block.

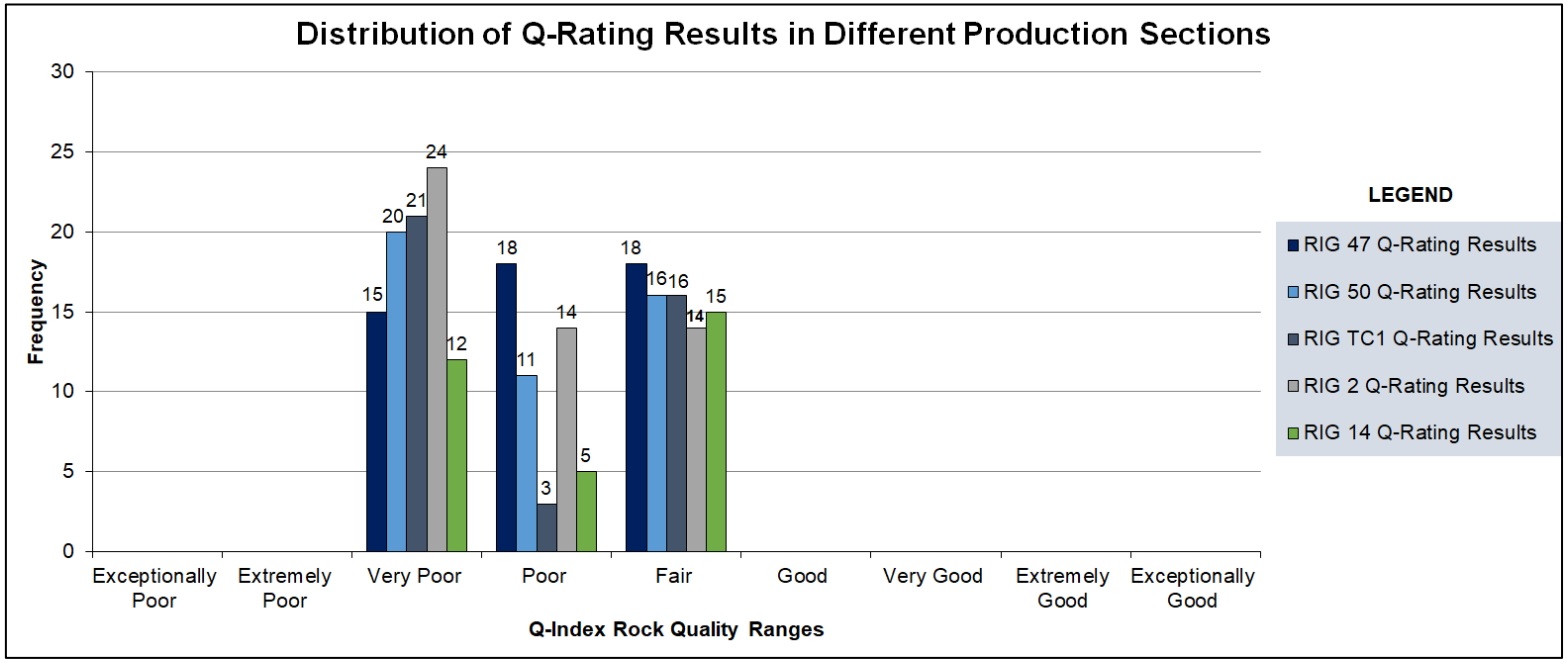


Figure 4-5: Frequency distribution of Q-Index values for all production sections

Table 4-14 provides the statistical analysis of each rock mass quality class according to the Q-system in each production section. A geometric mean was used since the Q-index values tend to make large fluctuations.

Table 4-14: Statistical analysis of the hanging wall Q-Rating results

(Q-Index) Rock Mass Quality	Statistical Parameters	RIG 47	RIG 50	TC1	RIG 2	RIG 14
Exceptionally Poor (0.001 – 0.01)	Minimum	-	-	-	-	-
	Maximum	-	-	-	-	-
	Mean	-	-	-	-	-
Extremely Poor (0.01 - 0.1)	Minimum	-	-	-	-	-
	Maximum	-	-	-	-	-
	Mean	-	-	-	-	-
Very Poor (0.1 - 1.0)	Minimum	0.28	0.39	0.40	0.19	0.19
	Maximum	0.92	0.83	0.83	0.90	0.83
	Mean	0.60	0.63	0.52	0.48	0.44
Poor (1 - 4)	Minimum	1.19	1.18	1.80	1.06	1.65
	Maximum	3.72	3.26	3.25	3.58	3.32
	Mean	2.18	1.91	2.43	1.89	2.55
Fair (4 - 10)	Minimum	4.84	4.44	4.82	4.74	4.85
	Maximum	9.99	9.82	9.90	9.77	9.95
	Mean	7.40	6.41	6.33	6.55	7.78
Good (10 - 40)	Minimum	-	-	-	-	-
	Maximum	-	-	-	-	-
	Mean	-	-	-	-	-
Very Good (40 - 100)	Minimum	-	-	-	-	-
	Maximum	-	-	-	-	-
	Mean	-	-	-	-	-
Extremely Good (100 - 400)	Minimum	-	-	-	-	-
	Maximum	-	-	-	-	-
	Mean	-	-	-	-	-
Exceptionally Good (400 - 1000)	Minimum	-	-	-	-	-
	Maximum	-	-	-	-	-
	Mean	-	-	-	-	-

4.3.4 Mining Rock Mass Rating ($MRMR_{2000}$) Results

The revised MRMR system proposed by Laubscher & Jakubec (2000), which introduces the rock block strength concept and incorporates the impact of the micro/mesoscale and cemented defects on rock mass strength, was used. $MRMR_{2000}$ ratings were also derived for 3 m runs of scanline mapping data and are included in the $MRMR_{2000}$ results in Appendix D. To cover all variations in jointed rock masses from very poor to very good, classification of MRMR values also ranges from 0 to 100 (five classes), which is consistent with the RMR_{89} scale (Laubscher, 1990). Table 4-15 summarises the adjustment factors which were used in the determination of $MRMR_{2000}$ values.

Table 4-15: Summary of $MRMR_{2000}$ Adjustment Factors

$MRMR_{2000}$ Adjustments	
Adjustment for the effect of weathering	1, for no exposure to weathering over the years
Adjustment for blasting effects	0.94, for good conventional blasting
Adjustment for orientation of discontinuities	1, for less than 3 discontinuity sets
	0.7, for 3 discontinuity sets with a 0-15 JC rating
Adjustment for mining induced Stress	1, no effect of mining induced stresses
Ajustment for the effects of water conditions	1, for a dry rock mass

The frequency distribution of $MRMR_{2000}$ results in each production section is presented in Figure 4-6. The $MRMR_{2000}$ values indicated that the quality of the hanging-wall rock mass generally ranges from fair to good. Poor ground conditions were only confirmed in the RIG 47 ore production block.

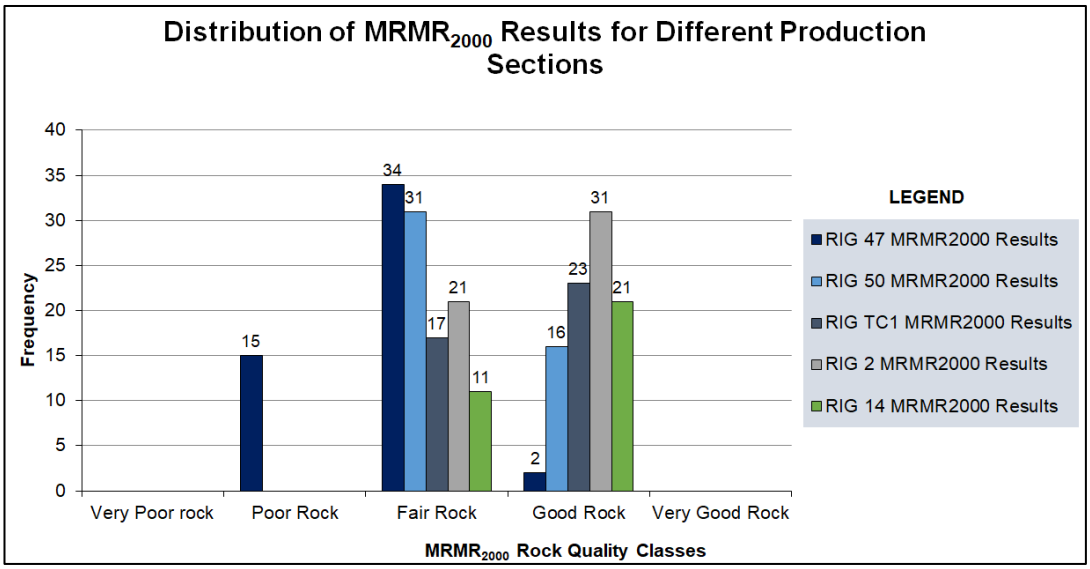


Figure 4-6: Frequency distribution of MRMR values for all production sections

The $MRMR_{2000}$ quantities were also statistically analysed, as shown in Table 4-16. The statistical analysis of the $MRMR_{2000}$ values in each production section confirmed that the variability in the rock mass quality is medium to high, which indicates an inconsistent rock mass that needs careful support design.

Table 4-16: Statistical Analysis of the $MRMR_{2000}$ Results

(MRMR) Rock Mass Quality	Statistical Parameters	RIG 47	RIG 50	TC1	RIG 2	RIG 14
Vey Poor Rock (<20)	Minimum	0	0	0	0	0
	Maximum	0	0	0	0	0
	Mean	0	0	0	0	0
Poor Rock (21-40)	Minimum	25.10	0	0	0	0
	Maximum	36.06	0	0	0	0
	Mean	30.40	0	0	0	0
Fair Rock (41-60)	Minimum	42.35	41.39	59.19	57.88	57.88
	Maximum	55.86	59.43	59.13	59.13	59.76
	Mean	49.49	53.78	59.07	58.93	59.07
Good Rock (61-80)	Minimum	67.52	62.18	61.85	61.85	61.85
	Maximum	72.81	67.68	68.70	68.70	69.64
	Mean	70.16	63.71	63.73	63.91	63.75
Very Good Rock (81-100)	Minimum	0	0	0	0	0
	Maximum	0	0	0	0	0
	Mean	0	0	0	0	0

4.4 Rock Test Results and Rock Mass Properties

Individual laboratory test results are attached in Appendix C. The properties derived from the test results were used to aid in the evaluation of different failure modes at the mine. Since rock testing data were limited, it was assumed that the obtained laboratory test results would also apply to the disseminated Chromitite seams and parting planes in the hangingwall.

4.4.1 Results of the Uniaxial Compression Test with Elastic Moduli (UCM)

Figure 4-7 and Figure 4-8 present the distribution of the UCS values for the Pyroxenite and Chromitite rocks, respectively. Based on the results of the UCS values, the Pyroxenite rock was classified as a ‘very strong rock’ and the Chromitite rock was classified as a ‘strong rock’ according to the ISRM (1978c) field classification of rock strength. The classification of rock based on the UCS is presented in Section 2.3.

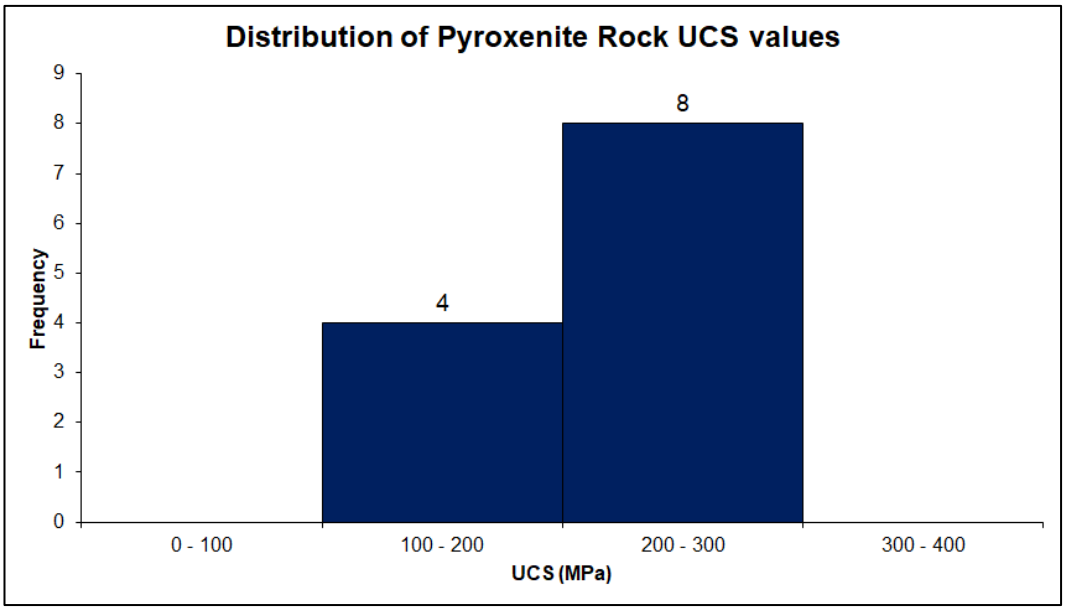


Figure 4-7: Frequency distribution of Pyroxenite UCS values

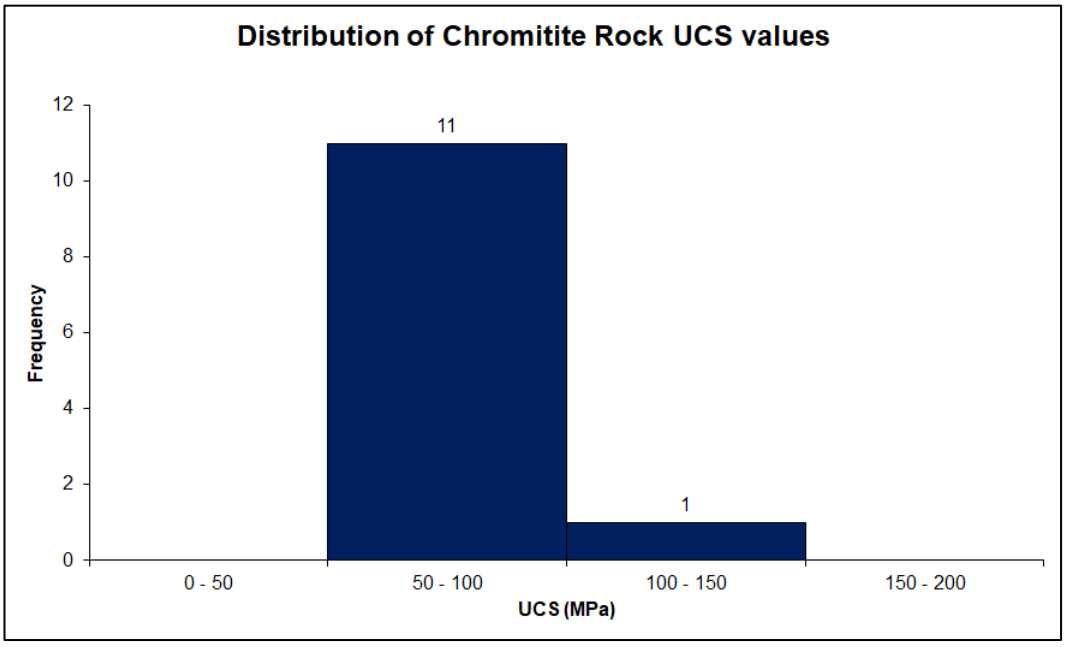


Figure 4-8: Frequency distribution of Chromitite UCS values

Table 4-17 present the statistical analysis of the UCM test results. In Table 4-17 outliers, which are UCM results for rock specimens that failed along discontinuities, were omitted from the dataset and excluded from the analysis to avoid distortion to the results.

Table 4-17: Statistical analysis of UCM results for Pyroxenite and Chromitite rock

Rock type	Statistical Parameter	UCS (MPa)	Density (g/cm³)	Tangent Elastic Modulus @ 50% UCS (GPa)	Secant Elastic Modulus @ 50% UCS (GPa)	Poisson's Ratio Tangent @ 50% UCS	Poisson's Ratio Secant @ 50% UCS
Pyroxenite	Mean	212.35	3.24	124.57	125.56	0.26	0.24
	Standard Dev.	17.01	0.11	15.78	18.27	0.02	0.02
	Minimum	186.49	3.09	99.80	87.00	0.24	0.18
	Maximum	243.21	3.55	149.00	151.00	0.33	0.28
Chromitite	Mean	74.41	3.68	95.23	96.29	0.36	0.28
	Standard Dev.	15.94	1.26	31.56	45.65	0.14	0.08
	Minimum	51.62	0.96	36.40	23.30	0.17	0.15
	Maximum	108.73	4.29	139.00	144.00	0.66	0.40

4.4.2 Results of the Triaxial Compressive Strength (TCS) Test

The intact rock TCS results were used to determine estimates of Pyroxenite and Chromitite rock mass strength parameters. The Rocscience program 'RocLab' was used to obtain estimates of rock mass strength parameters, which will serve as inputs in the design of stable bord spans. To determine the strength properties of the Pyroxenite rock, the triaxial laboratory test data were used. Figure 4-9 presents the output from RocLab for the Pyroxenite rock mass.

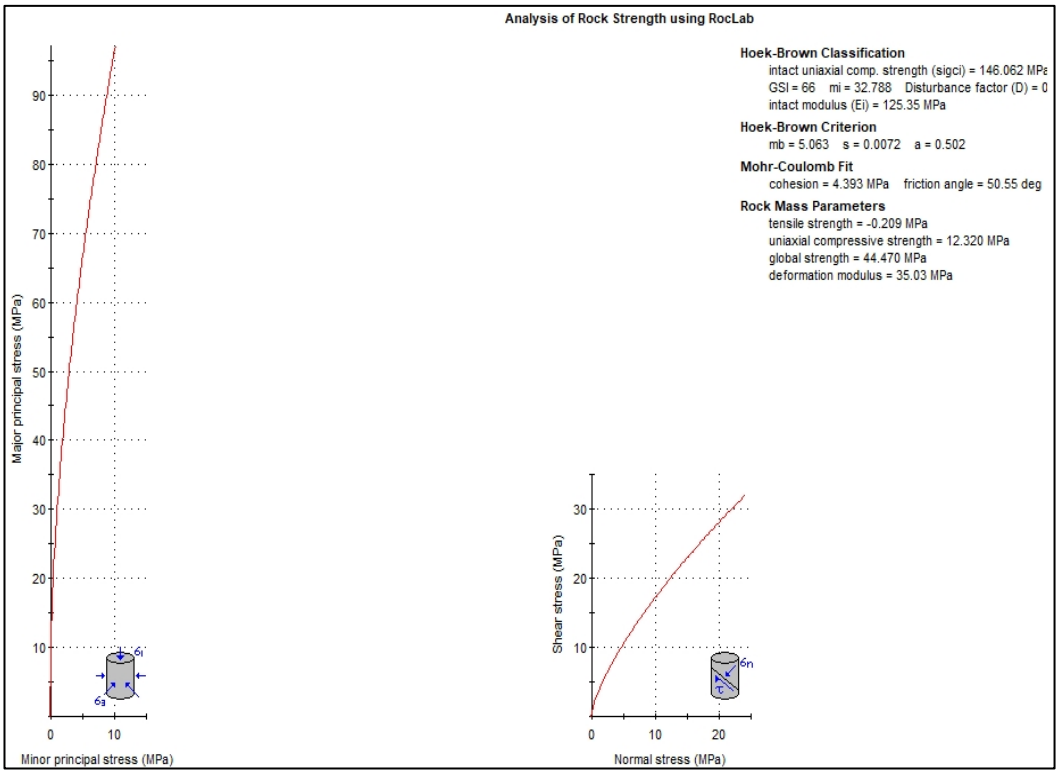


Figure 4-9: Output from RocLab for Pyroxenite rock

Since no TCS laboratory tests were conducted on Chromitite rock material in this case study, built-in charts and tables in the program (presented in Section 2.7.3) were used to estimate the mi and D inputs for Chromitite Rock (Hoek, et al., 2002). The GSI and intact rock UCS for Chromitite rock were obtained from rock mass classification systems and UCM test results, respectively. Average GSI values for all scanline mapping data points combined (provided in Appendix D) for both the Pyroxenite and Chromitite rocks in the mine were used. Figure 4-10 presents the output from RocLab for the Chromitite rock.

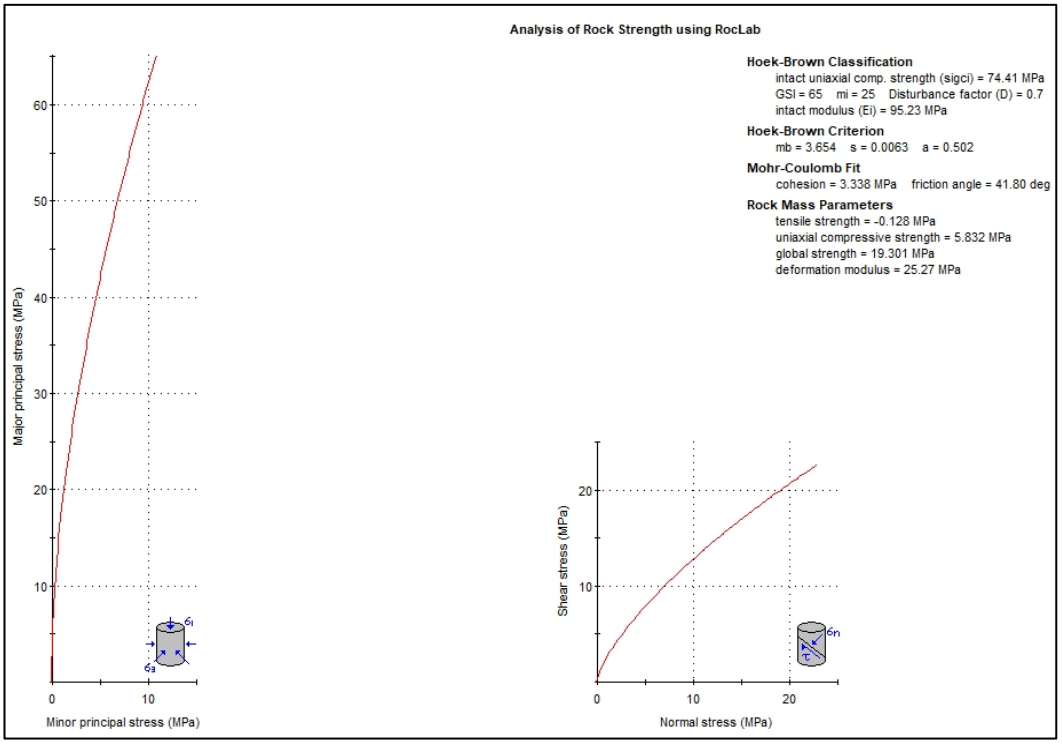


Figure 4-10: Output from RocLab for MG1 Chromitite rock

Table 4-18 summarises the strength, Hoek-Brown equivalent, Mohr-Coulomb parameters, and additional rock mass strength properties for Pyroxenite and Chromitite rock. The derived parameters were used in Chapters 5 and 6 for stability evaluation and estimation of support requirements.

Table 4-18: Rock mass properties for the hangingwall and the mineralised zone

Rock Mass Strength Parameters			
	Parameter	Lithological Unit	
		Pyroxenite (Hangingwall)	Chromitite Reef (Sidewall)
Hoek-Brown Failure Criterion for jointed rock masses	Hoek-Brown Strength Parameter, mb	5.06	3.65
	Hoek-Brown Strength Parameter, s	0.01	0.01
	Hoek-Brown Strength Parameter, a	0.50	0.50
Equivalent Mohr-Coulomb Failure Criterion	Cohesion (c) (MPa)	4.39	3.34
	Angle of Friction (Φ) (degrees)	50.55	41.80
Rock Mass Strength Parameters	Tensile Strength (σ_t) (MPa)	-0.21	-0.13
	Uniaxial Compressive Strength (σ_c) (MPa)	12.32	5.83
	Global Strength (MPa)	44.47	19.30
	Deformation Modulus (E_m) (GPa)	35.03	25.27
Geological Strength Index	GSI	66.00	65.00

Frictional properties of discontinuities with serpentinite infill material

The discussion of discontinuity properties in Section 4.2 indicated that most of the mapped discontinuities contain serpentine infill material, which has an impact on the shear strength of the discontinuities. Serpentine infill has a field strength (UCS) classification of 0.025 MPa – 0.05 MPa. Table 2-17 was used to estimate the peak friction by taking account of the joint roughness number (Jr) and joint alteration number (Ja) of discontinuities with serpentinite infill materials.

The Jr and Ja of 1.0 (for smooth, planar joints) and 2.0 (for slightly altered, non-softening, non-cohesive rock mineral or crushed rock filling), respectively, which are least favourable for stability in terms of shear resistance, were used. This resulted in a peak friction angle of 25°. The typical cohesion values for different types of infill material were also discussed in Section 2.7.4. A minimum and conservative cohesion of 0 kPa was assigned to the serpentine infill. Table 4-19 summarizes the shear strength properties assigned to discontinuities with serpentine infill material.

Table 4-19: Frictional properties of discontinuities with serpentine infill material

Properties of Discontinuties with Serpentine Infill	
Peak Friction Angle (°)	25
Cohesion (kPa)	0

4.5 Summary of Chapter

This chapter presented the use of acquired geotechnical data to derive the mechanical properties of intact rocks and characterization of the discontinuous rock mass at Thorncliffe mine. The quantitative description of the discontinuities and numerical values obtained from the rock mass classification exercise can then be used for bord stability evaluation and the determination of support appropriate requirements. The next chapter presents the design and evaluation of stable panel spans by using the design parameters determined in this chapter.

5 DESIGN OF STABLE BORD SPANS

Chapter 4 presented rock mass characterisation results which featured in-depth quantitative descriptions of the rock mass structure and characteristics of the discontinuous underground rock mass at Thorncliffe Mine. As discussed in Chapter 2, the correct characterisation of the jointed rock mass at the mine was important if a proper stability assessment of the rock mass was to be achieved. Chapter 5 firstly presents the determination of maximum safety spans without support, which is informed by different rock mass qualities. The instability of unsupported mining spans is then assessed to subsequently inform support requirements to ensure stable conditions in the spans between pillars.

5.1 Maximum Unsupported Bord Spans

The Norwegian Geotechnical Institute (NGI) (2022) stated that support design in underground excavations depends on the rock mass quality, safety requirements, and dimensions (span or height) of the underground openings. Therefore, it is vital to consider the purpose and life of various types of production drives in a mining section, which ultimately dictate safety requirements. Safety requirements are expressed by a factor called the Excavation Support Ratio (ESR) (Barton, et al., 1974). Low ESR values indicate high-level safety (support) requirements, while high ESR values indicate that lower safety levels can be accepted.

As discussed in Section 1.2.5, a typical bord and pillar production section at Thorncliffe Mine consists of strike conveyor belt drives, which continuously transport broken ore for the life of an ore block. Secondly, the mine requires the workforce and TMMs to use dedicated travelling roadways to reach the position of the working face (Glencore ECM, 2021). To quantify the life of these two excavation types Figure 5-1, which shows Thorncliffe Mine's life of mine (LOM) footprint (not to scale), was used. Figure 5-1 also shows depth below surface major contours from the current position of the declines to the LOM boundary.

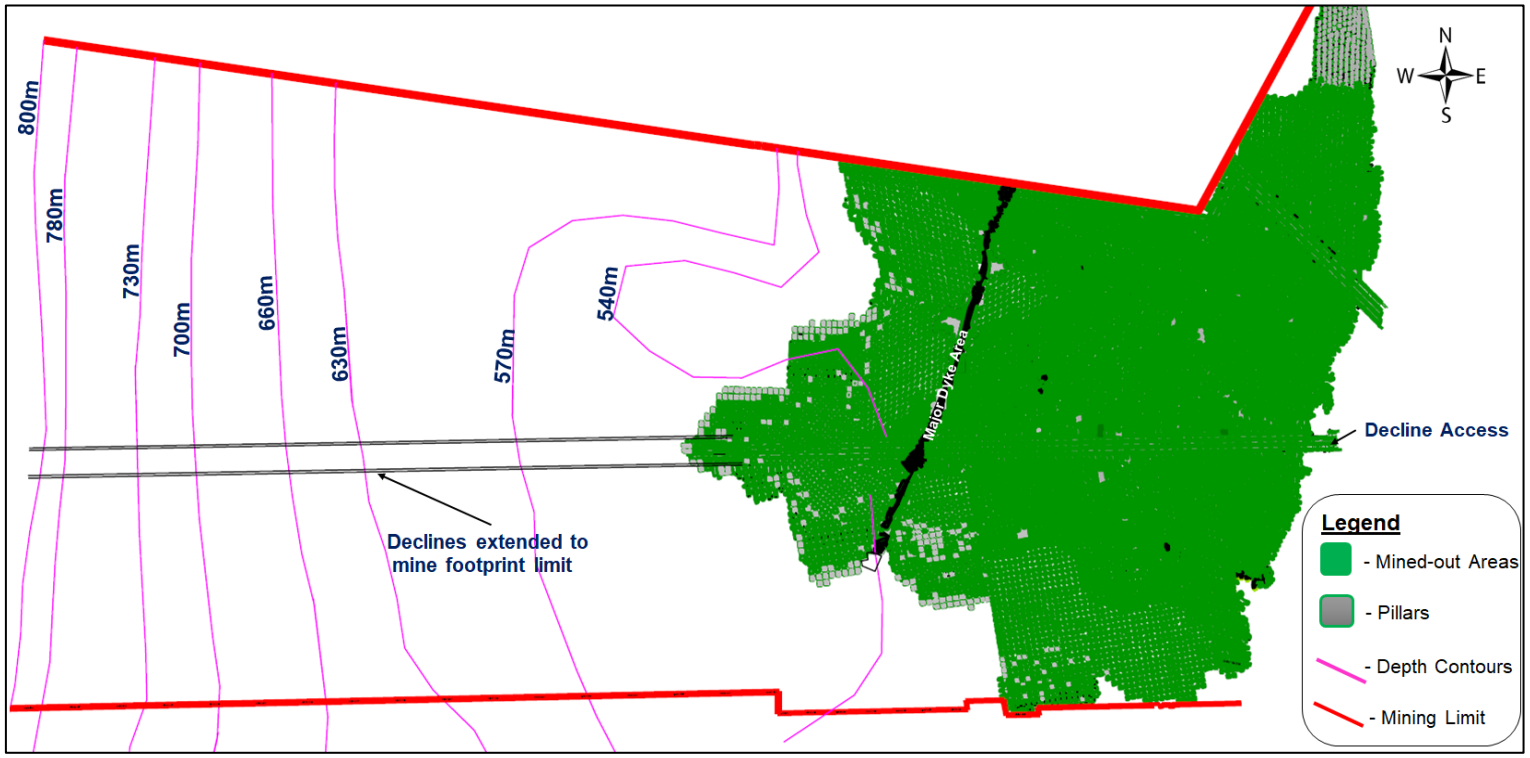


Figure 5-1: Thorncliffe Life of Mine (LOM) Footprint (not to scale)

The LOM is planned to end at a depth of 800 m below surface (mbs) on the boundary of the St George's Fault described in Section 1.2.4. The maximum strike length at 800 mbs was measured to be about 1240 m on the north side of the declines. It would take about 4 years and 3 months to completely mine out the above-mentioned two excavation types and reach the mining limit when using the current production rates of 4 m advance per blast and blasting each panel six times in a month. Travelling roadways and conveyor belt drives can then be classified as medium-term excavations according to mine planning and production scheduling principles (Gholamnejad, 2008).

Besides travelling roadways and conveyor belt drives, the rest of the bords are used solely for production at Thorncliffe Mine (Glencore ECM, 2021). To quantify the life of these production drives, the stope was divided into the working area and the back area, as illustrated in Figure 5-2. The working area is the area in which routine production operations are allowed to take place (Stacey, 2001). At Thorncliffe Mine, this area is measured as the distance between the current position of the working face to a distance that includes a maximum of two ventilation holings or splits behind the face and highlighted in green in Figure 5-2 (Glencore ECM, 2021). Beyond the working area is the back area (highlighted in red in Figure 5-2), where entry of workers is not permitted unless an entry examination is conducted and the area is declared safe. By using the largest pillar dimensions planned at 800 mbs (15 m on strike by 15 m on dip) and current ventilation holings of 8 m, the maximum length of the working area is 61 m. It would take a maximum of only about 2.5 months to establish a new working area when using the current advance per blast of 4 m and blasting each panel 6 times in a month. The previous working area would be declared as a back area after 2.5 months, and no entry would be allowed. This indicated that bords used solely for production can be classified as short-term excavations (Gholamnejad, 2008).

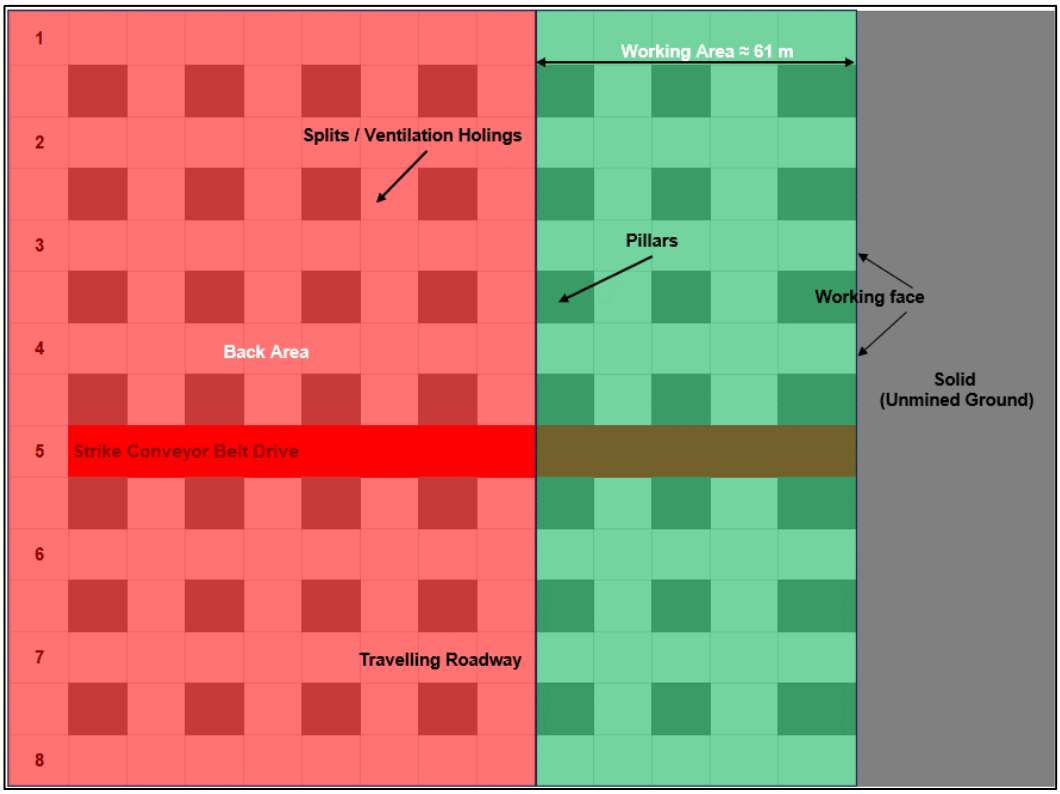


Figure 5-2: Enlarged typical bord and pillar layout showing the working area and back area

Based on their purpose and as medium-term excavations, strike conveyor belt drives and travelling roadways require higher levels of safety (or support) than bords used for production only. As summarised in Table 5-1, to indicate the established different safety requirements, an ESR of 1.6 was assigned to conveyor belt drives and travelling roadways. An ESR of 3 was assigned to panels used solely for production.

Table 5-1: ESR values assigned to different production drives in a bord and pillar section

Description	Ore Block Strike Length (m)	Number of Blasts per Month	Advance per Blast (m)	Number of Months (To deplete ore block)	Number of Years (To deplete ore block)	Life of Excavations (Short Term/Medium Term/Long Term)	Exacavation Support Ratio (ESR)
Conveyor belt drives and travelling ways (Longest strike length at 800 mbs)	1240.0	6.0	4.0	51.7	4 years and 3 Months	Medium Term	1.6
Working Area Length (800 mbs where planned pillars are 15 m x 15 m)	61.0	6.0	4.0	2.5	2 Months and 16 days	Short Term	3.0

The maximum unsupported span relationship by Barton et al (1974) (Equation B-10 in Appendix B) was used for the estimation of maximum safety bord spans without support for different rock mass qualities in each mining section. Maximum unsupported spans were determined for the identified short-term and medium-term panels in each production section.

Table 5-2 present the results of the maximum unsupported spans for short-term production drives for different rock mass qualities. According to the results, the maximum self-supporting spans for short-term panels can be as low as 3 m in very poor rock to a maximum of 15 m in fair rock qualities.

Table 5-2: Maximum unsupported spans for short-term panels in the five production sections

(Q-Index) Rock Mass Quality	Statistical Parameters	ESR for Short-Term Panels (Bords used for Production Only)	Maximum Unsupported Spans (m)				
			Rig 47	Rig 50	TC1	Rig 2	Rig 14
Exceptionally Poor (0.001 – 0.01)	Minimum	ESR = 3	-	-	-	-	-
	Maximum		-	-	-	-	-
	Mean		-	-	-	-	-
Extremely Poor (0.01 - 0.1)	Minimum		-	-	-	-	-
	Maximum		-	-	-	-	-
	Mean		-	-	-	-	-
Very Poor (0.1-1.0)	Minimum		4	4	4	3	3
	Maximum		6	6	6	6	6
	Mean		5	5	5	4	4
Poor (1 - 4)	Minimum		6	6	8	6	7
	Maximum		10	10	10	10	10
	Mean		8	8	9	8	9
Fair (4 - 10)	Minimum		11	11	11	11	11
	Maximum		15	15	15	15	15
	Mean		13	13	13	13	14
Good (10 - 40)	Minimum		-	-	-	-	-
	Maximum		-	-	-	-	-
	Mean		-	-	-	-	-
Very Good (40 - 100)	Minimum		-	-	-	-	-
	Maximum		-	-	-	-	-
	Mean		-	-	-	-	-
Extremely Good (100 - 400)	Minimum		-	-	-	-	-
	Maximum		-	-	-	-	-
	Mean		-	-	-	-	-
Exceptionally Good (400 - 1000)	Minimum		-	-	-	-	-
	Maximum		-	-	-	-	-
	Mean		-	-	-	-	-

Table 5-3 presents the results of the maximum unsupported spans for short-term and medium-term production drives for different rock mass qualities. Due to higher safety requirements in medium-term panels, the calculated maximum self-supporting spans were generally less, ranging between 2 m to a maximum of 8 m, as presented in Table 5-3.

Table 5-3: Maximum unsupported spans for medium-term panels in the five production sections

(Q-Index) Rock Mass Quality	Statistical Parameters	ESR for Medium-Term Panels (Conveyor Belt Drives and Travelling Roadways)	Maximum Unsupported Spans (m)				
			Rig 47	Rig 50	TC1	Rig 2	Rig 14
Exceptionally Poor (0.001 – 0.01)	Minimum	ESR = 1.6	-	-	-	-	-
	Maximum		-	-	-	-	-
	Mean		-	-	-	-	-
Extremely Poor (0.01 - 0.1)	Minimum		-	-	-	-	-
	Maximum		-	-	-	-	-
	Mean		-	-	-	-	-
Very Poor (0.1-1.0)	Minimum		2	2	2	2	2
	Maximum		3	3	3	3	3
	Mean		3	3	2	2	2
Poor (1 - 4)	Minimum		3	3	4	3	4
	Maximum		5	5	5	5	5
	Mean		4	4	5	4	5
Fair (4 - 10)	Minimum		6	6	6	6	6
	Maximum		8	8	8	8	8
	Mean		7	7	7	7	7
Good (10 - 40)	Minimum		-	-	-	-	-
	Maximum		-	-	-	-	-
	Mean		-	-	-	-	-
Very Good (40 - 100)	Minimum		-	-	-	-	-
	Maximum		-	-	-	-	-
	Mean		-	-	-	-	-
Extremely Good (100 - 400)	Minimum		-	-	-	-	-
	Maximum		-	-	-	-	-
	Mean		-	-	-	-	-
Exceptionally Good (400 - 1000)	Minimum		-	-	-	-	-
	Maximum		-	-	-	-	-
	Mean		-	-	-	-	-

Engineering requirements at the mine dictate 6 m minimum bord spans to accommodate the manoeuvrability of the equipment/machinery (such as Load-Haul Dump (LHD) trucks) that are used in production. The mine also requires 6 m minimum spans in strike conveyor belt drives to accommodate belt conveyor equipment and sufficient space for workers to travel (Glencore ECM, 2021). It is worth noting that for medium-term excavations, the required minimum span of 6 m was calculated only when the ground conditions were at least fair, indicating the importance of maintaining stability for longer. On the other hand, short-term production drives of at least 6 m in width can be created in very poor ground conditions.

In the following sections, different rock failure mechanisms will be evaluated to determine whether the different panel spans indicated as self-supporting will sustain their integrity when mining takes place. The stability evaluation will first indicate the actual maximum stable spans without support and will then inform

support requirements to maintain stability for *"the full life of the excavation, not only during development."* (Stacey, 2001).

5.2 Stability Evaluation of Bord Spans

It is important to note that the stability of the bords will be evaluated for the worst ground conditions to be encountered to ensure a conservative design. Bord span stability evaluation was limited to the following failure modes, as suggested by the MHSC (Murphy, et al., 2016):

(i) Rock Mass Failure,
(ii) Beam Failure,
(iii) Structural Failure, and
(iv) Intact Rock Mass Failure.

Watson & Gerber (2018) stated that an important consideration in the determination of stable spans in mechanized stopes is intersections or holings between orthogonal bords. Bord intersections represent areas of larger spans where the potential of collapses occurring is increased and where most FOGs occur.

In a bord and pillar mining layout, the critical span at an intersection is calculated by using the diagonal span across the intersection, as illustrated in Figure 5-3. Bord spans that can be safely mined must be designed to accommodate the critical diagonal span across the intersections. This means that the width of bord or panel spans must be designed to ensure that the diagonal span across the intersection does not exceed the critical span. An example is shown in Figure 5-3 where, for a critical diagonal span of 8 m, the safe span of two equal-sized bords would be 5.6 m (Watson & Gerber, 2018). Another approach to cater for intersections in the design of underground tunnels was described by Barton et al (1974) where Q-Index values are down-rated by multiplying the joint set number (Jn) by a factor of 3.

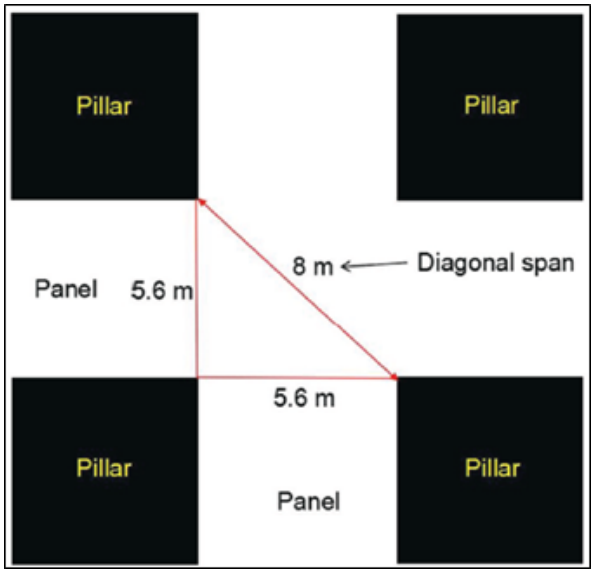


Figure 5-3: Bord spans are designed to accommodate the critical diagonal span across intersections (Watson & Gerber, 2018)

This research study focused on the design of diagonal spans across intersections as an additional safety factor in the design of bord/panel spans, as suggested by Watson & Gerber (2018). Six bord spans were selected for stability evaluation in the various rock mass quality classes shown in Table 5-2 and Table 5-3 as follows:

- 6 m minimum bord span (as dictated by engineering requirements at the mine),
- 8 m bord span, to verify or validate the stability of the current bord spans of 8 m used at the mine (current mine design criteria are presented in Section 1.2.5), and
- 10 m, 12 m, 14 m, and a maximum span of 15 m to assess the effect of increasing bord spans by 2 m, which represents improving underground ground conditions at the mine.

In this project report, intersecting orthogonal bords are assumed to be of equal size. The stability of diagonal spans of each of the above-selected bord spans will be evaluated to determine the critical diagonal span. The diagonal spans across the intersections of the selected orthogonal bords are presented in Table 5-4.

Table 5-4: Diagonal spans across intersections of various orthogonal bords

Spans of Orthogonal Bords/Panels (m)	Diagonal Span Across Intersections (m)
6	8
8	11
10	14
12	17
14	20
15	21

5.2.1 Rock Mass Failure

The Modified Stability Graph Method by Matthews et al. (1981) relating the stability number (N') of the hangingwall to the tunnel critical-hydraulic radius was used to assess rock mass failure. Determination of the hangingwall modified stability number incorporated the calculated values of the modified Rock Quality Index (Q') (described in Appendix B) for each mining section; and the three multiplying factors (A, B, and C) which consider the effect of rock stress conditions, joint orientation relative to hangingwall face, and influence of gravity, respectively.

Table 5-5 present the calculated modified rock quality index (Q') results. Q' values were determined by removing the effects of the stress reduction factor (SRF) and water inflow (J_w = 1 for dry conditions in the underground rock mass) from the calculated Q-index values.

Table 5-5: Results of the Modified Rock Quality Index (Q') per mining section

Q' - Stability Rating	Statistical Parameters	RIG 47	RIG 50	TC1	RIG 2	RIG 14
Exceptionally Poor (0.001 – 0.01)	Minimum	-	-	-	-	-
	Maximum	-	-	-	-	-
	Mean	-	-	-	-	-
Extremely Poor (0.01 - 0.1)	Minimum	-	-	-	-	-
	Maximum	-	-	-	-	-
	Mean	-	-	-	-	-
Very Poor (0.1 - 1.0)	Minimum	2.76	2.06	3.98	1.85	1.90
	Maximum	9.16	8.27	8.27	9.03	8.29
	Mean	6.05	5.87	5.23	4.83	4.39
Poor (1 - 4)	Minimum	3.96	3.95	6.17	4.09	4.11
	Maximum	18.60	16.37	17.95	35.83	8.29
	Mean	9.48	7.91	9.65	14.01	6.36
Fair (4 - 10)	Minimum	12.09	11.11	12.04	11.84	12.13
	Maximum	24.99	24.56	24.75	24.42	24.88
	Mean	18.50	16.03	15.84	16.38	19.44
Good (10 - 40)	Minimum	-	-	-	-	-
	Maximum	-	-	-	-	-
	Mean	-	-	-	-	-
Very Good (40 - 100)	Minimum	-	-	-	-	-
	Maximum	-	-	-	-	-
	Mean	-	-	-	-	-
Extremely Good (100 - 400)	Minimum	-	-	-	-	-
	Maximum	-	-	-	-	-
	Mean	-	-	-	-	-
Exceptionally Good (400 - 1000)	Minimum	-	-	-	-	-
	Maximum	-	-	-	-	-
	Mean	-	-	-	-	-

Table 5-6 presents the modified stability number multiplying factors. The factors were determined for each production section.

Table 5-6: Modified Stability Number Multiplying factors (A, B, and C) per production section

Production Sections	A - Factor	B - Factor	C - Factor
RIG 47	1.0	0.8	2.4
RIG 50	1.0	0.8	4.8
TC1	1.0	0.8	2.5
RIG 2	1.0	0.8	2.3
RIG 14	1.0	0.8	2.1

As shown in Table 5-6, maximum induced stress components could not be accurately estimated; therefore, the A-factor was set to one, as the UCS divided by the induced compressive stress is likely to be greater than ten in these shallow mining environments (Potvin, 1988). Since each production section consists of

several major discontinuity sets identified using stereonets, discontinuity sets with the smallest true dip angle were used in the determination of the B factor (Hutchinson & Diederichs (1996). Lastly, the average dip angle of the hangingwall (presented in Chapter 3) in each production section was used to determine the C factor (Hutchinson & Diederichs, 1996). The results of the calculated modified stability number for each production section are presented in Table 5-7 below.

Table 5-7: Calculated Modified Stability Number (N') in each section for different rock qualities

(Q-Index) Rock Mass Quality	Statistical Parameters	Modified Stability Number (N')				
		Rig 47	Rig 50	TC1	Rig 2	Rig 14
Exceptionally Poor (0.001 – 0.01)	Minimum	-	-	-	-	-
	Maximum	-	-	-	-	-
	Mean	-	-	-	-	-
Extremely Poor (0.01 - 0.1)	Minimum	-	-	-	-	-
	Maximum	-	-	-	-	-
	Mean	-	-	-	-	-
Very Poor (0.1 - 1.0)	Minimum	5.3	7.9	8.0	3.4	3.2
	Maximum	17.6	31.8	16.5	16.6	13.9
	Mean	11.6	22.5	10.5	8.9	7.4
Poor (1 - 4)	Minimum	7.6	15.2	12.3	7.5	6.9
	Maximum	35.7	62.9	35.9	65.9	13.9
	Mean	18.2	30.4	19.3	25.8	10.7
Fair (4 - 10)	Minimum	23.2	42.7	24.1	21.8	20.4
	Maximum	48.0	94.3	49.5	44.9	41.8
	Mean	35.5	61.6	31.7	30.1	32.7
Good (10 - 40)	Minimum	-	-	-	-	-
	Maximum	-	-	-	-	-
	Mean	-	-	-	-	-
Very Good (40 - 100)	Minimum	-	-	-	-	-
	Maximum	-	-	-	-	-
	Mean	-	-	-	-	-
Extremely Good (100 - 400)	Minimum	-	-	-	-	-
	Maximum	-	-	-	-	-
	Mean	-	-	-	-	-
Exceptionally Good (400 - 1000)	Minimum	-	-	-	-	-
	Maximum	-	-	-	-	-
	Mean	-	-	-	-	-

In bord and pillar mines, the bords have a large or an 'infinite' length. The hydraulic radius will then be approximately half the width of the bord, which also caters for spans across intersections (Murphy, et al., 2016). Therefore, the hydraulic radius was determined as half of the calculated spans. To design for the worst underground conditions, the minimum N' calculated for each rock mass quality class was used in assessing the stability of each selected diagonal span. These

are highlighted in red in Table 5-7. Table 5-8 to Table 5-12 present the selected N' values and calculated hydraulic radii for various spans mining in different ground conditions in each mining section. By plotting the selected stability numbers against the respective hydraulic radii, the stability of the selected diagonal spans across intersections in each section was evaluated. The N' versus hydraulic radius plots for each section are presented in Figure 5-4 to Figure 5-8.

Table 5-8: Bord spans, hydraulic radii, and stability number for the Rig 47 section

Modified Stability Number (N') and Hydraulic Radius for RIG 47				
Diagonal Spans Across Intersections (m)	**Hydraulic radius (m)**	**Minimum Modified Stability Number (N') - Very Poor ground**	**Minimum Modified Stability Number (N') - Poor ground**	**Minimum Modified Stability Number (N') - Fair ground**
8	4.0	5.3	7.6	23.2
11	5.5	5.3	7.6	23.2
14	7.0	5.3	7.6	23.2
17	8.5	5.3	7.6	23.2
20	10.0	5.3	7.6	23.2
21	10.5	5.3	7.6	23.2

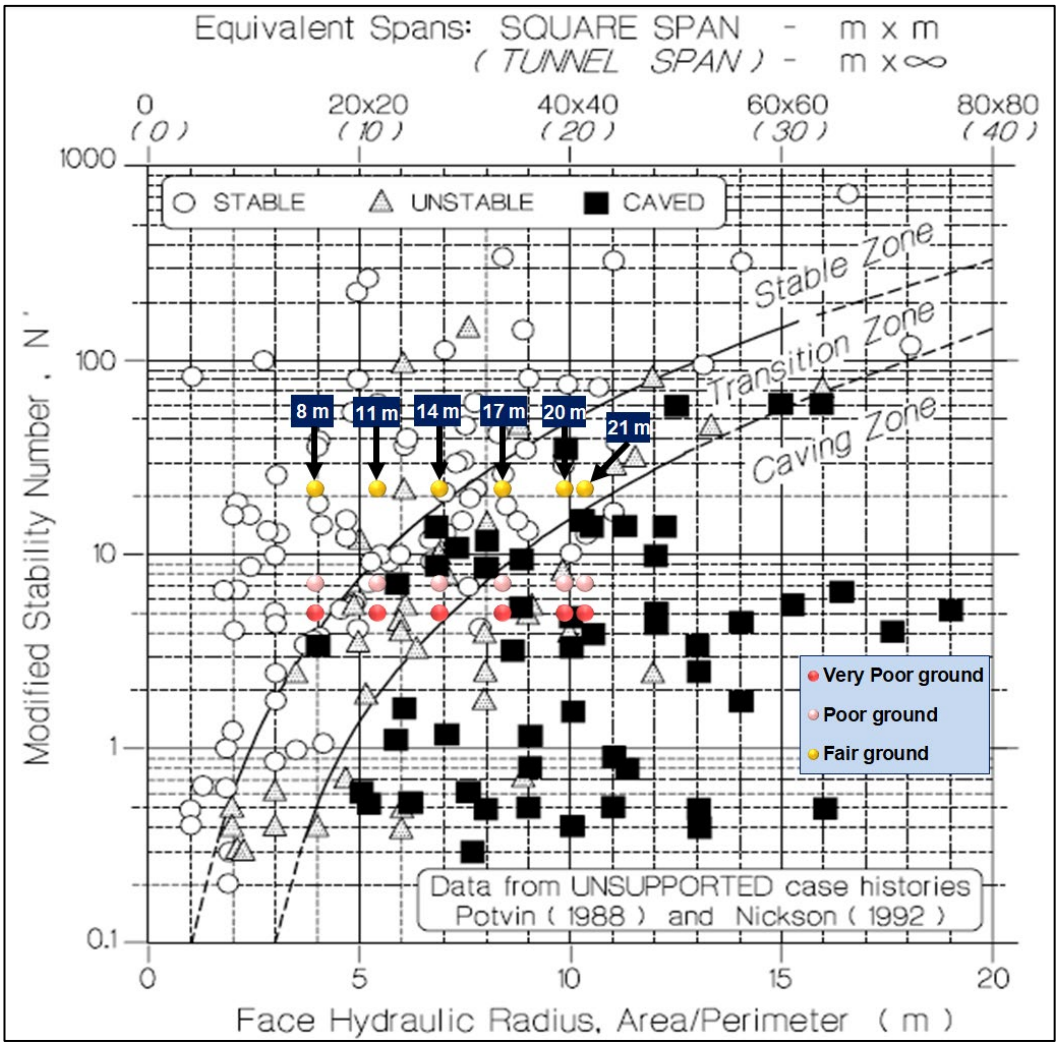


Figure 5-4: Stability number versus hydraulic radius for Rig 47 mining section

Table 5-9: Bord spans, hydraulic radii, and stability number for Rig 50 mining section

Modified Stability Number (N') and Hydraulic Radius for RIG 50				
Diagonal Spans Across Intersections (m)	**Hydraulic radius (m)**	**Minimum Modified Stability Number (N') - Very Poor ground**	**Minimum Modified Stability Number (N') - Poor ground**	**Minimum Modified Stability Number (N') - Fair ground**
8	4.0	7.9	15.2	42.7
11	5.5	7.9	15.2	42.7
14	7.0	7.9	15.2	42.7
17	8.5	7.9	15.2	42.7
20	10.0	7.9	15.2	42.7
21	10.5	7.9	15.2	42.7

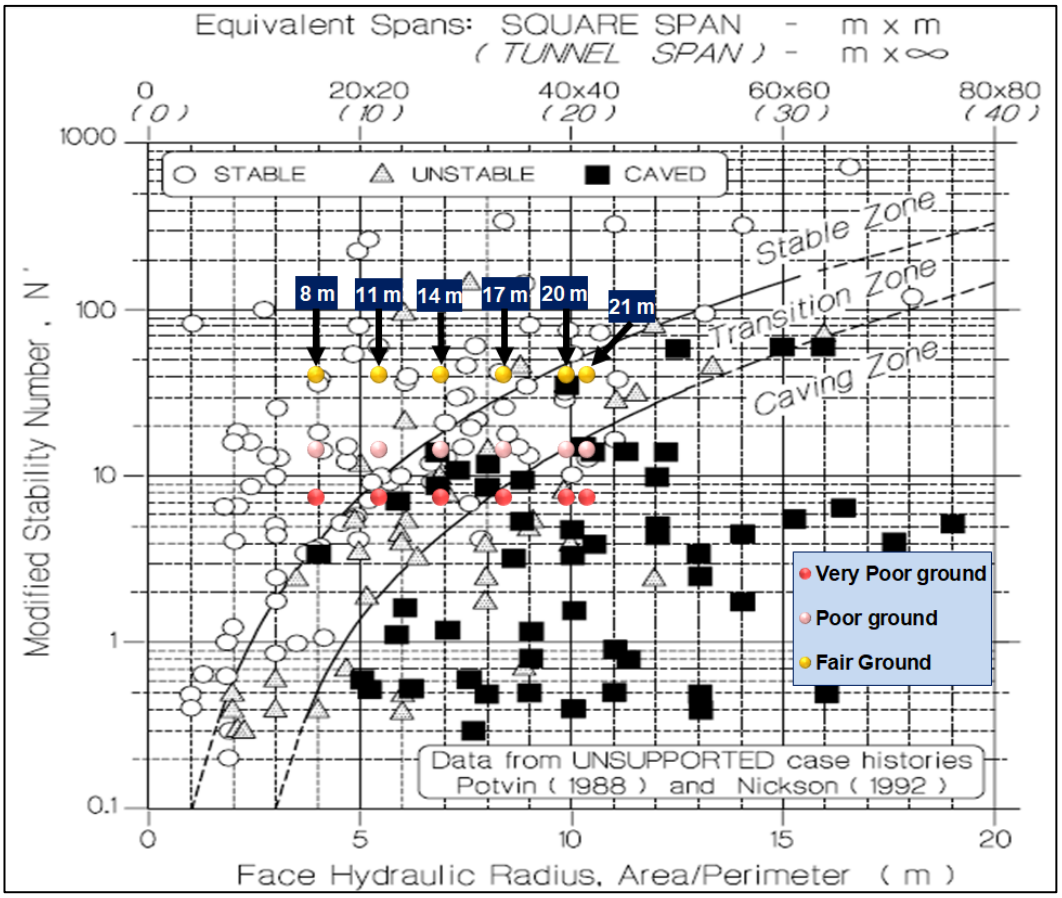


Figure 5-5: Stability number versus hydraulic radius for Rig 50 mining section

Table 5-10: Bord spans, hydraulic radii, and stability number for TC1 mining section

Modified Stability Number (N') and Hydraulic Radius for TC1				
Diagonal Spans Across Intersections (m)	Hydraulic radius (m)	Minimum Modified Stability Number (N') - Very Poor ground	Minimum Modified Stability Number (N') - Poor ground	Minimum Modified Stability Number (N') - Fair ground
8	4.0	8.0	12.3	24.1
11	5.5	8.0	12.3	24.1
14	7.0	8.0	12.3	24.1
17	8.5	8.0	12.3	24.1
20	10.0	8.0	12.3	24.1
21	10.5	8.0	12.3	24.1

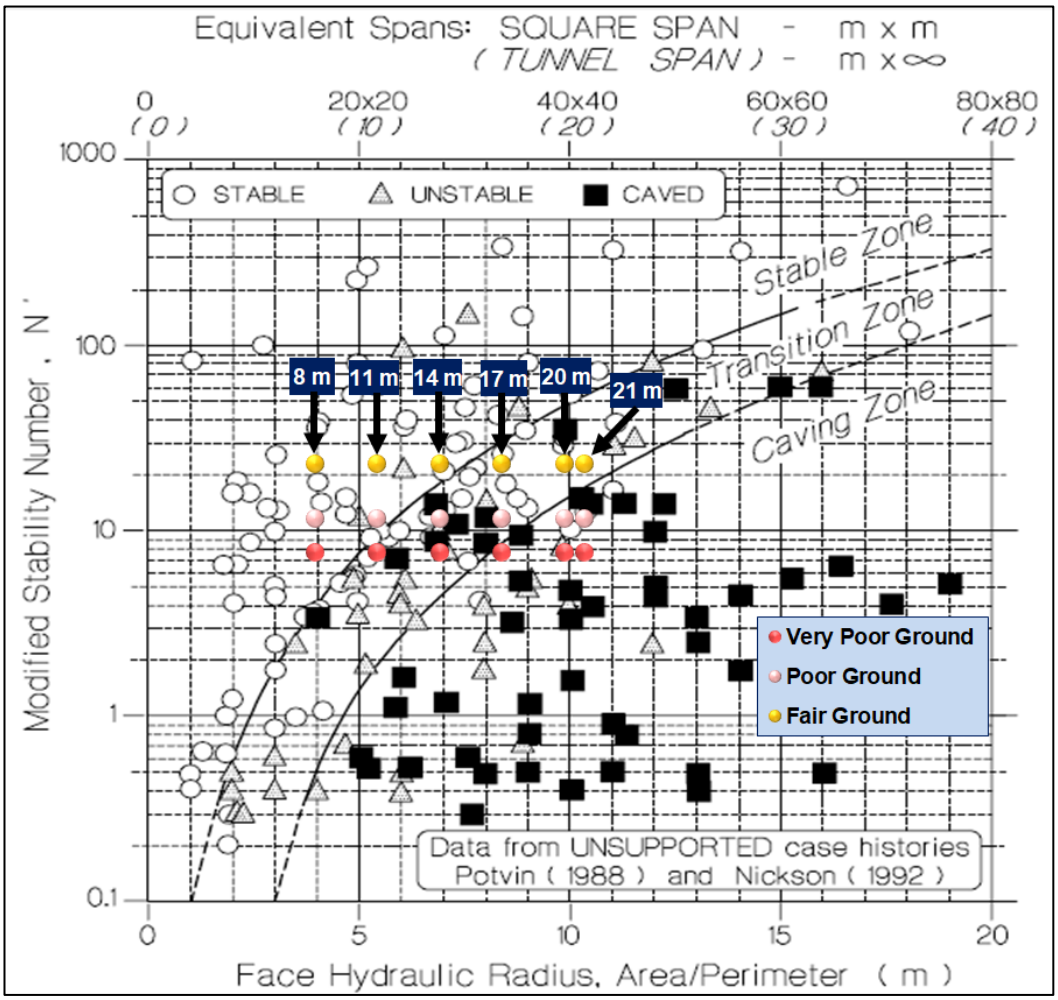


Figure 5-6: Stability number versus hydraulic radius for TC1 mining section

Table 5-11: Bord spans, hydraulic radii, and stability number for Rig 2 mining section

Modified Stability Number (N') and Hydraulic Radius for RIG 2				
Diagonal Spans Across Intersections (m)	**Hydraulic radius (m)**	**Minimum Modified Stability Number (N') - Very Poor ground**	**Minimum Modified Stability Number (N') - Poor ground**	**Minimum Modified Stability Number (N') - Fair ground**
8	4.0	3.4	7.5	21.8
11	5.5	3.4	7.5	21.8
14	7.0	3.4	7.5	21.8
17	8.5	3.4	7.5	21.8
20	10.0	3.4	7.5	21.8
21	10.5	3.4	7.5	21.8

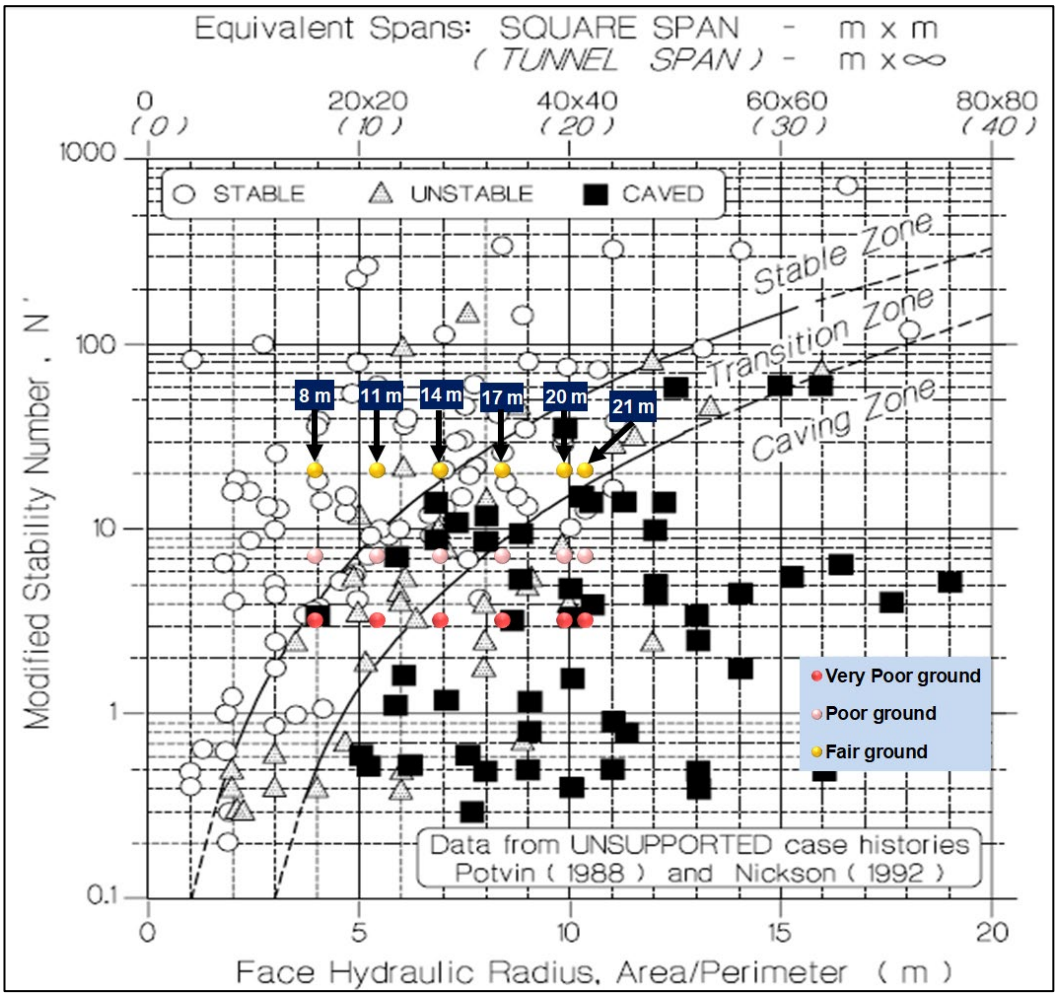


Figure 5-7: Stability number versus hydraulic radius for RIG 2 mining section

Table 5-12: Bord spans, hydraulic radii, and stability number for Rig 14 mining section

Modified Stability Number (N') and Hydraulic Radius for RIG 14				
Diagonal Spans Across Intersections (m)	Hydraulic radius (m)	Minimum Modified Stability Number (N') - Very Poor ground	Minimum Modified Stability Number (N') - Poor ground	Minimum Modified Stability Number (N') - Fair ground
8	4.0	3.2	6.9	20.4
11	5.5	3.2	6.9	20.4
14	7.0	3.2	6.9	20.4
17	8.5	3.2	6.9	20.4
20	10.0	3.2	6.9	20.4
21	10.5	3.2	6.9	20.4

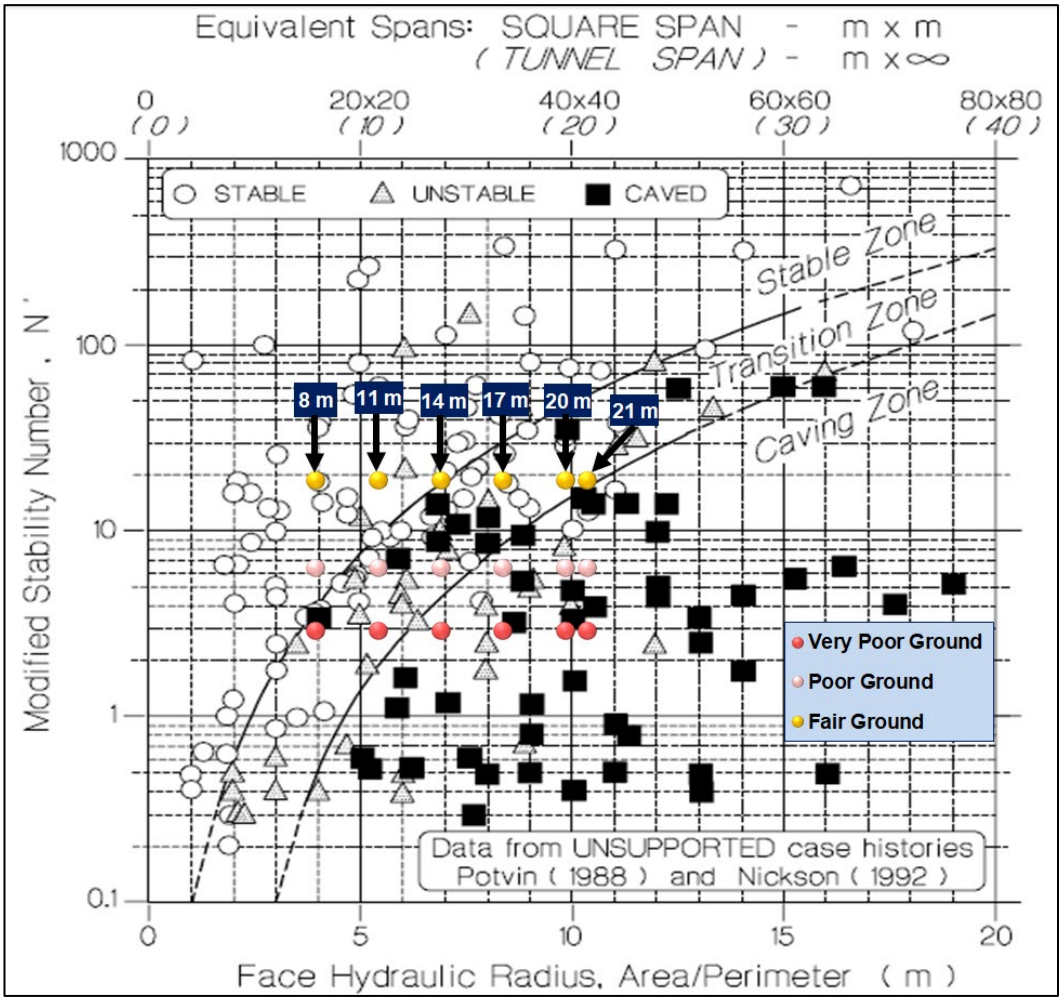


Figure 5-8: Stability number versus hydraulic radius for RIG 14 mining section

The results based on the modified stability graph method indicated that 8 m to 14 m diagonal spans (formed by 6 m to 10 m spans of orthogonal panels) are likely to

be stable without support in a fair-ground (stable zone). Additionally, stable conditions for diagonal spans ≥17 m to 21 m (formed by ≥12 m to 15 m spans of orthogonal bords) in fair-ground are likely to be achieved by the installation of support (transition zone).

In poor ground, only 8 m diagonal spans (formed by 6 m spans of orthogonal panels) fall in the stable zone, indicating the possibility of being stable without support. Diagonal spans ≥11 m to 14 m (formed by ≥8 m and 10 m spans of orthogonal bords) require support to achieve stability. Additionally, diagonal spans ≥17 m to 21 m (formed by ≥12 m to 15 m bord spans of orthogonal bords) are likely to collapse in poor ground (caved zone).

In very poor ground, it was only 8 m to 11 m diagonal spans (formed by 6 m to 8 m spans of orthogonal panels) that are likely to be stable with the installation of support (transition zone). The rest of the calculated spans fall within the caved zone and will suffer stability problems in very poor ground conditions

Stability evaluation based on the Mining Rock Mass Rating (MRMR) - The minimum $MRMR_{2000}$ values calculated under different rock mass quality classes in each production section (presented in Section 4.3.4) were also used for stability evaluation and design of the span between pillars. Again, the largest spans formed due to the intersection of equal-sized orthogonal panels (diagonal span across intersections) were used in the stability assessment. Table 5-13 to Table 5-17 present the minimum MRMR values and calculated hydraulic radii for various spans of mining in different ground conditions in each mining section.

By plotting the adjusted MRMR values obtained against the hydraulic radius, the stability of the selected diagonal spans across intersections in each section was evaluated. The adjusted MRMR versus hydraulic radius plots for each production section are presented in Figure 5-9 to Figure 5-13. In these figures, the arrows indicate the direction of increasing span from 8 m to 21 m since the individual plots are closely spaced and could not be labelled separately. The results are discussed below.

Table 5-13: Bord spans, hydraulic radii, and MRMRs for Rig 47 mining section

Mining Rock Mass Rating (MRMR) and Hydraulic Radius for RIG 47				
Diagonal Spans Across Intersections (m)	Hydraulic radius (m)	Minimum MRMR Rating - Poor ground	Minimum MRMR Rating - Fair ground	Minimum MRMR Rating - Good ground
8	4.0	25.1	42.3	67.5
11	5.5	25.1	42.3	67.5
14	7.0	25.1	42.3	67.5
17	8.5	25.1	42.3	67.5
20	10.0	25.1	42.3	67.5
21	10.5	25.1	42.3	67.5

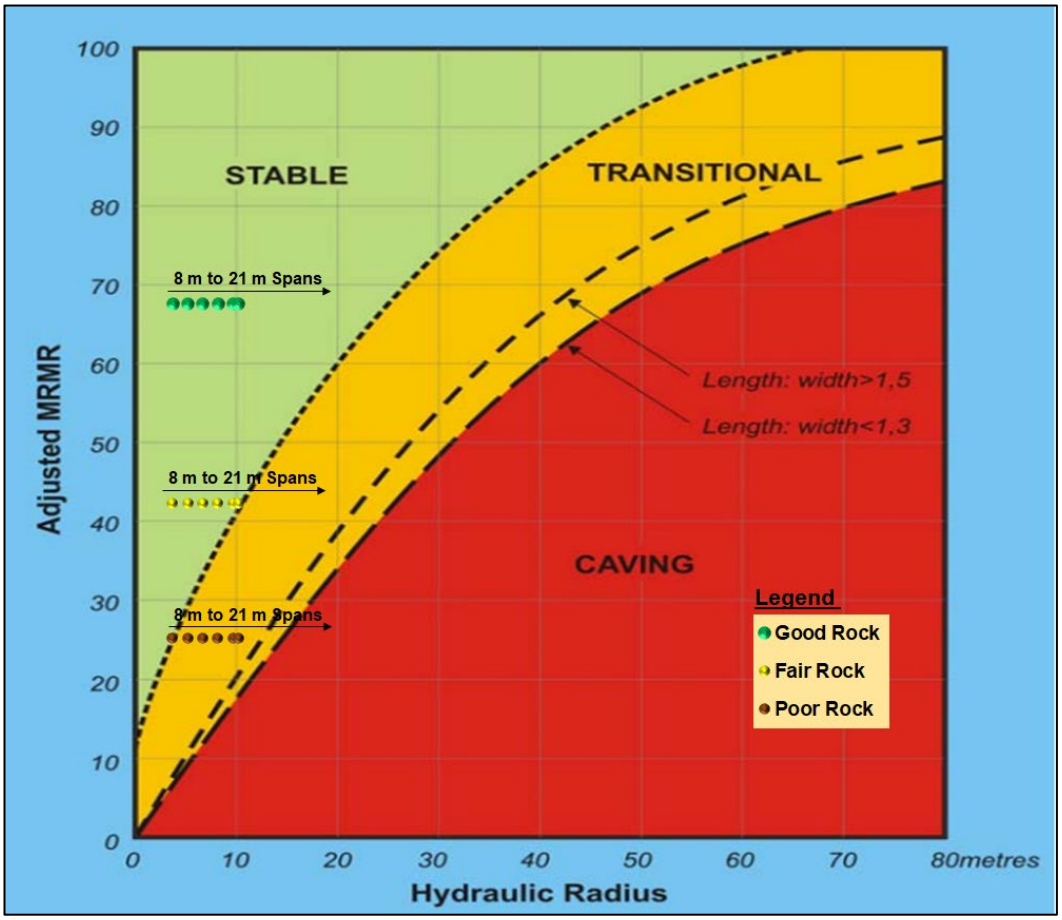


Figure 5-9: Adjusted MRMR versus hydraulic radius for RIG 47 mining section

Table 5-14: Bord spans, hydraulic radii, and MRMRs for Rig 50 mining section

Mining Rock Mass Rating (MRMR) and Hydraulic Radius for RIG 50			
Diagonal Spans Across Intersections (m)	Hydraulic radius (m)	Minimum MRMR Rating - Fair ground	Minimum MRMR Rating - Good ground
8	4.0	41.5	62.2
11	5.5	41.5	62.2
14	7.0	41.5	62.2
17	8.5	41.5	62.2
20	10.0	41.5	62.2
21	10.5	41.5	62.2

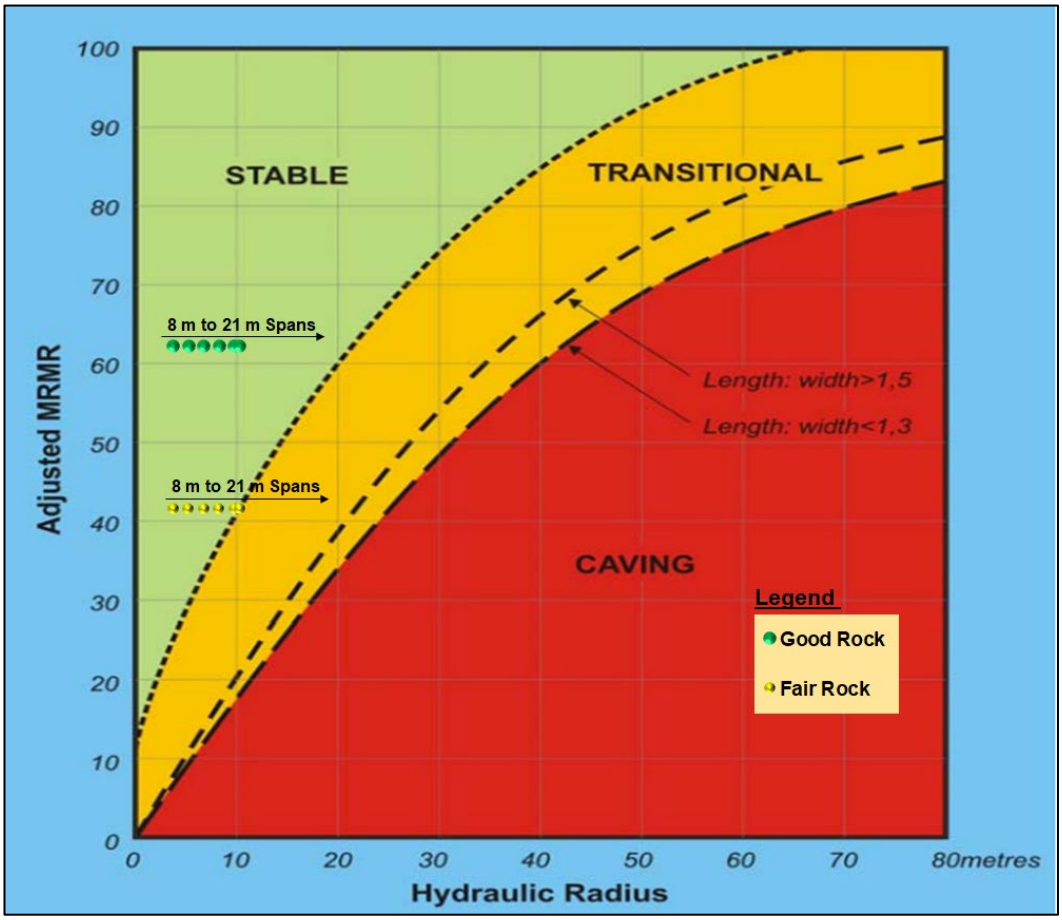


Figure 5-10: Adjusted MRMR versus hydraulic radius for RIG 50 mining section

Table 5-15: Bord spans, hydraulic radii, and MRMRs for TC1 mining section

Mining Rock Mass Rating (MRMR) and Hydraulic Radius for TC1			
Diagonal Spans Across Intersections (m)	Hydraulic radius (m)	Minimum MRMR Rating - Fair ground	Minimum MRMR Rating - Good ground
8	4.0	59.2	61.9
11	5.5	59.2	61.9
14	7.0	59.2	61.9
17	8.5	59.2	61.9
20	10.0	59.2	61.9
21	10.5	59.2	61.9

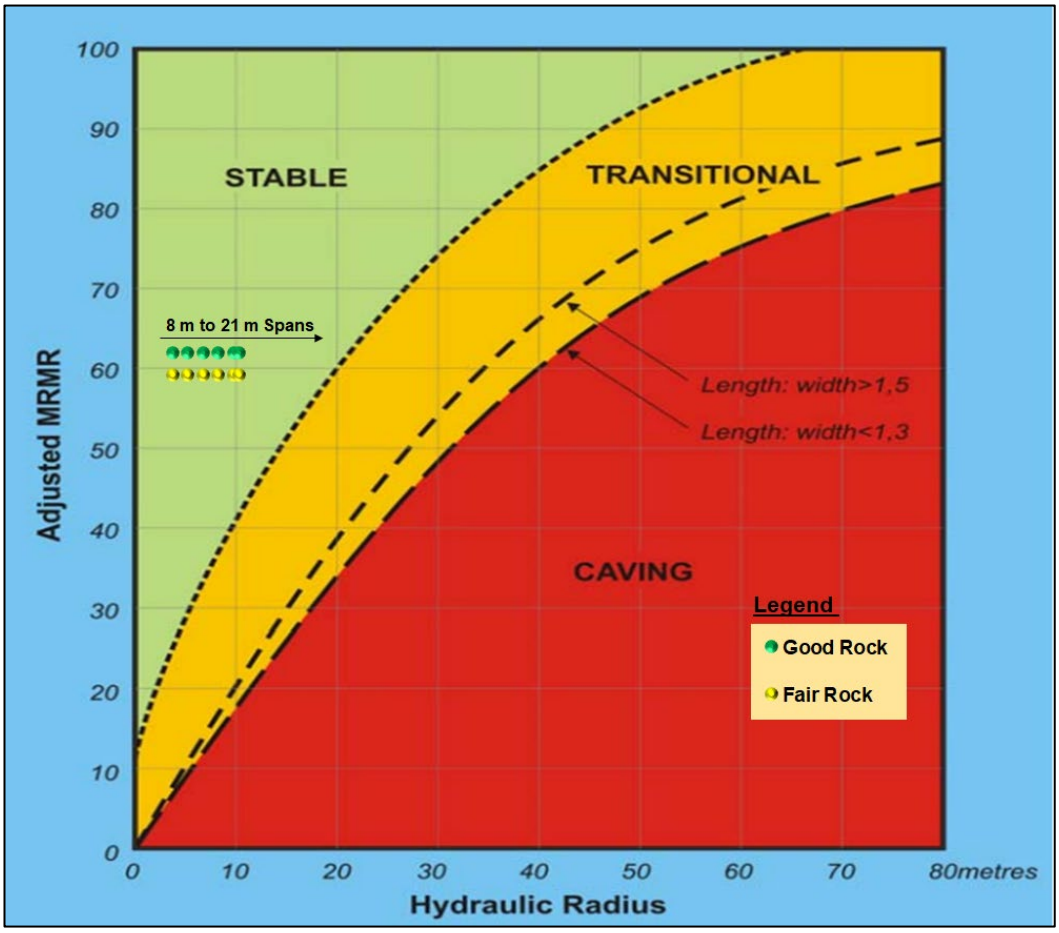


Figure 5-11: Adjusted MRMR versus hydraulic radius for TC1 mining section

Table 5-16: Bord spans, hydraulic radii, and MRMRs for Rig 2 mining section

Mining Rock Mass Rating (MRMR) and Hydraulic Radius for RIG 2			
Diagonal Spans Across Intersections (m)	Hydraulic radius (m)	Minimum MRMR Rating - Fair ground	Minimum MRMR Rating - Good ground
8	4.0	57.9	61.9
11	5.5	57.9	61.9
14	7.0	57.9	61.9
17	8.5	57.9	61.9
20	10.0	57.9	61.9
21	10.5	57.9	61.9

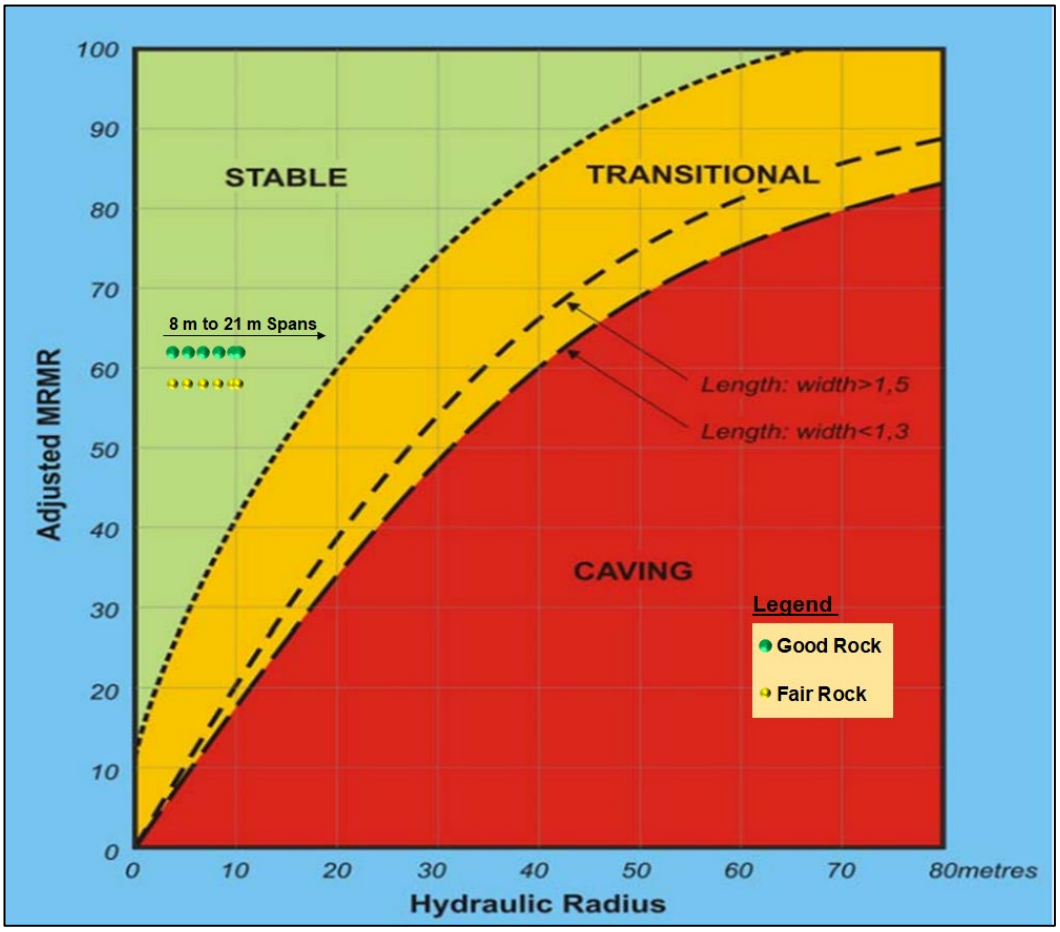


Figure 5-12: Adjusted MRMR versus hydraulic radius for Rig 2 mining section

Table 5-17: Bord spans, hydraulic radii, and MRMRs for Rig 14 mining section

Mining Rock Mass Rating (MRMR) and Hydraulic Radius for RIG 14			
Diagonal Spans Across Intersections (m)	Hydraulic radius (m)	Minimum MRMR Rating - Fair ground	Minimum MRMR Rating - Good ground
8	4.0	57.9	61.9
11	5.5	57.9	61.9
14	7.0	57.9	61.9
17	8.5	57.9	61.9
20	10.0	57.9	61.9
21	10.5	57.9	61.9

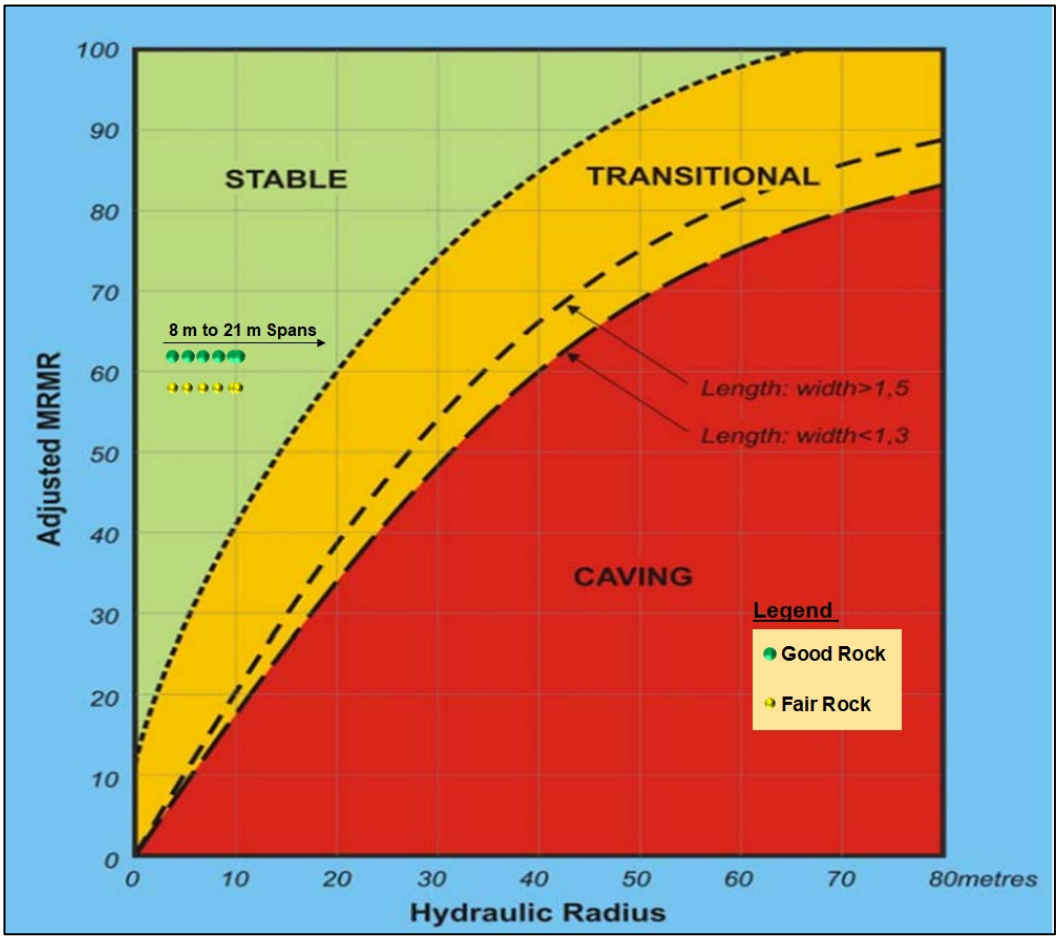


Figure 5-13: Adjusted MRMR versus hydraulic radius for Rig 14 mining section

The stability evaluation based on the MRMR indicated that when ground conditions are classified as ‘good’, all the calculated spans ranging between 8 m to 21 m (formed by 6 m to 15 m spans of orthogonal panels) are likely to be stable without

support (stable zone). Stacey (2001) stated, *"It is almost certain that, even in good quality rock masses, rock support will be required.".* The estimation of support requirements per span, mining in different ground conditions, will be presented in Chapter 6.

As ground conditions deteriorate to 'fair', stable conditions in larger spans of ≥20 m to 21 m (≥14 m to 15 m spans of orthogonal panels) can only be achieved by the installation of appropriate support (transitional zone). Additionally, the other spans of 8 m to 17 m (6 m to 12 m spans of orthogonal panels) are likely to be stable without support in fair-ground conditions. When ground conditions are classified as poor, stable conditions can only be achieved by the installation of support in all the calculated spans ranging between 8 m to 21 m (transitional zone).

5.2.2 Hangingwall Voussoir Beam Failure Analysis

The immediate pyroxenite hangingwall layer (MG1HW1) consists of a disseminated MG1 leader 1 Chromitite stringer (MG1L1), as described in Section 1.2.3. The MG1L1 is situated between 0.25 m to 0.45 m above the MG1 reef and has a thickness ranging between 0.02 m to 0.2 m. The stability assessment of the resulting rock beams between pillars is discussed below.

The characterization results in Section 4.1 indicated that the hangingwall consists of near-vertical discontinuities. Therefore, according to the literature review in Section 2.8.2, a stable rock beam will develop over a bord if a compressive arch (Voussoir arch) can form. The assessment of the stability of panel spans was conducted using the Voussoir beam theory, which assesses two Voussoir arch failure modes:

- Buckling of the roof beam resulting in 'snap-through' failure; and
- Shear failure along discontinuities at the abutments.

Table 5-18 presents all input parameters used for calculating the maximum deflection or displacement of the hangingwall for assessing buckling failure and the maximum compressive stress in the beam for computing beam shear strength at the abutments using the equations presented in Section 2.8.2. As mentioned in Section 5.1, Thorncliffe's LOM is planned to end at a depth of 800 mbs. To support future designs, the maximum compressive stress at mid-span for calculating the

maximum frictional resistance that can be mobilised was determined for various depths below the surface between 200 m and 1000 m. Local in situ stress measurements have never been conducted since the inception of Thorncliffe Mine (Glencore ECM, 2021). Therefore, estimation of in situ stress field conditions with increasing depth was based on the work by Stacey & Wesseloo (1998), as described in Section 2.5. The k-ratio was estimated by determining the average between the ratio of the major (k_1) and minor (k_3) horizontal in situ stress to vertical stress at the selected depths below the surface. This is provided in Appendix D. Table 5-18 presents the parameters for evaluating the Voussoir arch failure modes.

Table 5-18: Input parameters for Voussoir beam stability analysis

Depth Below Surface (m)	k-ratio	UCS of Pyroxenite Material (MPa)	Hangingwall Specific Weight (KN/m^2)	Rock mass Deformation Modulus (GPa)	Friction Angle, ϕ (°)	Thickness Coefficient, n
200	1.70	212.15	31.40	35.02	25.00	0.75
400	1.23					
600	0.88					
800	0.82					
1000	0.68					

Again, Voussoir beam failure analysis was conducted for the selected of 8 m to 21 m diagonal spans across intersections (representing 6 m to 15 m spans of orthogonal panels), which are the calculated self-supporting panel spans at different ground quality classes. The effect of increasing beam thickness from 0.1 m to 0.45 m on the Voussoir beam stability was also assessed.

Table 5-19 presents the Voussoir snap-through failure analysis, whilst Table 5-20 to Table 5-24 present the results of the Voussoir shear failure assessment for different depths below the surface at Thorncliffe Mine.

Table 5-19: Voussoir buckling or snap-through failure analysis at Thorncliffe Mine

Diagonal Spans Across Intersections (m)	Beam thickness (m)	10% of Beam Thickness (mm)	Maximum Deflection (mm)	Deflection (as % of the Beam Thickness)	FOS against elastic buckling or snap-through failure
8	0.10	10.00	11.61	12%	0.53
	0.15	15.00	5.16	3%	1.80
	0.20	20.00	2.90	1%	4.27
	0.25	25.00	1.86	1%	8.34
	0.30	30.00	1.29	0%	14.42
	0.35	35.00	0.95	0%	22.89
	0.40	40.00	0.73	0%	34.17
	0.45	45.00	0.57	0%	48.66
11	0.10	10.00	41.51	42%	0.15
	0.15	15.00	18.45	12%	0.50
	0.20	20.00	10.38	5%	1.20
	0.25	25.00	6.64	3%	2.33
	0.30	30.00	4.61	2%	4.03
	0.35	35.00	3.39	1%	6.40
	0.40	40.00	2.59	1%	9.56
	0.45	45.00	2.05	0%	13.61
14	0.10	10.00	108.93	109%	0.06
	0.15	15.00	48.41	32%	0.19
	0.20	20.00	27.23	14%	0.46
	0.25	25.00	17.43	7%	0.89
	0.30	30.00	12.10	4%	1.54
	0.35	35.00	8.89	3%	2.44
	0.40	40.00	6.81	2%	3.64
	0.45	45.00	5.38	1%	5.19
17	0.10	10.00	236.82	237%	0.03
	0.15	15.00	105.25	70%	0.09
	0.20	20.00	59.21	30%	0.21
	0.25	25.00	37.89	15%	0.41
	0.30	30.00	26.31	9%	0.71
	0.35	35.00	19.33	6%	1.12
	0.40	40.00	14.80	4%	1.68
	0.45	45.00	11.69	3%	2.39
20	0.10	10.00	472.93	473%	0.01
	0.15	15.00	210.19	140%	0.04
	0.20	20.00	118.23	59%	0.10
	0.25	25.00	75.67	30%	0.20
	0.30	30.00	52.55	18%	0.35
	0.35	35.00	38.61	11%	0.56
	0.40	40.00	29.56	7%	0.84
	0.45	45.00	23.35	5%	1.19
21	0.10	10.00	551.44	551%	0.01
	0.15	15.00	245.09	163%	0.04
	0.20	20.00	137.86	69%	0.09
	0.25	25.00	88.23	35%	0.18
	0.30	30.00	61.27	20%	0.30
	0.35	35.00	45.02	13%	0.48
	0.40	40.00	34.47	9%	0.72
	0.45	45.00	27.23	6%	1.02

Table 5-20: Voussoir beam shear failure analysis at 200 mbs at Thorncliffe Mine

Diagonal Spans Across Intersections (m)	Depth Below Surface (m)	Beam thickness (m)	Maximum Compressive stresses at Mid-span (MPa)	Shear Strength (Maximum Frictional Resistance (or Shear Force) that can be mobilised) (kN)	Abutment Shear Force (kN)	Shear FOS
8	200	0.10	20.98	366.83	12.71	28.85
	200	0.15	17.59	461.31	19.07	24.19
	200	0.20	15.89	555.80	25.43	21.86
	200	0.25	14.88	650.28	31.78	20.46
	200	0.30	14.20	744.77	38.14	19.53
	200	0.35	13.71	839.26	44.50	18.86
	200	0.40	13.35	933.74	50.86	18.36
	200	0.45	13.07	1028.23	57.21	17.97
11	200	0.10	30.04	525.23	17.48	30.05
	200	0.15	23.63	619.72	26.22	23.63
	200	0.20	20.42	714.20	34.96	20.43
	200	0.25	18.50	808.69	43.70	18.50
	200	0.30	17.22	903.17	52.44	17.22
	200	0.35	16.30	997.66	61.18	16.31
	200	0.40	15.61	1092.14	69.93	15.62
	200	0.45	15.08	1186.63	78.67	15.08
14	200	0.10	41.96	733.65	22.25	32.97
	200	0.15	31.57	828.14	33.37	24.81
	200	0.20	26.38	922.63	44.50	20.73
	200	0.25	23.27	1017.11	55.62	18.29
	200	0.30	21.19	1111.60	66.75	16.65
	200	0.35	19.71	1206.08	77.87	15.49
	200	0.40	18.59	1300.57	89.00	14.61
	200	0.45	17.73	1395.05	100.12	13.93
17	200	0.10	56.74	992.10	27.02	36.72
	200	0.15	41.43	1086.59	40.53	26.81
	200	0.20	33.77	1181.07	54.03	21.86
	200	0.25	29.18	1275.56	67.54	18.89
	200	0.30	26.12	1370.04	81.05	16.90
	200	0.35	23.93	1464.53	94.56	15.49
	200	0.40	22.29	1559.02	108.07	14.43
	200	0.45	21.01	1653.50	121.58	13.60
20	200	0.10	75.71	1323.92	32.12	41.22
	200	0.15	54.08	1418.40	48.17	29.44
	200	0.20	43.26	1512.89	64.23	23.55
	200	0.25	36.77	1607.37	80.29	20.02
	200	0.30	32.44	1701.86	96.35	17.66
	200	0.35	29.35	1796.34	112.41	15.98
	200	0.40	27.03	1890.83	128.47	14.72
	200	0.45	25.23	1985.32	144.52	13.74
21	200	0.10	80.89	1414.51	33.37	42.38
	200	0.15	57.53	1508.99	50.06	30.14
	200	0.20	45.85	1603.48	66.75	24.02
	200	0.25	38.84	1697.96	83.43	20.35
	200	0.30	34.17	1792.45	100.12	17.90
	200	0.35	30.83	1886.94	116.81	16.15
	200	0.40	28.33	1981.42	133.49	14.84
	200	0.45	26.38	2075.91	150.18	13.82

Table 5-21: Voussoir beam shear failure analysis at 400 mbs at Thorncliffe Mine

Diagonal Spans Across Intersections (m)	Depth Below Surface (m)	Beam thickness (m)	Maximum Compressive stresses at Mid-span (MPa)	Shear Strength (Maximum Frictional Resistance (or Shear Force) that can be mobilised) (kN)	Abutment Shear Force (kN)	Shear FOS
8	400	0.10	25.81	451.31	12.71	35.50
	400	0.15	22.42	588.03	19.07	30.83
	400	0.20	20.72	724.76	25.43	28.50
	400	0.25	19.71	861.49	31.78	27.10
	400	0.30	19.03	998.21	38.14	26.17
	400	0.35	18.54	1134.94	44.50	25.51
	400	0.40	18.18	1271.67	50.86	25.01
	400	0.45	17.90	1408.39	57.21	24.62
11	400	0.10	34.87	609.71	17.48	34.88
	400	0.15	28.46	746.44	26.22	28.47
	400	0.20	25.25	883.16	34.96	25.26
	400	0.25	23.33	1019.89	43.70	23.34
	400	0.30	22.05	1156.62	52.44	22.05
	400	0.35	21.13	1293.34	61.18	21.14
	400	0.40	20.45	1430.07	69.93	20.45
	400	0.45	19.91	1566.80	78.67	19.92
14	400	0.10	46.79	818.14	22.25	36.77
	400	0.15	36.40	954.86	33.37	28.61
	400	0.20	31.21	1091.59	44.50	24.53
	400	0.25	28.10	1228.31	55.62	22.08
	400	0.30	26.02	1365.04	66.75	20.45
	400	0.35	24.54	1501.77	77.87	19.29
	400	0.40	23.43	1638.49	89.00	18.41
	400	0.45	22.56	1775.22	100.12	17.73
17	400	0.10	61.57	1076.58	27.02	39.85
	400	0.15	46.26	1213.31	40.53	29.94
	400	0.20	38.60	1350.03	54.03	24.99
	400	0.25	34.01	1486.76	67.54	22.01
	400	0.30	30.95	1623.49	81.05	20.03
	400	0.35	28.76	1760.21	94.56	18.62
	400	0.40	27.12	1896.94	108.07	17.55
	400	0.45	25.84	2033.67	121.58	16.73
20	400	0.10	79.21	1385.05	31.78	43.58
	400	0.15	58.02	1521.78	47.68	31.92
	400	0.20	47.42	1658.50	63.57	26.09
	400	0.25	41.07	1795.23	79.46	22.59
	400	0.30	36.83	1931.96	95.35	20.26
	400	0.35	33.80	2068.68	111.25	18.60
	400	0.40	31.53	2205.41	127.14	17.35
	400	0.45	29.76	2342.14	143.03	16.38
21	400	0.10	85.72	1498.99	33.37	44.92
	400	0.15	62.36	1635.72	50.06	32.67
	400	0.20	50.68	1772.44	66.75	26.55
	400	0.25	43.67	1909.17	83.43	22.88
	400	0.30	39.00	2045.89	100.12	20.43
	400	0.35	35.66	2182.62	116.81	18.69
	400	0.40	33.16	2319.35	133.49	17.37
	400	0.45	31.21	2456.07	150.18	16.35

Table 5-22: Voussoir beam shear failure analysis at 600 mbs at Thorncliffe Mine

Diagonal Spans Across Intersections (m)	Depth Below Surface (m)	Beam thickness (m)	Maximum Compressive stresses at Mid-span (MPa)	Shear Strength (Maximum Frictional Resistance (or Shear Force) that can be mobilised) (kN)	Abutment Shear Force (kN)	Shear FOS
8	600	0.10	26.95	471.32	12.71	37.07
	600	0.15	23.56	618.05	19.07	32.41
	600	0.20	21.87	764.78	25.43	30.08
	600	0.25	20.85	911.51	31.78	28.68
	600	0.30	20.17	1058.24	38.14	27.75
	600	0.35	19.69	1204.97	44.50	27.08
	600	0.40	19.32	1351.70	50.86	26.58
	600	0.45	19.04	1498.43	57.21	26.19
11	600	0.10	36.01	629.72	17.48	36.02
	600	0.15	29.60	776.45	26.22	29.61
	600	0.20	26.40	923.18	34.96	26.40
	600	0.25	24.47	1069.91	43.70	24.48
	600	0.30	23.19	1216.64	52.44	23.20
	600	0.35	22.28	1363.37	61.18	22.28
	600	0.40	21.59	1510.10	69.93	21.60
	600	0.45	21.06	1656.84	78.67	21.06
14	600	0.10	47.93	838.14	22.25	37.67
	600	0.15	37.55	984.88	33.37	29.51
	600	0.20	32.36	1131.61	44.50	25.43
	600	0.25	29.24	1278.34	55.62	22.98
	600	0.30	27.17	1425.07	66.75	21.35
	600	0.35	25.68	1571.80	77.87	20.18
	600	0.40	24.57	1718.53	89.00	19.31
	600	0.45	23.70	1865.26	100.12	18.63
17	600	0.10	62.71	1096.59	27.02	40.59
	600	0.15	47.40	1243.32	40.53	30.68
	600	0.20	39.75	1390.05	54.03	25.73
	600	0.25	35.15	1536.78	67.54	22.75
	600	0.30	32.09	1683.51	81.05	20.77
	600	0.35	29.90	1830.24	94.56	19.36
	600	0.40	28.26	1976.98	108.07	18.29
	600	0.45	26.99	2123.71	121.58	17.47
20	600	0.10	80.35	1405.06	31.78	44.21
	600	0.15	59.16	1551.79	47.68	32.55
	600	0.20	48.57	1698.52	63.57	26.72
	600	0.25	42.21	1845.25	79.46	23.22
	600	0.30	37.97	1991.98	95.35	20.89
	600	0.35	34.94	2138.71	111.25	19.23
	600	0.40	32.67	2285.44	127.14	17.98
	600	0.45	30.91	2432.17	143.03	17.00
21	600	0.10	86.87	1519.00	33.37	45.51
	600	0.15	63.51	1665.73	50.06	33.27
	600	0.20	51.82	1812.46	66.75	27.15
	600	0.25	44.82	1959.19	83.43	23.48
	600	0.30	40.14	2105.92	100.12	21.03
	600	0.35	36.81	2252.65	116.81	19.29
	600	0.40	34.30	2399.38	133.49	17.97
	600	0.45	32.36	2546.11	150.18	16.95

Table 5-23: Voussoir beam shear failure analysis at 800 mbs at Thorncliffe Mine

Diagonal Spans Across Intersections (m)	Depth Below Surface (m)	Beam thickness (m)	Maximum Compressive stresses at Mid-span (MPa)	Shear Strength (Maximum Frictional Resistance (or Shear Force) that can be mobilised) (kN)	Abutment Shear Force (kN)	Shear FOS
8	800	0.10	31.02	542.46	12.71	42.67
	800	0.15	27.63	724.76	19.07	38.00
	800	0.20	25.94	907.06	25.43	35.67
	800	0.25	24.92	1089.37	31.78	34.27
	800	0.30	24.24	1271.67	38.14	33.34
	800	0.35	23.76	1453.97	44.50	32.67
	800	0.40	23.39	1636.27	50.86	32.18
	800	0.45	23.11	1818.57	57.21	31.79
11	800	0.10	40.08	700.86	17.48	40.09
	800	0.15	33.67	883.16	26.22	33.68
	800	0.20	30.47	1065.47	34.96	30.47
	800	0.25	28.54	1247.77	43.70	28.55
	800	0.30	27.26	1430.07	52.44	27.27
	800	0.35	26.34	1612.37	61.18	26.35
	800	0.40	25.66	1794.67	69.93	25.67
	800	0.45	25.12	1976.98	78.67	25.13
14	800	0.10	52.00	909.29	22.25	40.87
	800	0.15	41.62	1091.59	33.37	32.71
	800	0.20	36.42	1273.89	44.50	28.63
	800	0.25	33.31	1456.19	55.62	26.18
	800	0.30	31.23	1638.49	66.75	24.55
	800	0.35	29.75	1820.80	77.87	23.38
	800	0.40	28.64	2003.10	89.00	22.51
	800	0.45	27.77	2185.40	100.12	21.83
17	800	0.10	66.78	1167.73	27.02	43.22
	800	0.15	51.47	1350.03	40.53	33.31
	800	0.20	43.81	1532.34	54.03	28.36
	800	0.25	39.22	1714.64	67.54	25.39
	800	0.30	36.16	1896.94	81.05	23.40
	800	0.35	33.97	2079.24	94.56	21.99
	800	0.40	32.33	2261.54	108.07	20.93
	800	0.45	31.06	2443.85	121.58	20.10
20	800	0.10	84.42	1476.20	31.78	46.44
	800	0.15	63.23	1658.50	47.68	34.79
	800	0.20	52.63	1840.81	63.57	28.96
	800	0.25	46.28	2023.11	79.46	25.46
	800	0.30	42.04	2205.41	95.35	23.13
	800	0.35	39.01	2387.71	111.25	21.46
	800	0.40	36.74	2570.01	127.14	20.21
	800	0.45	34.98	2752.31	143.03	19.24
21	800	0.10	90.94	1590.14	33.37	47.65
	800	0.15	67.57	1772.44	50.06	35.41
	800	0.20	55.89	1954.74	66.75	29.29
	800	0.25	48.88	2137.05	83.43	25.61
	800	0.30	44.21	2319.35	100.12	23.17
	800	0.35	40.87	2501.65	116.81	21.42
	800	0.40	38.37	2683.95	133.49	20.11
	800	0.45	36.42	2866.25	150.18	19.09

Table 5-24: Voussoir beam shear failure analysis at 1000 mbs at Thorncliffe Mine

Diagonal Spans Across Intersections (m)	Depth Below Surface (m)	Beam Thickness (m)	Maximum Compressive stresses at Mid-span (MPa)	Shear Strength (Maximum Frictional Resistance (or Shear Force) that can be mobilised) (kN)	Abutment Shear Force (kN)	Shear FOS
8	1000	0.10	31.78	555.80	12.71	43.72
	1000	0.15	28.39	744.77	19.07	39.05
	1000	0.20	26.70	933.74	25.43	36.72
	1000	0.25	25.68	1122.71	31.78	35.32
	1000	0.30	25.00	1311.68	38.14	34.39
	1000	0.35	24.52	1500.66	44.50	33.72
	1000	0.40	24.16	1689.63	50.86	33.22
	1000	0.45	23.87	1878.60	57.21	32.84
11	1000	0.10	40.84	714.20	17.48	40.85
	1000	0.15	28.39	744.77	19.07	39.05
	1000	0.20	26.70	933.74	25.43	36.72
	1000	0.25	25.68	1122.71	31.78	35.32
	1000	0.30	25.00	1311.68	38.14	34.39
	1000	0.35	24.52	1500.66	44.50	33.72
	1000	0.40	24.16	1689.63	50.86	33.22
	1000	0.45	23.87	1878.60	57.21	32.84
14	1000	0.10	52.76	922.63	22.25	41.47
	1000	0.15	42.38	1111.60	33.37	33.31
	1000	0.20	37.19	1300.57	44.50	29.23
	1000	0.25	34.07	1489.54	55.62	26.78
	1000	0.30	32.00	1678.51	66.75	25.15
	1000	0.35	30.51	1867.48	77.87	23.98
	1000	0.40	29.40	2056.45	89.00	23.11
	1000	0.45	28.54	2245.43	100.12	22.43
17	1000	0.10	67.54	1181.07	27.02	43.72
	1000	0.15	52.23	1370.04	40.53	33.81
	1000	0.20	44.58	1559.02	54.03	28.85
	1000	0.25	39.98	1747.99	67.54	25.88
	1000	0.30	36.92	1936.96	81.05	23.90
	1000	0.35	34.74	2125.93	94.56	22.48
	1000	0.40	33.10	2314.90	108.07	21.42
	1000	0.45	31.82	2503.87	121.58	20.60
20	1000	0.10	85.18	1489.54	31.78	46.86
	1000	0.15	63.99	1678.51	47.68	35.21
	1000	0.20	53.40	1867.48	63.57	29.38
	1000	0.25	47.04	2056.45	79.46	25.88
	1000	0.30	42.80	2245.43	95.35	23.55
	1000	0.35	39.78	2434.40	111.25	21.88
	1000	0.40	37.51	2623.37	127.14	20.63
	1000	0.45	35.74	2812.34	143.03	19.66
21	1000	0.10	91.70	1603.48	33.37	48.05
	1000	0.15	68.34	1792.45	50.06	35.81
	1000	0.20	56.66	1981.42	66.75	29.69
	1000	0.25	49.65	2170.39	83.43	26.01
	1000	0.30	44.97	2359.37	100.12	23.57
	1000	0.35	41.64	2548.34	116.81	21.82
	1000	0.40	39.13	2737.31	133.49	20.51
	1000	0.45	37.19	2926.28	150.18	19.48

The results indicated that the probability of both assessed Voussoir beam failure modes (based on safety factors against failure) occurring decreases with increasing beam thickness and increases with increasing span dimension. As presented in

Table 5-19, the onset of snap-through failure occurs when a beam thickness of 0.30 m in a 17 m span has a minimum deflection of 26.31 mm (highlighted in green colour). This means for beam thicknesses of less than 0.30 m, there will be potential for snap-through failure. This is also confirmed by the factor of safety against elastic buckling failure in the results (FOS<1).

Interestingly, analysis of the historic FOG database at the mine in Section 1.2.6 indicated that 48% of all FOGs are due to hangingwall parting planes situated at a modal fallout height of 0.25 m (less than 0.30 m thickness). The mine can include the MG1L1 stringer in the mining cut as a strategy for eliminating the source of many FOGs.

Finally, as presented in Table 5-20 to Table 5-24 the calculated FOS against abutment shear failure indicated that there is no potential for shear-type beam failure (FOS>1) for all the spans evaluated up to the depth of 1000 mbs. The results also indicated that the shear FOS generally increases with increasing depth below the surface but decreases with increasing beam thickness.

5.2.3 Structural Stability Analysis

Different maximum unsupported bord spans were calculated for various underground ground conditions. The stability of individual keyblocks or unstable wedges defined by structural features between pillars must still be considered to ensure stable conditions. The Dips stereonet plots in Section 4.1 gave an early indication that there is the possibility of unstable wedges forming in three of the five current production ore-blocks. These are Rig 47, Rig 50, and TC1.

To determine support requirements which will ensure the stability of the wedges forming, it was vital to determine the actual size of the wedges and wedge failure modes. As discussed in Section 2.8.3, there are computer programs recommended for evaluating the stability of wedges forming in underground excavations.

Rocscience's software '*UNWEDGE*' was used to evaluate the stability of the wedges forming in Rig 47, Rig 50, and TC1. The discontinuity sets identified in each production section were entered into the program, with the cross-section and

orientation of the bords in each mining block. The program also required the specification of discontinuity shear strength properties. Mohr-Coulomb failure criterion, frictional parameters of discontinuities with serpentinite infill material (worst case) were entered. The program then determined the location, size, and failure mode of the largest wedges which are formed in the hangingwall, footwall, and sidewalls of the bords.

The programme followed a conservative approach to determining the size and safety factors of the largest possible unstable wedges that can be formed between pillars. However, the program also allowed the formed wedges to be 'scaled down' to more realistic dimensions by using site-specific recorded FOG data. Indeed, the initial wedges formed by the program in each mining section were too large and did not reflect the typical observed fallouts at the mine.

The historical FOG data at Thorncliffe Mine occurred between the last line of permanent support and the face. This means the FOGs occurred in an unsupported area. These FOGs were used to scale down the formed wedges to more realistic sizes based on observed wedge sizes. Specifically, the wedges formed were scaled down using the fallout thickness, discontinuity trace lengths, and persistence since these factors dictate the actual wedge sizes formed in the rock mass. A maximum fallout thickness of 0.8 m (from the FOG database) was used to scale down the maximum apex of the wedges formed. A modal discontinuity trace length and persistence of 10 m were used to allow maximum lateral extents (area) of the wedges to be defined in all the sections. This gave realistic results, which were predicted by the preliminary structural stability assessment in Section 4.1.

Since in-situ stresses can have a stabilising effect (due to clamping forces) on the wedges formed in the roof, in-situ stresses were ignored in the analysis. This ensured that the analysis and support design were conservative. A design factor of safety of 1.5 was used in the program to assess the stability of the formed wedges. In each production section, the effect of advancing the bords along strike and dip direction on the stability of wedges formed was also assessed. However, in-depth analysis, such as the effect of a change in strike direction, was excluded

from this case study. The results of RIG 47, RIG 50, and TC1 wedge stability analysis are presented below.

Rig 47 Unwedge Analysis Results

The interaction of Rig 47 strike bords and splits with the identified discontinuity sets is presented in Figure 5-14 and Figure 5-16, respectively. The trend of the axis of the stope excavations is represented with a chain dotted line, whilst the plunge is marked with a cross. Figure 5-15 and Figure 5-17 present a multi-view of the Rig 47 strike and dip stope panels showing the wedges formed in the roof, sidewalls, and floor by the three discontinuity sets. Table 5-25 summarises the stability parameters of each wedge formed, which includes wedge FOS, volume, excavation face area, support pressure required to accomplish design FOS, and wedge failure mode. Upper and lower right or left roof wedges are formed by prominent discontinuities (mostly pegmatite veins and joints) which terminate at the reef-hangingwall/footwall contact as observed underground.

As shown in the results in Table 5-25 and Table 5-26, the size of all the unstable wedges (wedges with FOS<1) is quite small, with a maximum volume of 0.002 m^3, which indicates a blocky rock mass structure. The maximum support pressure required to accomplish the wedge design factor of safety in Rig 47 is 12 kPa, which is quite small. The type of support systems required to stabilize the wedges will be discussed in Chapter 6. According to the results, fewer wedges formed in the splits than in the strike bords.

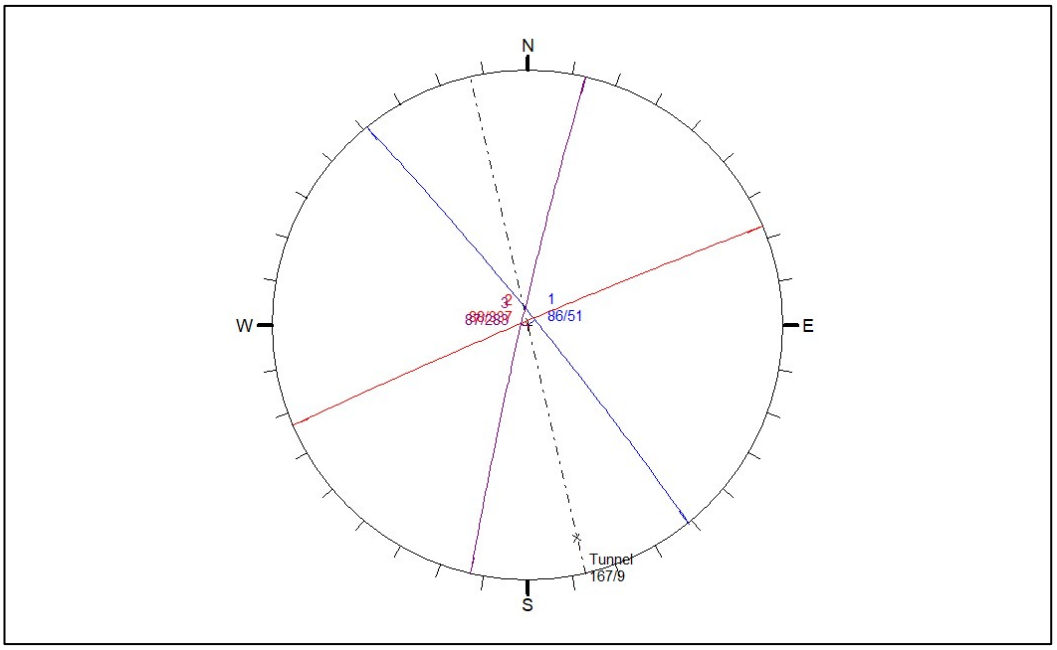


Figure 5-14: Interaction of a Rig 47 strike bords with the identified discontinuity sets

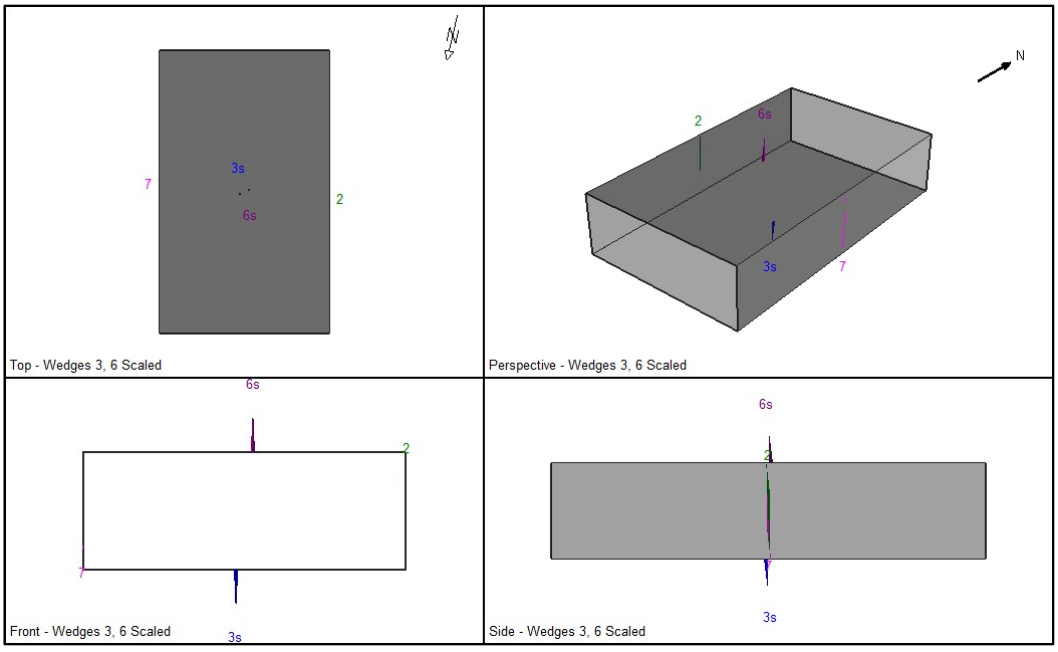


Figure 5-15: Wedges formed in the hangingwall, footwall, and sidewall of RIG 47 strike bords

Table 5-25: Results of the maximum wedges formed in RIG 47 strike bord

Parameters	Roof Wedge	Upper Right wedge	Lower Left wedge	Floor
Factor of Safety	0.016	0.038	0.024	Stable
Wedge Volume (m^3)	0.001	0.000	0.000	0.001
Excavation Face Area (m^2)	0.000	0.060	0.060	0.060
Support Pressure Required (KPa)	12.0	1.0	1.0	0.0
Failure Mode	Sliding on Joint Set 2	Wedge sliding along line of intersection of Joint Set 1 and 2	Sliding on Joint Set 3	Unconditionaly stable wedge

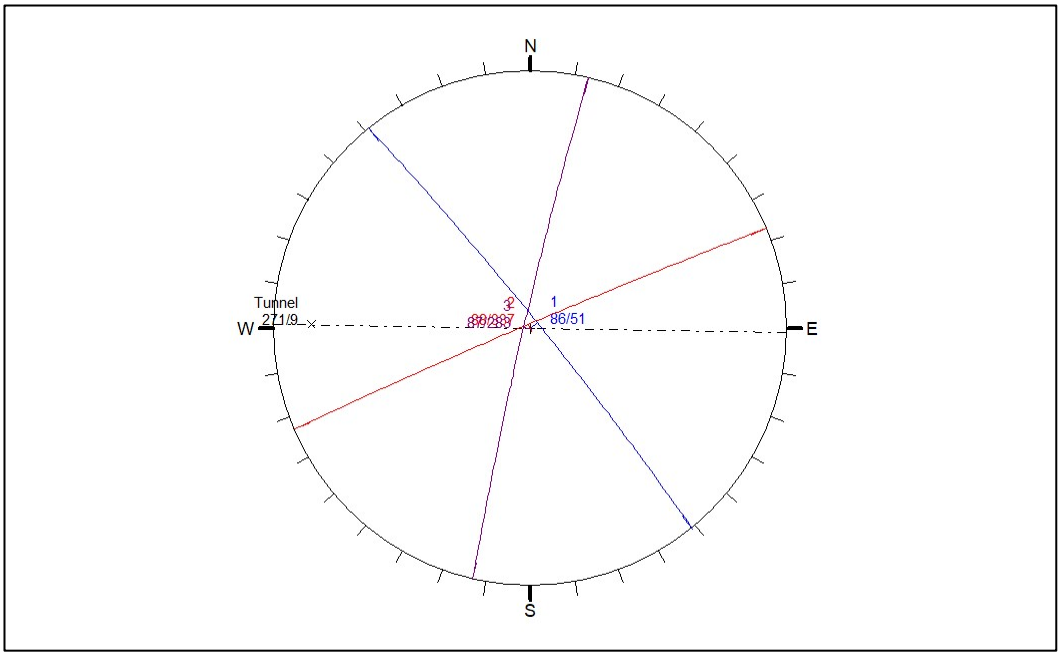


Figure 5-16: Interaction of a Rig 47 ventilation holings with the identified discontinuity sets

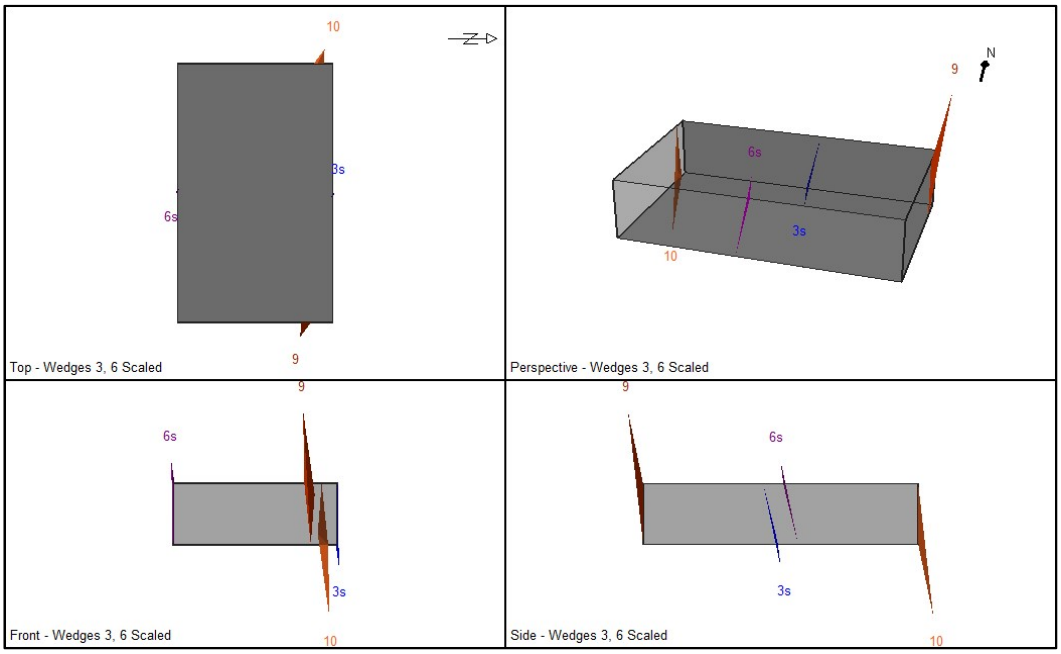


Figure 5-17: Wedges formed in the hangingwall, footwall, and sidewall of RIG 47 ventilation holings

Table 5-26: Results of the maximum wedges formed in RIG 47 ventilation holings

Parameters	Upper Left wedge	Lower Right wedge
Factor of Safety	0.016	Stable
Wedge Volume (m^3)	0.002	0.002
Excavation Face Area (m^2)	0.080	0.080
Support Pressure Required (kPa)	2.0	0.0
Failure Mode	Sliding on Joint Set 2	Unconditionally stable wedge

Rig 50 Unwedge Analysis Results

In Figure 5-18 and Figure 5-20, the five discontinuity sets are shown to interact with the strike bords and splits in the RIG 50 mining block. The Unwedge program has an inherent limitation of being unable to compute the interaction of more than three discontinuity sets simultaneously. However, a function called 'Joint Combination Analyser' was used to automatically compute the most critical discontinuity set combinations since more than three discontinuity sets were defined. Ten possible combinations consisting of three discontinuity sets were determined and used to assess the formation of wedges in different locations of

the bords and splits in the Rig 50 section. Figure 5-19 and Figure 5-21 present a multi-view of the wedges formed in different areas of the strike bords and splits. The results in Table 5-27 to Table 5-37 show the formation of relatively small wedges in both the strike bords and splits, with a maximum volume of 0.3 m^3. While the support pressure required to maintain stability for most of the Rig 50 wedges formed is slightly higher than Rig 47 wedges, the maximum support pressure required to achieve the design FOS is 13 kPa, which is also quite small. Again, in Rig 50, the splits or ventilation holings indicated the formation of fewer wedges than strike bords.

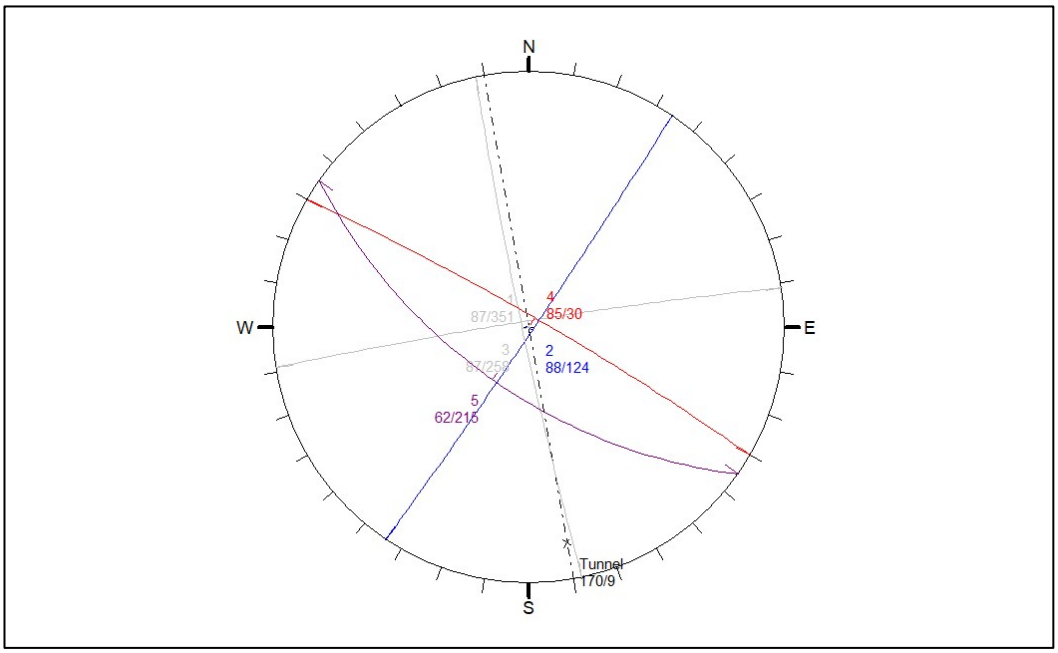


Figure 5-18: Interaction of Rig 50 strike bords with the identified discontinuity sets

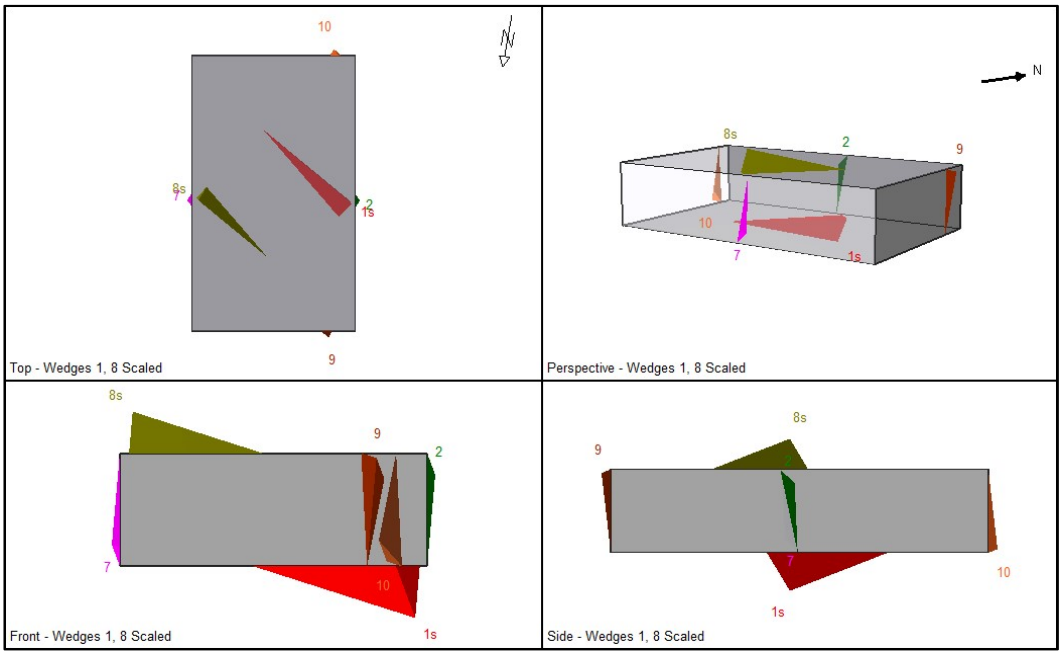


Figure 5-19: Wedges formed in the hangingwall, footwall, and sidewall of RIG 50 strike bords

Table 5-27: Results of the maximum wedges formed in the hangingwall of RIG 50 strike bords

Wedges formed in the Roof - Strike Bords							
Combination	Joint A	Joint B	Joint C	Factor of Saftey	Required Support Pressure (kPa)	Wedge Volume (m^3)	Excavation Area (m^2)
	2	3	4	0.00	13.3	0.003	0.013
	1	3	4	0.02	12.4	0.001	0.005
	1	2	5	No wedges formed	-	-	-
	1	2	4	No wedges formed	-	-	-
	1	2	3	No wedges formed	-	-	-
	1	4	5	No wedges formed	-	-	-
	3	4	5	No wedges formed	-	-	-
	1	3	5	No wedges formed	-	-	-
	2	3	5	No wedges formed	-	-	-
	2	4	5	No wedges formed	-	-	-

Table 5-28: Results of the maximum wedges formed in the upper right side of RIG 50 strike bords

Wedges formed in the Upper Right Side - Strike Bords							
Combination	Joint A	Joint B	Joint C	Factor of Saftey	Required Support Pressure (kPa)	Wedge Volume (m^3)	Excavation Area (m^2)
	1	2	3	0.00	13.0	0.002	0.008
	2	4	5	0.06	3.0	0.018	0.336
	2	3	4	0.06	1.0	0.009	0.372
	1	4	5	0.07	2.0	0.007	0.140
	1	3	4	0.07	1.0	0.003	0.145
	1	2	5	0.13	2.0	0.013	0.226
	3	4	5	No wedges formed	-	-	-
	1	3	5	No wedges formed	-	-	-
	2	3	5	No wedges formed	-	-	-
	2	4	5	No wedges formed	-	-	-

Table 5-29: Results of the maximum wedges formed in the upper left side of RIG 50 strike bords

Wedges formed in the Upper Left Side - Strike Bords							
Combination	Joint A	Joint B	Joint C	Factor of Saftey	Required Support Pressure (kPa)	Wedge Volume (m^3)	Excavation Area (m^2)
	1	2	3	No wedges formed	-	-	-
	2	4	5	0.06	13.0	0.246	0.915
	2	3	4	No wedges formed	-	-	-
	1	4	5	0.07	12.0	0.205	0.765
	1	3	4	No wedges formed	-	-	-
	1	2	5	0.00	13.0	0.041	0.152
	3	4	5	0.02	8.0	0.333	2.873
	1	3	5	0.02	5.0	0.113	2.129
	2	3	5	0.13	3.0	0.067	1.757
	1	2	4	3.40	0.0	0.001	0.009

Table 5-30: Results of the maximum wedges formed in the lower left side of RIG 50 strike bords

Wedges formed in the Lower Left Side - Strike Bords							
Combination	Joint A	Joint B	Joint C	Factor of Saftey	Required Support Pressure (kPa)	Wedge Volume (m^3)	Excavation Area (m^2)
	1	2	3	0.02	2.0	0.006	0.242
	2	3	4	0.02	2.0	0.009	0.372
	1	3	4	0.05	2.0	0.003	0.145
	1	2	5	0.25	3.0	0.013	0.226
	2	4	5	0.25	3.0	0.018	0.336
	1	4	5	0.81	1.0	0.007	0.140
	3	4	5	No wedges formed	-	-	-
	1	3	5	No wedges formed	-	-	-
	2	3	5	No wedges formed	-	-	-
	2	4	5	No wedges formed	-	-	-

Table 5-31: Results of the maximum wedges formed in the lower right side of RIG 50 strike bords

Wedges formed in the Lower Right Side - Strike Bords							
Combination	Joint A	Joint B	Joint C	Factor of Saftey	Required Support Pressure (kPa)	Wedge Volume (m^3)	Excavation Area (m^2)
	1	2	4	0.07	2.5	0.001	0.009
	2	3	5	3.40	0.0	0.067	1.757
	1	4	5	3.40	0.0	0.205	0.765
	3	4	5	3.40	0.0	0.333	2.873
	2	4	5	3.40	0.0	0.246	0.915
	1	2	5	3.40	0.0	0.041	0.152
	1	3	5	3.40	0.0	0.113	2.129
	1	3	5	No wedges formed	-	-	-
	2	3	5	No wedges formed	-	-	-
	2	4	5	No wedges formed	-	-	-

Table 5-32: Results of the maximum wedges formed in the floor of RIG 50 strike bords

Wedges formed in the Floor - Strike Bords							
Combination	Joint A	Joint B	Joint C	Factor of Saftey	Required Support Pressure (kPa)	Wedge Volume (m^3)	Excavation Area (m^2)
	2	3	4	3.40	0.0	0.003	0.013
	1	3	4	3.40	0.0	0.001	0.005
	2	3	5	No wedges formed	-	-	-
	3	4	5	No wedges formed	-	-	-
	1	2	5	No wedges formed	-	-	-
	2	4	5	No wedges formed	-	-	-
	1	4	5	No wedges formed	-	-	-
	1	3	5	No wedges formed	-	-	-
	2	3	5	No wedges formed	-	-	-
	2	4	5	No wedges formed	-	-	-

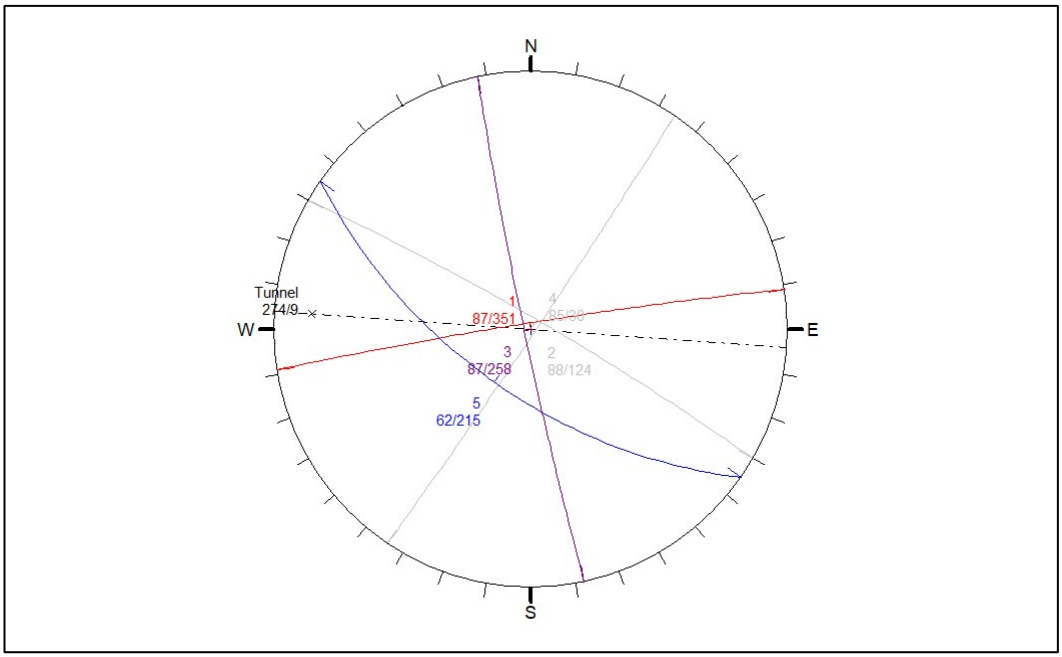


Figure 5-20: Interaction of Rig 50 ventilation holings with the identified discontinuity sets

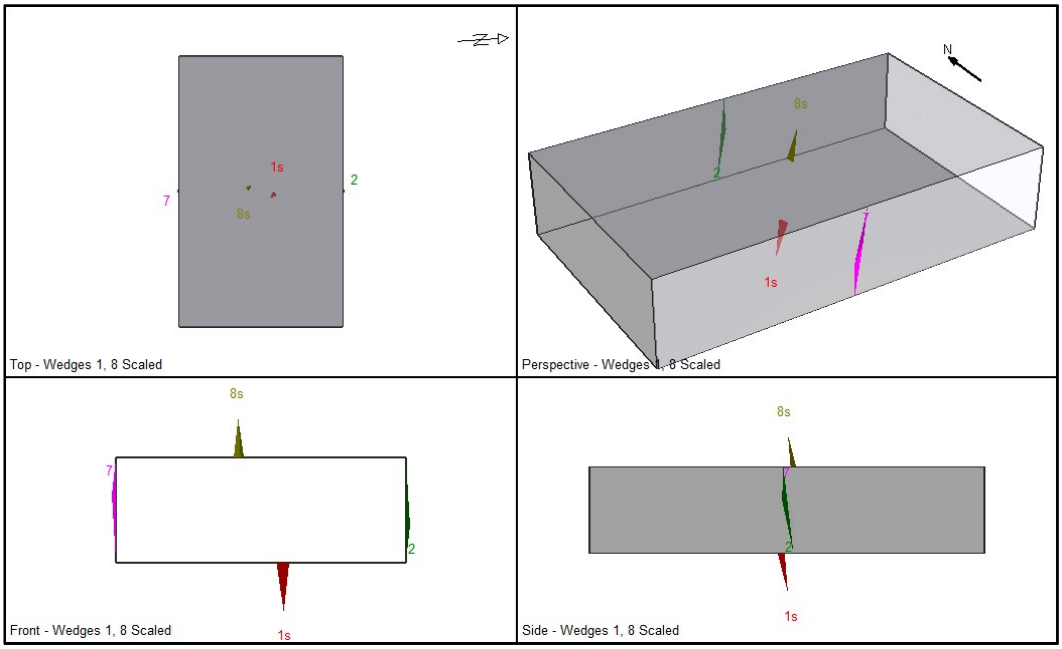


Figure 5-21: Wedges formed in the hangingwall, footwall, and sidewall of RIG 50 ventilation holings

Table 5-33: Results of the maximum wedges formed in the roof of RIG 50 ventilation holings

Wedges formed in the Roof - Splits/Ventilation Holings							
Combination	Joint A	Joint B	Joint C	Factor of Saftey	Required Support Pressure (kPa)	Wedge Volume (m^3)	Excavation Area (m^2)
	1	2	3	0.00	13.0	0.002	0.008
	2	3	4	0.00	13.0	0.003	0.013
	1	4	5	No wedges formed	-	-	-
	3	4	5	No wedges formed	-	-	-
	2	3	5	No wedges formed	-	-	-
	1	3	4	No wedges formed	-	-	-
	1	2	4	No wedges formed	-	-	-
	1	2	5	No wedges formed	-	-	-
	1	3	5	No wedges formed	-	-	-
	2	3	5	No wedges formed	-	-	-

Table 5-34: Results of the maximum wedges formed in the upper right side of RIG 50 ventilation holings

Wedges formed in the Upper Right Side - Splits/Ventilation Holings							
Combination	Joint A	Joint B	Joint C	Factor of Saftey	Required Support Pressure (kPa)	Wedge Volume (m^3)	Excavation Area (m^2)
	1	2	3	No wedges formed	-	-	-
	2	3	4	No wedges formed	-	-	-
	1	4	5	No wedges formed	-	-	-
	3	4	5	No wedges formed	-	-	-
	2	3	5	0.13	4.0	0.032	0.263
	1	3	4	No wedges formed	-	-	-
	1	2	4	3.40	0.0	0.001	0.013
	1	2	5	0.00	13.0	0.046	0.171
	1	3	5	0.02	13.0	0.062	0.229
	2	3	5	No wedges formed	-	-	-

Table 5-35: Results of the maximum wedges formed in the upper left side of RIG 50 ventilation holings

Wedges formed in the Upper Left Side - Splits/Ventilation Holings							
Combination	Joint A	Joint B	Joint C	Factor of Saftey	Required Support Pressure (kPa)	Wedge Volume (m^3)	Excavation Area (m^2)
	1	2	3	0.02	2.0	0.003	0.156
	2	3	4	0.04	3.0	0.004	0.146
	1	4	5	0.04	3.0	0.026	0.751
	3	4	5	0.20	4.0	0.046	0.509
	2	4	5	0.04	4.0	0.013	0.340
	1	3	4	0.02	4.0	0.011	0.269
	1	2	4	No wedges formed	-	-	-
	1	2	5	0.13	2.0	0.020	0.545
	1	3	5	0.02	2.0	0.009	0.390
	2	3	5	No wedges formed	-	-	-

Table 5-36: Results of the maximum wedges formed in the lower left side of RIG 50 ventilation holings

Wedges formed in the Lower Left Side - Splits/Ventilation Holings							
Combination	Joint A	Joint B	Joint C	Factor of Saftey	Required Support Pressure (kPa)	Wedge Volume (m^3)	Excavation Area (m^2)
	1	2	3	No wedges formed	-	-	-
	2	3	4	No wedges formed	-	-	-
	1	4	5	No wedges formed	-	-	-
	3	4	5	No wedges formed	-	-	-
	2	3	5	0.04	0.0	0.032	0.263
	1	3	4	No wedges formed	-	-	-
	1	2	4	0.07	12.0	0.001	0.013
	1	2	5	0.13	0.0	0.046	0.171
	1	3	5	0.02	0.0	0.062	0.229
	2	3	5	No wedges formed	-	-	-

Table 5-37: Results of the maximum wedges formed in the floor of RIG 50 ventilation holings

Wedges formed in the Floor - Splits/Ventilation Holings							
Combination	Joint A	Joint B	Joint C	Factor of Saftey	Required Support Pressure (kPa)	Wedge Volume (m^3)	Excavation Area (m^2)
	1	2	3	3.40	0.0	0.002	0.008
	2	3	4	3.40	0.0	0.003	0.013
	1	4	5	No wedges formed	-	-	-
	3	4	5	No wedges formed	-	-	-
	2	3	5	No wedges formed	-	-	-
	1	3	4	No wedges formed	-	-	-
	1	2	4	No wedges formed	-	-	-
	1	2	5	No wedges formed	-	-	-
	1	3	5	No wedges formed	-	-	-
	2	3	5	No wedges formed	-	-	-

TC1 Unwedge Analysis Results

Figure 5-22 shows that the area defined by the intersection of the three TC1 mining block discontinuity sets is quite small. As a result, the trend of the axis of the stope excavations does not pass through that defined area. This was a preliminary indication that only a few wedges may form. Figure 5-23 to Figure 5-25, show that no roof wedges were likely and only stope excavation perimeter wedges were formed, which still needed to be stabilized. The results in Table 5-38 and Table 5-39 show that the perimeter wedges are small, with a maximum wedge volume of only 0.001 m^3. Some of the wedges formed were stable, with only 1 kPa required to accomplish design FOS.

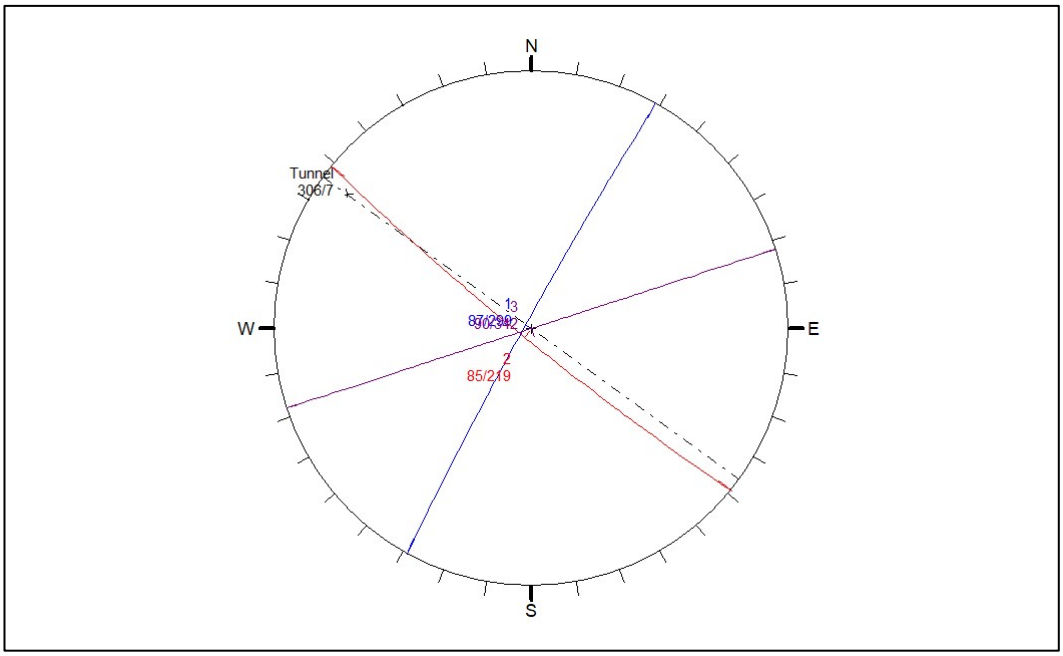


Figure 5-22: Interaction of TC1 strike bords with the identified discontinuity sets

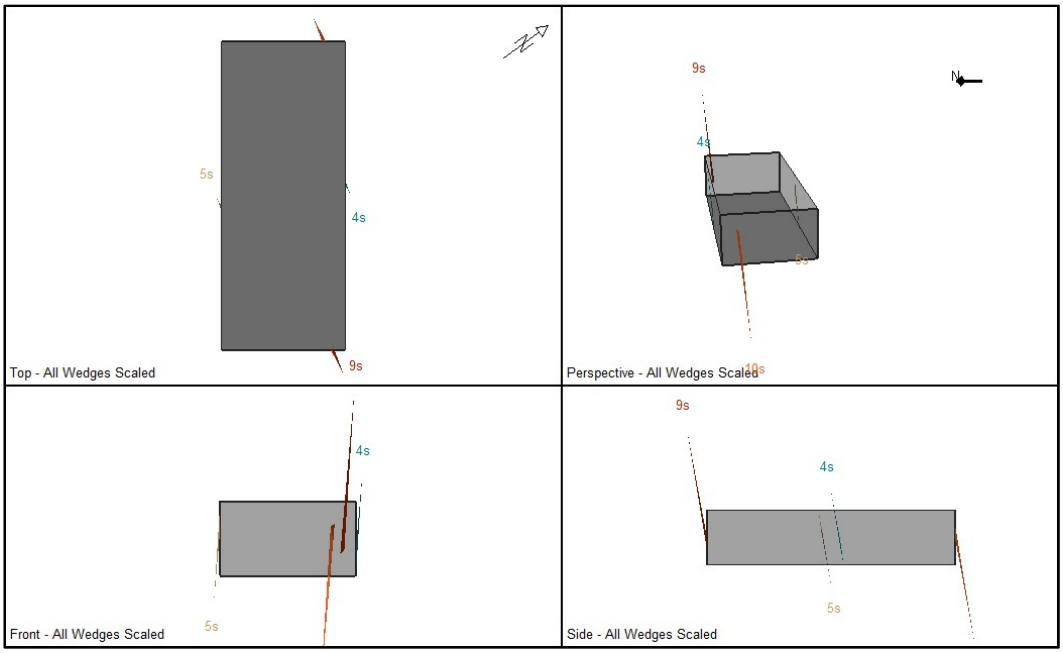


Figure 5-23: Wedges formed in the hangingwall, footwall, and sidewall of TC1 strike bords

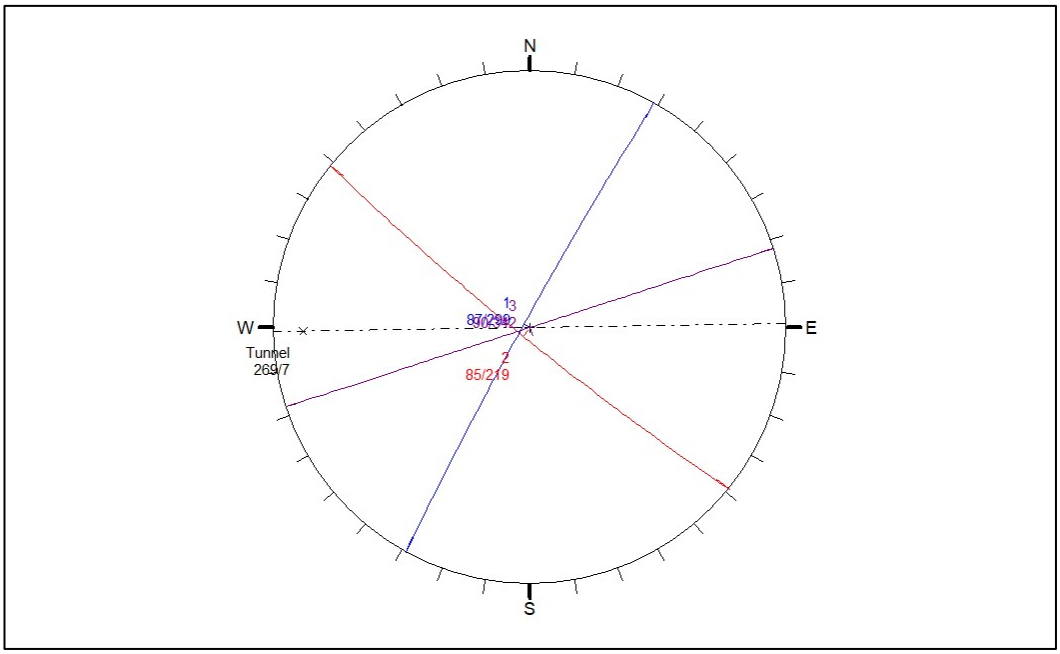


Figure 5-24: Interaction of TC1 ventilation holings with the identified discontinuity sets

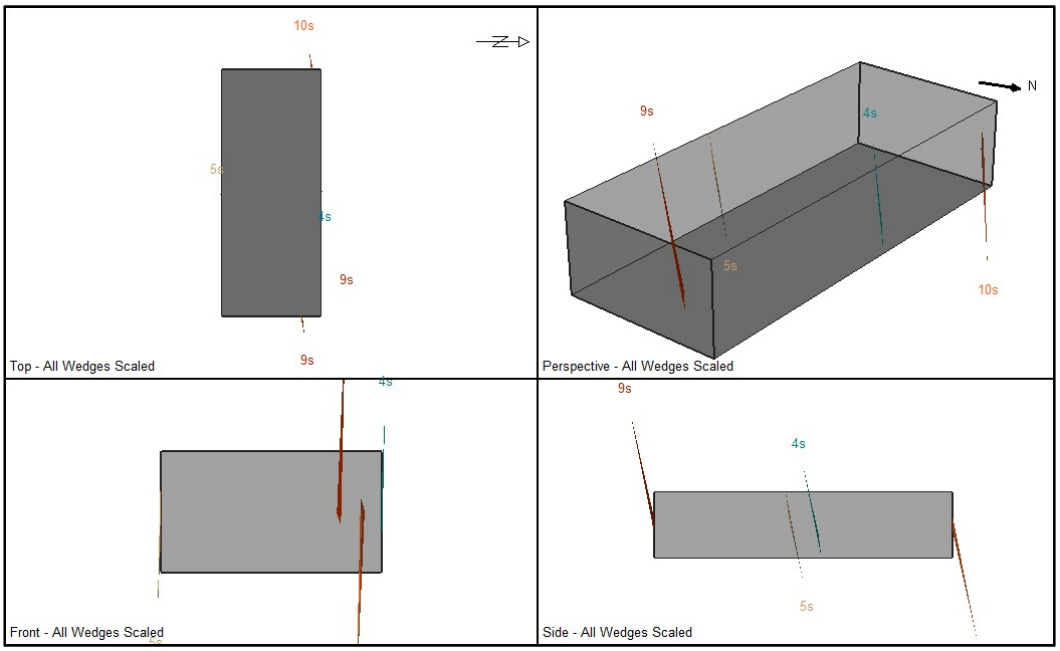


Figure 5-25: Wedges formed in the hangingwall, footwall, and sidewall of TC1 ventilation holings

Table 5-38: Results of the maximum wedges formed in TC1 strike bords

Parameters	Upper Right wedge	Lower Left wedge
Factor of Safety	0.091	Stable
Wedge Volume (m^3)	0.001	0.001
Excavation Face Area (m^2)	0.020	0.020
Support Pressure Required (kPa)	2.00	0.00
Failure Mode	Wedge sliding along line of intersection of Joint Set 1 and 3	Unconditionaly stable wedge

Table 5-39: Results of the maximum wedges formed in TC1 ventilation holings

Parameters	Upper Right wedge	Lower Left wedge
Factor of Safety	0.091	Stable
Wedge Volume (m^3)	0.001	0.001
Excavation Face Area (m^2)	0.040	0.040
Support Pressure Required (kPa)	1.000	0.000
Failure Mode	Wedge sliding along line of intersection of Joint Set 1 and 3	Unconditionaly stable wedge

The UNWEDGE stability analysis conducted in this section focused on the determination of stability parameters of the maximum possible wedges that can form in the bords and splits of each production section. However, the effect of varying stope excavation spans on the frequency of keyblocks formed, size and risk of rock falls was not studied here. The Jblock stability analysis in Chapter 6, which evaluates the effectiveness of proposed support systems, will include such analysis.

5.2.4 Intact Rock Mass Failure Analysis

Section 2.8.4 showed that the areas above shallow stopes, where the vertical stress is tensile (the tensile zone), promote hangingwall failure in the form of bed separation and large collapses. The goal of this rock mass failure assessment was to use the determined maximum vertical tensile zone heights (height of potential instability) to inform the length of artificial support. The influence of panel span, depth below the surface, and the existence of disseminated Chromitite stringers on the resulting height of the tensile zone was also evaluated.

Physical calculations (analytical design equations presented in Section 2.8.4) and the Rocscience 2D finite element numerical modelling program RS2 were used to

determine comparable estimates of the tensile zone heights. The analytical solution determined the tensile zone height as a function of depth below the surface and bord widths. The numerical modelling program included in-situ field stress conditions, increasing depth below the surface, bord widths, and the MG1L1 Chrome stringer in the hangingwall. The calculated diagonal (largest) spans across intersections (which represent 6 m to 15 m spans of orthogonal panels) were evaluated in each method.

While mining is currently taking place at a maximum depth below the surface of about 590 m, the estimation of the vertical tensile zone heights was done from a depth of 200 m to 1000 m below the surface. As stated in Section 5.2.2, estimation of the in-situ stress field conditions (the k-ratio) was based on the work by Stacey & Wesseloo (1998). The average of the major (k_1) and minor (k_3) horizontal in situ stress was divided by the vertical stress at selected depths below the surface.

RS2 model set-up

RS2 models were used to assess the vertical tensile zone in various spans with increasing depth below the surface. The parameters used in the RS2 models are discussed below and summarised in

Table 5-40 and Table 5-41:

- The pyroxenite host rock (footwall and hangingwall) and the MG1 Chromitite reef geological domains were defined in the model and assigned unique properties;
- The MG1L1 Chromitite stringer of a maximum thickness of 0.2 m was defined at a maximum position of 0.45 m above the MG1 Chromitite reef hangingwall contact, and these were assigned similar material properties;

Gravity field stress type was used, and the parameters used for defining field stress conditions in each production section are summarised in

- Table 5-40;
- Strength properties and Hoek-Brown parameters of each material are summarised in Table 5-41; and

- Pillar widths of 8.0 m were used in the modelling exercise.

Table 5-40: In-situ field stress parameters

Depth Below Surface (DBS) (m)	Ratio of major horizontal principal stress to vertical stress (K_3)	Ratio of major horizontal principal stress to vertical stress (K_1)	Average K-Ratio
200	1.19	2.20	1.70
400	0.80	1.65	1.23
600	0.75	1.00	0.88
800	0.80	0.84	0.82
1000	0.55	0.80	0.68

Table 5-41: Summary of material properties used in the RS2 model

Input Parameter	Pyroxenite Host Rock	MG1 Chromitite Reef
UCS (MPa)	212.15	74.41
Unit Weight (MN/m^3)	0.03	0.04
Stiffness Paramaters		
(i) Poisson's Ratio	0.26	0.36
(ii) Young's Modulus (GPa)	124.57	95.23
Strength Paramaters		
(i) Failure Criterion	Hoek-Brown	Hoek-Brown
(ii) Material Type	Elastic	Elastic
(iii) mb Parameter	5.06	3.65
(iv) s Parameter	0.01	0.01

To construct RS2 models in which boundary conditions have no impact on the simulation results, external vertical and horizontal boundaries which define the model domain were both defined at seven times the span being considered (Corkum, 2017). This rule of thumb was applied in all modelled spans from a depth of 200 m to 1000 m below the surface. Rollers were applied in the vertical boundaries (models fixed in the x-axis) to create planes of symmetry.

A six-noded triangular-shaped graded mesh was applied to the model with a gradation factor of 0.1 to enable the computation of accurate results. Figure 5-26 shows one of the constructed RS2 model domains with MG1L1 Chrome stringer. Figure 5-27 gives a closer look at the RS2 model, showing different materials, as well as the position and thickness of the MG1L1 stringer. Figure 5-28 shows an

example of the result where measurements were made on-screen to estimate tensile zone heights.

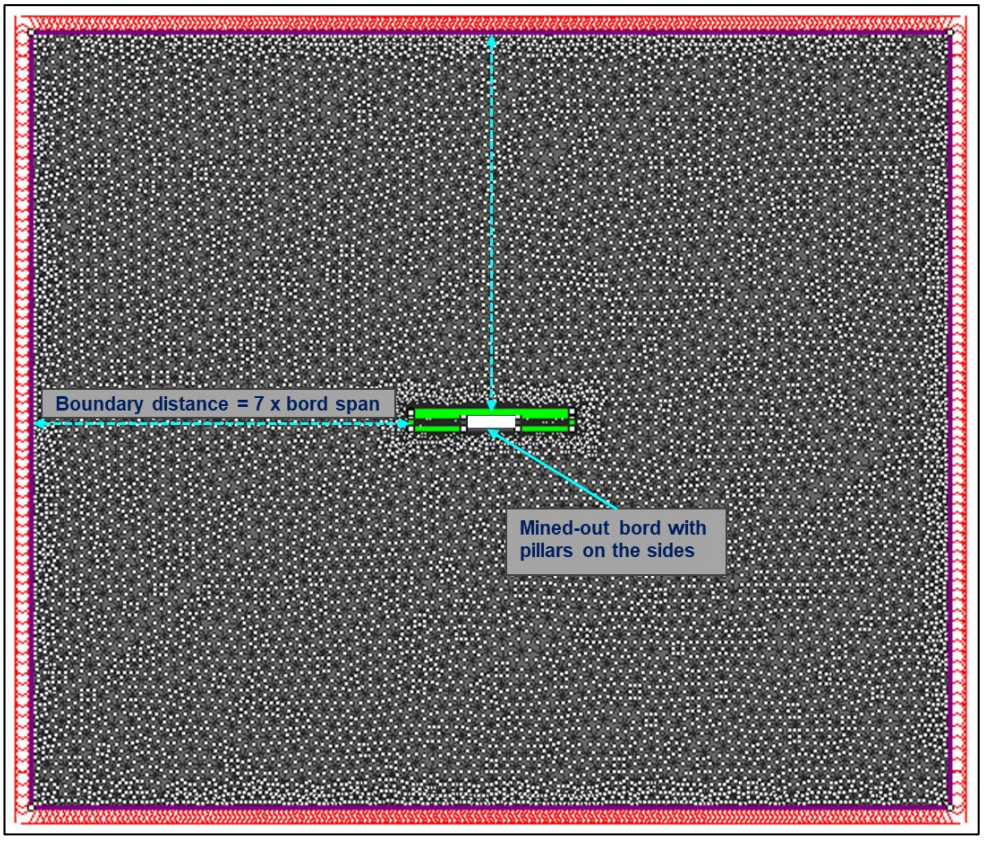


Figure 5-26: Constructed RS2 model with MG1L1 Chrome stringer

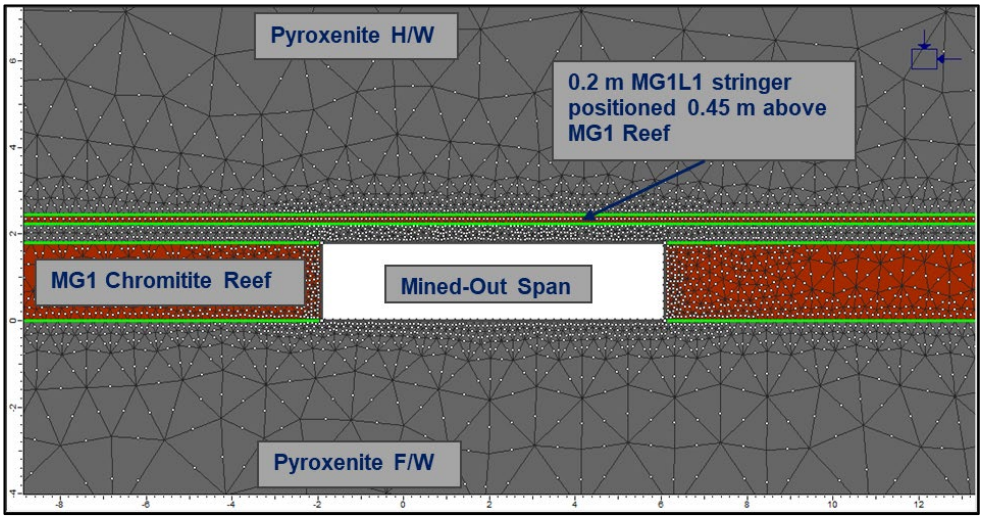


Figure 5-27: Enlarged section of the RS2 model showing the position and thickness of the MG1L1 stringer

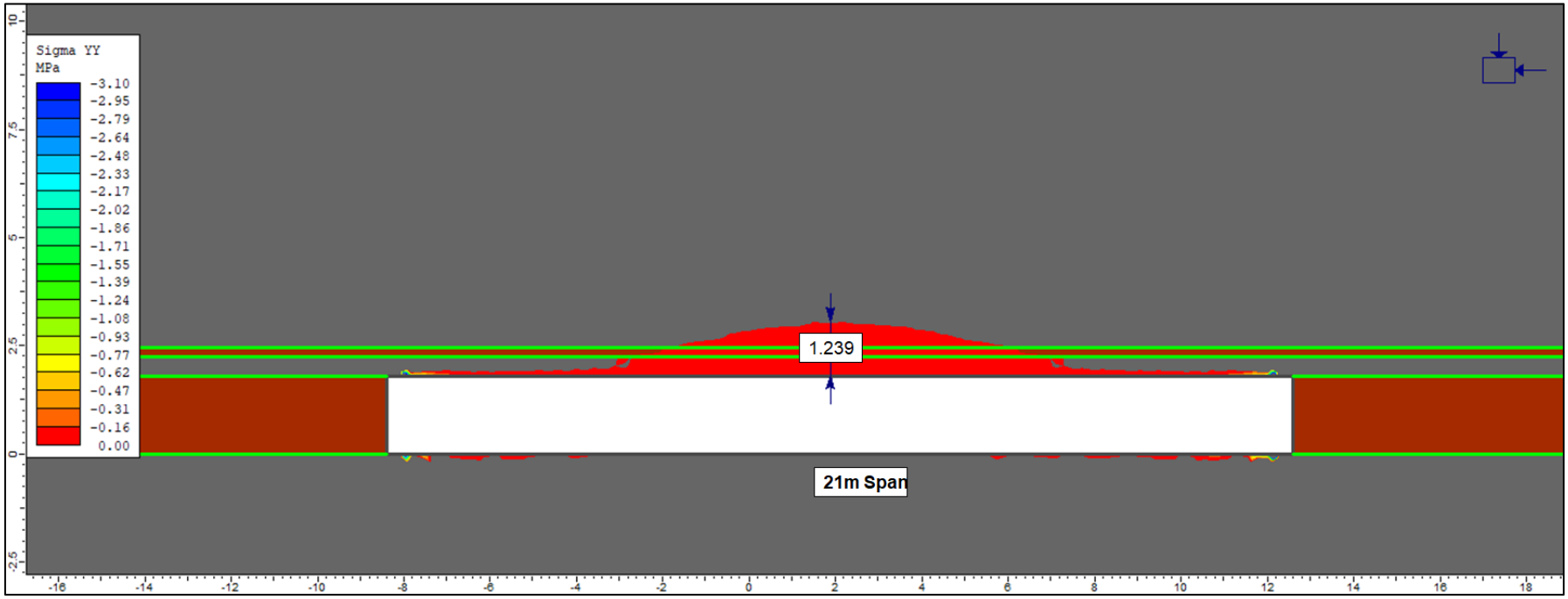


Figure 5-28: RS2 results showing measurements of the vertical tensile zone

In the example of the RS2 simulation results in Figure 5-28, the red colour represents areas where vertical stress is tensile (the tensile zone). The grey colour in the figure represents a vertical compressive stress zone. Table 5-42 to Table 5-46 summarise and compare the results obtained from analytical equations and RS2 modelling for the selected spans with increasing depth below the surface. All RS2 modelling results for the various spans evaluated with increasing depth are provided in Appendix E. The results are discussed below.

Table 5-42: Empirical and modelled tensile zone height results at 200 mbs

Depth below surface = 200 m			
Spans of Orthogonal Bords/Panels (m)	Diagonal Span Across Intersections (m)	Vertical Tensile Zone Height (m) (Analytical Equations)	RS2 Modelled Tensile Zone Height - with MG1L1 Stringer (m)
6	8	0.57	0.21
8	11	0.93	0.45
10	14	1.35	0.79
12	17	1.81	1.25
14	20	2.32	1.71
15	21	2.51	1.88

Table 5-43: Empirical and modelled tensile zone height results at 400 mbs

Depth below surface = 400 m			
Spans of Orthogonal Bords/Panels (m)	Diagonal Span Across Intersections (m)	Vertical Tensile Zone Height (m) (Analytical Equations)	RS2 Modelled Tensile Zone Height - with MG1L1 Stringer (m)
6	8	0.40	0.16
8	11	0.65	0.29
10	14	0.94	0.48
12	17	1.26	0.81
14	20	1.61	1.12
15	21	1.74	1.24

Table 5-44: Empirical and modelled tensile zone height results at 600 mbs

Depth below surface = 600 m			
Spans of Orthogonal Bords/Panels (m)	Diagonal Span Across Intersections (m)	Vertical Tensile Zone Height (m) (Analytical Equations)	RS2 Modelled Tensile Zone Height - with MG1L1 Stringer (m)
6	8	0.33	0.08
8	11	0.53	0.23
10	14	0.76	0.37
12	17	1.02	0.69
14	20	1.31	0.90
15	21	1.41	1.04

Table 5-45: Empirical and modelled tensile zone height results at 800 mbs

Depth below surface = 800 m			
Spans of Orthogonal Bords/Panels (m)	Diagonal Span Across Intersections (m)	Vertical Tensile Zone Height (m) (Analytical Equations)	RS2 Modelled Tensile Zone Height - with MG1L1 Stringer (m)
6	8	0.28	0.07
8	11	0.46	0.18
10	14	0.66	0.29
12	17	0.88	0.50
14	20	1.13	0.77
15	21	1.21	0.82

Table 5-46: Empirical and modelled tensile zone height results at 1000 mbs

Depth below surface = 1000 m			
Spans of Orthogonal Bords/Panels (m)	Diagonal Span Across Intersections (m)	Vertical Tensile Zone Height (m) (Analytical Equations)	RS2 Modelled Tensile Zone Height - with MG1L1 Stringer (m)
6	8	0.25	0.06
8	11	0.41	0.17
10	14	0.59	0.27
12	17	0.79	0.46
14	20	1.01	0.70
15	21	1.08	0.30

Higher vertical tensile zone height values were generally obtained from the analytical equation than measured values from the RS2 modelling. In both methods of evaluation, the height of the tensile zone increased with increasing span and decreased with increasing depth below the surface. As mentioned in Section 2.8.4, the analytical equation gives a crude estimate of the tensile zone

height. It does not consider the deformation properties of the hangingwall rock or the presence of a parting plane. The RS2 simulation results, which consider important factors in the estimation of the vertical tensile zone height in stopes, were then used to inform the required length of support units to maintain stability. The RS2 results indicated that at a maximum depth of 200 m below the surface (Table 5-42), the vertical tensile zone height is less than 1 m for intersecting orthogonal panel spans of at most 10 m (where the maximum diagonal span across intersections is 14 m). When the orthogonal bord spans are increased beyond 10 m, the vertical tensile zone height increases beyond 1 m and is measured approximately 2 m at the maximum orthogonal panel spans of 15 m. Vertical tensile zones extending further into the hangingwall require support units of greater length to clamp the unstable zone with competent rock above the unstable zone. When the depth below the surface was increased to a maximum of 400 m (Table 5-43), a maximum vertical tensile zone height of 1.2 m was calculated at orthogonal panel spans of 15 m (where the maximum diagonal span is 21 m). Furthermore, the vertical tensile zone increased beyond 1 m when orthogonal bord spans were increased beyond 12 m (17 m diagonal span across intersections). When the depth below the surface is 600 m (Table 5-44), the vertical tensile zone extended to a maximum of 1 m into the hangingwall only at the maximum diagonal span of 21 m (orthogonal panel spans of 15 m). Lastly, when the depth below the surface increased beyond 600 m (Table 5 45 and Table 5-46), the vertical tensile zone extended to less than 1 m into the hangingwall for all the spans which were selected for evaluation. The results from this failure analysis will be used to inform support element recommendations at the mine.

5.3 Chapter Summary

The holistic design of stable bord spans involved the identification and evaluation of all rock mass failure mechanisms. In this chapter, factors such as rock mass quality, safety requirements, and stope dimensions were considered in the design or prediction of maximum stable panel spans and stability evaluation. A conservative approach to designing for the largest spans formed due to intersecting orthogonal bords was used. The assessment of various rock mass failure mechanisms identified critical spans at which failure may occur if not

supported. The next chapter will focus on the determination of standard support systems to stabilize the stope excavations.

6 DETERMINATION OF IN-STOPE SUPPORT REQUIREMENTS

Chapter 5 presented the determination of maximum unsupported stope spans in different underground rock quality classes. Through a detailed stability evaluation exercise, different rock mass failure mechanisms or instabilities were identified in the area between pillars. The MHSC systematic design methodology applied in this study recommended the revision and determination of appropriate support systems required to address the various failure modes. Chapter 6 presents the determination of optimal standard in-stope support systems required to overcome the identified instabilities. The in-stope support design in this chapter outlines the philosophies followed in the determination of the following standard support specifications:

- minimum rockbolt length;
- minimum rockbolt support resistance (capacity);
- optimum support spacing; and
- secondary support specifications (if any are required).

The selected standard support system must ensure the safety of stope excavations while improving mining productivity and being economical for the mine. A brief review of current support practices is included below to later compare and check the validity of the support strategies currently employed at the mine. Table 6-1 and Table 6-2 present the standard primary tendon and secondary support types currently used at the mine.

Table 6-1: Current in-stope tendon support used at Thorncliffe mine (Glencore ECM, 2021)

Tendon Support Type	Bolt Length (m)	Bolt Dimater (mm)	Bolt Capoacity (kN)	Tensioning Capacity (ton)
Primary Support				
(i) Resin Grouted Bolt	1.5	18	180	1
Secondary Support				
(i) Flexibolts	3	18	250	20
(ii) Cable Anchors	4.5	18	380	20
(iii) Cable Anchors	6.5	18	380	20

Table 6-2: Specifications of the shotcrete support used at Thorncliffe Mine (Glencore ECM, 2021)

Shotcrete Secondary Support	
Shear Strength (MPa)	≈ 1.3
Thickness (mm)	50

The mine uses hand-operated Autorock drills for the installation of hangingwall support, presented in Table 6-1. To achieve optimal bond strength and a rigid anchorage system, 28 mm diameter drill holes are used for the resin-grouted bolts and flexibolts (Glencore, 2021). This results in a 5 mm drillhole annulus, which falls within the recommended resin annulus range of 3 mm to 6 mm to ensure effective roof bolt performance (Canbulat, et al., 2005). Cable anchors are installed using 38 mm diameter drill holes, resulting in a 10 mm annulus, which ensures grout flow (Sandvik Mining and Rock Technology, 2023).

Previously, the Eastern Chrome Mines (ECM) reported a combined 95% cumulative fallout thickness of 0.5 m. However, to determine the support resistance that the primary support system is required to meet, ECM used a conservative maximum height of instability of 1.0 m to account for 100% of potential fallouts. Each primary support unit is therefore required to provide a support resistance of 31.4 kN/m^2 (using a density of 3200 kg/m^3). As shown in Table 6-1, the primary support system consists of 1.5 m long, 18 mm diameter full-column resin grouted bolts with an ultimate capacity of 180 kN. The bolts are installed at a maximum grid spacing of 1.5 m x 1.5 m, which equates to a supported area of 2.25 m^2. The bolt yield limit of 150 kN is used to quantify its support resistance of 66.7 kN/m^2. This support system, therefore, has a FOS of 2.1 against potential rock falls (Glencore ECM, 2021).

The determination of in-stope support requirements in this case study is presented in this chapter. To ensure a holistic support design, various failure mechanisms were considered. The requirements of the support are:

- support for rock mass failure (using rock mass classification systems);
- fallout thickness and support resistance;
- support for identified keyblocks and wedges;

- support informed by stress analysis; and
- support for a stratified rock mass.

Lastly, the effectiveness of the selected standard primary support system was evaluated to check if the desired stable conditions were achieved. This was done using the Jblock Software, which follows a stochastic keyblock analysis to determine the effectiveness of the proposed support system.

6.1 Support Requirements using Rock Mass Classification Systems

The Barton and Grimstad (1993) empirical support design chart (discussed in Appendix B) was used to provide initial indications of support requirements. This approach provides support guidelines, particularly in terms of rock bolts and areal coverage (shotcrete) requirements. Since the rock mass stability in the stope excavations was evaluated for the worst ground conditions (minimum rock qualities), the corresponding support requirements were determined for the worst conditions to be encountered in each production section, to ensure a conservative support design.

A typical production section consists of various types of production drives with unique purposes and life which dictate safety requirements. It was concluded that travelling roadways and conveyor belt drives are medium-term excavations and therefore require higher levels of safety (or support) than bords used for production only. Production bords were determined to be short-term excavations. This means that installed support must provide a higher degree of security against instability in medium-term than short-term production drives. To express the required safety requirements, an ESR of 1.6 and 3 were assigned to medium-term excavations and short-term production drives, respectively. These safety requirements were considered in the estimation of support requirements.

Additionally, the estimation of support requirements considered the largest spans (diagonals across intersections of orthogonal bords) as an additional safety factor in the support design for short-term and medium-term production drives. Table 6-3 and Table 6-4 summarise the equivalent dimension (De) for medium-term and short-term production drives, respectively.

Table 6-3: Equivalent dimension (De) for medium-term production drives

Spans of Orthogonal Bords	Diagonal Span Across Intersections	ESR	Equivalent Dimension (Diagonal Span (m)/ESR)
6	8	1.6	5.0
8	11		6.9
10	14		8.8
12	17		10.6
14	20		12.5
15	21		13.1

Table 6-4: Equivalent dimension (De) for short-term production drives

Spans of Orthogonal Bords	Diagonal Span Across Intersections	ESR	Equivalent Dimension (Diagonal Span (m)/ESR)
6	8	3	2.7
8	11		3.7
10	14		4.7
12	17		5.7
14	20		6.7
15	21		7.0

By plotting the equivalent dimension (De) of the different stope spans against the minimum calculated Q-ratings, reinforcement requirements were derived for different spans mining in various ground conditions in each production section. The calculated Q-ratings in each production section were presented in Section 4.3.3. Figure 6-1 illustrates an example of the support design chart for an 11.0 m medium-term (diagonal) span in RIG 47. All the support design charts for the different spans evaluated in each production section are provided in Appendix E.

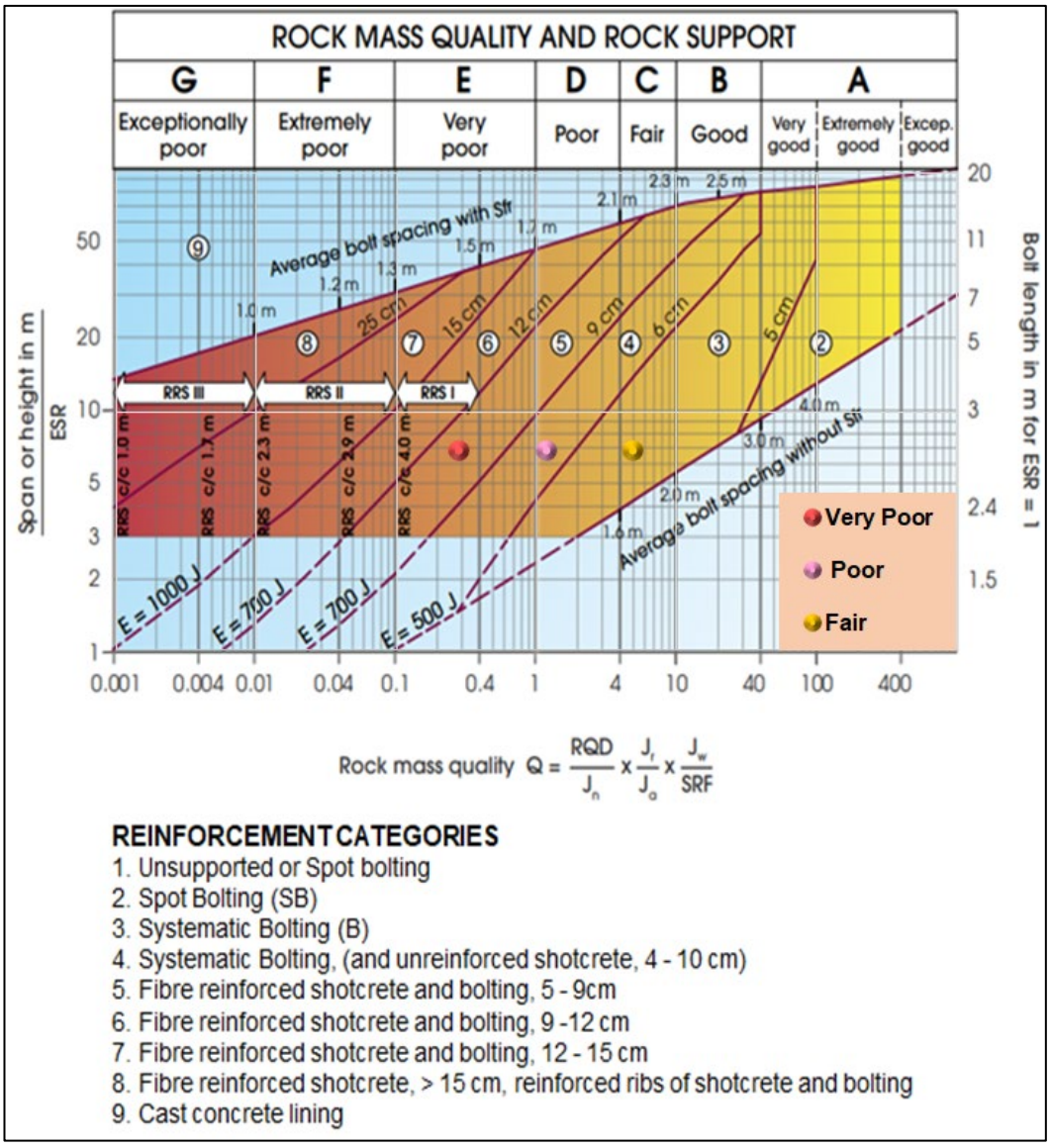


Figure 6-1: Q-support design chart for an 8.0 m medium-term span in RIG 47

Table 6-5 to Table 6-10 present the estimated support requirements for various medium-term spans when mining in various ground conditions from all the ore production sections. Table 6-11 to Table 6-16 provide the estimated support requirements for short-term panel spans in various ground conditions. The various ground conditions represent a different risk category area in the mine.

Table 6-5: Support requirements for an 8.0 m medium-term span in different ground conditions

(Q-Index) Rock Mass Quality	Span (m)	Reinforcement Category	Tendon length (m)	Areal coverage Required?	Bolt spacing (m)
Exceptionally Poor (0.001 – 0.01)	8.0 m diagonal span (for 6 m medium-term orthogonal production drives)	-	-	-	-
Extremely Poor (0.01 - 0.1)		-	-	-	-
Very Poor (0.1-1.0)		Ranges between: • (4) Systematic Bolting & 4 - 10 cm Unreinforced shotcrete, and • (5) 5 - 9 cm Fibre Reinforced shotcrete and bolting	2.4 to 3.0	Yes	1.3 to 1.5
Poor (1 - 4)		Ranges between: • (3) Systematic Bolting, and • (4) Systematic Bolting & 4 - 10 cm Unreinforced shotcrete	2.4 to 3.0	Yes	1.7 to 2.1
Fair (4-10)		• (3) Systematic Bolting	2.4 to 3.0	No	2.1 to 2.3
Good (10-40)		-	-	-	-
Very Good (40-100)		-	-	-	-
Extremely Good (100-400)		-	-	-	-
Exceptionally Good (400-1000)		-	-	-	-

Table 6-6: Support requirements for an 11.0 m medium-term span in different ground conditions

(Q-Index) Rock Mass Quality	Span (m)	Reinforcement Category	Tendon length (m)	Areal coverage Required?	Bolt spacing (m)
Exceptionally Poor (0.001 – 0.01)	11.0 m diagonal span (for 8 m medium-term orthogonal production drives)	-	-	-	-
Extremely Poor (0.01 - 0.1)		-	-	-	-
Very Poor (0.1-1.0)		Ranges between: • (5) 5 - 9 cm Fibre reinforced shotcrete and bolting, and • (6) 9 - 12 cm Fibre reinforced shotcrete and bolting	2.4 to 3.0	Yes	1.3 to 1.5
Poor (1 - 4)		Ranges between: • (3) Systematic Bolting, and • (4) Systematic Bolting & 4 - 10 cm unreinforced shotcrete	2.4 to 3.0	Yes	1.7 to 2.1
Fair (4-10)		• (3) Systematic Bolting	2.4 to 3.0	No	2.1 to 2.3
Good (10-40)		-	-	-	-
Very Good (40-100)		-	-	-	-
Extremely Good (100-400)		-	-	-	-
Exceptionally Good (400-1000)		-	-	-	-

Table 6-7: Support requirements for a 14.0 m medium-term span in different ground conditions

(Q-Index) Rock Mass Quality	Span (m)	Reinforcement Category	Tendon length (m)	Areal coverage Required?	Bolt spacing (m)
Exceptionally Poor (0.001 – 0.01)	14.0 m diagonal span (for 10 m medium-term orthogonal production drives)	-	-	-	-
Extremely Poor (0.01 - 0.1)		-	-	-	-
Very Poor (0.1-1.0)		Ranges between: • (5) 5 - 9 cm Fibre reinforced shotcrete and bolting, and • (6) 9 - 12 cm Fibre reinforced shotcrete and bolting	2.4 to 3.0	Yes	1.3 to 1.5
Poor (1 - 4)		• (4) Systematic Bolting & 4 - 10 cm unreinforced shotcrete	2.4 to 3.0	Yes	1.7 to 2.1
Fair (4-10)		• (3) Systematic Bolting	2.4 to 3.0	No	2.1 to 2.3
Good (10-40)		-	-	-	-
Very Good (40-100)		-	-	-	-
Extremely Good (100-400)		-	-	-	-
Exceptionally Good (400-1000)		-	-	-	-

Table 6-8: Support requirements for a 17.0 m medium-term span in different ground conditions

(Q-Index) Rock Mass Quality	Span (m)	Reinforcement Category	Tendon length (m)	Areal coverage required?	Bolt spacing (m)
Exceptionally Poor (0.001 – 0.01)	17.0 m diagonal span (for 12 m medium-term orthogonal production drives)	-	-	-	-
Extremely Poor (0.01 - 0.1)		-	-	-	-
Very Poor (0.1-1.0)		Ranges between: • (5) 5 - 9 cm Fibre reinforced shotcrete and bolting, and • (6) 9 - 12 cm Fibre reinforced shotcrete and bolting	3.0 to 5.0	Yes	1.3 to 1.5
Poor (1 - 4)		Ranges between: • (4) Systematic Bolting & 4 - 10 cm unreinforced shotcrete, and • (5) 5 - 9 cm Fibre reinforced shotcrete and bolting	3.0 to 5.0	Yes	1.7 to 2.1
Fair (4-10)		• (3) Systematic Bolting	3.0 to 5.0	No	2.1 to 2.3
Good (10-40)		-	-	-	-
Very Good (40-100)		-	-	-	-
Extremely Good (100-400)		-	-	-	-
Exceptionally Good (400-1000)		-	-	-	-

Table 6-9: Support requirements for a 20.0 m medium-term span in different ground conditions

(Q-Index) Rock Mass Quality	Span (m)	Reinforcement Category	Tendon length (m)	Areal coverage Required?	Bolt spacing (m)
Exceptionally Poor (0.001 – 0.01)	20.0 m diagonal span (for 14 m medium-term orthogonal production drives)	-	-	-	-
Extremely Poor (0.01 - 0.1)		-	-	-	-
Very Poor (0.1-1.0)		• (6) 9 - 12 cm Fibre reinforced shotcrete and bolting	3.0 to 5.0	Yes	1.3 to 1.5
Poor (1 - 4)		Ranges between: • (4) Systematic Bolting & 4 - 10 cm unreinforced shotcrete, and • (5) 5 - 9 cm Fibre Reinforced shotcrete and bolting	3.0 to 5.0	Yes	1.7 to 2.1
Fair (4-10)		Ranges between: • (3) Systematic Bolting, and • (4) Systematic Bolting & 4 - 10 cm unreinforced shotcrete	3.0 to 5.0	Yes	2.1 to 2.3
Good (10-40)		-	-	-	-
Very Good (40-100)		-	-	-	-
Extremely Good (100-400)		-	-	-	-
Exceptionally Good (400-1000)		-	-	-	-

Table 6-10: Support requirements for a 21.0 m medium-term span in different ground conditions

(Q-Index) Rock Mass Quality	Span (m)	Reinforcement Category	Tendon length (m)	Areal coverage Required?	Bolt spacing (m)
Exceptionally Poor (0.001 – 0.01)	21.0 m diagonal span (for 15 m medium-term orthogonal production drives)	-	-	-	-
Extremely Poor (0.01 - 0.1)		-	-	-	-
Very Poor (0.1-1.0)		Ranges between: • (6) 9 - 12 cm Fibre reinforced shotcrete and bolting, and • (7) 12 - 15 cm Fibre reinforced shotcrete and bolting	3.0 to 5.0	Yes	1.3 to 1.5
Poor (1 - 4)		Ranges between: • (4) Systematic Bolting & 4 - 10 cm unreinforced shotcrete, and • (5) 5 - 9 cm Fibre reinforced shotcrete and bolting	3.0 to 5.0	Yes	1.7 to 2.1
Fair (4-10)		Ranges between: • (3) Systematic Bolting, and • (4) Systematic Bolting & 4 - 10 cm unreinforced shotcrete	3.0 to 5.0	Yes	2.1 to 2.3
Good (10-40)		-	-	-	-
Very Good (40-100)		-	-	-	-
Extremely Good (100-400)		-	-	-	-
Exceptionally Good (400-1000)		-	-	-	-

Table 6-11: Support requirements for an 8.0 m short-term span in different ground conditions

(Q-Index) Rock Mass Quality	Span (m)	Reinforcement Category	Tendon length (m)	Areal coverage Required?	Bolt spacing (m)
Exceptionally Poor (0.001 – 0.01)	8.0 m diagonal span (for 6 m short-term orthogonal production drives)	-	-	-	-
Extremely Poor (0.01 - 0.1)		-			
Very Poor (0.1-1.0)		• (4) Systematic Bolting & 4 - 10 cm Unreinforced shotcrete	1.5 to 2.4	Yes	1.3 to 1.5
Poor (1 - 4)		• (3) Systematic Bolting	1.5 to 2.4	No	1.7 to 2.1
Fair (4-10)		• (1) Unsupported or Spot bolting	1.5 to 2.4	No	1.6 to 2.0
Good (10-40)		-	-	-	-
Very Good (40-100)		-	-	-	-
Extremely Good (100-400)		-	-	-	-
Exceptionally Good (400-1000)		-	-	-	-

Table 6-12: Support requirements for a 11.0 m short-term span in different ground conditions

(Q-Index) Rock Mass Quality	Span (m)	Reinforcement Category	Tendon length (m)	Areal coverage Required?	Bolt spacing (m)
Exceptionally Poor (0.001 – 0.01)	11.0 m diagonal span (for 8 m short-term orthogonal production drives)	-	-	-	-
Extremely Poor (0.01 - 0.1)		-	-	-	-
Very Poor (0.1-1.0)		Ranges between: • (4) Systematic Bolting & 4 - 10 cm Unreinforced shotcrete, and • (5) 5 - 9 cm Fibre reinforced shotcrete and bolting	2.0 to 2.4	Yes	1.3 to 1.5
Poor (1 - 4)		Ranges between: • (3) Systematic Bolting, and • (4) Systematic Bolting & 4 - 10 cm unreinforced shotcrete	2.0 to 2.4	Yes	1.7 to 2.1
Fair (4-10)		Ranges between: • (1) Unsupported or Spot bolting, and • (2) Spot Bolting	2.0 to 2.4	No	1.6 to 2.0
Good (10-40)		-	-	-	-
Very Good (40-100)		-	-	-	-
Extremely Good (100-400)		-	-	-	-
Exceptionally Good (400-1000)		-	-	-	-

Table 6-13: Support requirements for a 14.0 m short-term span in different ground conditions

(Q-Index) Rock Mass Quality	Span (m)	Reinforcement Category	Tendon length (m)	Areal coverage Required?	Bolt spacing (m)
Exceptionally Poor (0.001 – 0.01)	14.0 m diagonal span (for 10 m short-term orthogonal production drives)	-	-	-	-
Extremely Poor (0.01 - 0.1)		-	-	-	-
Very Poor (0.1-1.0)		Ranges between: • (4) Systematic Bolting & 4 - 10 cm Unreinforced shotcrete, and • (5) 5 - 9 cm Fibre reinforced shotcrete and bolting	2.4 to 3.0	Yes	1.3 to 1.5
Poor (1 - 4)		Ranges between: • (3) Systematic Bolting, and • (4) Systematic Bolting & 4 - 10 cm unreinforced shotcrete	2.4 to 3.0	Yes	1.7 to 2.1
Fair (4-10)		• (3) Systematic Bolting	2.4 to 3.0	No	2.1 to 2.3
Good (10-40)		-	-	-	-
Very Good (40-100)		-	-	-	-
Extremely Good (100-400)		-	-	-	-
Exceptionally Good (400-1000)		-	-	-	-

Table 6-14: Support requirements for a 17.0 m short-term span in different ground conditions

(Q-Index) Rock Mass Quality	Span (m)	Reinforcement Category	Tendon length (m)	Areal coverage required?	Bolt spacing (m)
Exceptionally Poor (0.001 – 0.01)	17.0 m diagonal span (for 12 m short-term orthogonal production drives)	-	-	-	-
Extremely Poor (0.01 - 0.1)		-	-	-	-
Very Poor (0.1-1.0)		• (5) 5 - 9 cm Fibre reinforced shotcrete and bolting	2.4 to 3.0	Yes	1.3 to 1.5
Poor (1 - 4)		Ranges between: • (3) Systematic Bolting, and • (4) Systematic Bolting & 4 - 10 cm unreinforced shotcrete	2.4 to 3.0	Yes	1.7 to 2.1
Fair (4-10)		• (3) Systematic Bolting	2.4 to 3.0	No	2.1 to 2.3
Good (10-40)		-	-	-	-
Very Good (40-100)		-	-	-	-
Extremely Good (100-400)		-	-	-	-
Exceptionally Good (400-1000)		-	-	-	-

Table 6-15: Support requirements for a 20.0 m short-term span in different ground conditions

(Q-Index) Rock Mass Quality	Span (m)	Reinforcement Category	Tendon length (m)	Areal coverage Required?	Bolt spacing (m)
Exceptionally Poor (0.001 – 0.01)	20.0 m diagonal span (for 14 m short-term orthogonal production drives)	-	-	-	-
Extremely Poor (0.01 - 0.1)		-	-	-	-
Very Poor (0.1-1.0)		• (5) 5 - 9 cm Fibre reinforced shotcrete and bolting	2.4 to 3.0	Yes	1.3 to 1.5
Poor (1 - 4)		• (4) Systematic Bolting & 4 - 10 cm unreinforced shotcrete	2.4 to 3.0	Yes	1.7 to 2.1
Fair (4-10)		• (3) Systematic Bolting	2.4 to 3.0	No	2.1 to 2.3
Good (10-40)		-	-	-	-
Very Good (40-100)		-	-	-	-
Extremely Good (100-400)		-	-	-	-
Exceptionally Good (400-1000)		-	-	-	-

Table 6-16: Support requirements for a 21.0 m short-term span in different ground conditions

(Q-Index) Rock Mass Quality	Span (m)	Reinforcement Category	Tendon length (m)	Areal coverage Required?	Bolt spacing (m)
Exceptionally Poor (0.001 – 0.01)	21.0 m diagonal span (for 15 m short-term orthogonal production drives)	-	-	-	-
Extremely Poor (0.01 - 0.1)		-	-	-	-
Very Poor (0.1-1.0)		Ranges between: • (5) 5 - 9 cm Fibre reinforced shotcrete and bolting, and • (6) 9 - 12 cm Fibre reinforced shotcrete and bolting	2.4 to 3.0	Yes	1.3 to 1.5
Poor (1 - 4)		• (4) Systematic Bolting & 4 - 10 cm unreinforced shotcrete	2.4 to 3.0	Yes	1.7 to 2.1
Fair (4-10)		• (3) Systematic Bolting	2.4 to 3.0	No	2.1 to 2.3
Good (10-40)		-	-	-	-
Very Good (40-100)		-	-	-	-
Extremely Good (100-400)		-	-	-	-
Exceptionally Good (400-1000)		-	-	-	-

Due to higher safety requirements, medium-term production drives generally indicate higher demand for support than short-term production drives of the same span dimension, mining in similar ground conditions. In both excavation types, the thickness and strength requirements of the skin support decreased with improving ground conditions. The spacing between rockbolt units increased (decreasing support unit density) with improving ground conditions. The tendon length increased with increasing mining span.

Specifically, in very poor ground conditions, both short-term and medium-term production drives required a support system consisting of a combination of closely spaced (1.3 m ≤ spacing ≤1.5 m) systematic rock bolting and thick reinforced skin support (shotcrete). Medium-term excavations frequently required thicker reinforced shotcrete than short-term excavations in the same rock quality class. In very poor rock ground conditions, larger medium-term spans (≥17.0 m) required longer tendons (3.0 m to 5.0 m) than short-term spans (2.4 m to 3.0 m).

When mining in poor ground conditions, all short-term mining spans greater than 8.0 required a maximum support system comprised of a combination of systematic bolting and 40 mm – 100 mm unreinforced shotcrete support. Larger medium-term spans (≥17.0 m) mining in poor ground conditions required a maximum support system consisting of a combination of 50 mm – 90 mm, fibre-reinforced shotcrete and systematic bolting. In poor ground, larger medium-term spans (≥17.0 m) still required longer tendons (3.0 m to 5.0 m) than short-term spans (2.4 m to 3.0 m). Support spacing requirements were, however, similar in both short-term and medium-term production drives in poor ground, which ranged between 1.7 m to 2.1 m.

When ground conditions improved to fair, all the short-term mining spans required only systematic bolting and sometimes only spot bolting to maintain stability. However, larger medium-term production drives (> 17.0 m) required a maximum support system comprised of a combination of systematic bolting and 40 mm – 100 mm unreinforced shotcrete in fair ground. All medium-term production drives mining in fair-ground conditions required the support spacing to be maintained between 2.1 m to 2.3 m. Short-term production drives with smaller spans (≤11 m) required a support spacing of between 1.6 m to 2.0 whilst larger spans (≥14.0 m)

generally required a wider spacing of between 2.1 m to 2.3 m. Larger medium-term spans (≥17.0 m) required longer tendons (3.0 m to 5.0 m) than short-term spans (2.4 m to 3.0 m

To supplement the support recommendations suggested in the original 1974 publication, Barton, et al. (1977) proposed guidelines for the design of primary support systems based on the Q system. The proposed empirical equations are used for providing estimates of the rockbolt length (Equation B-9), ultimate support pressure required to stabilize the roof of an excavation (Equation B-11) and spacing of primary support (Equation B-12). The equations are provided in Appendix B.

In the equations, the tendon length is purely a function of the size of the excavation. The required roof support pressure for a given set of Q values depends on the dilatational properties of the weakest joint, that is, the roughness (J_r) of the discontinuity on which failure is likely to occur (Barton, et al., 1977). Lastly, the spacing between rock bolts and skin support requirements is a function of the rock mass quality and strength of the bolts.

Table 6-17 and Table 6-18 present the parameters used for the primary support design of short-term and medium-term production drives based on the Q system, respectively. To design for the worst case, the minimum Q values at which each bord span was selected for evaluation were calculated in all the production sections. Additionally, the joint roughness number (Jr) values of the weakest joint set (the least favourable for stability in terms of shear resistance) in each production section were used.

Table 6-17: Parameters used for primary support design of short-term panels

Bord Span (m)	Q Values	Joint Roughness Number (J_r)
6	0.83, Maximum Q value of the very poor class in Rig 50, TC1, and Rig 14.	1.5, for Slickensided, undulating discontinuities
8	1.80, Minimum Q value of the poor class in TC1	1.5, for Slickensided, undulating discontinuities
10	3.25, Maximum Q value of the poor class in TC1	1.5, for Slickensided, undulating discontinuities
12	4.84, Minimum Q value of the Fair ground in Rig 47	1.5, for Rough or irregular, planar discontinuities
14	7.78, Geomean Q value of the Fair ground in Rig 14	1.5, for Rough or irregular, planar discontinuities
15	9.77, Maximum Q value of the Fair ground in Rig 2	1.5, for Rough or irregular, planar discontinuities

Table 6-18: Parameters used for primary support design of medium-term panels

Bord Span (m)	Q Values	Joint Roughness Number (J_r)
6	4.44, Minimum Q value of the Fair ground in Rig 50	1.5, for Rough or irregular, planar discontinuities
8	9.77, Maximum Q value of Fair ground in Rig 2	1.5, for Rough or irregular, planar discontinuities

Again, the support design using the Q-system's empirical equations considered the largest spans (diagonals across intersections). In Section 5.1, the calculated maximum self-supporting spans for medium-term bords ranged between 2 m to a maximum of 8 m. Therefore, only a minimum bord span of 6 m and a maximum of 8 m were evaluated for medium-term span support design. A yield strength or tendon capacity of 0.15 MN (currently used at the mine) was used in computing the roof support pressure. Table 6-19 and Table 6-20 present the design of primary support systems for short-term and medium-term production drives based on the Q system, respectively. The results are discussed below.

Table 6-19: Design of primary support systems for short-term production drives

Spans of Orthogonal Bords (m)	Diagonal Span Across Intersections (m)	Excavation Support Ratio (ESR)	Rockbolt Length (m)	Yield Strength or Capacity of Tendon Unit (MN)	Support pressure (MN/m^2)	Tendon Spacing (m)
6	8	3	2.4	0.15	0.14	1.03
8	11		2.6		0.11	1.17
10	14		2.7		0.09	1.29
12	17		2.9		0.08	1.38
14	20		3.0		0.07	1.49
15	21		3.1		0.06	1.54

Table 6-20: Design of primary support systems for medium-term production drives

Spans of Orthogonal Bords (m)	Diagonal Span Across Intersections (m)	Excavation Support Ratio (ESR)	Rockbolt Length (m)	Yield Strength or Capacity of Tendon Unit (MN)	Support pressure (MN/m^2)	Tendon Spacing (m)
6	8	1.6	2.8	0.15	0.08	1.36
8	11		3.0		0.06	1.54

Again, the results indicated that the required primary support tendon length increases with increasing span dimension. The required support pressure decreased with improving ground conditions. Medium-term production drives still

required a support system comprised of longer tendon lengths than short-term production drives of the same span dimension. Section 5.1 showed that for medium-term excavations, the required minimum span of 6 m was calculated only when the ground conditions were at least fair (improved ground), which explains indications of less support pressure requirements and wider tendon spacing. However, medium-term excavations developed in the same ground conditions as short-term excavations would still require a primary support system which provides a higher degree of security against instabilities than support systems for short-term excavations.

6.2 Case Study Support Requirements

O'Ferrall & Malan (2012) stated that *"once operations have commenced, the design is adjusted based upon the support system performance. This performance is measured by recording the size and location of all falls of ground that occur during operations."* According to Jager & Ryder (1999), the support design process shifts from the desired mechanistic or structural analyses to the use of rock mass classification systems, to simple empirical design rules (the last two are conservative and often costly) when there is little understanding of the mine's rock mass failure mechanisms.

The use of local experience gained over time allows for a structural and mechanistic analysis, which considers properties of rock mass discontinuities, mechanisms of potential rock mass failure, and the physics of the interaction between support and the rock mass (Jager & Ryder, 1999). This emphasizes the importance of using the mine's historical FOG data to produce a refined support design which ensures safety in existing and future excavations.

This section presents the use of the historical FOG data to determine support requirements for maintaining stability at the mine. The historical FOGs were used to inform the determination of the standard tendon support resistance, support length, support spacing, and support FOS against instabilities.

6.2.1 Fallout Thickness and Support Resistance at Thorncliffe Mine

As discussed in the literature review, the support system in the mine must be designed to cater for rockfalls (and not rock bursts) as the mine is situated in a shallow mining environment. The Department of Mineral Resources recommended that the mine standard support system be designed to prevent 95% of all potential fallout heights (O'Ferrall & Malan, 2012). The 95% fallout thickness at Thorncliffe Mine, as determined in Section 1.2.6, is 0.5 m. However, the remaining 5% of fallout occurrences were analysed, and it was determined that these historical fallouts do not represent a separate ground control district or were not caused by anomalies at the mine.

In this case study, a support design optimisation approach was therefore taken where the support resistance criterion of the standard support system was designed to prevent 100% of all potential fallouts based on the available FOG database. This gives a maximum height of instability or 100% fallout height of 0.8 m. Table 6-21 presents the minimum demand (tendon support resistance) that each support unit is required to meet based on the 100% fallout height.

Table 6-21: Support demand at Thorncliffe based on 100% fallout height

Support Paramaters	Case study: Thorncliffe Mine
95% Fallout thickness (m)	0.5
100% Fallout thickness (m)	0.8
Overburden density (kg/m^3)	3240
Support Demand (pgt) (kN/m^2) (Based on 100% fallouts)	25.4

6.2.2 Standard Bolt Support Length

The practical determination of standard primary support units' length takes account of the fallout thickness and the critical bond length of the support unit. Stacey (2001) stated that a tendon should be designed to be a minimum of 0.2 m longer than the determined fallout thickness.

A rockbolt also consists of a threaded portion, which is usually about 0.1 m, enabling tensioning of the bolt. The calculated minimum bolt length when using the 100% maximum fallout height is 1.2 m. ECM currently uses 1.5 m long rockbolts

as reviewed above. Table 6-22 summarises the philosophies followed when determining the minimum standard tendon length in this case study and at ECM.

Table 6-22: Determination of standard bolt minimum length

	Standard Bolt Minimum Length
Eastern Chrome Mines (ECM)	1.0 m 100% fallout thickness + 0.3 minimum critical bond length + 0.1 m bolt thread = 1.4, ≈ 1.5 m
Thorncliffe Mine: Case Study	0.8 m 100% fallout thickness + 0.2 m minimum critical bond length + 0.1 bolt thread = 1.1 , ≈ 1.2 m

According to these results, Thorncliffe Mine may have an opportunity to use shorter support units of the same capacity and therefore save costs. However, the investigation of the influence of reducing support unit length (while maintaining the same capacity) will be presented later in this chapter.

6.2.3 Support Zone of Influence, Bolt Spacing, and Support Pattern.

As discussed in Chapter 2, the important factors considered in determining appropriate standard support spacing include the tributary area and tendon support zone of influence. The tendon zone of influence must fall within the support tributary area, which represents the maximum area that can be supported by a support unit. According to Roberts (1999), the zone of influence of tendon support typically ranges between 1.0 and 1.5 m.

Therefore, a systematic grid support spacing ranging between 1.0 m to 1.5 m was chosen. However, the scenarios evaluating the influence of support spacing will be assessed to determine the optimum standard support spacing.

6.2.4 Support Factor of Safety and Analysis

According to the results above, shorter full-column resin-grouted rockbolts can be used to maintain stability at the mine. If the current rockbolt capacity is adopted, a comparison can then be made between the current standard rockbolts used at the mine and the standard rockbolts determined in this case study. Table 6-23 summarises the comparison of the FOS of support units against FOGs in the current support system and the case study support system. The current standard tendon support has a FOS of 2.12, whilst the tendon support in this Case Study

has a FOS of 2.62 due to a lower demand. Both tendon support systems fulfil the industry-recommended rock bolting design FOS of between 1.5 to 3.

Table 6-23: Comparison of ECM and Case Study primary support FOS

Support Paramaters	Eastern Chrome Mines (ECM)	Thorncliffe Mine: Case Study
95% Fallout thickness (m)	0.5	0.5
100% Fallout thickness (m)	1.0	0.8
Support Demand (pgt) (kN/m^2) (Based on 100% fallouts)	31.4	25.4
Full Column Resin Grouted Bolt Capacity (kN)	180	180
Full Column Resin Grouted Bolt Yield Capacity (kN)	150	150
Support Grid Spacing (m)	1.5 x 1.5 square	1.5 x 1.5 square
Support Tributary Area (m^2)	2.25	2.25
Support Resistance (Tensile Strength/ Tributary Area) (kN/m^2)	66.67	66.67
FOS of Resin Grouted Bolt (Capacity/Demand)	2.12	2.62
Recommended rockbolting design FOS	1.5 - 3	

As illustrated in Table 6-23, the current standard support used is adequate and validated. However, in this case study, it was illustrated that a lower support demand is required to be supported by each unit. Thorncliffe Mine can then use shorter resin-grouted bolts of the same 180 kN capacity. However, this will be investigated further below.

6.3 Support for Identified Keyblocks and Wedges

In Chapter 5, limit equilibrium wedge analyses were conducted to determine the FOS of the largest possible wedges that can form in the area between pillars at Thorncliffe Mine. The UNWEDGE analysis gave indications of the support pressure required to stabilise the unstable keyblocks in the three ore production sections consisting of at least three discontinuity sets.

To determine an optimal standard support system at Thorncliffe Mine, this section presents the use of the UNWEDGE program to evaluate the capabilities of various support scenarios for stabilising the identified unstable key blocks. The support scenarios are presented in Table 6-24.

Table 6-24: Support scenarios evaluated in Unwedge

Support scenarios modelled in Unwedge				
No Support	1.5 m long bolts at 1.5 m x 1.5 m spacing	1.5 m long bolts at 1 m x 1 m spacing	1.2 m long bolts at 1.5 m x 1.5 m spacing	Application of 30 mm shotcrete with 1.5 m bolts at 1.5 m x 1.5 m spacing

Support properties were kept constant in all the simulation models. Table 6-25 and Table 6-26 summarise bolt and shotcrete properties used in the models.

Table 6-25: Bolt properties specified in Unwedge

Bolt Poperties	
Bolt Type	Resin Grouted
Tensile Capacity (MN)	0.15
Plate Capacity (MN)	0.1
Bond Strength (MN/m)	0.51
Bond Length (m)	0.3

Table 6-26: Shotcrete support specified in Unwedge

Shotcrete Properties	
Shear Strength (MPa)	1.0
Thickness (mm)	30.0
Unit Weight (MN/m^3)	0.026

Figure 6-2 to Figure 6-12 show the application of the various support scenarios. Table 6-27 to Table 6-32 summarise the results of the FOS of the formed wedges with different support scenarios in each production section. The results obtained from all the models in the three production sections were consistent. The FOS of the wedges did not improve when both the 1.5 m and 1.2 m bolts were installed at 1.5 m x 1.5 m grid spacing. Installing both bolts at a reduced spacing did stabilize some wedges, but not all of them, due to the variable sizes (or stabilization areas) of the formed wedges. Lastly, by applying a 30 mm shotcrete layer on the skin of the stope excavations, the FOS of all the individual wedges was not only brought up to acceptable levels but was drastically increased. The effect of the shotcrete is due to the small keyblocks as shown in Chapter 5. Shotcrete support should

therefore form part of the standard support. However, this can be a costly and counterproductive approach. Alternatively, the small keyblocks between support units can be managed by adequate barring during entry examination and/or the application of mesh or straps.

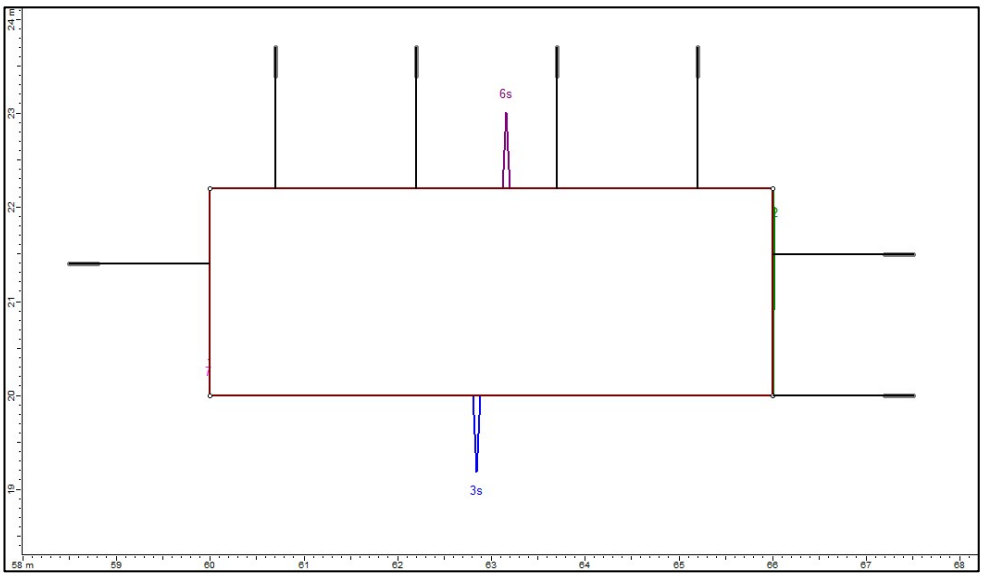


Figure 6-2: 1.5 m long resin grouted bolts installed on a 1.5 m by 1.5 m grid spacing in RIG 47

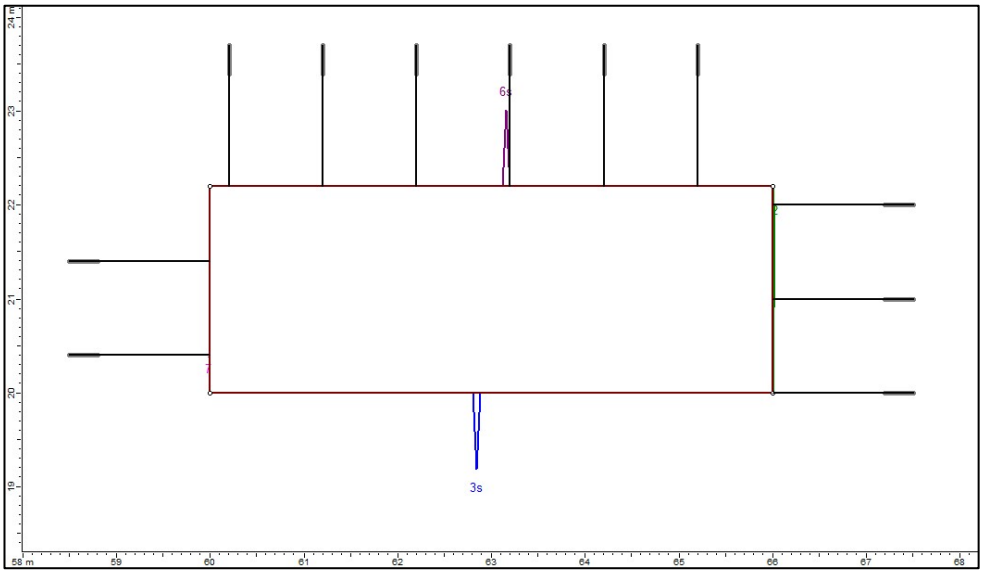


Figure 6-3: 1.5 m long resin grouted bolts installed on a 1.0 m by 1.0 m grid spacing in RIG 47

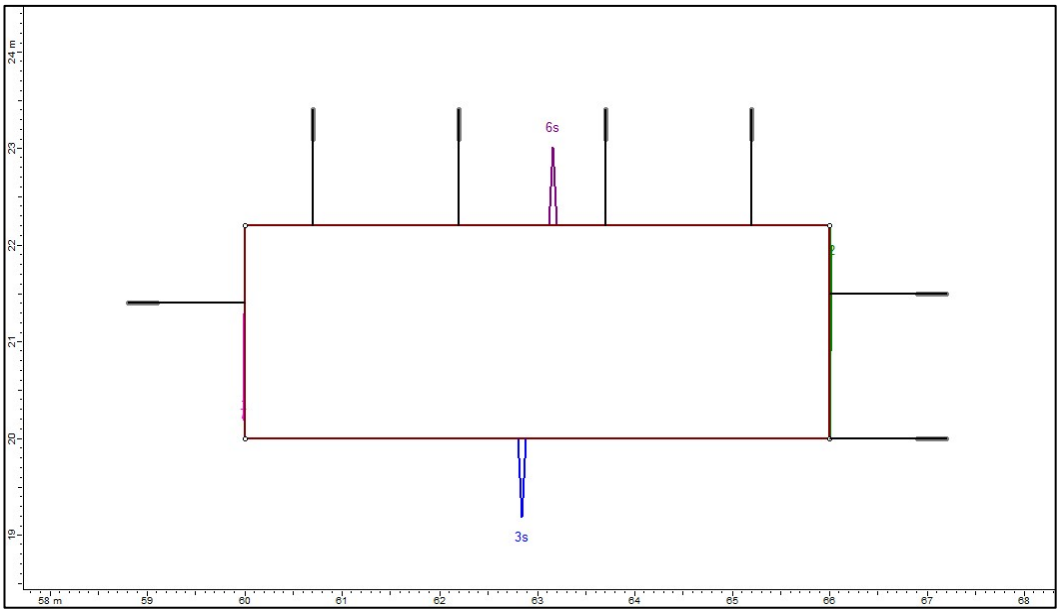


Figure 6-4: 1.2 m long resin grouted bolts installed on a 1.5 m by 1.5 m grid spacing in RIG 47

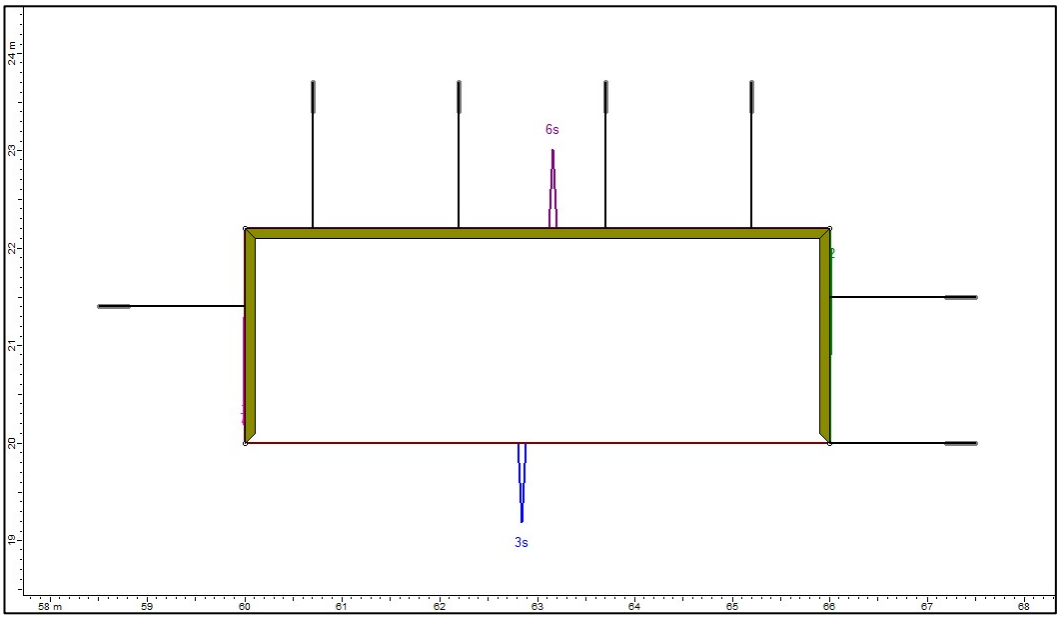


Figure 6-5: 30 mm Shotcrete and 1.5m long resin grouted bolts installed on a 1.5 m by 1.5 m grid spacing in RIG 47

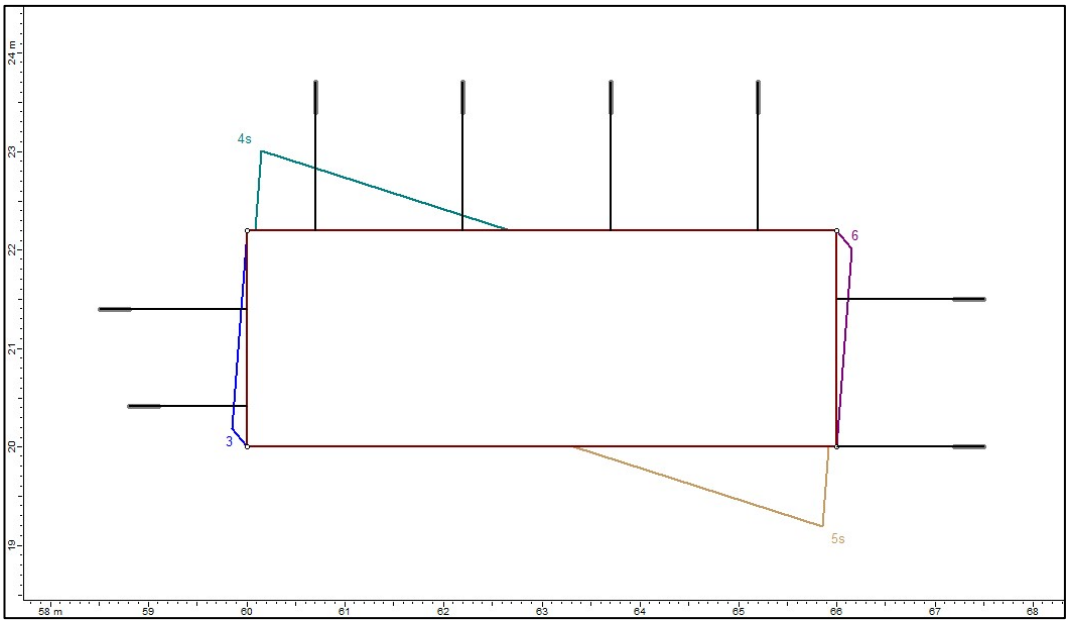


Figure 6-6: 1.5 m long resin grouted bolts installed on a 1.5 m by 1.5 m grid spacing in RIG 50

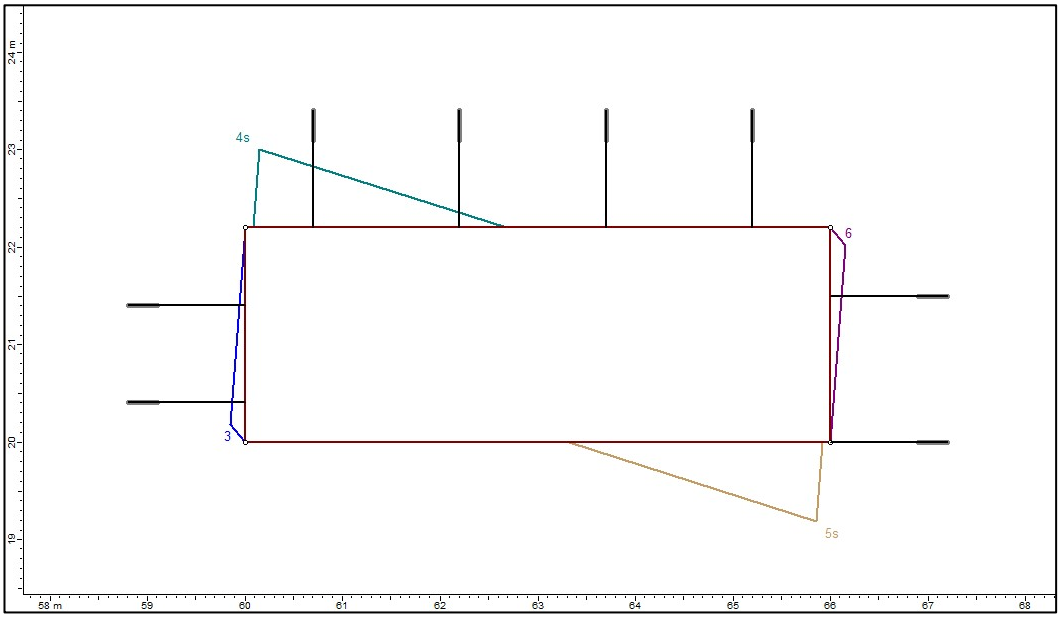


Figure 6-7: 1.2 m long resin grouted bolts installed on a 1.0 m by 1.0 m grid spacing in RIG 50

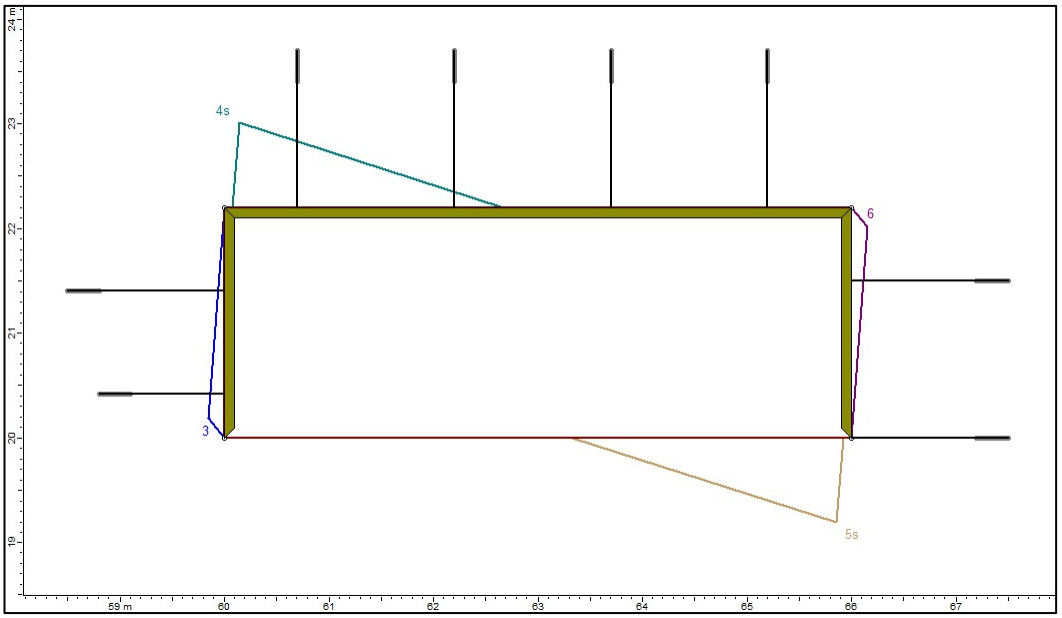


Figure 6-8: 30 mm Shotcrete and 1.5m long resin grouted bolts installed on a 1.5 m by 1.5 m grid spacing in RIG 50

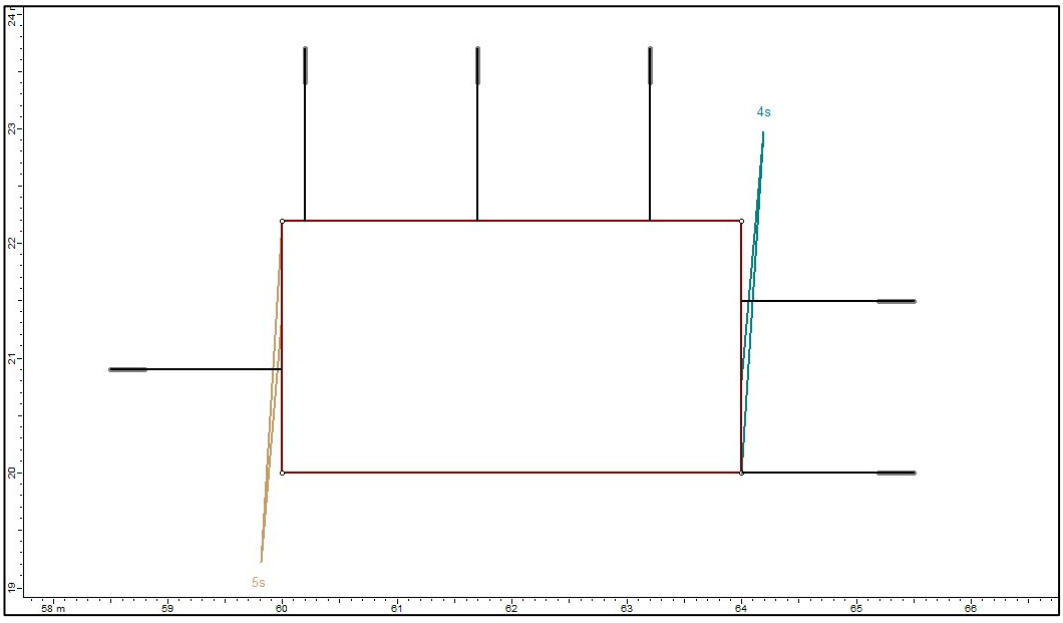


Figure 6-9: 1.5 m long resin grouted bolts installed on a 1.5 m by 1.5 m grid spacing in TC1

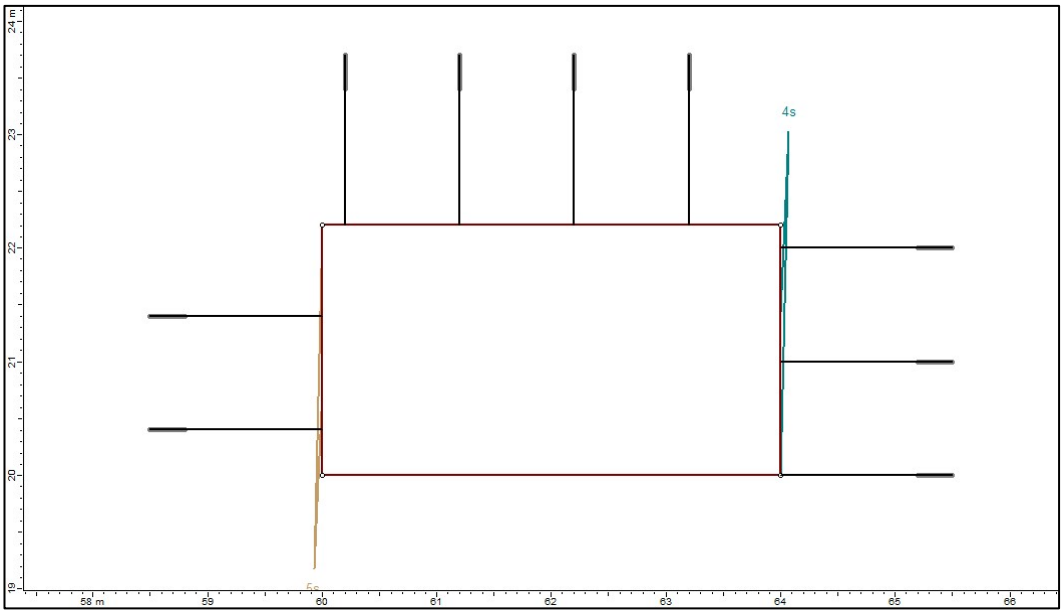


Figure 6-10: 1.5 m long resin grouted bolts installed on a 1.0 m by 1.0 m grid spacing in TC1

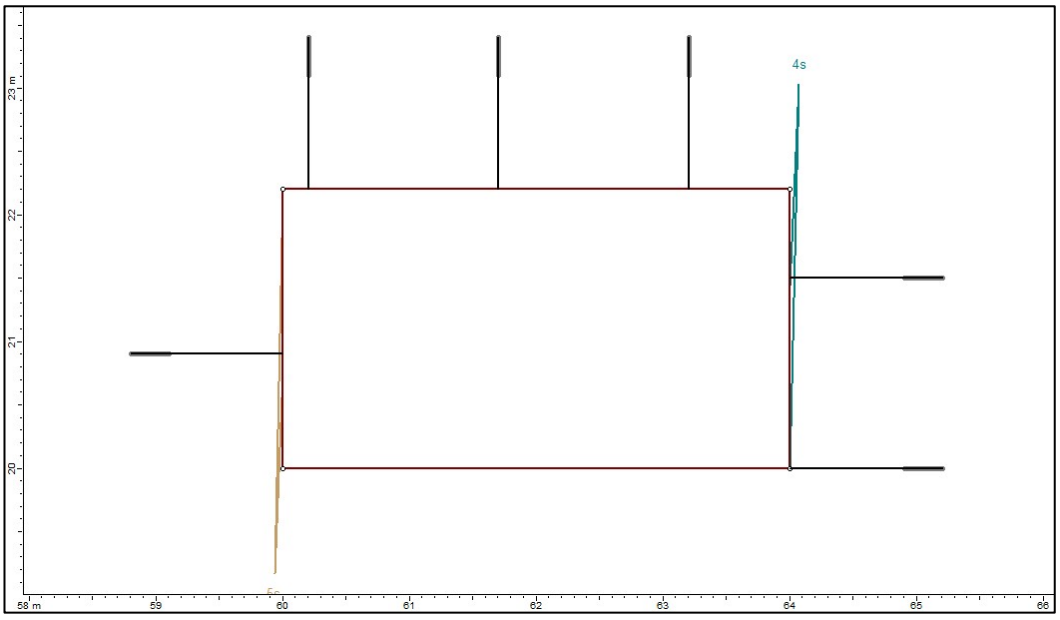


Figure 6-11: 1.2 m long resin grouted bolts installed on a 1.5 m by 1.5 m grid spacing in TC1

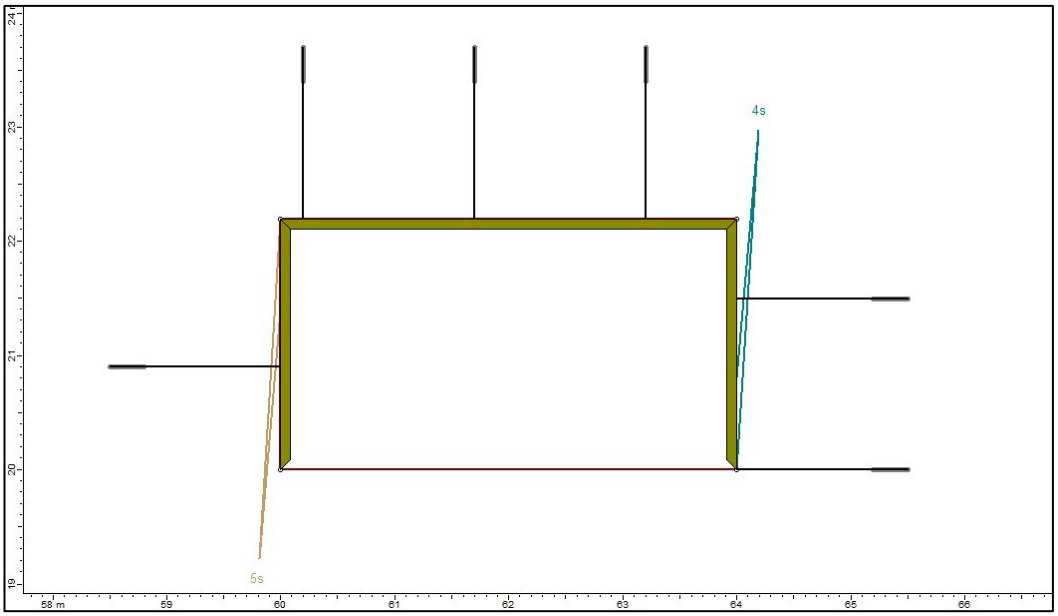


Figure 6-12: 30 mm Shotcrete and 1.5m long resin grouted bolts installed on a 1.5 m by 1.5 m grid spacing in TC1

Table 6-27: FOS results of generated wedges after applying various support systems

Wedge Position	Wedge Factor of Safety (FOS) for Different Support Scenarios in RIG 47				
	No Support	1.5 m long bolts at 1.5 m x 1.5 m spacing	1.5 m long bolts at 1 m x 1 m spacing	1.2 m long bolts at 1.5 m x 1.5 m spacing	Application of 30 mm shotcrete with 1.5 m bolts at 1.5 m x 1.5 m spacing
Roof Wedge	0.02	0.02	0.02	0.02	262.09
Upper Right Wedge	0.04	242.63	242.63	242.63	1173.20
Lower Left Wedge	0.02	0.02	0.02	0.02	982.69

Table 6-28: Results of the FOS of the roof wedge in RIG 50 after applying different support

Roof Wedge Factor of Safety (FOS) for Different Support Scenarios in RIG 50 Strike Bords								
Combination	Joint A	Joint B	Joint C	No Support	1.5 m long bolts at 1.5 m x 1.5 m spacing	1.5 m long bolts at 1 m x 1 m spacing	1.2 m long bolts at 1.5 m x 1.5 m spacing	Application of 30 mm shotcrete with 1.5 m bolts at 1.5 m x 1.5 m spacing
1	2	3	4	0.00	0.00	0.00	0.00	132.70
2	1	3	4	0.02	0.02	0.02	0.02	237.00
3	1	2	5	No wedges formed	-	-	-	-
4	1	2	4	No wedges formed	-	-	-	-
5	1	2	3	No wedges formed	-	-	-	-
6	1	4	5	No wedges formed	-	-	-	-
7	3	4	5	No wedges formed	-	-	-	-
8	1	3	5	No wedges formed	-	-	-	-
9	2	3	5	No wedges formed	-	-	-	-
10	2	4	5	No wedges formed	-	-	-	-

Table 6-29: Results of the FOS of the lower left wedge in RIG 50 after applying different support

Lower Left Wedge Factor of Safety (FOS) for Different Support Scenarios in RIG 50 Strike Bords								
Combination	Joint A	Joint B	Joint C	No Support	1.5 m long bolts at 1.5 m x 1.5 m spacing	1.5 m long bolts at 1 m x 1 m spacing	1.2 m long bolts at 1.5 m x 1.5 m spacing	Application of 30 mm shotcrete with 1.5 m bolts at 1.5 m x 1.5 m spacing
1	1	2	3	0.02	0.02	0.02	0.02	136.53
2	2	3	4	0.02	0.81	28.71	0.81	145.84
3	1	3	4	0.05	19.15	53.33	19.15	3.40
4	1	2	5	0.248	26.69	56.53	26.69	189.17
5	2	4	5	0.248	41.38	82.5	41.38	203.07
6	1	4	5	0.807	56.54	0.81	56.54	339.44
7	3	4	5	No wedges formed	-	-	-	-
8	1	3	5	No wedges formed	-	-	-	-
9	2	3	5	No wedges formed	-	-	-	-
10	2	4	5	No wedges formed	-	-	-	-

Table 6-30: Results of the FOS of the upper left wedge in RIG 50 after applying different support

Upper Left Wedge Factor of Safety (FOS) for Different Support Scenarios in RIG 50 Strike Bords								
Combination	Joint A	Joint B	Joint C	No Support	1.5 m long bolts at 1.5 m x 1.5 m spacing	1.5 m long bolts at 1 m x 1 m spacing	1.2 m long bolts at 1.5 m x 1.5 m spacing	Application of 30 mm shotcrete with 1.5 m bolts at 1.5 m x 1.5 m spacing
1	1	2	3	No wedges formed	-	-	-	-
2	2	4	5	0.00	Stable	0.00	Stable	47.52
3	2	3	4	No wedges formed	-	-	-	-
4	1	4	5	0.02	Stable	15.64	Stable	44.41
5	1	3	4	No wedges formed	-	-	-	-
6	1	2	5	0.00	Stable	0.04	Stable	37.87
7	3	4	5	0.02	Stable	18.05	Stable	24.22
8	1	3	5	0.02	Stable	0.76	Stable	29.43
9	2	3	5	0.13	Stable	1.19	Stable	34.79
10	1	2	4	3.40	0.07	Stable	0.07	Stable

Table 6-31: Results of the FOS of the lower right wedge in RIG 50 after applying different support

Lower Right Wedge Factor of Safety (FOS) for Different Support Scenarios in RIG 50 Strike Bords								
Combination	Joint A	Joint B	Joint C	No Support	1.5 m long bolts at 1.5 m x 1.5 m spacing	1.5 m long bolts at 1 m x 1 m spacing	1.2 m long bolts at 1.5 m x 1.5 m spacing	Application of 30 mm shotcrete with 1.5 m bolts at 1.5 m x 1.5 m spacing
1	1	2	4	0.07	0.07	0.07	0.07	1959.00
2	2	3	5	3.40	Stable	Stable	Stable	Stable
3	1	4	5	3.40	Stable	Stable	Stable	Stable
4	3	4	5	3.40	Stable	Stable	Stable	Stable
5	2	4	5	3.40	Stable	Stable	Stable	Stable
6	1	2	5	3.40	Stable	Stable	Stable	Stable
7	1	3	5	3.40	Stable	Stable	Stable	Stable
8	1	3	5	No wedges formed	-	-	-	-
9	2	3	5	No wedges formed	-	-	-	-
10	2	4	5	No wedges formed	-	-	-	-

Table 6-32: Results of the FOS of different wedges in TC1 after applying different support

Wedge Position	Wedge Factor of Safety (FOS) for Different Support Scenarios in TC1				
	No Support	1.5 m long bolts at 1.5 m x 1.5 m spacing	1.5 m long bolts at 1 m x 1 m spacing	1.2 m long bolts at 1.5 m x 1.5 m spacing	Application of 30 mm shotcrete with 1.5 m bolts at 1.5 m x 1.5 m spacing
Upper Right Wedge	0.09	0.09	0.09	0.09	1173.20

6.4 Support from Stress Analysis

In Section 5.2.4, the evaluation of intact rock mass failure involved the determination of the maximum vertical tensile zone height. This height was assumed to control hangingwall failure and was affected by mining spans and depths below the surface. It was established that the height of the tensile zone increased with increasing mining span but decreased with increasing mining depth below the surface. This means that spans at shallower depths require support systems consisting of longer tendons. According to the results, when the depth below the surface is increased beyond 500 m, the vertical tensile zone extends to a maximum of 1 m into the hangingwall only at the maximum diagonal span of 21 m (i.e. a bord span of 15 m). Additionally, when the depth below the surface increased beyond 600 m, the vertical tensile zone extended to less than 1 m into the hangingwall for all the spans evaluated.

Since the mine has passed mining at depths below 500 m, the 1.2 m resin-grouted rockbolts determined above are adequate to provide support to bord spans of less

than or equal to 15.0 m and can be used as standard support. This also supports future mining as the vertical tensile zone is less than 1 m for the evaluated spans when the mining depth below the surface exceeds 600 m.

6.5 Support for a Stratified Rock Mass

The hanging wall at Thorncliffe Mine consists of interlayering between the MG1L1 disseminated Chrome reef and pyroxenite host rock. It was determined that the onset of snap-through failure in the mine occurs when a beam thickness of smaller or equal to 0.30 m in a 17.0 m diagonal span (formed by a 12 m span of orthogonal bords) has deflected by 26.31 mm. The length of a standard support of 1.2 m determined in this case study is adequate to suspend or clamp together unstable strata to the stable beam above the excavation. Alternatively, the mining cut at the mine can include the MG1L1 Chromitite stringer, which would eliminate a source of many FOGs at the mine.

6.6 JBlock Probabilistic Stability Analysis

Finally, the JBlock programme enabled a risk-based standard support design which involved using characteristics of discontinuity sets for simulating and assessing the stability of hangingwall keyblocks in each production section. The Jblock program followed a probabilistic approach to determine the size and frequency of keyblocks that can occur in the stope excavations. The programme was then used to assess the effectiveness and validity of different standard support systems on the probability of failure of the formed keyblocks. Support effectiveness is determined by the number of keyblocks prevented from falling by the support system in place.

In the model setup, two ‘hazard zones’ were defined in the working area of production sections. The face area, which is measured 3 m from the position of the advancing face and the focus of this study (area of interest), and the ‘back area’, which extends 15 m from the back of the face area, are in the working area. Support was applied in both hazard zones. Since the exposure of the workforce to unsafe areas in the panels, two personnel were allowed in the face area for 30% of the

production shift, with only one person allowed to work in the back area 15% of the production shift (Maepa, 2024).

Table 6-33 presents the support scenarios that were analysed in the Jblock Software. Support properties used in the models are presented in Table 6-25 and Table 6-26. The modelled standard support layouts consist of varying bolt lengths, support spacing, and the application of shotcrete. Table 6-34 summarises the characteristics of each discontinuity set which were used as inputs into the Jblock models. Input parameters consist of discontinuity set orientation data, trace lengths, spacing, and shear strength properties. In all the production sections, a mining span of 10 m was selected to evaluate and demonstrate the effectiveness of different support layouts. A hazard analysis of rockfalls was conducted per mining step (one face advance of one blast) since the fallout of keyblocks is likely to occur during a blast, and only a few will fall after blasting. An advance of 4 m per blast was used.

Table 6-33: Support scenarios to assess the effect of support spacing, bolt length, and shotcrete

Support scenarios modelled in Jblock Software	
Scenario 1	No Support
Scenario 2	1.5 m long bolt at 1.5 m x 1.5 m spacing
Scenario 3	1.5 m long bolt at 1.0 m x 1.0 m spacing
Scenario 4	1.2 m long bolt at 1.5 m x 1.5 m spacing
Scenario 5	Application of 30 mm shotcrete with 1.5 m resin bolts

Table 6-34: Summary of discontinuity characteristics in each mining section

Mining Section	Joint Set (JS)	Dip (°)		Dip Direction (°)		Discontinuity Spacing (m)			Discontinuity Trace Lengths (m)			Cohesion (kPa)		Friction Angle	
		Average	Standard Dev	Average	Standard Dev	Min	Max	Mean	Min	Max	Mean	Cohesion (kPa)	Standard Dev	Mean	Standard Dev
RIG 47	JS1	86	4.1	051	25.2	0.001	2.48	0.45	3.0	10.0	7.0	0.0	0.0	25.0	0.0
	JS2	88	3.4	337	11.6	0.001	8.27	1.49	3.0	10.0	7.0	0.0	0.0	25.0	0.0
	JS3	87	2.5	283	7.0	0.166	8.07	2.23	3.0	10.0	7.0	0.0	0.0	25.0	0.0
RIG 50	JS1	87	3.1	258	12.1	0.001	4.90	0.92	3.0	10.0	7.0	0.0	0.0	25.0	0.0
	JS2	85	3.9	030	7.6	0.001	6.21	1.37	3.0	10.0	7.0	0.0	0.0	25.0	0.0
	JS3	87	4.1	351	17.8	0.002	6.06	0.72	3.0	10.0	7.0	0.0	0.0	25.0	0.0
	JS4	88	3.2	124	9.5	0.015	5.55	0.93	3.0	10.0	7.0	0.0	0.0	25.0	0.0
	JS5	62	5.6	215	4.4	0.021	4.13	0.68	3.0	10.0	7.0	0.0	0.0	25.0	0.0
TC1	JS1	87	3.2	299	14.2	0.147	9.85	1.26	3.0	10.0	7.0	0.0	0.0	25.0	0.0
	JS2	85	5.4	219	25.4	0.021	3.35	0.46	3.0	10.0	7.0	0.0	0.0	25.0	0.0
	JS3	90	3.6	342	3.9	0.085	4.88	1.14	3.0	10.0	7.0	0.0	0.0	25.0	0.0

Figure 6-13 and Figure 6-14 illustrate the Jblock scenarios modelled with no support and with support installed at 1.5 m by 1.5 m spacing, respectively. The red outlines represent unstable keyblocks, which are mostly concentrated behind the advancing face, whilst the blue outlines represent stable keyblocks and are seen mostly in the back of the working area. A few keyblocks become unstable further behind the face. The green blocks are formed outside of the excavation.

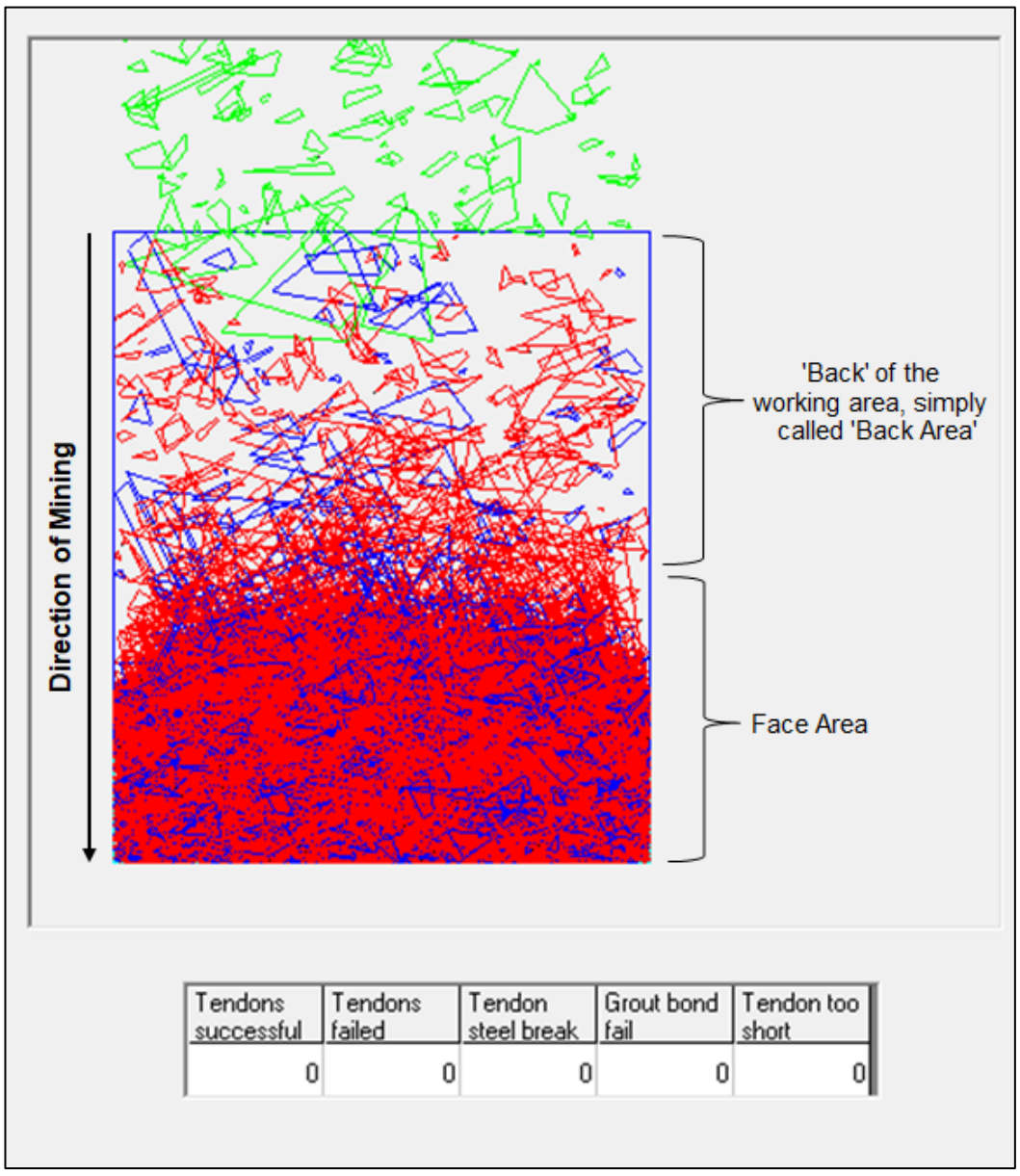


Figure 6-13: JBlock Model of a 10 m Span with no support in Rig 47

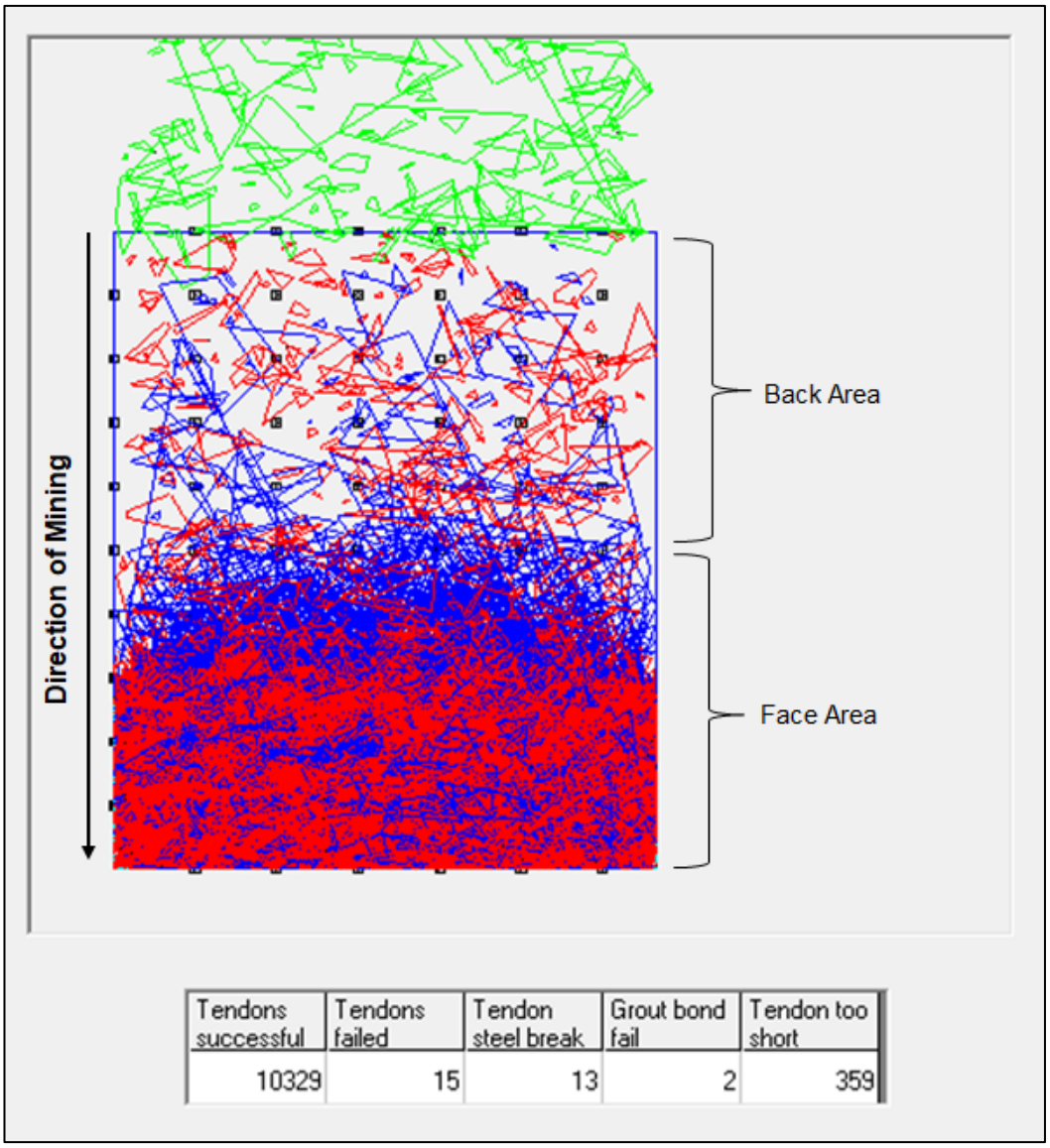


Figure 6-14: JBlock Model of a 10 m Span with support installed at 1.5 m by 1.5 m in Rig 47

The interpretation of the results is summarised in three parts, namely the number of falls per blast, as illustrated by Figure 6-15 and Figure 6-18 for unsupported and supported, respectively. Secondly, block stability outlines the key block size distribution, indicating the frequency of blocks that failed in each size class (Figure 6-16 and Figure 6-19). Lastly, the hazard and risk results for each hazard zone outline the total number of falls per mining step, average failure volume per mining step, and expected injuries per mining step in Figure 6 17 and Figure 6-20. All the

scenarios modelled in Jblock for all three production sections are provided in Appendix E.

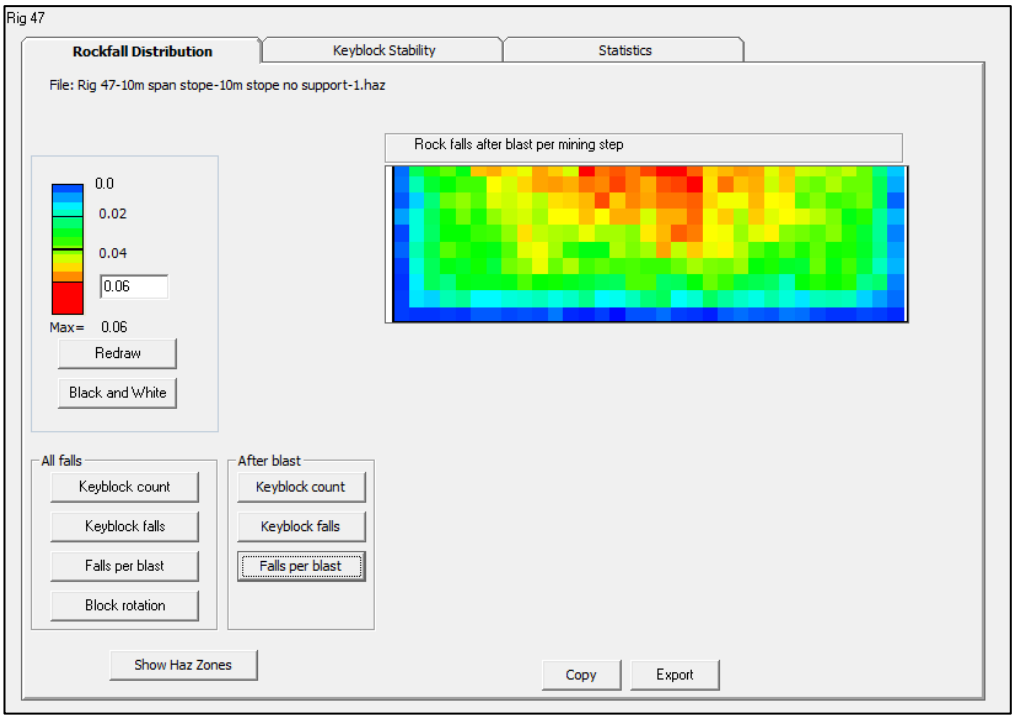


Figure 6-15: Distribution of rockfalls in the face area of a 10 m bord span with no support in Rig 47

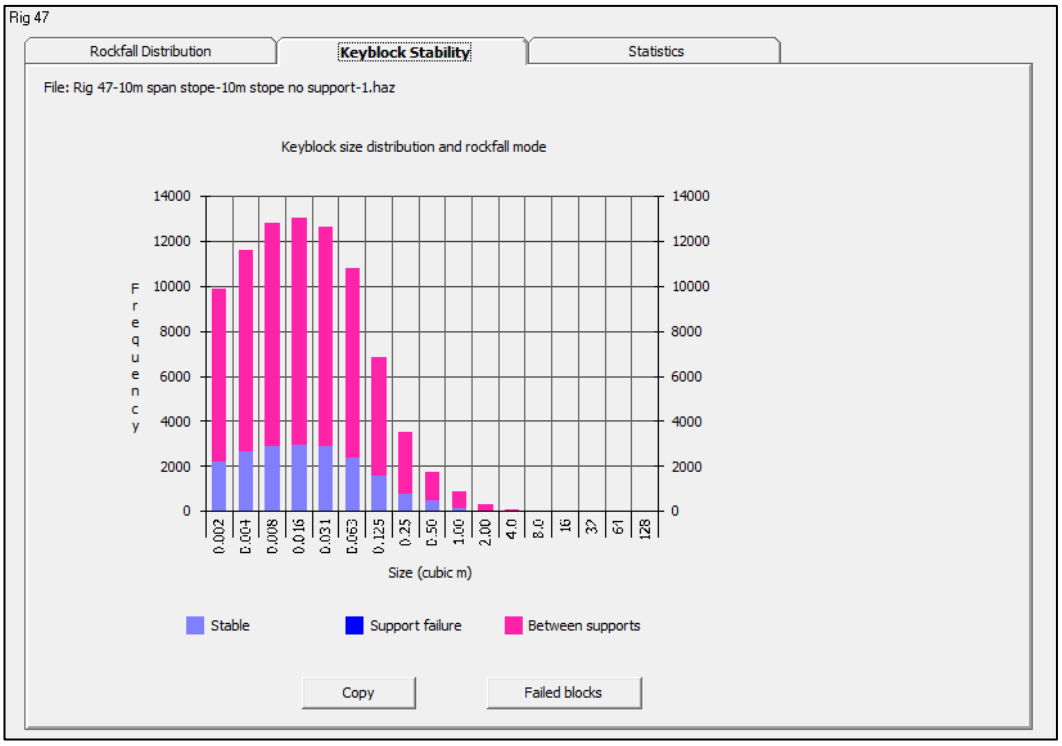


Figure 6-16: Key block stability frequency distribution chart for a 10 m bord span with no support in Rig 47

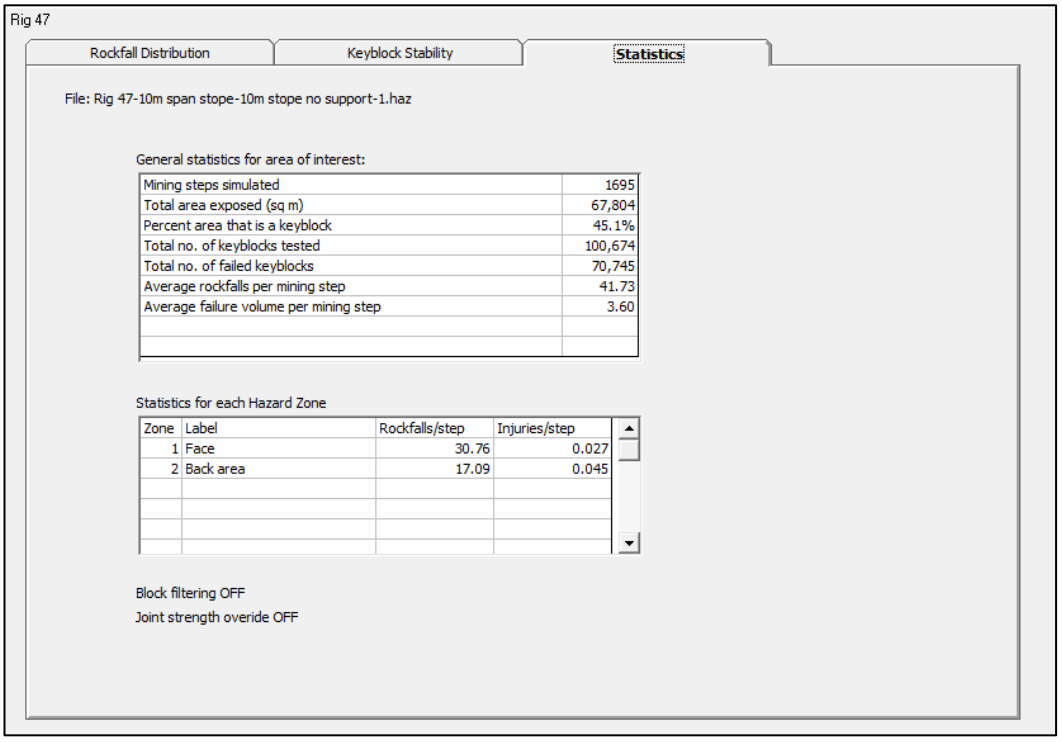


Figure 6-17: Hazard and risk results for a 10 m bord span with no support in Rig 47

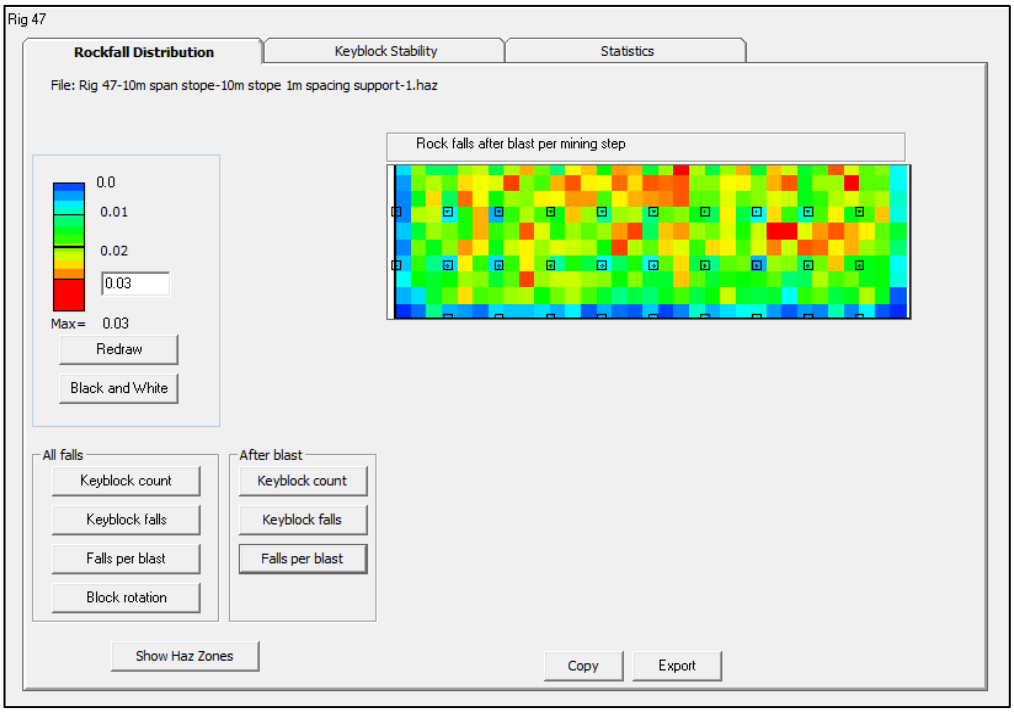


Figure 6-18: Distribution of rockfalls in the face area of a 10 m bord span with support in Rig 47

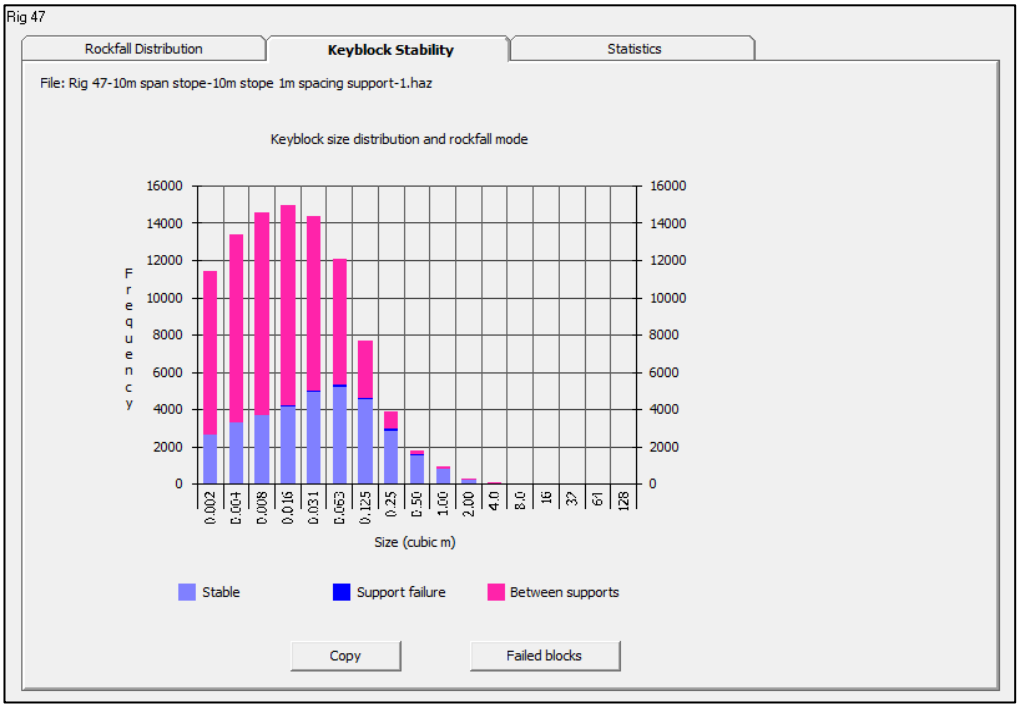


Figure 6-19: Keyblock stability frequency distribution chart for a 10 m bord span with support in Rig 47

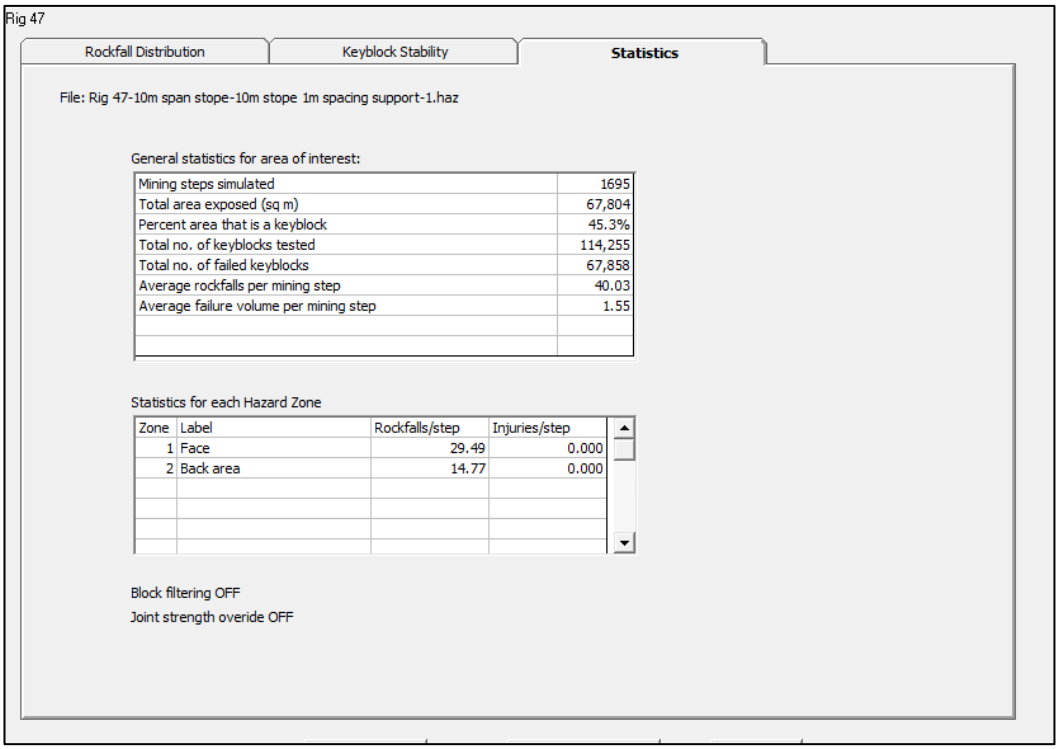


Figure 6-20: Hazard and risk results for a 10 m bord span with support in Rig 47

Table 6-35 to Table 6-37 summarise the results from the three production sections. It is worth noting that more than 95% of the keyblocks formed in all the mining sections are less than or equal to 1.0 m^3, which confirms the formation of small keyblocks in the hangingwall. This is demonstrated in Figure 6-19. Firstly, the results indicated that when no support is applied, a small percentage of blocks are still held in position by friction and are stable. The percentage of failed blocks in the 'no support scenarios' varied between 68.7% to 78.9% in the three production sections. The results indicated that the installation of the tendon support units decreased the number of failed blocks by a small percentage. Only a small number of blocks were stabilized. The keyblocks still failed between support units due to their small dimensions. Importantly, the 1.5 m and 1.2 m long resin grouted bolts installed at 1.5 m by 1.5 m grid spacing had the same effect in terms of providing support in all three mining sections, which provides further evidence of an opportunity to decrease the standard support length to 1.2 m. Installing 1.5 m long bolts on a grid spacing of 1 m by 1 m reduced the percentage of keyblocks by a maximum of about 11% but this was considered insignificant in this environment due to the increased support density, which translates to increased support costs.

The application of areal coverage of 30 mm shotcrete stabilized all the keyblocks, which agrees with the results in Section 6.3 (Unwedge analysis of keyblocks).

Table 6-35: Results of statistical keyblock analysis, Rig 47 10 m span

Support scenarios modelled in Jblock Software		Hazard Zone: Face Area, Rig 47 10 m Span			
		% of failed keyblocks	Rockfall per Mining Step	Average Failure Volume per Mining Step	Injuries per Mining Step
Scenario 1	No Support	70%	30.76	3.60	1 per 37 Blasts
Scenario 2	1.5 m long bolt at 1.5 m x 1.5 m spacing	64.76%	42.46	2.11	1 per 17 Blasts
Scenario 3	1.5 m long bolt at 1.0 m x 1.0 m spacing	59.39%	29.49	1.55	0.00
Scenario 4	1.2 m long bolt at 1.5 m x 1.5 m spacing	64.75%	31.71	2.13	0.00
Scenario 5	Application of 30 mm shotcrete with 1.5 m resin bolts	0%	0.00	0.00	0.00

Table 6-36: Results of statistical keyblock analysis, Rig 50 10 m span

Support scenarios modelled in Jblock Software		Hazard Zone: Face Area, Rig 50 10 m Span			
		% of failed keyblocks	Rockfall per Mining Step	Average Failure Volume per Mining Step	Injuries per Mining Step
Scenario 1	No Support	78.85%	73.82	15.48	1 per 16 Blasts
Scenario 2	1.5 m long bolt at 1.5 m x 1.5 m spacing	75.71%	129.62	12.40	0.00
Scenario 3	1.5 m long bolt at 1.0 m x 1.0 m spacing	72.41%	98.14	10.69	1 per 15 Blasts
Scenario 4	1.2 m long bolt at 1.5 m x 1.5 m spacing	76%	96.01	12.84	0.00
Scenario 5	Application of 30 mm shotcrete with 1.5 m resin bolts	0%	0.00	0.00	0.00

Table 6-37: Results of statistical key block analysis, TC1 10 m span

Support scenarios modelled in Jblock Software		Hazard Zone: Face Area, TC1 10 m Span			
		% of failed keyblocks	Rockfall per Mining Step	Average Failure Volume per Mining Step	Injuries per Mining Step
Scenario 1	No Support	68.68%	39.61	3.92	0.00
Scenario 2	1.5 m long bolt at 1.5 m x 1.5 m spacing	64.72%	41.81	2.36	1 per 9 Blasts
Scenario 3	1.5 m long bolt at 1.0 m x 1.0 m spacing	60.39%	40.23	1.87	1 per 10 Blasts
Scenario 4	1.2 m long bolt at 1.5 m x 1.5 m spacing	64.64%	41.87	2.36	1 per 9 Blasts
Scenario 5	Application of 30 mm shotcrete with 1.5 m resin bolts	0.002%	0.00	0.00	0.00

Note the formation of relatively bigger blocks (volume) in RIG 50 in Table 6-36, as this production section consists of five discontinuity sets, which create bigger keyblocks. However, even the biggest blocks were completely stabilised by the application of shotcrete. Table 6-38 summarises results from assessing the impact of varying the bord width dimension on the risk of rock falls (frequency of rockfalls and fallout size) in unsupported and supported bords, respectively. To carry out this exercise, the calculated spans ranging from 6 m to 15 m mining in the TC1 ore production block were evaluated. Exports of the Jblock results for each scenario are also provided in Appendix E. The results are discussed below.

Table 6-38: Effect of increasing supported bord spans on rockfall risk

Hazard Zone: Face Area. Support: 1.5 m long bolts at 1.5 m x 1.5 m spacing			
Bord Spans (m)	% of failed keyblocks	Rockfall per Mining Step	Average Failure Volume per Mining Step
6	63%	24.70	1.37
8	63%	35.38	1.82
10	65%	41.81	2.36
15	66%	63.60	4.05

The results indicated that while the improvement was considered small, reducing bord spans mitigated the rockfall risk by reducing the percentage of failed blocks, rockfalls per mining step, and the size of the fallouts. The results from all the spans evaluated still indicated that more than 95% of blocks are small (< 1 m^3) and fail between support units. Again, the application of shotcrete stabilized all the keyblocks due to their small dimensions.

6.7 Support Cost Saving Analysis

Currently, Glencore ECM installs the 1.5 m long full-column resin grouted rockbolts with one 500 mm long fast set capsule and one 900 mm long medium set capsule (Glencore ECM, 2019). The optimised or proposed bolt length of 1.2 m in this study will be installed with one 500 mm long fast set capsule and one 600 mm long medium set capsule. Both primary support systems require 2 capsules per support hole. Table 6-39 presents the prices of the roof bolts and resin capsules used in the current and optimised primary support systems.

Table 6-39: Roof bolts and resin capsules pricing (Sandvik Rocbolt Technologies , 2025)

Description	Quantity	Unit of Measure	Total Price (ZAR)
18 mm diameter, 1.5 m long resin bolt	1	Each	88.98
18 mm diameter, 1.2 m long resin bolt	1	Each	79.79
Resin Capsule Box - contains 12 x 25 mm diameter, 500 mm long fast set capsules, and 12 x 25 mm diameter, 900 mm long medium set capsules	1	Box	313.36
Resin Capsule Box - contains 15 x 25 mm diameter, 500 mm long fast set capsules, and 15 x 25 mm diameter, 600 mm long medium set capsules	1	Box	340.67

Table 6-39 indicates that the resin capsule box used in the installation of the 1.5 m long rockbolts contains 24 capsules, with each capsule costing about R13.06. The resin capsule box, which can be used in the installation of the optimised 1.2 m long rockbolts, contains 30 capsules, with each capsule costing about R11.26 (Sandvik Rocbolt Technologies , 2025).

To demonstrate the potential of saving costs on support in this study, a standard 1.5 m grid bolt spacing in an 8 m face length was used. The mine's support procedure requires that resin bolts be always installed at a maximum of 1.5 m from the side wall (Glencore ECM, 2019). This means approximately 4 rock bolts will be installed per support line along the dip of an 8 m panel. After an advance per blast of 4 m, the mine installs 3 lines of rock bolts spaced at 1.5 m along strike. This equates to 12 bolts installed in each production face after each blast. Each production cycle consists of 2 shifts. To meet production targets 10 crews or production sections blast about 5 panels per shift for an average of 21 days each month in a year (Glencore ECM, 2021). These parameters were used in Table 6-40 to demonstrate the potential of saving support costs in a year when using the optimised bolt of 1.2 m in length.

Table 6-40: Support cost saved annually

Support, production, and costing parameters	ECM Current Primary Support	Case Study Optimised Primary Support
Roofbolt length (m)	1.5	1.2
Bolt spacing (m)	1.5 m by 1.5m	1.5 m by 1.5m
Advance/blast (m)	4	4
Panel length (m)	8	8
Bolts/panel	12	12
Number of capsules/panel	24	24
Panels blasted/shift/crew	5	5
No. of production crews	10	10
Shifts/day	2	2
Average production days/month	21	21
Production months/year	12	12
Cost/bolt (R)	88.98	79.79
Cost/capsule (R)	13.06	11.36
Roofbolts Cost/year (R)	26 907 552.00	24 128 496.00
Cost of capsules per year (R)	7 896 672.00	6 867 907.20
Total support cost per year (R)	34 804 224.00	30 996 403.20
Costs saved annually (R)	**3 807 820.80**	
Notes: (i) Roofbolts cost/year = Bolts/panel × Panels blasted/shift/crew × No. of production crews × Shifts/day × Average production days/month × Production months/year × Cost/bolt (ii) Cost of capsules per year = Number of capsules/panel × Panels blasted/shift/crew × No. of production crews × Shifts/day × Average production days/month × Production months/year × Cost/capsule (Chikande, 2018)		

Table 6-40 demonstrates that Thorncliffe Mine can potentially save R 3 807 820.80 annually while maintaining safe in-stope working conditions if 1.2 m rock bolts are adopted as standard primary support. The support system consisting of 1.2 m long rock bolts is effective yet overall cheaper than the support system consisting of 1.5 m long rock bolts.

6.8 Chapter Summary

This chapter aimed at determining optimum standard support requirements to stabilize the rock mass at Thorncliffe Mine. A review of the current support practices at the mine was conducted. It was concluded that the current standard support system, consisting of 1.5 m long full-column resin-grouted bolts, is adequate. However, deterministic and probabilistic analyses suggest that a cost-saving alternative exists by using 1.2 m long bolts with the same capacity and spacing. This is because, according to the evaluation of stability assessments, the

unstable keyblocks forming between pillars are small in dimension, and all potential instability modes can be managed by the 1.2 m resin rockbolts. The small keyblocks occurring between support units can be managed by adequate barring during stope entry examination or the application of shotcrete. The next chapter rounds up all the key findings from the research project.

7 PROJECT FINDINGS

The MHSC systematic methodology for designing maximum stable stope spans in shallow mining conditions was applied in this research project. The study involved the identification and evaluation of various hangingwall failure mechanisms, which led to the determination of a standard support system required to stabilize the roof between pillars. An important (safety) factor considered in the design of maximum bord spans that can be safely mined was areas of the largest spans where the potential of large collapses occurring is increased. This area is defined by the diagonal span across intersections of equal-sized orthogonal panels. Bord widths were also tailored to engineering requirements, local rock engineering environment, and the degree of safety required in different production drives. This Chapter discusses key findings of the research project.

7.1 Rock Mass Failure Analysis

The study included in-depth rock mass characterization, which resulted in geotechnical data that were used as input parameters in different rock mass classification systems to quantify rock mass quality. The RMR_{89}, GSI, Q-system, and $MRMR_{2000}$ classification systems were used to quantify the quality of the hangingwall rock mass at Thorncliffe Mine. Rock mass classification schemes were also used to provide indications of likely dimensions of stable spans under different ground conditions and corresponding support requirements. The evaluation of stability of stope spans was conducted using the modified stability graph method using the modified stability number, *N*', originally developed by Mathews et al. (1980) and the mining rock mass rating (MRMR) system originally developed by Laubscher (1977). The findings from using empirical methods based on rock mass classification systems are summarized as follows:

- The quality of the hangingwall rock mass at Thorncliffe Mine's underground workings ranged from very poor to very good ground conditions. Only the Q-system identified the existence of very poor ground conditions in all the ore production sections. Both the Q-system and $MRMR_{2000}$ results confirmed the occurrence of poor ground conditions. All rock mass classification systems used to quantify rock mass quality confirmed the

existence of fair ground at the mine, whilst good ground conditions were identified by all rock mass classification methods used, excluding the Q-system. Very good ground conditions were confirmed by both the RMR_{89} and the GSI classification systems.

- Results from the characterization and rock mass classification exercises indicated that areas of very poor and poor ground quality were caused by the existence of adverse geological discontinuities. These include discontinuities such as pegmatite veins, shear zones, joint zones, fracturing associated with dykes, minor faults, and domes. These areas consisted of the intersection of discontinuities (or discontinuity sets) that are closely spaced, where most individual discontinuities have planar, Slickensided or smooth surfaces with thick infill material of low strength, such as serpentine serpentinite infill.
- It was determined that support design in underground excavations depends on rock mass quality, safety requirements, and planned span dimension. Therefore, the unique purposes and life of the different types of production drives in a bord and pillar mining section were considered in determining maximum spans that can be safely mined. Travelling roadways and conveyor belt drives were classified as medium-term excavations and required higher levels of safety than bords used for production only, which were classified as short-term excavations.
- Due to the different degrees of safety required in the different production drives, it was determined that the maximum self-supporting spans for short-term panels can be as low as 3 m in very poor rock to a maximum of 15 m in fair rock qualities. Due to higher safety requirements in medium-term panels, the calculated maximum self-supporting spans were generally low. The values ranged between 2 m in very poor ground to a maximum of 8 m in fair ground.
- Engineering requirements dictated that the mine maintain minimum bord spans of 6 m to accommodate the manoeuvrability of the TMMs. The mine also required 6 m minimum spans in strike conveyor belt drives to accommodate belt conveyor equipment and provide sufficient space for workers to travel to working places.
- In the stability evaluation of the calculated bord spans under different rock mass qualities, results from the modified stability graph method and MRMR

correlated well. As ground conditions deteriorate from good to poor, the mining spans indicate the likelihood of stability problems. In good ground, results from the MRMR indicated that all calculated diagonal spans ranging between 8 m to 21 m spans (formed by 6 m to 15 m spans of orthogonal bords) are likely to be stable without support (stable zone). However, according to Stacey (2001), rock support is still required even in good-quality rock masses.

- In fair ground, stable conditions in larger spans ranging between 17 m to 21 m diagonal spans (formed by 12 m to 15 m spans of orthogonal bords) could only be achieved by the installation of appropriate support (transitional zone). However, smaller spans of 8 m to 14 m (formed by 6 m to 10 m spans of orthogonal panels) were likely to be stable without support in fair-ground conditions. When ground qualities further deteriorated to poor, stable conditions could only be achieved by the installation of support in all the calculated spans, ranging between 8 m to 21 m (formed by 6 m to 15 m spans of orthogonal panels).
- As outlined above, the existence of very poor ground conditions was confirmed in all the ore production sections by the Q-system. The modified stability graph method indicated that in very poor ground, 8 m to 11 m diagonal spans only (formed by 6 m to 8 m spans of orthogonal bords) were likely to be stable with the installation of support, while the rest of the calculated spans will fail.

7.2 Hangingwall Beam Failure Analysis

It was outlined that the interlayering between the MG1L1 disseminated Chrome reef and pyroxenite host rock in the hanging wall at Thorncliffe Mine resulted in a pseudo-stratified rock mass (formed from beams of rock). The Voussoir beam theory was utilised to determine the stability and deflection of the (compressive) Voussoir arch. The stability evaluation focused on the assessment of two Voussoir arch failure modes, namely buckling of the roof beam resulting in ‘snap-through’ failure, and shear failure along discontinuities at the abutments. The findings are as follows:

- The probability of both the assessed Voussoir beam failure modes occurring increases with decreasing beam thickness and increasing span dimension;
- The onset of snap-through failure in the hangingwall occurred when a beam thickness of smaller or equal to 0.30 m in a 17.0 m diagonal span (formed by 12 m spans of orthogonal bords) had deflected by 26.3 mm. Therefore, the potential of rock beams buckling is increased where the rock beam thickness is less than or equal to 0.30 m;
- These findings correlated with the mine's recorded historic FOG database, which indicated that 48% of all FOGs are due to hangingwall parting planes situated at a modal fallout height of 0.25 m (less than 0.30 m rock beam thickness). As a strategy for eliminating the source of many FOGs, the mine can include the entire MG1L1 stringer in the mining cut; and
- Lastly, the calculated FOS against abutment shear failure indicated that there is no potential for shear-type beam failure for all the spans evaluated up to the depth of 1000 mbs (life of mine).

7.3 Structural Failure Analysis

To cover all ground conditions likely to be encountered at the mine, scanline mapping data was collected in the current five ore production blocks. The orientation data of the mapped discontinuities enabled the identification of major discontinuity sets in each of the five mining sections. The acquired structural data also enabled detailed mechanistic and structural stability analyses, which consider the frictional characteristics of the discontinuities. The purpose of the structural stability analyses was to determine the actual size of the wedges and failure modes of individual keyblocks, which informed the determination of support required to ensure the stability of the wedges. The findings from the structural stability analysis are summarised as follows:

- Major discontinuity sets having similar trends and plunges were identified in the five production sections. This confirmed the orientation of major structural features at the mine. It was also determined that the mine's underground workings consist of random discontinuities that are 'scattered' throughout the mine and do not form part of any discontinuity set;

- Analysis of the structural data acquired at Thorncliffe Mine's underground workings indicated that only the three sections (ore blocks) mining towards the South direction (RIG 47, RIG 50, and TC1) consist of the intersection of three or more major discontinuity sets. This was an indication that there were potentially unstable blocks. The two sections mining towards the North direction both indicated an intersection of less than three major discontinuity sets, which indicated the probability of fewer instabilities occurring; and
- Results from the analysis carried out using Rocscience's software '*UNWEDGE*' indicated that the size of the formed and unstable wedges is quite small, with a maximum volume of 0.3 m^3. This analysis further indicated that the reinforcing forces required to accomplish the wedge design FoS are small, with a maximum support pressure of 13 kPa. The probabilistic stability analysis conducted using the Jblock programme confirmed the formation of small keyblocks in the hangingwall in all the mining sections.

7.4 Intact Rock Failure Analysis

The intact rock failure analysis focused on the determination of the maximum vertical tensile zone height above the shallow stopes. This provided predictions of the maximum extent of fracturing in the hangingwall above the stope excavations and therefore guided the design of standard support and maximum spans. Analytical design methods, which include physical calculations and numerical assessment using the Rocscience 2D finite element program RS2, were used to determine estimates of the vertical tensile zone height. The calculated diagonal spans across intersections (which are formed by 6 m to 15 m spans of equal-sized orthogonal panels) were used in each method from a depth of 200 m to 1000 m below the surface. The findings from this analysis are as follows:

- Results from both analytical design methods indicated an increase in the height of the vertical tensile zone with increasing mining span and a decrease with increasing depth below the surface;
- It was decided to use results from the RS2 simulation to inform the length of tendon support units required to maintain stability. This is because the

RS2 numerical assessment considered important factors such as the deformation properties of hangingwall and ore-zone materials, in-situ field stress, depth below the surface, bord widths, and the existing MG1L1 Chrome stringer in the hangingwall. The analytical equation only considered the depth below the surface and bord widths to give crude estimates of the vertical tensile zone height; and

- Principally, the results indicated that when the depth below the surface is increased beyond 500 m, the vertical tensile zone extended to a maximum of 1 m into the hangingwall at the maximum diagonal span of 21 m (when orthogonal bord spans are a maximum of 15 m). Additionally, at a depth below the surface of more than 600 m, the vertical tensile zone extended to less than 1m into the hangingwall for all the spans evaluated. This indicates that the current and future standard support system does not have to consist of longer tendon units since production is currently taking place at a depth below the surface of about 590 m.

7.5 Support Requirements

Various failure mechanisms between pillars were considered in the determination of an optimal standard support system. While empirical rock mass classification systems provided initial indications of support requirements in different ground conditions, the importance of using the mine's historical FOG database in the determination of standard support specifications was demonstrated. Support specifications include the rockbolt length, rockbolt support resistance (capacity), and support spacing. The proposed standard support system was backed up by a risk-based support design using the JBlock program. The following support strategies were derived:

- Poor ground conditions and larger spans (≥17.0 m) require a combination of both closely spaced long systematic rock bolting and reinforced shotcrete;
- When ground conditions improve to fair or good, the spacing between rockbolt units in smaller spans (<17.0 m) can be increased, which decreases support unit density and therefore decreases support costs;
- Unreinforced shotcrete and sometimes no shotcrete support can be used in fair to good ground conditions and smaller spans;

- The current standard support system, consisting of a 1.5 m long full-column resin grouted, was validated. However, deterministic and probabilistic analyses indicated that a cost-saving alternative exists of using 1.2 m long bolts with the same capacity;
- The unstable keyblocks forming between pillars are small. It was demonstrated that the various potential instability modes can be managed by a standard support system consisting of 1.2 m rockbolts;
- The small keyblocks occurring between support units can be managed by adequate barring or application of shotcrete; and
- A cost-saving analysis demonstrated that Thorncliffe Mine can potentially save R 3 807 820.80 annually while maintaining safe in-stope working conditions if a support system consisting of 1.2 m rock bolts is adopted.

7.6 Chapter Summary

The research project findings demonstrated the importance of considering various critical factors governing stability to ensure the safe creation of stope excavations in current and future mining. The next chapter concludes the research project by rounding up key findings and observations from the research study and providing recommendations to the mine.

8 CONCLUSIONS AND RECOMMENDATIONS

The research aimed at providing Thorncliffe Chrome Mine with maximum stable bord spans and a support design that ensures that the standard support system is adequate for most of the expected ground conditions at the mine. This involved the application of a systematic and holistic design methodology proposed by the MHSC for the design of shallow stope excavations. The method enabled the use of a combination of different rock engineering design methods to evaluate various rock instability modes which can occur in the stope excavations. The stability analyses subsequently informed the design of a standard support system required to maintain stability in the mine. This Chapter concludes the research report by providing a summary of the key findings and observations, research contributions, and research limitations, and provides recommendations to the mine.

8.1 Summary of Chapters

This report has presented seven chapters that cover the following:

- Chapter 1 introduced the research report by outlining the research context and background, which focused on providing background information on Thorncliffe Chrome Mine. This included Thorncliffe Mine's locality, geology (regional and local), mine design criteria, and the analysis of historical FOG incidents. The chapter presented the problem statement, which highlighted the need for Thorncliffe Mine to follow an engineering approach which takes critical factors into account for the stability of bords. This was followed by a discussion on the justification and main objectives of the research study. Finally, the research methods employed to achieve the objectives of the study were introduced in this stage.
- Chapter 2 presented the research study literature review, which firstly outlined the different rock engineering methods available for the design of underground stope excavations. This was followed by detailing all the components of the systematic MHSC methodology for designing maximum stable bord spans in shallow mining operations in the BC. Lastly, the chapter covered different industry approaches for the determination of support requirements in shallow mining environments.

- Chapter 3 presented the geotechnical investigation undertaken at Thorncliffe Mine's underground workings. The data were used to determine critical parameters that adequately quantify and describe the rock mass structure. Geotechnical data gathering consisted of the scanline mapping of underground exposed hangingwall and pillar rock surfaces, and laboratory testing of rock material.
- Chapter 4 presented the underground rock mass characterisation results, which involved using the acquired geotechnical data to quantitatively describe the geotechnical character of the discontinuous rock mass. The characterisation exercise provided an in-depth understanding of the rock mass structure in the mining environment, and critical mine design parameters were derived in this stage.
- In Chapter 5, results from the characterisation exercise in Chapter 4 were used as input in the design of maximum stable bord spans between pillars. The possible instability modes in the stope excavations were evaluated, which subsequently informed the determination of support required to maintain stability. Additionally, maximum bord widths that can be safely mined were tailored to engineering requirements, local rock engineering environment, and the degree of safety required in different production drives.
- Chapter 6 presented the application of various approaches to determine optimal standard in-stope support systems required to overcome the identified instabilities between pillars. The chapter outlined the philosophies followed in the determination of support specifications such as the rockbolt length, support resistance (capacity), support spacing, and areal coverage. This chapter included a support cost-saving analysis, which demonstrated the impact of adopting a primary support system consisting of the support specifications proposed in this study.
- Lastly, Chapter 7 rounded up the key findings from the different analyses conducted in the research project. This included findings from the rock mass failure analysis, hangingwall beam failure analysis, structural failure analysis, intact rock failure analysis, and the evaluation of support requirements.

8.2 Research Key Findings and Observations

The research study involved the application of an improved method for determining maximum stable bord spans that can be safely mined. The current support system was also investigated. The following are key findings and observations of the research project:

- The quality of the hangingwall rock mass at Thorncliffe Mine's underground workings ranges from very poor to very good ground conditions. The existence of these different ground conditions was confirmed using the RMR_{89}, GSI, Q-system, and $MRMR_{2000}$ classification systems;
- Areas of poor ground quality consisted of the intersection of adverse discontinuities (or discontinuity sets) that are closely spaced, where most individual discontinuities have planar, slickenside or smooth surfaces with thick infill material of low strength, such as serpentinite infill. These include discontinuities such as pegmatite veins, shear zones, joint zones, fracturing associated with dykes, minor faults, and domes;
- The production ore blocks mining towards the South direction consisted of the intersection of three or more major discontinuity sets, which indicated that there are more potentially unstable blocks. The production sections mining towards the North direction indicated an intersection of less than three major discontinuity sets, which indicated the probability of fewer instabilities occurring;
- In addition to the critical geotechnical parameters which characterise the discontinuous rock mass structure, important factors considered in designing maximum bord widths were engineering (equipment) requirements, local rock engineering environment, and the degree of safety required in different production drives. This degree of safety was dictated by the unique purpose and life of the different types of production drives in a bord and pillar ore production section;
- Travelling roadways and conveyor belt drives were classified as medium-term excavations, indicating higher levels of safety (support requirements) than bords used for production only, which were classified as short-term excavations;
- The design of maximum stable bord widths considered the largest spans where the potential of large collapses occurring is increased. The spans

were defined by the diagonal span across intersections of equal-sized orthogonal panels;

- Initial stability analyses indicated that maximum self-supporting spans for short-term panels can be as low as 3 m in very poor rock to a maximum of 15 m in fair rock qualities. Due to higher safety requirements in medium-term panels, the calculated maximum self-supporting spans were generally less, ranging between 2 m in very poor ground to a maximum of 8 m in fair ground;
- Engineering requirements dictated that the mine maintain 6 m minimum bord spans to accommodate the manoeuvrability of the TMMs used in production. The mine also required 6 m minimum spans in strike conveyor belt drives, to accommodate belt conveyor equipment and space for workers to travel. The 6 m requirement equates to 8 m at intersections;
- Results from the modified stability graph method and MRMR stability evaluation correlated well. As ground conditions deteriorated from good to poor, the spans indicated the likelihood of experiencing stability problems. Results from the MRMR indicated that in good ground, all calculated spans ranging between 8 m to 21 m spans (formed by 6 m to 15 m spans of orthogonal bords) are likely to be stable without support. However, rock support is still required in good-quality rock masses according to Stacey (2001);
- In fair-quality ground, stable conditions in larger spans ranging between 17 m to 21 m diagonal spans (formed by 12 m to 15 m spans of orthogonal bords) can only be achieved by the installation of appropriate support. However, smaller spans of 8 m to 14 m (formed by 6 m to 10 m spans of orthogonal panels) are likely to be stable without support in fair-ground conditions;
- When ground conditions further deteriorate to poor, stable conditions can only be achieved by the installation of support in all the calculated spans ranging between 8 m to 21 m (formed by 6 m to 15 m spans of orthogonal panels);
- The modified stability graph method indicated that in very poor ground, only 8 m to 11 m diagonal spans (formed by 6 m to 8 m spans of orthogonal bords) are likely to be stable with the installation of support, while the rest of the calculated spans will fail;

- Results from the Voussoir beam failure analysis indicated that the onset of snap-through failure in the hanging wall occurred when a beam thickness of smaller or equal to 0.30 m in a 17.0 m diagonal span (formed by 12 m spans of orthogonal bords) had deflected by 26.3 mm. Therefore, the potential of rock beam buckling is increased where rock beam thickness is less than or equal to 0.30 m. These findings correlated with the mine's recorded historic FOG database, which indicated that 48% of all FOGs are due to hangingwall parting planes situated at a modal fallout height of 0.25 m (less than 0.30 m rock beam thickness);
- In the Voussoir beam failure analysis, the calculated FOS against abutment shear failure indicated that there was no potential for shear-type beam failure for all the spans evaluated up to the depth of 1000 mbs (life of mine);
- Results from the structural stability analysis confirmed that the size of the formed and unstable wedges between pillars is small, with a maximum volume of 0.3 m^3. The reinforcing forces required to accomplish the unstable wedges' design factor of safety are small, with a maximum support pressure of 13 kPa. The formation of small keyblocks in the hangingwall in the production sections was confirmed by probabilistic stability analysis using the Jblock programme;
- Results from the intact rock mass failure analysis indicated that when the depth below the surface is increased beyond 500 m, the vertical tensile zone extends to a maximum of 1 m into the hangingwall at the maximum diagonal span of 21 m (when orthogonal bord spans are a maximum of 15 m). Additionally, when the depth below the surface exceeds 600 m, the vertical tensile zone extends to less than 1m into the hangingwall for all the spans evaluated. This indicated that the current and future standard support system can consist of shorter tendon units since production is currently taking place at a depth below the surface of about 590 m;
- Rock mass failure analysis indicated that poor ground conditions and larger spans (≥17.0 m) require a combination of both closely spaced long systematic rock bolting and reinforced shotcrete for stability;
- The spacing between rockbolt units in fair-ground conditions and smaller spans (<17.0 m) can be increased, which decreases support unit density and therefore decreases support costs;

- In good or fair-ground conditions and smaller spans, stable conditions can be maintained by application of unreinforced shotcrete, and in some cases no shotcrete support is required;
- While empirical methods provided initial indications of support requirements in different ground conditions, the importance of using the mine's historical FOG database in the determination of standard support specifications was demonstrated;
- The current standard support system, consisting of 1.5 m long full-column resin-grouted bolts was validated. However, deterministic, and probabilistic analyses indicated that a cost-saving alternative exists of using 1.2 m long bolts with the same capacity;
- The various potential instability modes identified between pillars can be managed by a standard support system consisting of 1.2 m rockbolts;
- The mine can potentially save approximately R 3 807 820.80 annually on support costs while maintaining safe in-stope working conditions if a primary support system consisting of 1.2 m long rock bolts is adopted; and
- Lastly, the small keyblocks which occur between support units in the bords can be managed by adequate barring or application of shotcrete.

8.3 Research Contributions

This research work formed an essential part of the GCMP of the mine and aimed to assist in improving the mine's mandatory COP to combat rock falls. The research study made the following valuable contributions to Glencore ECM Operations:

- The geotechnical investigation completed in 2022 at Thorncliffe Mine for this research project added approximately 1500 m of reliable scanline mapping data to the existing limited geotechnical data collected by the mine in 2019. The updated data can be used for conducting value-adding mine planning and design studies in the mine;
- The research provided the mine with maximum stable bord spans that can be safely mined in different ground conditions. This ensured the maximum extraction of ore under safe working conditions;
- Geotechnical scanline mapping covered all ground conditions likely to be encountered at the mine. Additionally, a support design optimisation

approach was taken where the support resistance criterion of the standard support system was designed to prevent 100% of all potential fallouts based on the available FOG database. This means the proposed primary tendon support system design will be adequate for most of the expected ground conditions at the mine; and

- The research study identified a cost-saving opportunity for the mine to reduce the tendon length from 1.5 m to 1.2 m, while maintaining the same support capacity. The newly proposed primary tendon support system would still achieve the desired stable conditions whilst reducing support costs for the mine. Approximately R 3 807 820.80 can be saved on support costs if a support system consisting of 1.2 m rock bolts is adopted.

8.4 Research Limitations

The successful application of the MHSC methodology for designing maximum safety bord spans and support requirements at Thorncliffe Mine was reliant on a proper rock mass characterization study of the mining environment. A few limitations and challenges were identified in the geotechnical investigation and rock mass characterization stages of the project, which highlight opportunities for future research at the mine. These are:

- Incomplete rock testing database - Tensile tests are important to sufficiently tie down the rock mass characterisation, however, these tests were not done in the data collection stage of this research project due to budget constraints at the mine. Additionally, the research involved the estimation of frictional properties of discontinuities with serpentinite infill material (which dominates the underground workings). Rock material specimens containing discontinuities with infill minerals have not been sampled for laboratory testing to derive accurate frictional properties of discontinuities; and
- Estimation of in situ stress field – Local in situ stress measurements have never been conducted since the inception of Thorncliffe Mine in 2006. Therefore, the estimation of in situ stress field conditions was based on the *in situ* stress measurements collated by Stacey & Wesseloo (1998). The in-

situ field stress is an important input parameter for evaluating stability of stope excavations using numerical modelling techniques.

8.5 Recommendations to Thorncliffe Mine

A review and revision of the current mine design criteria used at Thorncliffe Mine enabled the application of an improved method for the determination of maximum stable bord spans and appropriate support requirements. Based on the learnings from the research project, the following recommendations were made:

- The mine should include the entire MG1L1 stringer in the mining cut as a strategy for eliminating the source of many FOGs;
- The mine should consider reducing the standard tendon support length from 1.5 m to 1.2 m. It was demonstrated that stable conditions can still be achieved using resin-grouted rockbolts of a reduced length but the same capacity. This can reduce support costs for the mine;
- To confirm the quality of the rock mass in the underground workings, the mine should always use more than one rock mass classification system for quantifying rock mass quality. It is recommended to use the RMR_{89}, Q-system, and $MRMR_{2000}$ classification systems. Additionally, the mine should always use a combination of analytical, empirical and observational methods to obtain the best possible design of mining spans between pillars;
- The mine should apply areal coverage support only in areas consisting of poor ground conditions and adverse geological occurrences. This is to avoid high operating costs and production delays if areal coverage were made a standard support requirement. Rock Engineering personnel should conduct underground routine visits to determine whether areas of concern require areal coverage support;
- In the determination of support requirements, ensure the largest spans are considered, as the potential of large collapses occurring is increased in this area. The largest span is defined by the diagonal span across intersections of orthogonal panels;
- Install monitoring devices in bord intersections, as the risk of FOG occurrences is increased in these areas;

- Since large FOGs are infrequent at Thorncliffe Mine, the mine should adopt a cost-effective approach of installing longer and stronger support units, such as cable anchors, only when it is required;
- The mine should enforce good barring practices to ensure the correct management of potential rock fallouts between support units;
- The FOG database indicated that FOGs occur mostly during drilling of the face, installation of support, and barring of loose rocks. The mine should attempt complete mechanisation, which will involve rolling out TMMs such as scalers (for barring) and bolters. This will limit the exposure of personnel to FOG incidents and limit injuries related to FOG incidents;
- The introduction of high-density areal coverage will not eliminate the risk associated with some adverse geological structures. The TARP system is still a vital daily risk assessment tool for dictating the required level of response to hazards presented by adverse ground conditions and geological structures;
- As the mine develops, the ground support standards are expected to evolve further; the FOG database should be regularly updated and used to review and improve support systems at the mine;
- The mine should identify GCDs within the mine, which will dictate specific support requirements for similar ground conditions at the mine. Therefore, improves overall stability;
- Discontinuities with serpentinite infill material dominate the underground workings; it is strongly recommended that rock specimens with discontinuities that have serpentine infill be sent for laboratory testing to derive accurate frictional properties;
- GPRs should be routinely used to confirm the position of disseminated stringers in the hangingwall. This will continually inform both optimal mining and support strategies;
- The mine should conduct local in situ stress measurements to determine the *in situ* field stress in the mining environment. This input will enable more valid stress calculations in the stability evaluation of stope excavations and significantly improve the safety of the mining operation;
- Extensometers should be used to monitor the displacement which promotes the opening of discontinuities; and

- Short encapsulations pull out tests (SEPT) should be conducted to validate the bond strength used and to verify tendon support performance.

9 REFERENCE LIST

Abbas, S. M. & Konietzky, H. H., 2017. *Rock Mass Classification Systems* , Freiberg: The Technische Universität Bergakademie Freiberg.

Abioye, A. V., 2019. Determination of Class I and Class II rocks from Conventional method based on the Mechanism of rock Deformation Process. *Insights in Mining Science and Technology,* 1(4), pp. 108-117.

Amadei, B., 2019. *CVEN 5768 - Lecture Notes 10: Rock Discontinuities,* Boulder: University of Colorado Boulder.

Ayamamani, C., 2014. *Introducing RS2.* [Online] Available at: https://www.scribd.com/document/364712561/Introducing-RS2 [Accessed 15 August 2025].

Barton, N., Lien, R. & Lunde, J., 1974. Engineering classification of rock masses for the design of tunnel support. *Rock Mechanics,* 6(4), pp. 189-239.

Barton, N., Lien, R. & Lunde, J., 1977. *Estimation of support requirements for underground excavations..* Minnesota, Norwegian Geotechnical Institute (NGI).

Bieniawski, Z. T., 1973. Engineering classification of jointed rock masses. *Transactions of the South African Institution of Civil Engineers,* Volume 15, pp. 335-343.

Bieniawski, Z. T., 1984. *Rock Mechanics Design in Mining and Tunneling.* Rotterdam : Balkema.

Bieniawski, Z. T., 1989. *Engineering Rock Mass Classifications,* Canada: John Wiley and Sons, Inc.

Bieniawski, Z. T., Franklin, J. A. & Bernede, M. J., 1979. Suggested Method for Determining Deformability of Rock Materials in Uniaxial Compression.

International Journal of Rock Mechanics and Mining Sciences & Geomechanics, 16(2), pp. 135-140.

Brady, B. G. & Brown, E. T., 2004. Rock Mass Structure and Characterisation. In: *Rock Mechanics for Underground Mining.* Dordrecht: Kluwer Academic Publishers, pp. 46-85.

Cai, M., Kaiser, P. K., Tasaka, Y. & Minami, M., 2004. Estimation of rock mass deformation modulus and strength of jointed hard rock masses using the GSI system. *International Journal of Rock Mechanics and Mining Sciences,* 41(1), pp. 3-19.

Canbulat, I., Wilkinson, A. & Prohaska, G., 2005. *An Investigation into the Support Systems in South African Collieries,* Johannesburg: Safety in Mines Research Advisory Committee (SIMREC).

Canbulat, I., Wilkinson, A. & Prohaska, G., 2006. *Roof Bolting Guidelines in South African Collieries,* Johannesburg: Safety in Mines Research Advisory Committee (SIMRAC).

Chikande, T., 2018. *Reflections on Support Design in Geotechnically Challenging Ground Conditions: A Case Study of Zimbabwean Great Dyke Platinum Mining.* Johannesburg: University of Witwatersrand.

Chiwaye, H. T., 2010. *A Comparison of the Limit Equilibrium and Numerical Modelling Approaches to Risk Analysis for Open Pit Mine Slopes,* Johannesburg: University of Witwatersrand.

Corkum, A., 2017. *RS2 (Phase2) Boundary and Initial Conditions.* [Online] Available at: https://www.youtube.com/watch?v=g41Sq1qHqUI [Accessed 08 August 2024].

Daehnke, A., van Zyl, M. & Roberts, M. K., 2001. Review and application of stope support design criteria. *The Journal of The South African Institute of Mining and Metallurgy (SAIMM),* pp. 135-164.

Deere, D. U., 1989. *Rock Quality Designation (RQD) After 20 Years,* Vicksburg: US Army Corps Engineers.

Deere, D. U., Hendron, A. J., Patton, F. D. & Cording, E. J., 1967. *Design of surface and near surface construction in rock.* New York, American Institute of Mining, Metallurgical, and Petroleum Engineers (AIME), pp. 237-302.

Department of Mineral Resources, 2007. *Codebook for Mines: South African Mines Reportable Accidents Statistics System (SAMRASS),* Pretoria: Department of Mineral Resources.

Deseta, N., 2020. *Geology of the PGE Deposits in the Bushveld Complex, South Africa.*[Online] Available at: https://www.geologyforinvestors.com/geology-of-the-pge-deposits-in-the-bushveld-complex-south-africa/

du Preez, L. D. V., 2018. *Investigating the different support methods for various geological structures encountered in hard rock mining within the Eastern Limb of the Bushveld Igneous Complex, South Africa.* Pretoria: University of Pretoria.

Edelbro, C., 2004. *Evaluation of rock mass strength criteria,* Luleå: Luleå University of Technology.

Egerton, F. M., 2004. Presidential Address: The mechanisation of UG2 mining in the Bushveld Complex. *The Journal of The South African Institute of Mining and Metallurgy (SAIMM),* pp. 439-450.

Esterhuizen , G. S. & Streuders, S. B., 1998. Rockfall hazard evaluation using probabilistic analysis. *The Journal of The South African Institute of Mining and Metallurgy (SAIMM),* 98(2), pp. 59-64.

Esterhuizen, G. S., 2007. *An evaluation of the strength of slender pillars,* Pittsburgh: National Institute for Occupational Safety and Health (NIOSH).

Garg, P., 2018. *Behaviour of laminated roof under high horizontal stress,* Morgantown: West Virginia University.

Gholamnejad, J., 2008. A zero-one integer programming model for open pit mining sequences. *The Journal of The Southern African Institute of Mining and Metallurgy (SAIMM),* Volume 108, pp. 759-762.

Giwangkara, G. G. et al., 2020. Analysis of Internal Friction Angle and Cohesion Value for Road Base Materials in a Specified Gradation. *Journal of Advanced Civil and Environmental Engineering (JACEE),* 3(2), pp. 58-65.

Glencore Eastern Chrome Mines (ECM), 2019. *Support Procedure,* Burgersfort: Glencore ECM Operations.

Glencore Eastern Chrome Mines (ECM), 2021. *Technical Support Document,* Burgersfort: Glencore ECM Operations.

Goodman, R. E. & Shi, G., 1985. *Block theory and Its Application to Rock Engineering.* Englewood Cliffs: Prentice-Hall.

Grimstad, E. & Barton, N., 1993. *Updating the Q-System for NMT.* Fagernes, Olso: Norwegian Concrete Association (NCA), pp. 46-66.

Hammah, R., 2025. *Reversing the Paradigm in the Use of RS3 and RS2.* [Online] Available at: https://www.rocscience.com/learning/reversing-the-paradigm-in-the-use-of-rs3-and-rs2 [Accessed 15 August 2025].

Harshil, B., Meena, M. & Badhwar, M., 2018. Design Principles of Rockbolting. *International Journal of Advanced Research in Science and Engineering (IJARSE),* 07(02), pp. 298-303.

Hasch, M. & Latypov, R., 2021. Too large to be seen: Regional structures in Lower and Middle Group chromitites of the Bushveld Complex, South Africa. *Ore Geology Reviews.*

Hoek, E., 1994. Strength of rocks and rock masses. *ISRM News Journal,* 2(2), pp. 4-16.

Hoek, E., 2007. *Practical Rock Engineering,* North Vancouver: Evert Hoek Consulting Engineer Inc.

Hoek, E. & Brown, E. T., 1977. Practical Estimates of Rock Mass Strength. *International Journal of Rock Mechanics and Mining Sciences,* 34(8), pp. 1165-1186.

Hoek, E. & Brown, E. T., 1980. Classification of Rock Masses. In: *Underground Excavations in Rock.* Boca Raton, London, New York: Taylor and Francis Group, pp. 14-36.

Hoek, E. & Brown, E. T., 1997. Practical estimates of rock mass strength. *International Journal of Rock Mechanics & Mining Sciences,* Volume 34, pp. 1165-1186.

Hoek, E. & Brown, E. T., 2019. The Hoek–Brown failure criterion and GSI – 2018 edition. *Journal of Rock Mechanics and Geotechnical Engineering,* 11(3), pp. 445-463.

Hoek, E., Carranza-Torres, C. T. & Corkum, B., 2002. *Hoek-Brown failure criterion - 2002 edition.* Toronto, Proceedings of the 5th North American Rock Mechanics Symposium, pp. 73-267.

Hoek, E., Carter, T. G. & Diederichs, M. S., 2013. Quantification of the Geological Strength Index Chart. *American Rock Mechanics Association (ARMA),* 13(672), pp. 1-8.

Hoek, E. & Diederichs, M. S., 2006. Empirical estimation of rock mass modulus. *International Journal of Rock Mechanics and Mining Sciences,* Volume 43, pp. 203-215.

Hoek, E., Kaiser, P. K. & Bawden, W. F., 1995. *Support of underground excavations in hard rock,* Rotterdam: A.A. Balkema.

Hoek, E., Marinos, P. & Benissi, M., 1998. Applicability of the Geological Strength Index (GSI) classification for very weak and sheared rock masses. The case

of the Athens Schist Formation. *Bulletin of Engineering Geology and the Environment*, pp. 151-160.

Hoek, E. & Martin, C. D., 2014. Fracture initiation and propagation in intact rock - A review. *Journal of Rock Mechanics and Geotechnical Engineering,* pp. 1-14.

Hutchinson, D. J. & Diederichs, M. S., 1996. *Cablebolting in underground mines.* Canada: BiTech Publishers Ltd.

Hyldahl, J., 2018. *Effects of Jointing on Fragmentation: Design and Influence of Joints in Small Scale Testing,* Luleå: Department of Civil, Environmental and Natural Resources Engineering, Luleå University of Technology.

International Society for Rock Mechanics (ISRM), 1978a. Suggested Methods for Determining The Strength of Rock Materials in Triaxial Compression. *International Journal for Rock Mechanics and Mining Sciences and Geomechanics,* Volume 15, pp. 47-51.

International Society for Rock Mechanics (ISRM), 1978b. Suggested Methods for Determining Tensile Strength of Rock Materials. *International Journal of Rock Mechanics and Mining Sciences and Geomechanics,* Volume 15, pp. 99-103.

International Society for Rock Mechanics (ISRM), 1978c. Suggested Methods for the Quantitative Description of Discontinuities in Rock Masses. *International Journal of Rock Mechanics and Mining Science & Geomechanics Abstracts,* Volume 15, pp. 319-368.

International Society for Rock Mechanics (ISRM), 1985. Suggested Method for Determining Point Load Strength. *International Journal for Rock Mechanics and Mining Sciences and Geomechanics,* 22(2), pp. 51-60.

ITASCA Software, 2025. *FLAC2D: Continuum Modelling for Geomechanics in 2D.* [Online]

Available at: https://itascasoftware.com/products/flac2d/ [Accessed 15 August 2025].

ITASCA Software, 2025. *UDEC version 7.0. Distinct-Element Modelling of Jointed and Blocky Material in 2D.* [Online] Available at: https://www.itascacg.com/software/udec [Accessed 16 August 2025].

Jacubec, J., 2013. *Role of defects in rock mass classification.* Perth, Australian Centre for Geomechanics (ACG).

Jager , A. J. & Ryder, J. A., 1999. Chapter 2: Overview of Rock Engineering Strategies. In: *A handbook on Rock Engineering Practice for tabular hardrock mines.* Johannesburg: The Safety in Mines Research Advisory Committee (SIMRAC), pp. 29-43.

Jager, A. J. & Ryder, J. A., 1999. Chapter 10: Monitoring and Auditing. In: *A handbook on Rock Engineering Practice for tabular hard rock mines.* Johannesburg: The Safety in Mines Research Advisory Committee (SIMRAC), pp. 311-327.

Jager, A. J. & Ryder, J. A., 1999. Chapter 6: Tunnel Support. In: *A handbook on Rock Engineering Practice for tabular hard rock mines.* Johannesburg: The Safety in Mines Research Advicory Committee (SIMRAC), pp. 207 - 223.

Jager, A. J. & Ryder, J. A., 2002. Chapter 7: Support of Mine Excavations. In: *A textbook on rock mechanics for tabular hard rock mines.* Johannesburg: Safety in Mines Research Advisory Committee (SIMRAC), pp. 305-391.

Jager, A. J. & Ryder, J. A., 2002. Chapter 9: Underground Monitoring and Instrumentation. In: *A textbook on rock mechanics for tabular hard rock mines.* Johannesburg: Safety in Mines Research Advisory Committee (SIMRAC), pp. 445 - 481.

Jager, A. & Ryder, J., 2002. Chapter 4: Analytic Elasticity and Inelasticity. In: *A Textbook on Rock Mechanics for Tabular Hard Rock Mines.* Johannesburg:

The Safety in Mines Research Advisory Committee (SIMRAC), CSIR, pp. 147-189.

Jakubec, J., 2013. *Role of defects in rock mass classification.* Vancouver, Canada, Australian Centre for Geomechanics (ACG).

Jakubec, J. & Laubscher, D. H., 2000. *The MRMR Rock Mass Rating Classification System in Mining Practice.* Brisbane, Queensland, Australasian Institute of Mining and Metallurgy (AusIMM).

Keykha, H. A., Huat, B. B., Asadi, A. & Moayedi, H., 2011. The effect of discontinuities on stability of rock blocks in tunnel. *International Journal of the Physical Sciences (IJPS),* 6(31), pp. 7132-7138.

Korkanç, M. & Savran, A., 2017. *Impact of the surface roughness of stones used in historical buildings on biodeterioration,* Niğde: ELSEVIER.

Larsson, J., 2021. *Quality aspects in direct shear testing of rock joints,* Stockholm, Sweden: KTH Royal Institute of Technology.

Laubscher, D. H., 1977. Geomechanics classifications of jointed rock masses - mining applications. *Transactions of the Institution of Mining and Metallurgy,* pp. A1-A7.

Laubscher, D. H., 1984. Design aspects and effectiveness of support systems in different mining conditions. *Transactions of the Institution of Mining and Metallurgy,* Volume 93, pp. A70-A82.

Laubscher, D. H., 1990. A Geomechanics Classification System for Rating of Rock Mass in Mine Design. *Journal of the Southern African Institute of Mining and Metallurgy (SAIMM),* 90(10), pp. 257-273.

Laubscher, D. H. & Taylor, H. W., 1976. The importance of geomechanics classification of jointed rock masses in mining operations. In: Z. Bieniawski, ed. *Exploration for rock engineering.* Cape Town: Balkema, pp. 119-128.

Laubscher, D. & Page, C. H., 1990. *The design of rock support in high stress or weak rock environments..* Ottawa, Canadian Institute of Mining, Metallurgy and Petroleum (CIM).

Lauffer, H., 1958. Gebirgsklassifizierung für den Stollenbau. *Geologie und Bauwesen,* 24(1), pp. 46-51.

Leach, A. R., Naidoo, K., Rangasamy, T. & Spencer, D., 2002. *Guidelines for Anomalous Geotechnical Areas in Platinum and Gold Mine Stopes,* Johannesburg: The Safety in Mines Research Advisory Committee (SIMRAC).

Lee, S., 2025. *UDEC Mastery: Geomechanics Essentials.* [Online] Available at: https://www.numberanalytics.com/blog/ultimate-guide-udec-geomechanics#google_vignette
[Accessed 16 August 2025].

Lousteau, R., 2014. *Pillar Optimization for Glencore Operations in the Eastern Limb,* Johannesburg: Middindi Consulting.

Maepa, K., 2024. *Personal Communication* [Interview] (14 October 2024).

Malan, D. F., Napier, J. A. & Janse van Rensburg, A. L., 2007. Stope deformation measurements as a diagnostic measure of rock behaviour: a decade of research. *The Journal of The Southern African Institute of Mining and Metallurgy (SAIMM),* Volume 107, p. 743.

Malan, D. F. & Napier, J. L., 2011. The design of stable pillars in the Bushveld Complex Mines: A problem solved?. *The Journal of the Southern African Institute of Mining and Metallurgy (SAIMM),* Volume 111, pp. 821-836.

Marinos, P. G., Marinos, V. & Hoek, E., 2005. *The Geological Strength Index (GSI): A characterization tool for assessing engineering properties for rock masses.* Athens, s.n., pp. 87-94.

Merafe Resources, 2021. *Appendix 1: Mineral Resource and Mineral Reserve Report.* Rustenburg: Merafe Resources Limited.

Miller, D. R., Barret, J. R. & Bamford, W. E., 1986. *A field classification for uniaxial strength of diamond drill core using simple index tests,* North Melbourne, Australia: Bamford Rock Testing Services.

Milne, D., Hadjigeorgiou, J. & Pakalnis, R., 1999. Rock Mass Characterization for Underground Hard Rock Mines. *Tunnelling and Underground Space Technology,* 13(4), pp. 383-391.

Monsalve, J. J., Baggett, J., Bishop, R. & Ripepi, N., 2018. *A Preliminary Investigation for Characterization and Modelling of Structurally Controlled Underground Limestone Mines by Integrating Laser Scanning with Discrete Element Modelling.* Virginia, Virginia Polytechnic Institute and State University.

Muralha, J., Grasselli, G. & Tatone, B., 2013. *ISRM Suggested Method for Laboratory Determination of the Shear Strength of Rock Joints: Revised Version,* s.l.: Springer-Verlag Wien.

Murphy, S. K., Joughin, W. C., Walls, E. J. & Zermatten, C., 2016. *A handbook on practical design methodology for spans (bord widths) in bord and pillar mining on platinum and chrome mines in the Bushveld Complex,* Johannesburg: The Safety in Mines Research Advisory Committee (SIMRAC).

Norwegian Geotechnical Institute (NGI), 2022. *Using the Q-System - Rock mass classification and support design.* June 2022 ed. Olso, Norway: Norwegian Geotechnical Institute (NGI).

O'Ferrall, G. C. & Malan, D. F., 2012. *Case Studies of Tendon Support Design In Bord And Pillar Operations In Two South African Platinum Mines.* Stockholm, International Society for Rock Mechanics (ISRM).

Oliveira, D. A. & Pells, P. J., 2014. *Revisiting the applicability of voussoir beam theory for tunnel design in Sydney,* Sydney: Australian Geomechanics Journal.

Pacher, F., Rabcewicz, L. & Golser, J., 1974. *Zum der seitigen Stand der Gebirgsklassifizierung in Stollen-und Tunnelbau.* Salzburg, Proc. XXII Geomech. Colloq., pp. 31-34.

Palmström, A., 1982. *The volumetric joint count - a useful and simple measure of the degree of rock jointing.* Delhi 5, 4th Congr. Int. Assn. Engg. Geol., pp. 221-228.

Perras, M. & Diederichs, M., 2014. *A Review of The Tensile Strength of Rock: Concepts and Testing ,* Switzerland : Springer International Publishing .

Potvin, Y., 1988. *Empirical open stope design in Canada. Ph.D Dissertation,* Vancouver: University of British Columbia.

Priest, S. D. & Hudson, J., 1976. Discontinuity spacing in rock. *International Journal of Rock Mechanics and Mining Sciences & Geomechanics ,* 13(5), pp. 135-148.

Read, J. & Stacey, P., 2008. Field Data Collection. In: *Guidelines for Open Pit Slope Design.* Collingwood: CSIRO PUBLISHING, pp. 15-52.

Read, J. & Stacey, P., 2008. Rock Mass Model. In: *Guidelines for Open Pit Slope Design.* Collingwood: CSIRO PUBLISHING, pp. 83-140.

Rehman, Z. U. et al., 2021. *Slope Engineering: Design Techniques in Rock and Soil Engineering,* London: Istanbul University Cerrahpaşa.

Ritter, W., 1879. *Die Statik der Tunnelgewölbe.* Berlin: Springer.

Roberts, D., 2020. *FLAC(3D) - Numerical Modelling Techniques in Rock Engineering Lecture Notes.* Johannesburg: University of Witwatersrand.

Roberts, M. K., 1999. *The Design of Stope Support Systems in South African Gold and Platinum Mines. Ph.D. thesis,* Johannesburg: University of Witwatersrand .

Rocscience Inc, 2022. *Rocscience | Geotechnical Software for Tunnelling.* [Online] Available at: https://www.geoengineer.org/news/rocscience-geotechnical-software-for-tunnelling
[Accessed 15 August 2025].

Rocscience, 2023. *Dips: Graphical and Statistical Analysis of Orientation Data.* [Online] Available at: https://www.rocscience.com/software/dips [Accessed 19 May 2023].

Roscscience, 2007. *RocLab 1.0: Rock Mass Strength Analysis using the Generalised Hoek-Brown failure criterion.* [Online] Available at: https://www.resolutionmineeis.us/documents/rocscience-2007 [Accessed 13 August 2025].

Sandvik Mining and Rock Technology, 2023. *Pioneering Solutions in Ground Support for Your Sustainable Future,* s.l.: Sandvik Mining and Rock Solutions.

Sandvik Rocbolt Technologies , 2025. *Roofbolts and Resin Capsules Sales - Quote.* Johannesburg: Sandvik Mining and Rock Technology.

Scoon, R. & Viljoen, M., 2016. *Africa's Top Geological Sites 8. The Eastern Limb of the Bushveld Complex,* Grahamstown: Rhodes University.

Sellers, E. J., Coetzer, S. J. & Kamstra, R., 2002. *Understanding and determining the variability of the primititve stress environment,* Johannesburg: Safety in Mines Research Advisory Committee (SIMRAC).

Shabanimaschool, M., Jing, L. & Li, C., 2014. *Discontinuous Modelling of Stratum Cave-in in a Longwall Coal Mine in the Arctic Area,* Switzerland: Springer International Publishing.

Shacker, D., 2019. *Research into the interpretation of deformation measured by extensometers,* Saskatoon, Canada: University of Saskatchewan.

Singh, B. & Geol, R. K., 1999. *Rock mass classification: a practical approach in civil engineering,* Amsterdam: Elsevier Science.

Spross, J., 2016. *Toward a reliability framework for the observational method,* Stockholm, Sweden: KTH Royal Institute of Technology.

Stacey, T. R., 1981. A simple extension strain criterion for fracture of brittle rock. *International Journal of Rock Mechanics and Mining Sciences,* pp. 469-474.

Stacey, T. R., 2001. *Best practice rock engineering handbook for "other" mines,* Johannesburg: The Safety in Mines Research Advisory Committee (SIMRAC).

Stacey, T. R., 2021. *Mechanical properties of rocks and rock masses: A Design Process,* Johannesburg: University of the Witwatersrand.

Stacey, T. R. & Wesseloo, J., 1998. *Evaluation and Upgrading of Records of Stress Measurements Data in the Mining Industry,* Johannesburg: The Safety in Mines Research Advisory Committee (SIMRAC).

Stavrou, A., Vazaios, I., Murphy, W. & Vlachopoulos, N., 2019. Refined Approaches for Estimating the Strength of Rock Blocks. *Geotechnical and Geological Engineering ,* Volume 37, p. 5409–5439.

Stini, I., 1950. *Tunnul baugeologie.* Vienna: Springet-Verlag.

Swart, A. H., 2005. *Investigation of factors governing the stability of stope panels in hard rock mines in order to define a suitable methodology for shallow mining operations,* Pretoria: University of Pretoria.

Swart, A. H. & Handley, M. F., 2005. The design of stable stope panels for near-surface and shallow mining operations. *The South African Institute of Mining and Metallurgy (SAIMM),* pp. 275-286.

Swart, A. H., Stacey, T. R. & Wesseloo, J., 2000. *Investigation of factors governing the stability/instability of stope panels in order to define a suitable design methodology for near surface and shallow mining operations. SIMRAC Project Report OTH 501,* Johannesburg: The Safety in Mines Research Advisory Committee (SIMRAC).

Terzaghi, K., 1946. Rock defects and loads on tunnel supports. *Rock Tunneling with Steel Support,* Volume 1, p. 17.

Torkan, M., Janiszewski, M., Uotinen, L., Baghbanan. A. 2022. *Photogrammetric Method to Determine Physical Aperture and Roughness of a Rock Fracture.* [Online]
Available at: https://www.mdpi.com/1424-8220/22/11/4165 [Accessed 27 November 2023].

Watson, B., 2003. *The feasibility of using rock mass ratings for the design of panel spans and support in the shallow to intermediate depth Bushveld platinum mines. MSc Thesis,* Johannesburg: Department of Mining Engineering, University of Witwatersrand.

Watson, B. P. & Gerber, R., 2018. Determination of stable spans in UG2 excavations. *The Journal of the Southern African Institute of Mining and Metallurgy (SAIMM),* Volume 118, pp. 1-12.

Watson, B. P., Lamos, R. A. & Roberts, D. P., 2021. PlatMine Pillar Strength Formula for the UG2 Reef. *Journal of the Southern African Institute of Mining and Metallurgy (SAIMM),* 121(8), pp. 437-448.

Wickham, G. E., Tiedmann, H. R. & Skinner, E. H., 1972. *Support determination based on geologic predictions.* Chicago, 1st Rapid Excavation and Tunn. Conf, pp. 43-64.

Xtrata Alloys, 2005. *Helena MG1 Project Geological Summary Report,* s.l.: Xtrata Alloys.

Yilmaz, H., 2010. Rock Testing and Mechanical Properties of Rocks. *The Southern African Institute of Mining and Metallurgy (SAIMM),* pp. 145-162.

Yun, B., 2018. *Underground Engineering: Planning, Design, Construction and Operation of the Underground Space.* First Edition ed., Shanghai: College of Civil Engineering, Tongji University.

Zerradi, Y., Lahmili, A. & Souissi, M., 2020. *Stability of a rock mass using the key block theory: a case study.* Morocco, EDP Sciences.

Zhang, L., 2016. Determination and applications of rock quality designation (RQD). *Journal of Rock Mechanics and Geotechnical Engineering,* 8(3), pp. 389-397.

Zhang, N., Li, C. C. & Lu, A., 2019. Experimental Studies on the Basic Friction Angle of Planar Rock Surfaces by Tilt Test. *Journal of Testing and Evaluation.*

Zhao, K., Gu, S. & Yan, Y., 2018. *Rock Mechanics Characteristics Test and Optimization of High-Efficiency Mining in Dajishan Tungsten Mine,* Ganzhou: Wiley Hindawi.